Organically Templated Inorganic Membranes

for

Gas Separation

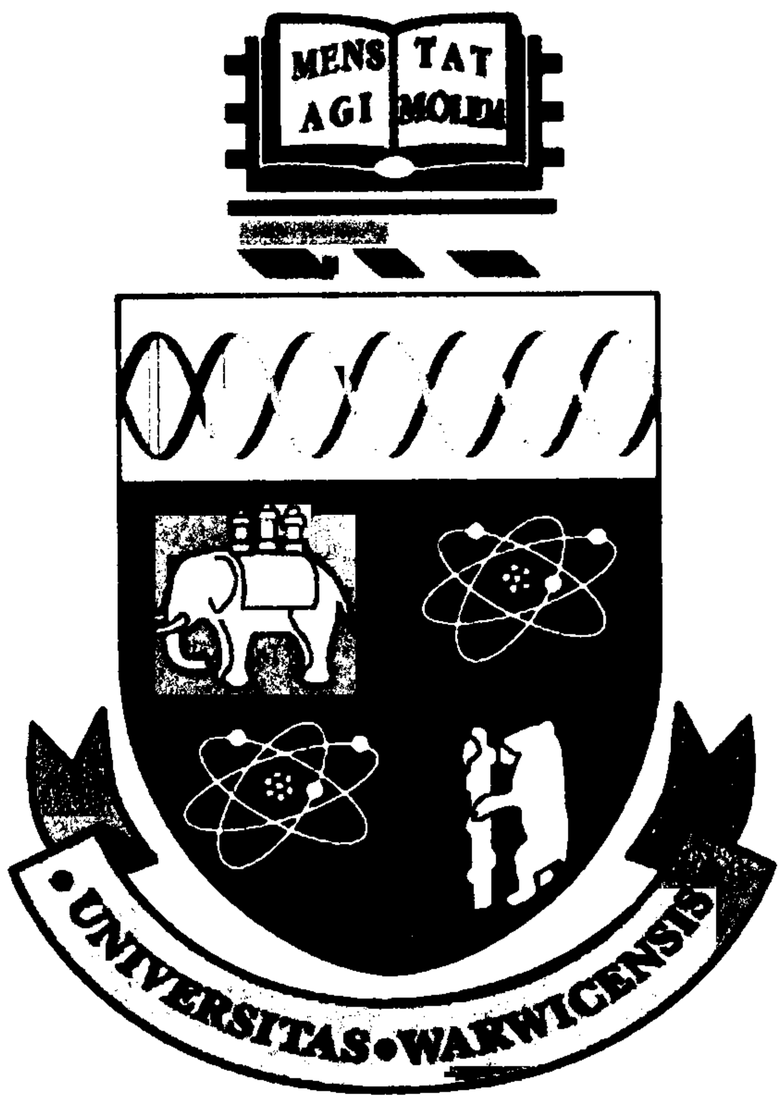

Geoffrey Graham Diamond M.Sc

Thesis submitted for the award of
Doctor of Philosophy

Department of Physics
Centre for Advanced Materials

November 2001

Acknowledgements

Grateful thanks and acknowledgements are extended to my supervisor, Prof. M.H. Lewis for both his scientific expertise and personal support over the period of this thesis.

Acknowledgement is also made to ESPRC for their financial support.

I would like to extend my thanks to the staff and technicians who assisted me greatly: Dr M Smith Mr N. Dajda and all the staff of the NMR group who provided much help and assistance, Dr A.M. Wootton, Mr K Briggs, Mr S. York and Mr R. Bridgeland who allowed permitted full and open access to the facilites of the machine workshop.

Special thanks are expressed towards Mr G. West whose mature judgements and practical support have been greatly appreciated.

Declaration

This thesis is the result of my own research and has not been submitted for any other degrees. Parts of this work have been previously published as:

1) U. Stefan Björket, M. H. Lewis, D. Holland "*Novel Planar Membranes for Gas Separation: 12 Month Progress Report*", Centre for Advanced Materials, Dept of Physics, University of Warwick

2) U. Stefan Björket, M. H. Lewis, D. Holland "*Novel Planar Membranes for Gas Separation: 18 Month Progress Report*", Centre for Advanced Materials, Dept of Physics, University of Warwick

3) "Gas separation Mechanisms through Micro-porous Silica Membranes" G. West, G. Diamond, D. Holland, M.E. Smith, M.H. Lewis. Accepted for publication in "Journal of Membrane Science" November 2001

4) "Structural Evolution of Membrane Materials" G. West, G. Diamond, N. Dajda, M.E. Smith, M.H. Lewis. Submitted for publication in "Journal of Sol Gel Science and Technology" October 2001

Summary

This work is an attempt to develop inorganic gas separation membranes for the purposes of separating high temperature binary gaseous mixtures. Carbon dioxide and nitrogen mixtures are the focus of this work but other mixtures could be used.

The membrane synthesis route is derived from the sol-gel technique. It relies upon micropores being produced within the membrane and this is accomplished by the thermal removal of organic ligands (the "templates"). The thermal stability and structural evolution with temperature of these materials has been characterised with TGA, DTA, FTIR, ^{13}C CP MAS NMR ^{11}B MAS NMR and ^{29}Si MAS NMR investigations.

The research was demarcated into the comparisons between two systems: non-borosilicate and borosilicate. The borosilicate systems were thought to merit special investigation due to the known property of the boron atom in borosiloxane bonds to act as a network enhancer.

Three different organic ligands; methyl, ethyl and phenyl have been investigated. The higher thermal stability (~770K) and the known CO_2 affinity of the phenyl ligand, led to the production of materials containing both the methyl ligand (to generate porosity) and the phenyl ligand (to hopefully provide CO_2 affinity). Other structures with methyl as a backbone but containing boron were found to have superior performance in terms of separation factors, robustness and durability.

The permeability of CO_2, N_2, Ar and He was measured through all the membranes systems , as a function of pressure, temperature and time. In both the borosilicate and non-borosilicate systems, CO_2 was found to permeate preferentially over He in the best specimens. This was despite its much larger molecular diameter and for both classes of system, permeance was observed to decrease with elevated temperatures. The general conclusion that for both classes of system the mechanism of preferential CO_2 transport is activated surface diffusion. Evidence of gradual absorption of CO_2 by the non-borosilicate systems was indicated by their steady decrease in performance with time when exposed to this species. (Such degradation in permeance performance was not observed for those non-borosilicate systems that had not been exposed to CO_2 but just N_2, He or Ar. The borosilicate systems however, were far more robust. Any decrease in permeance with time, after exposure to CO_2 under pressure, was orders of magnitude slower than with the non-borosilicate systems.

For the non-borosilicate systems the decrease in permeability is deemed to be due to CO_2 chemisorption and must be related to the surface diffusion. For the non-borosilicate systems however, chemisorption appears to play a far less important role.

Structural studies (NMR and FTIR) of all the systems indicated that the pyrolysis of the organic templates produces both siloxane and in the case of the borosilicate systems, borosiloxane linkages as well. These are assumed to be the generators of the sites through which surface diffusion occurs.

For the non-borosilicate systems, surface diffusion seems to be improved by the incorporation of phenyl ligands within the siloxane network. However, this is associated with accelerated adsorption and decrease in overall performance. For the borosilicate systems, the most successful system had a methyl backbone and decreased in performance very gradually and after that remained

constant except for long-term modulations which were mirrored by the inert species as well. Thermally rejuvenating the degraded non-borosilicate membranes did not meet with success. However, the borosilicate systems did partially respond to this treatment and regained a significant fraction of their original performance. The conclusion is that in the non-borosilicate system chemisorption dominates over physisorption as a CO_2 selectivity mechanism, whilst for the borosilicate systems the reverse appears to be true.

Contents

List of Illustrations

Chapter 1

Chapter 2

Chapter 3

Chapter 4

Chapter 5

Chapter 1

Introduction

1.1 Project Background

The aim of this research project was to investigate a method of producing micro-porous inorganic gas-separation membranes, which would be suitable for the separation of the various components of high-temperature gas mixtures.

The chosen approach for the production of such membranes is that of using an organic "template" [1]. This technique revolves around the principle of taking silicate precursor gels containing organic molecules, which can then be removed via pyrolysis. (The process of removing the organic component(s) creates an array of voids - or "templates" – that then provide the porosity necessary for the separation of gases).

Initially, the precise goal of this project was to develop a flat membrane, specifically designed for the purpose of separating CO_2 and N_2 from the flue gases of commercial power stations.

The motivation for attempting this particular separation process is that it would reduce the amounts of CO_2 emitted into the atmosphere. Atmospheric concentrations of CO_2 are considered in many quarters to be one of the most significant contributing factors to the supposed "greenhouse effect" and the (unproven) phenomenon of "global warming". This popular perception, together with heavy political involvement, now means that there are very lucrative

commercial incentives to develop and exploit technologies capable of performing this separation process.

However, once separated, the collected CO_2 must somehow be isolated in a form that does not permit its escape into the atmosphere. This means that for it to be fixed in a more or less permanent form, the CO_2 must be chemically bound. Such solutions (e.g. combination with calcium ions) involve highly endothermic chemical reactions.

The fact that the flue emission gases are already heated to between 700K to 900K, provides the energy for the CO_2 binding reactions mentioned above. However, the main problem is that whilst membranes capable of separating a binary mixture of N_2 and CO_2 can be made using current techniques - all of the membranes currently available to accomplish this are low-temperature organic polymer films [2].

Basically, there is currently no membrane available which is capable of separating out CO_2 and which does not also undergo irreversible physical and structural damage when exposed to such a high-temperature environment.

Cooling of the flue gases prior to filtration is not a commercially feasible option. In order for the process to be cost effective and economically viable for large-scale industrial application, other savings must offset the amortisation costs of the large capital investments required to install such a separation process. This means that no external heat can be provided in the secondary stage of chemically binding the CO_2. Hence, ideally any separating membrane should be thermally stable up to 900K. (Other problems such as low fracture toughness do also have to be addressed, but in the main they are of secondary importance in comparison with the central issue of thermal stability).

Inorganic membranes have the potential to be resistant to both high temperatures and corrosive environments. If a successful solution to the present problem of gas

separation described above could be found, then the "spin-offs" for such a separation process could have an enormous range of applications in many other industries and processes. Some examples, which could readily be capitalised upon, are: nitrogen and oxygen separation from air; the purification of methane; high-temperature recovery of hydrogen in coal gasification; the removal of acidic gases from gas streams and catalytic membrane reactors.

1.1.1 Related Research At Warwick .

The current research project commenced in October 1998. However, it stems from a commission originally accepted by the Centre for Advanced Materials Research at the University of Warwick in 1993, from the NEDO Corporation of Japan .

Previously, the Centre had not pursued the "template" method, but had instead chosen two different approaches to this problem [3]:-

1) Diphasic ceramic materials: These are micro-porous and actually channel the gas via one or more of three possible mechanisms – viscous flow (undesirable), Knudsen flow and surface absorption along the pore walls (section 1.3).

Augmentation of a preferential permselectivity of CO_2 over N_2 was attempted by introducing dopants to enhance chemisoprtion of the permeate species. This species is then transported along a pore wall by a transmembrane pressure difference that drives a surface diffusion mechanism. Alumina was the chosen membrane microstructure with a titania second phase. Dopants for the purpose of enhancing chemical affinity between CO_2 and the membrane material were either lanthanum oxide or magnesium oxide.

2) Interpenetrating Networks (IPN's) These materials possess a large molecular framework and selectivity should arise as a result of a difference in the diffusion constants of each component of a binary gas mixture.

1.2 Membrane Types

For the purposes of this thesis, a membrane is defined as being a semi-permeable barrier between different phases that are not in thermodynamic equilibrium with each other. The main purpose of *any* membrane is to control the mass transport of different species in a selective fashion. Separation of gases by a membrane involves separating a feed gas of two (or more) species by use of the semi-permeable barrier, through which, one or more of the species moves faster than other(s). The basic membrane separation process involves a mixed-species feed gas and is illustrated in Figure 1.1. This is then separated into a *retentate* (that part of the feed gas that does not pass through the membrane and is retained) and a *permeate* (that part of the feed gas that passes through the membrane).

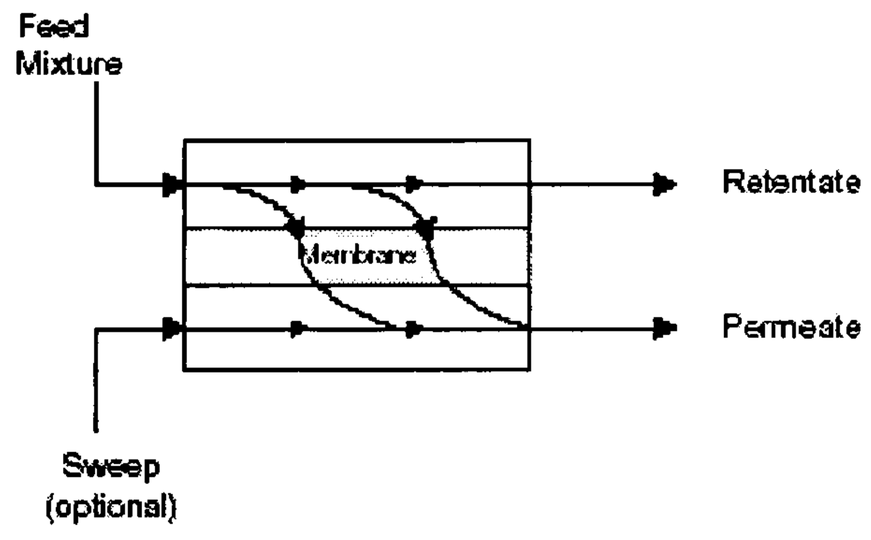

FIGURE 1.1 – Schematic of basic membrane operation.

Membranes are usually categorised in accordance with their separation behaviour and their structure. The usual demarcation is between the inorganic and organic types. However, organic membranes can only withstand mild chemical and thermal conditions. As mentioned previously, the intended

application of this research is to be for such environments as the flues of commercial power stations. Therefore, pure organic membranes will not be discussed further owing to their inability to withstand exposure to such elevated temperatures and aggressive chemical environments.

1.2.1 Inorganic membranes.

There are two general classes of inorganic membranes: dense and porous.

1.2.1.1 Dense inorganic membranes

Strictly speaking, non-porous membranes were not the subjects of this research. However, superficially they would appear to be sufficiently robust in terms of their mechanical and thermal properties to be suitable for an environment such as the flue of commercial power stations. They are therefore briefly discussed below for the sake of completeness. (Included are the reasons why they were ultimately not suitable for the purposes of this project).

This class of inorganic membrane can be subdivided into metal membranes and nonporous oxide membranes.

<u>Metal membranes</u>

Palladium membranes are the most commonly used metal membranes. These membranes are made of Pd alloys that adsorb hydrogen atoms that are then transported via diffusion – hence resulting in the selective permeation of hydrogen. Near total conversion of the reactants is possible with these membranes as they let only one component permeate. At present, the only other metal membrane apart from palladium to have been successfully used in membrane reactors is silver and its function is for the separation of oxygen.

An initial reaction might be that metal membranes were the material of choice for the harsh thermal and chemical environment of the flue of a commercial

power station. However, metal membranes have several disadvantages. These metals are expensive, difficult to form and not as durable as other more common metals. More seriously, carbon and sulphur compounds can poison these classes of membranes. (This is an extreme disadvantage for the aim of this project if one considers that carbon and sulphur combustion products are a significant fraction of the exhaust gases of a power station). Other handicaps for metal membranes are their intrinsically low permeabilities and problems of metal sintering.

Oxide Membranes

At present, the only use for this class of membrane has been for the separation of oxygen and hydrogen from mixed-gas streams. Therefore, as this thesis is specifically concerned with N_2 and CO_2, their range of practical applications is somewhat restricted and inappropriate for the aim of this research.

1.2.1.1.1 Gas transport Mechanism in Non-Porous Membranes.

Metal membranes.

The nonporous metal membranes described in section 1.2.1.1 have only one separation mechanism. This is the so-called "atomic diffusion" process where hydrogen molecules adsorb and dissociate into atoms on the metal surface. These atoms then diffuse through the metal membrane due to the solubility of hydrogen atoms in palladium. On the obverse side of the membrane the hydrogen atoms recombine and desorb from the surface. Although there are other gas species that are capable of being dissociated upon contact with palladium, there are none that possess a sufficiently high solubility in palladium. Hence, theoretically unlimited separation factors should be possible when separating out hydrogen from other gases. However, in practice the hydrogen flux is proportional to the square root of the partial pressure of hydrogen [4].

Oxygen transport through silver membranes is via a similar mechanism to hydrogen transport through palladium alloy membranes. Oxygen atoms dissociate, diffuse through the membrane and recombine on the opposite side. The permeability of the gas (into a vacuum) is proportional to the square root of the partial pressure of oxygen. However, the transport of oxygen is affected by the presence of other species that can also adsorb on the silver surface. The rate of transport of oxygen through silver is far less than hydrogen through palladium.

Amorphous non-porous membranes.

Nonporous silica glass also displays a high affinity for hydrogen and very large separation factors are possible. This selectivity results from small voids within the glass network. Transport is then accomplished via an adsorption process in combination with a solution/diffusion mechanism.

Crystalline non-porous membranes

Calcium-stabilised zirconia is used as a membrane with a high selectivity that favours oxygen. Oxygen is transported through the membrane via dissociation on the surface, followed by conduction through the structure. Electron conduction in the opposite direction to the oxygen flow maintains overall charge neutrality and so no external charge-balancing circuit is required.

1.2.1.2 Porous Inorganic Membranes

These are usually categorised into three basic types [5]:

Macro-porous : pore diameter (d_p) > 50 nm

Meso-porous : 2 nm < d_p < 50 nm

Micro-porous : d_p < 2 nm

When the pore size is of the order of angstroms then the micro-porous membranes are usually described as molecular sieves. As the name implies, the

pores are so small that they can discriminate between molecular species according to their kinetic diameters. However, it must be emphasised that most micro-porous membranes do not rely solely upon a pure sieving mechanism. Instead, they affect the transport of differing chemical species by varying degrees.

Inorganic micro-porous membranes are classed as either amorphous or crystalline. Zeolite membranes are the most significant of the crystalline variety. However, as the specific goal of this research is gas separation membranes that are synthesised from sols, only the amorphous silica-backboned structures will be discussed in below.

1.2.2 Micro-Porous Silica Membranes

Only one type of micro-porous silica membrane is currently available on a limited commercial basis: Chemical Vapour Infiltrated (CVI) based membranes. These are synthesised by reacting a silica precursor such as tetraethylorthosilicate (TEOS) with an oxidising agent. This reaction actually occurs within the pores of a macro- or meso-porous support.

Uhlhorn *et al* [6], Kitao and Asaeda [7] and Kuraoka *et al* [8] report upon sol and CVD derived silica membranes. The overall conclusion is that in these systems, activated diffusion is the main mass-transport mechanism.

Commercial versions of these membrane systems display a high selectivity for hydrogen [9]. The disadvantage is that their absolute permeabilities are quite low (due to the presence of almost fully dense silica plugs within the pores of the support substrate).

This is the classic dilemma of membrane separation technology: high selectivity often comes at the cost of low volume throughputs. The efficiency of a permselective membrane is generally dependent upon it possessing as

small a pore size (and as narrow a pore size distribution) as possible. However, smaller pore sizes means larger impedance of mass-transport. For practical reactor design, one has to calculate a "trade off" between these two requirements.

1.2.3 Sol-Gel derived Micro-Porous Silica Membranes

Sol-gel derived silica membranes are not yet available on a commercial basis. However, since the late 1980's the development of this class of membrane has been the focus of much research. The usual approach to producing gas separation membranes is to take thin films that have been deposited from polymeric sols and to expose them to drying regimes that encourage the extreme collapse of the structure[10].

Ideally, this should result in the formation of a material possessing sub-nanometre sized pores. (A review of the applicable techniques employed to synthesise this class of membrane has been conducted by Klein and Woodman [11] and Brinker *et al* [12]). The drawback is that small pore size is attained at the cost of high resistance to mass-transport and low gas fluxes. The alternative approach to producing microporous sol-derived materials of small pore sizes within a narrow distribution range – and also affording a high level of porosity - is the template method which is discussed in section 1.5.4

Because of their small pore sizes, sol-gel derived silica membranes display high permeability towards small-moleculed gas species such as H_2, O_2 CO_2 and He but very low permeabilities for the larger molecules such as for example, aromatic hydrocarbons and SF_6.

These materials are ideal candidates for this research. They offer high thermal and chemical robustness combined with the potential for both high fluxes and selectivities found that are characteristic of micro-porous silica membranes.

Hence, if satisfactorily synthesised, the sol gel approach could produce membranes which would be ideal for the goal of this research.

1.3 Membrane Separation and Mass Transport Mechanisms

The degree to which the various constituents of a gaseous mixture can be separated by a membrane is dependent upon the mass-transport mechanism(s) that are operative under given environmental conditions.

The mass-transport mechanism(s) of the membrane dictates the relative fluxes of the gaseous species, which in turn affect the separating ability of the membrane. A thorough discussion of the interaction between substrate and separation membrane layer(s) is presented by Meixner and Dyer [13]. (Another consideration is the interaction between the mobile species themselves).

1.3.2 Gas Transport through Porous Membranes.

Porous membranes are the subject of this research. Hence, the treatment of their mass transport mechanisms will be more rigorously treated than the classes of membrane described above.

The sol-gel derived silica backboned structures, which are the subject of this thesis, were originally intended to have pore sizes that were comparable to the kinetic diameter of small gas molecules. Therefore, even a very thin membrane atop of a porous support substrate would offer a large resistance to the flow of gas through it.

The selectivity of such a multi-layered porous membrane system is predominantly determined by the micro-porous layer (analogous to the conductance of electrical resistances in series). However, the porous support substrate of such a membrane also affects the mass-transport of gas species.

This is especially true for small fast-moving molecules where the resistance that is offered by the active separation layer is small. In these instances, the resistance to flow of the membrane support substrate becomes more influential. From a design point of view, modelling the separation characteristics of the entire multi-layered, multi component, membrane system has to take account of all the mass-transport features of each layer [13].

The above discussion has emphasised the situation for micro-porous membranes (d_p < 2 nm). However the same reasoning applies (though to a lesser degree) to porous substrates supporting active membrane layers with pores in the meso-porous regime (2 nm < d_p < 50 nm). The further the active membrane's pore size deviates from this lower limit, then the greater will be the influence of the support substrate

There are five major mass-transport mechanisms[14,15,16,17]. In order of their relative effectiveness they are:

- Poiseuille (viscous) flow;
- Knudsen diffusion;
- Surface diffusion;
- Capillary condensation;
- Molecular sieving.

(For macro- and meso-porous media the mechanism of mass-transport of gases is determined by the ratio of the mean free path (σ) of the molecules to the pore diameter d_p). These mechanisms are discussed in detail in sections 1.3.2.1 to 1.3.2.5 below.

Overview of Mass Transport Mechanisms

One main criterion dictates whether or not permeation is to be controlled by either viscous or molecular flow. This is whether the molecules of the gas species experience a greater number of collisions with the pore walls or with other gas molecules. Viscous and molecular flow can occur simultaneously and the degree to which these two fundamental processes exert their respective influences is determined by the pore size (d_p) and the mean free path (σ) of the gas molecules. The ratio of d_p to σ is a gauge of the relative mass-transport contribution from each process. If $d_p/\sigma << 1$ then molecular processes dominate at the expense of viscous flow and if $d_p/\sigma >> 1$ then the reverse is true.

For miscible fluids such as gases, Poiseuille (viscous) flow is ineffectual as a mechanism for separation purposes. This is because the pore size is many times larger than the mean free path of the gas molecule. Under Poiseuille flow, the mean free path of the gas molecules is small in comparison with the pore diameter. Molecules of different gas species will collide more often with each other than with pore walls. Hence, the molecules in a gaseous mixture cannot act independently in the viscous flow regime. The result is that the pore size is too large to discriminate against gas species according to their size. In addition, as the velocities of the molecules of each species becomes similar then there remains no gross physical difference between the species that can be exploited to provide separation.

Knudsen diffusion allows only relatively low separation factors when compared to surface diffusion and capillary condensation. Molecular sieving is theoretically the most selective process of all and has the potential to offer extremely high separation factors. For all these mass-transport mechanisms, the performance is highly dependent upon pore size and pore size distribution, temperature, transmembrane pressure difference, interactions between the mobile gases and also the state of the membrane's surface.

1.3.2.1 Poiseuille (Viscous) Flow.

In the viscous flow regime (macro-pores), the mean free path of the gas molecules is very much smaller than the pore diameter. When a transmembrane pressure gradient is present, momentum transport leads to drift velocities of the molecules.

If one assumes cylindrical pore geometry (with its Reynolds number of 2000) then it is reasonable to assume laminar flow for the transmembrane pressures involved. The permeability (F) of such a membrane for incompressible gases is described by Equation (1.1) below and illustrated in Figure 1.2.

$$F = \frac{\varepsilon_p \bar{r}^2 P_{av}}{8RT\eta\tau L} \qquad \textbf{(1.1)}$$

(Where ε_p is volume fraction porosity; r is mean pore radius; P_{av} is the mean transmembrane pressure difference; R is the universal gas constant; T is the thermodynamic temperature; η is viscosity, τ is a tortuosity coefficient and L is membrane thickness.)

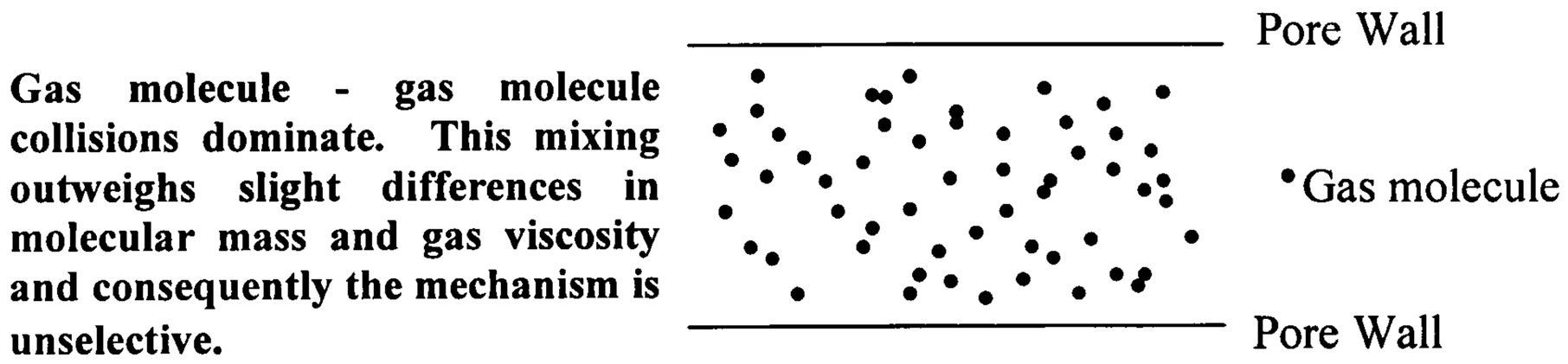

Figure 1.2 - POISEUILLE FLOW – pore size >60 nm).

1.3.2.2 Knudsen Diffusion

As the ratio d_p/σ decreases (either as a result of the pressure being lowered and/or the pore radius becoming smaller) the gas molecules experience more collisions with the pore walls than with each other. Gas molecules then proceed through the pores more independently of each other and independently of the transmembrane pressure difference.

During each collision with the pore wall, the gas molecule briefly adsorbs onto the pore surface and loses some momentum to the surface. The momentum vector is completely random. The overall result is that mass-transport becomes a function of the speed of gas flow, which in turn is inversely proportional to the square root of the molecular weight. This process is illustrated pictorially in Figure 1.3 below.

The majority of collisions are with the pore wall (as opposed to other gas molecules). These interactions with the pore walls cause the flow speed to be inversely proportional to the square root of the molecular weight, and therefore dependent on the gas species.

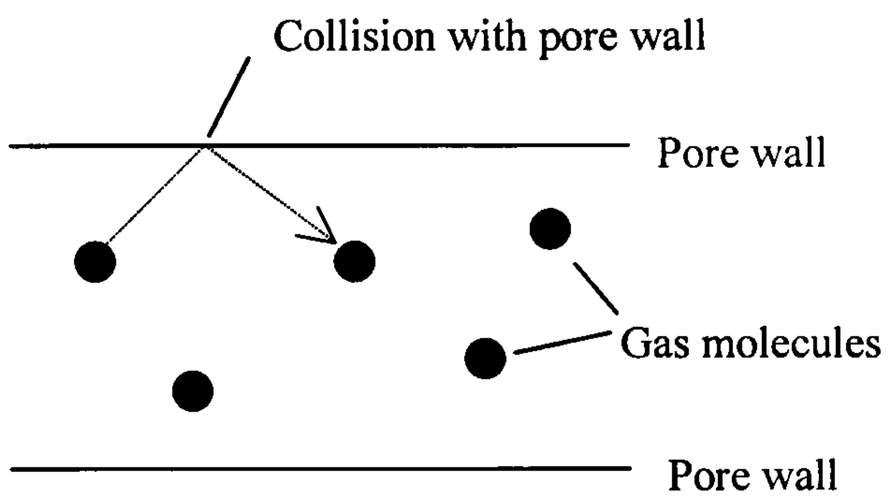

Figure 1.3 - Representation of Knudsen Diffusion (pore size 2-60 nm).

Within this mass-transport regime, a 50:50 molar mix of feed gas will have a separation factor that is equal to the square root of the ratio of the molecular weights of each gas species. (But only when the low-pressure side is a vacuum – otherwise the separation factor will be slightly lower if a pressure is maintained in the low-pressure side instead of a vacuum).

The mean pore size of most ceramic membranes is sufficiently small to permit separation via Knudsen diffusion. In multi-layered membrane structures (including the support substrate), the pore size of the thin separation layer usually falls within the Knudsen diffusion regime that provides separation, whilst the mean pore size of the supporting layers are much larger and flow occurs according to viscous flow.

The derivation of the relationship describing Knudsen diffusion is given in Equation 1.2 to 1.4 below [14]. These Equations are expressed as permeance Q, which is a measure of a membrane's permeability per unit thickness. ε_p and τ are porosity and tortuosity coefficients respectively. (Although attempts have been made to find a theoretical expression for τ it is highly material-specific. It is normally dealt with as an empirical correction factor between the results and the theoretical Knudsen diffusion value.) Elsewhere, v and r are the mean velocity and pore radii respectively, R is the universal gas constant and T is the thermodynamic temperature.

$$Q = \frac{2\varepsilon_p \bar{v} \bar{r}}{3RT\tau} \qquad \textbf{(1.2)}$$

but,

$$\bar{v} = \sqrt{\frac{8RT}{\pi M}} \qquad \textbf{(1.3)}$$

therefore,

$$Q = \frac{8\varepsilon_p \bar{r}}{3\tau\sqrt{2\pi RTM}} \qquad \textbf{(1.4)}$$

From inspection of eqns. 1.2 to 1.4 in can be seen that this particular mass-transport mechanism is independent of the transmembrane pressure difference. However, it is inversely proportional to the square root of temperature. In addition, the separation factor (α) for two species A and B can be represented by Equation 1.5 below:

$$\alpha_{\frac{A}{B}} = \sqrt{\frac{M_B}{M_A}} \qquad \textbf{(1.5)}$$

Separation of gases within the Knudsen regime has the limitation that only the lighter component can be preferentially removed. When the molecular weights of the components do not differ by a significant amount, an economical separation by Knudsen diffusion is not possible. This is certainly the case for a binary mixture of CO_2 and N_2 where the ideal Knudsen separation factor is just 0.8.

(Viscous flow can also be present in porous membranes if the transmembrane pressure difference is sufficiently high. However, as discussed in the previous section, viscous flow mass-transport does not result in the separation of a gaseous mixture).

1.3.2.3 Surface Diffusion

A gas molecule can chemisorb or physisorb onto the pore walls and migrate along the surface. The conditions that most favour the adsorption of molecules onto the surface of the pore walls are a sufficiently low temperature and/or a sufficiently high transmembrane pressure difference. When these adsorbed molecules are mobile, surface diffusion can occur. The degree of surface diffusion is determined largely by the fraction of the surface covered by an adsorbent monolayer of atoms and their subsequent mobility.

Several descriptions of surface diffusion have been proposed. The essence of all the theoretical models is that an adsorbed gas molecule will "sit" on a surface site until its fluctuating energy exceeds the activation energy E_d, allowing it to jump onto an adjacent vacant site. This process repeats until the gas molecule migrates through the membrane. This process is illustrated below in Figure 1.4.

Gas molecules adsorb on the surface and diffuse through the membrane along adsorption sites on the pore wall (i.e. the gas molecule 'hops' along the surface).

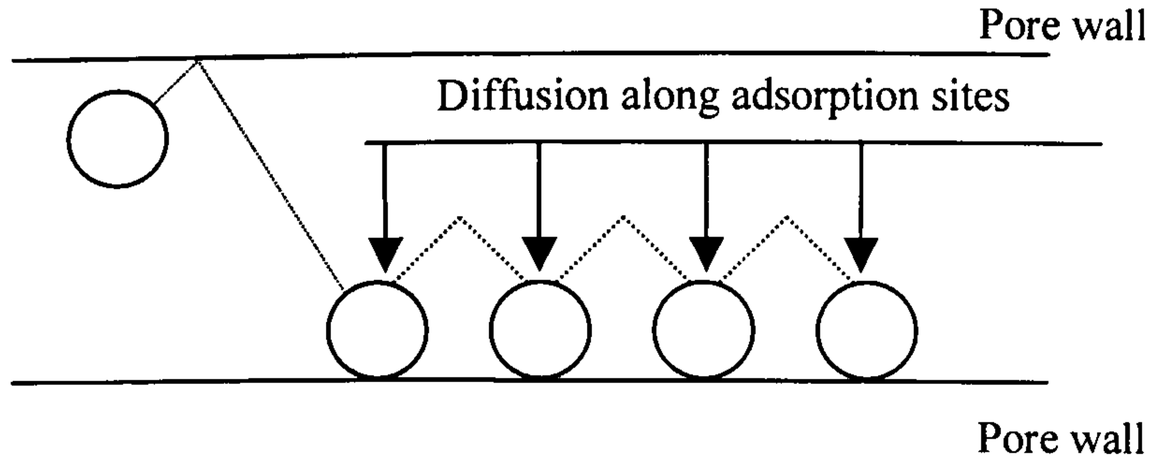

FIGURE 1.4 – Schematic of the surface diffusion process (pore size <2 nm).

The surface diffusion coefficient D is given by Equation (1.6) below [14]

$$D = \frac{\omega_E a^2}{2\pi} \exp^{-\frac{E_d}{kT}} \qquad \textbf{(1.6)}$$

(Where ω_E is the circular vibrational energy of an adsorbed atom and a is the lattice separation in the plane of the surface). This relation shows that the mass-transport due to surface diffusion should increase with temperature. However, in practice any increase in diffusivity is often negated by a corresponding decrease in surface concentration. Hence overall, the rate of mass-transport due to surface diffusion is generally observed to decrease with temperature.

Having attained the expression for the surface diffusion coefficient (D), Equation (1.6) permits the calculation of the permeability associated with surface diffusion (F_s) to be made. This relation is presented below in Equation (1.7):

$$F_s = \frac{2\varepsilon D}{r\tau A_O N_A} \frac{\partial\theta}{\partial p} \qquad \textbf{(1.7)}$$

(Where: ε and τ are the porosity and tortuosity coefficients respectively; θ is the fraction of coverage by the adsorbent as a monolayer on the available

surface; A_o is the surface area that a molecule occupies; N_A is Avogadro's number; p is the mean pressure and r is the pore radius).

From the above discussions, it is apparent that the surface diffusion mechanism effectively increases the permeability of the more readily adsorbed components in a gaseous feed mix. However, a consequence of this is that it also works antagonistically towards the other species by actually *reducing* their permeabilities. This is due to the decrease in the effective pore diameter that occurs when the entrance to the pore is occluded by the adsorbed species. It follows therefore, that this mechanism's two-fold way of increasing selectivity will have a greater influence for those membranes that possess the smaller pore sizes.

Whenever surface diffusion is active, its effect on selectivity always has to be considered. Usually the procedure to do this is to assume that the total flux through the membrane is the sum of the fluxes due to selective adsorption and Knudsen diffusion. One could even take this modelling one stage further and include the contribution from viscous flow. Therefore, by combining Equations (1.1, 1.2) and (1.7) we come to the combined expression of Equation (1.8) below:

$$F = F_K + F_P + F_S = \frac{2\varepsilon\overline{vr}}{3\tau RT} + \frac{\varepsilon r^2 \overline{p}}{8\eta\tau RT} + \frac{2\varepsilon D}{r\tau A_O N_A}\frac{\partial\theta}{\partial p} \qquad \textbf{(1.8)}$$

From inspection of Equation (1.8), several interesting aspects of mass transport through porous membranes become apparent:

- As the temperature increases, the relative strength and influence of the differing transport mechanisms changes. For example, gas molecules will desorb more easily from the surface, which will retard surface diffusion and allow Knudsen diffusion to dominate.

- In the absence of surface diffusion, the total permeability is a function of the mean transmembrane pressure difference.

Usually the presence of a surface diffusion component has to be established from empirical observations. Should the recorded permeability and separation factor(s) of a single species constituent of a feed gas stream be higher than those predicted by Knudsen-diffusion modelling, then the increase is normally indicative of surface diffusion.

Of all the gases examined in this thesis, CO_2 was always the most likely to possess a contribution of surface diffusion to permeance.

1.3.2.4 Capillary Condensation.

If one of the constituents of a multi-component gas is a condensable vapour and if the pores of the membrane are small enough, then the condensate can inhibit gaseous diffusion of other (non-condensable) species through the membrane (by clogging its pores). This condensate will then evaporate on the low partial-pressure side of the membrane. Hence, selective mass-transport of just one species of the original mixture is achieved.

For a narrow pore size distribution the Kelvin Equation [16] can be represented by Equations (1.9) and (1.9a) below. The first relationship describes the case where condensate collects as a film on the side of the pore wall and the second describes an actual droplet that has the same radius as the pore.

$$\frac{P}{P_0} = \exp\left(\frac{-2\gamma V_m \cos\theta}{r_p RT}\right) \qquad \textbf{(1.9)}$$

$$\frac{P}{P_0} = \exp\left(\frac{-2\gamma V_m}{r_p RT}\right) \qquad \textbf{(1.9a)}$$

(Where P is the vapour pressure of a droplet of radius r, r_p is the radius of the pore, γ is the surface tension of the condensed fluid, V_m its molar volume, T is absolute temperature, R is the universal gas constant, and P_o is the condensation vapour pressure in the bulk phase at the experimental temperature).

The Kelvin Equation represents thermodynamic equilibrium between gas and condensate in pores. It predicts that condensation will occur in small pores, *even when the partial pressure of the condensable vapour component is below its normal equilibrium vapour pressure (SVP).* As a result of capillary condensation, the pores of a membrane can completely fill with the condensed liquid. Therefore, if all the pores were filled then the fluxes of the gas species through the membrane would be very low and limited by their solubility in the condensable component.

Theoretically if the right feed mixture is used, then extremely high separation factors are possible. However, remembering the goal of this research, in the case of CO_2 and N_2, only the CO_2, with its slight solubility in water would be affected. However, the molar fraction of the feed gas that could be dissolved under the experimental conditions would be negligible.

1.3.2.5 Molecular Sieving

The majority of inorganic membranes currently in commercial use do not possess pore sizes that are small enough to selectively admit specific molecules in a gaseous mixture (and exclude others) based solely upon their kinetic diameters. Hence, the available separation factors from these membranes are intrinsically low.

However, the pore sizes of micro-porous materials are of molecular dimensions. In membranes that are synthesised from these materials, the smallest molecules of a gas mixture are the most likely to diffuse through the pore. Larger molecules will be almost totally excluded.

The concepts of gas transport discussed in the sections above concerned macro- and meso-porous materials. These descriptions however no longer apply in the micro-porous size regime. Essentially this is because the macroscopic models of surfaces do not apply upon such a small scale.

In the basic model, a membrane that is synthesised from a micro-porous material can be considered as being a three-dimensional, highly interconnected network of energetically identical (but totally independent) voids. This means that there are periodic constraints within a micro-porous membrane that are similar in size to that of the mobile gas molecule itself, Therefore, then the potential energy of the gas molecule varies with position.

The result is that the mobile gas molecule ceases to behave in a gaseous fashion according to the descriptions determining transport through macro- and meso-porous materials. In basic terms, the Lennard-Jones potentials vary as a function of distance across the pore surface and the potential barrier decreases with a reduction in the kinetic diameter of the gas species.

The ideal case in terms of gas selectivity would be where the pore diameter d_p lay between the two kinetic diameters of gas species A and B. (i.e. $A< d_p< B$). In such a situation, species B will be totally excluded and the separation factor will be theoretically infinite. This situation is represented pictorially in Figure 1.5 below.

Separation is based on size exclusion. Gas molecules with diameters larger than that of the pore cannot permeate.

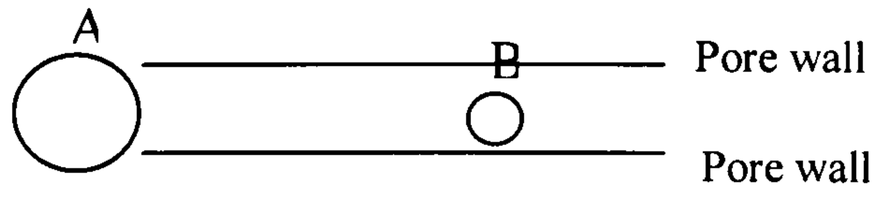

Only gas B can permeate.

Figure 1.5 - Schematic of ideal molecular sieving (pores of molecular size).

It has been observed empirically that the flux through a micro-porous membrane is a function of temperature according to the relationship presented below in Equation (1.10) [18]:

$$J \propto J_0 \exp \frac{-E_{act}}{RT} \qquad \textbf{(1.10)}$$

(Where E_{act} is assumed to be an apparent activation energy coefficient). Literature values for this activation energy range from ~2 to 40 kJ.mol^{-1} [18]. This energy is also pore size and gas species dependent. The activation energy for CO_2 is much lower than other gases such as N_2. So, although permeability increases with elevated temperatures, selectivity will be reduced.

There is also a "rule of thumb" for calculating a selectivity coefficient that estimates the degree of discrimination that a microporous membrane (of pore radius R) will show towards two molecules of differing size (r_A and r_B). Basically, this is that the separation factor between two species of differing kinetic diameters is such that the selectivity they experience is proportional to the relation in Equation (1.11):

$$Selectivity \propto \left(\frac{R - r_A}{R - r_B} \right) \qquad \textbf{(1.11)}$$

1.4 Design Considerations

The choice of membrane support substrate was a planar one, consisting of two strata. First, there was a macroporous sintered stainless steel base with a much finer titania overlayer on top. It is upon this titania layer that the active membrane would be deposited. (Full details are given in section 5.1.1). This particular material was chosen mainly because of its flatness and graded porosity and also because it was very suited to the membrane deposition process of spin-coating.

However, the aim of this thesis was to attempt the synthesis of a high-temperature inorganic membrane that might be suitable for industrial application. Hence, a discussion is presented here as to the possible reactor construction(s) that may result from of this type of research [19] [40] [41].

Koros and Flemming review the two main types of design are common in commercial applications of this sort: tubular and planar . Tubular arrangements are for the most part those membranes that are deposited upon the outside of a hollow porous support-tube. Feed gas is then passed through the hollow central axis of the tube and then permeates outwards through the walls. These "tubes" can even be very small-diameter hollow fibres employing the same principle. This general class of reactor has the advantage that the ratio of surface area to volume can be made very high indeed. (Neglecting a tubular close-packing coefficient, this ratio is proportional to 1/r). However, to obtain the maximum advantage from this asymptotic relation, the radius of the tubular membrane modules soon reaches the point where the mechanical rigidity of such inflexible inorganic materials can cause fracture problems.

In contrast, an arrangement of planar membrane modules (of constant thickness) has a fixed ratio of surface area to volume. These planar membrane

modules are easier to fabricate, implement on a large scale and are probably more appropriate for prototype plants.

Whatever arrangement is eventually chosen (i.e. tubular or planar), there would still be serious engineering issues to address if applying the type of membrane investigated within this thesis on an industrial scale. Some of the more influential factors are listed below:

1) **The construction of very thin, uniform, defect free layers of large area.** (This is difficult enough to accomplish under laboratory conditions with 25mm diameter specimens).
2) **The sealing of the membrane into a device that operates at high temperatures.** A sealing material must be used that is both capable of withstanding the aggressive thermal and chemical environment of an exhaust flue but also be capable of being matched to the thermal expansion coefficient of the composite membrane assembly. (Polymer-based sealing cannot be used at temperatures higher than 473 K).
3) **Extreme durability at temperature cycling.**
4) **The adherence of the deposited membrane layer to the substrate support under repetitive temperature cycling**.
5) **The use of large volumes of sweep gas might be required**. This introduces the problem of separation of the CO_2 filtrate from the sweep gas. Air cannot be used as it would defeat the point of separation of N_2 in the first instance. The use of other gases may actually turn out to be too expensive for commercial application. Steam could not be used, as it would turn what is supposedly a passive process in terms of energy consumption, into one that required additional cost (financial as well as energetic) to operate.
6) **The possible susceptibility of membranes to poisoning and fouling.** Fouling in a power-station exhaust flue would probably come from the intrusion into the pores by the fine carbon particulates of fossil fuel

combustion. Considering the high temperatures, the formation of coke could also be a problem.

7) **Quality control**. Measuring pore sizes on a laboratory scale is difficult enough, to do so on an industrial scale for a membrane of very large area would be a daunting prospect. One might not know if a module worked until it was actually installed and failure could be very expensive in terms of materials and time required to replace on a "trial and error" basis.

8) **A successful membrane**. Strangely enough, the decrease in pore size necessary for high separation factors might also result in such low permeabilities that actual use of the membranes would be uneconomical.

1.5 Membrane Synthesis

1.5.1 Overview

As mentioned previously, the primary aim of this research was to synthesise a thin-film membrane, which was capable of separating the components of a binary mixture of CO_2 and N_2 at a temperature around 700K.

Unfortunately, from a separation point of view, these two species have very similar kinetic diameters (3.681 Å and 3.996 Å for N_2 and CO_2 respectively) [20]. This small size difference, coupled with the required high operating temperature, imposes severe restrictions upon the choice of separation mechanism(s) and type of materials that can be used.

Only two practical separation mechanisms could apply under these conditions. They fall into two basic categories: those where the separation process is relatively insensitive to molecular weight and size and those which are processes where molecular weight and size are extremely important. Surface diffusion and physio-chemical attraction fall into this first category and processes such as Knudsen diffusion and molecular sieving fall into the latter.

Whatever separation process(es) are chosen, one design consideration remains paramount: that the required high thermal stability, durability and possibility of thermally regenerating "spent" membranes, necessitates that the material is based upon an inorganic backbone.

The sol-gel method is the chosen approach of this thesis to synthesise networks with such a backbone. The major advantage the sol-gel method in this respect is that its chemistry (section 1.5.2.2) is based upon the hydrolysis-condensation reactions of metal alkoxides. These reactions eventually result in inorganic metal-oxo polymers. Moreover, the use of organoalkoxide precursors allows non-hydrolysable organic ligands to be directly attached to the central metal atom. These organic groups enable carbon atoms to be incorporated into the inorganic backbone and have been shown to stimulate a surface-diffusion separation mechanism.

1.5.2 The Sol-Gel Process

1.5.2.1 Overview.

As mentioned previously, the method of synthesising and applying membranes relied upon the sol-gel production process [21]. This process is basically a wet-chemical technique used for the preparation of inorganic oxides, and involves the particle aggregation of colloids.

In essence, this process enables the production of glass and/or ceramics from liquids. A *sol* is a solution containing colloids; a *gel* is a structure whose (interconnected) elements are no more than a hundred nanometres across.

More fully, a *sol* is a dispersion of colloids in a liquid. If put into an aqueous solution, colloidal particles will never settle due to the action of Brownian

notion. The term *gel* describes a three-dimensional network with interspersed liquid. Polymeric sol-gels are in the sol state when the atomic clusters (dimers, trimers, and short chains) reach colloidal size. The nature and extent of this polymerisation process can be regulated and controlled by careful selection of the metal alkoxide precursors and the reaction conditions. The gel state is achieved when these dimers, trimers and short chains begin to form a three dimensional network.

Hence, sol-gel processing enables materials to be mixed on a molecular level to produce polymerised macromolecular networks, whilst still containing solvent. The molecular structure of the organometallic precursor, and subsequent pyrolysis conditions, control the composition of the ceramic material and its properties).

Once desiccated by a process of ageing and drying, the result is a solid (xerogel) with a very high level of very fine porosity. The consequence of having a solid with such an extremely high porosity is that it also has a high internal surface area. A high surface area also means a high surface energy. This high surface energy enables sintering to be accomplished at much lower temperatures than one would expect from conventional powder processing. (For example, silica is normally sintered at circa 1750°C - compared with approximately 1100 °C via the sol-gel route [22]).

To summarise the advantages of the sol gel process:-

- It can by-pass phase separation or crystallisation (non-equilibrium mixing) and it offers the opportunity of forming novel, metastable materials;
- It lends itself very well to the formation of thin films that are suitable for membrane synthesis via the processes of spin-coating (the preferred technique of this thesis see, chapter 2) and dip-coating;
- The property of low-temperature crystallisation and densification;

- It can accommodate the production of fibres and thin films without using powder technology.

The main disadvantage to the sol-gel process, which has been the biggest impediment so far to more widespread commercial application, is that it is prone to cracking during drying (see chapter 5). This makes monolithic manufacture difficult, slow and expensive.

1.5.2.2 Generic Sol-Gel Reactions

The generic sol-gel reaction[21] [22] has two basic stages: hydrolysis followed by condensation.

Metal alkoxides $M(OR)_n$ where *M* is the metal and *R* is the specific alkyl group, react readily with water and experience hydrolysis and subsequent polycondensation reactions to yield oxides or hydroxides. (The precise reaction product is dependent upon the nature of the precursors and the precise reaction conditions). This ready reactivity between alkoxide and water is the main appeal of sol-gel precursors.

A summary of the two stages of this generic reaction appears below in Equations (1.12) to (1.14).

1) Hydrolysis of organometallic precursor;

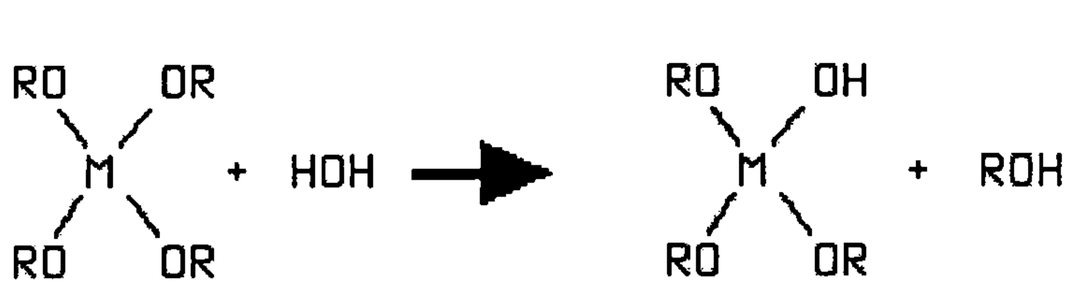

$$M(OR)_n + H_2O \rightarrow M(OR)_{n-1}OH + ROH \qquad \textbf{(1.12)}$$

2) Condensation (alcohol);

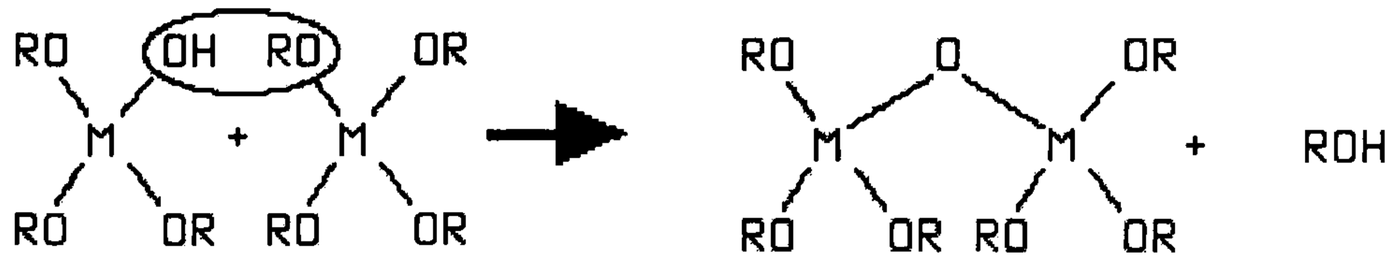

$$M(OR)_n + M(OR)_{n-1}OH \rightarrow (OR)_{n-1}MOM(OR)_{n-1} + ROH \qquad \textbf{(1.13)}$$

3) Condensation (water);

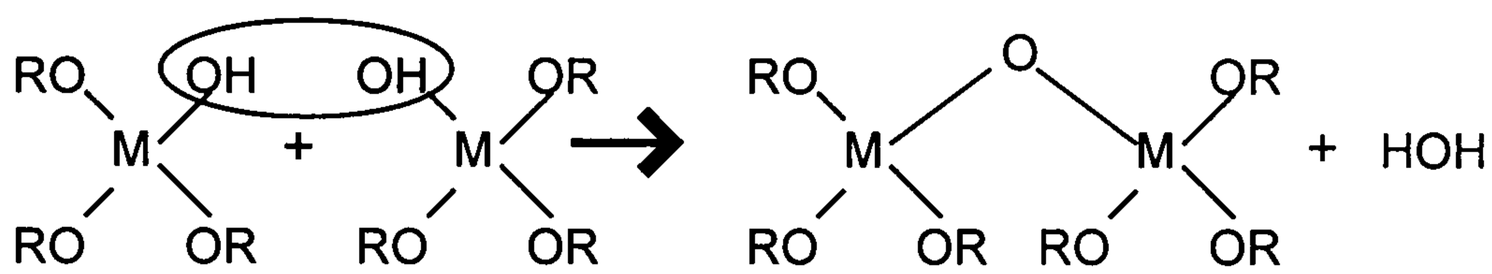

$$2M(OR)_{n-1}OH \rightarrow (OR)_{n-1}MOM(OR)_{n-1} + H_2O \qquad \textbf{(1.14)}$$

(Note: for Equations (1.12) to (1.14) above, *n* represents the valence of the metalloid *M*; and *R* is the alkyl group).

With increasing amounts of water, the monomers first group into dimers, trimers, and short chains. They then form long linear chains that then proceed to cross-link to form a coherent three-dimensional network, the basic model of which is illustrated in fig 1.6 below.

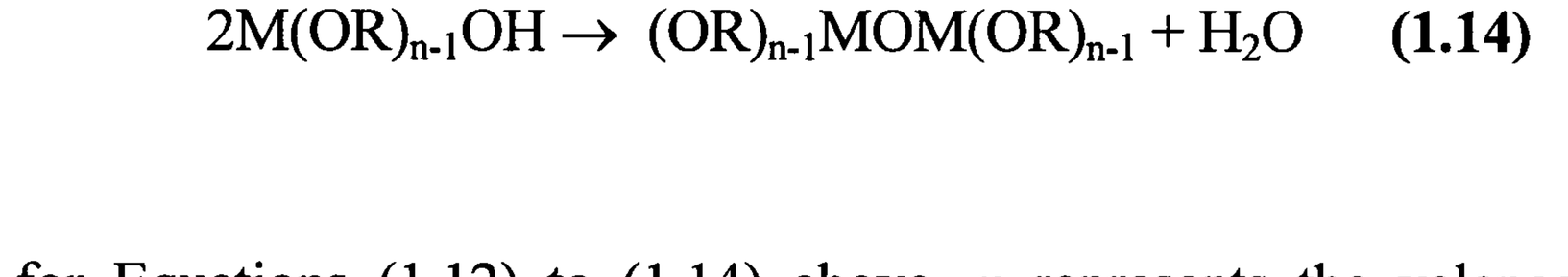

Figure 1.6 - Generic polymerisation mechanism

One caveat is that if reaction conditions are not maintained, then the processes detailed above are all reversible. Hydrolysis can switch to esterification and the condensation reactions can return to their starting points via alcoholysis and pyrolysis.

The hydrolysis reaction described by Equation (1.12) is an example of a partially hydrolysed system. Substituting Si as the metalloid, the reaction described by Equation (1.12) would have represented a reaction that had produced $Si(OR)_3(OH)$. The reaction might actually proceed until all the RO groups are substituted by OH groups. The extent to which substitution by OH groups occurs depends greatly upon the type choice of precursor; the hydrolysis ratio (i.e. molar ratio of water to alkoxide) and the choice (and concentration) of catalyst. The practical implementation of manipulating the initial hydrolysis reaction amounts to controlling the dilution of the alkoxides and water with alcohol.

1.5.2.3 Details of Generic Polymerisation Process

After the primary hydrolysis reaction has occurred, a series of condensation reactions will follow. These condensation reactions create secondary species that are susceptible to being linked by the action of bridging oxygens. The consequence is that eventually even larger molecules will appear as a result of polymerisation.

The nature and extent of condensation that arises depends upon the functionality of the precursor. This functionality is defined as the number of hydrolysable ligands attached to the metalloid precursor. Functionality normally ranges from f=1 to f=4. (Though functionalities greater than four are sometimes possible for metalloids that exhibit higher coordination such as Al, Zr and Ti). Monomers with a functionality of f=2 polymerise into rings or chains. Following gelation and drying, they do not form solids.

Monomers with a functionality greater than 2 form chains that may then be conjoined by cross-links. This results in the formation of a three-dimensional structure. It must be noted however, that reaction conditions have great influence upon the nature of the final structure(s). The key factors which affect the final polymerised structure are:

- The size of the initial clusters of dimers, trimers and short chains at the gel point and their concentration in solution;
- The pH and alkoxide concentration;
- Temperature and ageing time;
- Stresses that develop within the gel's pore-network during drying and solvent evaporation.

By being conscious of these various influences, it is possible to manipulate the reaction conditions and physical treatments to which the gel is exposed. Hence, one could, in principle, direct the growth of the polymer towards developing into either linear or cross-linked networks. Such control of polymer formation mainly takes the form of:-

- Care in the choice of precursor to select the size of alkoxide ligand;
- Choosing the appropriate catalyst and also its concentration (i.e. pH);
- Changing the hydrolysis ratio – i.e. the molar ratio of H_2O: *M*;
- Selection and molar ratio of the organic solvent.

1.5.2.4 Generic Sol-Gel Production Route

The generic sol-gel production route takes several slightly differing forms that depend upon what the desired end-product should be. For the sake of clarity, they are presented pictorially in Figure 1.7

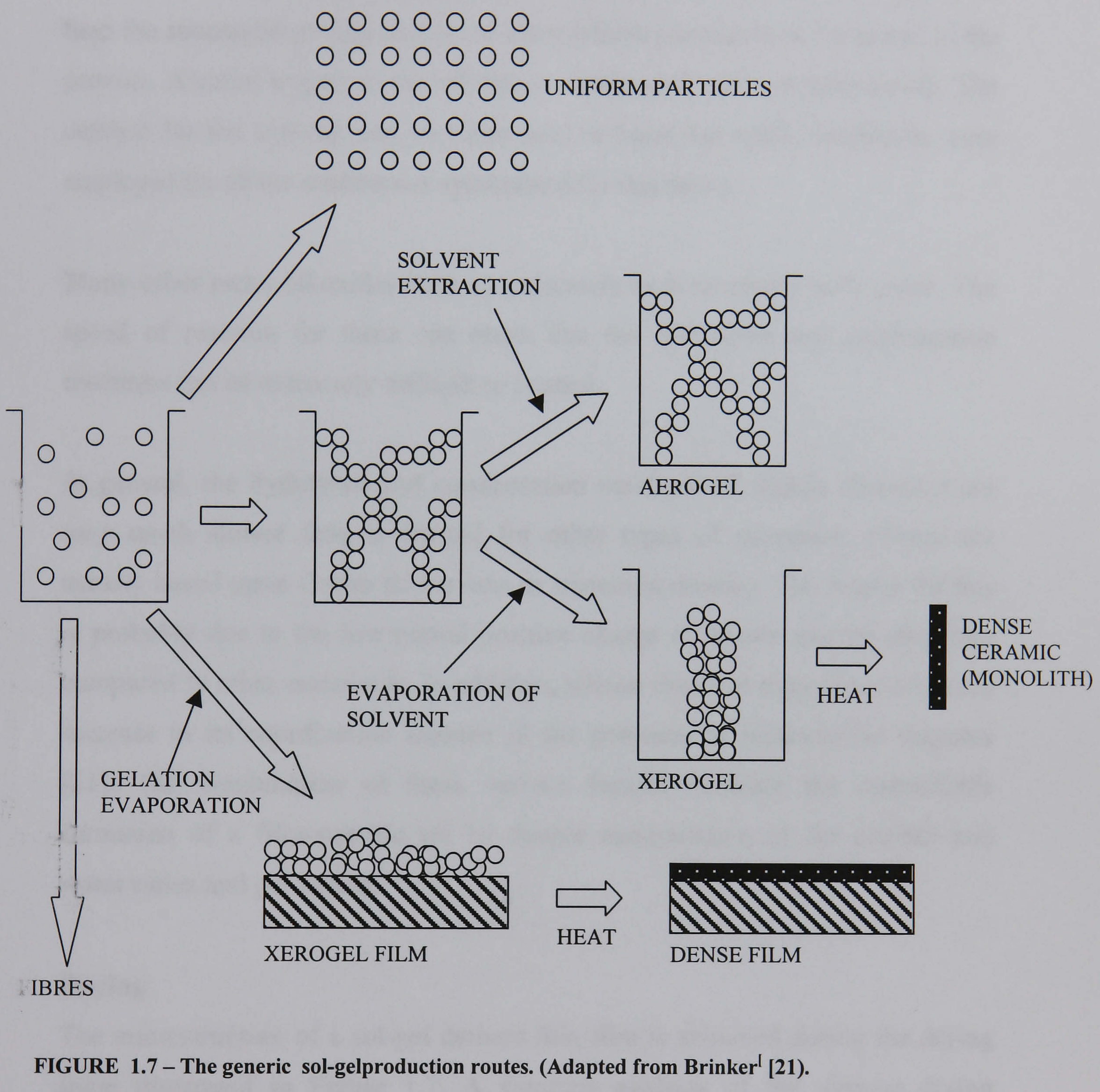

FIGURE 1.7 – The generic sol-gelproduction routes. (Adapted from Brinker[l] [21).

1.5.2.5 Silicon Alkoxide Based Sol-Gel Processes

As described by the generic description (section 1.5.2.4), the synthesis of silicate sol-gel systems proceeds via hydrolysis and condensation reactions. However, here the successful polymerisation of alkoxysilane precursors is the kernel of the process. Alcohol is used as the solvent as silanes and water are immiscible. The catalyst for the reaction can be either acid or basic but acidic conditions were employed for all the membranes synthesised for this thesis.

Many other metal alkoxides have an extremely high reactivity with water. The speed of reaction for these can mean that the hydrolysis and condensation reactions can be extremely difficult to control.

In general, the hydrolysis and condensation reactions of silicon alkoxides are very much slower than is normal for other types of precursor. (These are usually based upon Group III systems or transition metals). The reason for this is probably due to the low partial positive charge of silicon and its alkoxides compared to other metalloids. In addition, silicon does not experience a sudden increase in its coordination number in the presence of nucleophilic reagents [21]. The combination of these various factors facilitate the controllable formation of a film-suitable sol by simple manipulation of the alcohol and water ratios and pH values.

Drying

The microstructure of a sol-gel derived thin film is achieved during the drying stage illustrated in Figure 1.7. A rigorous analysis of the various drying processes for silica sols has been performed by Scherer [10] [23] [24] [25]. Most importantly, one paper [23] examines the effect of a gel layer upon a rigid substrate. However, not only must the drying process be suitable for the formation of the appropriately dense microstructure, it must also be consistent

with the pyrolysis regime devised for the removal of the template molecule for that particular sol system.

1.5.2.6 Pre-Requisites for Sols Intended for Thin-Film Formation

The basic purpose of the sols so far discussed is to be deposited onto a porous substrate as a thin-film and then transformed into a separation membrane. Hence, theses sols must satisfy certain physical and chemical requirements [26]. A more precise understanding of these stages improve the prospect of successfully synthesising a sol that is suitable for thin-film formation. These specifications, and how they might be met, are discussed in detail below.

Choice of Silane

The size of the alkoxy ligand always has an impact upon reaction rates. This is because the larger organic groups can give rise to greater steric obstruction of mobility and are therefore less reactive than smaller alkoxy ligands.

Hydrolysis Ratio (*r*)

The hydrolysis ratio is critical in influencing the evolution of the sol's structure. With acid-catalysed reactions, low values of *r* result in polymeric sols and high values of *r* in combination with base catalysts result in the creation of particulate sols. In between these two extremes, there is a whole spectrum of possible intermediate structures that are formed by altering the values and relative proportions of these two variables.

Solvent

Hydrolysis and condensation of the silane uses alcohol as the solvent, as silanes and water are immiscible. However, alcohol itself can also affect the progression of the polymerisation process. Inspection of Equations (1.12) and (1.13) indicate that excess alcohol can shift the chemical equilibrium of the sol so that the hydrolysis and alcohol condensation reactions will reverse. In addition, excess

alcohol might also dilute concentration of the reactants to such an extent that these reactions will be significantly slowed.

From the point of view of applying the sol as a thin film, the alcohol ratio has another effect as it will control the viscosity of the sol and hence its susceptibility to centrifugal spreading during the spin coating procedure. Porosity of the final film is greatly influenced by the drying process, which in turn is dictated in large part by the vapour pressure of the solvent. (The rate of evaporation is one of the main factors responsible for inducing the capillary stresses that arise during the drying process).

Hydrolysis and Condensation Reactions and Resultant Polymer Network

The sols should be capable of forming thin uniform layers with thicknesses of the order of one micron or less. These films should also be based upon structures that are capable of withstanding the capillary stresses that arise during drying. This requirement is satisfied if weakly branched short-range polymer containing sols are used.

The formation of these types of network is thought to result from a monomer clustering process [21]. The supposition is that monomers form clusters by randomly colliding with each other. Spatially separated clusters then eventually meet and condense with each other. Upon collision, these clusters either permanently join at their point of contact (diffusion limited), or only have a probability of adhesion (chemically limited).

As mentioned previously, hydrolysis and condensation reactions direct what form the final structures takes. All the sols in this thesis were based upon acid-catalysed reactions.

Hydrolysis reaction

With an acid catalyst, the hydrolysis reaction proceeds via the electrophilic action of the hydrogen ion upon the oxygen of the alkyl group. The next stage in the process is the nucleophilic action of the water's oxygen atom upon the silicon atom. This process determines the hydrolysis reaction's overall speed .

Condensation Reaction

The condensation reaction's rate can be minimised by consideration of the cluster-cluster model discussed above. It follows that if the rate of the condensation reaction is a function of the probability that these clusters irreversibly stick together upon contact, then reducing this probability should slow down the condensation reaction rate.

This is accomplished by bringing the solution as close as possible to the isoelectric point. For silica, this point is reached when the acidic conditions of the sol are equal to pH 2. More acidic conditions than this result in the deprotonation of the silanol group and becoming more alkaline results in the protonation of the group. There is enormous practical difficulty applying this rationale in an attempt to experimentally fine-tune the condensation reaction rate. This is that the pH of a sol is in a gradual state of flux and this causes the system to become more acidic as the condensation reaction proceeds.

1.5.3 Ormosils

"Ormosils" is the acronym for Organically Modified Silicates and the variety that is pertinent to this thesis describes a system where the organic component of the precursor becomes covalently bonded to the central silicon atom.

Ormosils are essentially an inorganic-organic hybrid whose principles and brief discussion as a possible class of membrane material are presented by Schmidt and Wolter [27]. In principle, ormosils should combine the large free volumes of organic polymers with rigid networks of inorganic structures. The large molecular framework of these materials possess a large molecular framework should permit permselectivity as a result of a difference in the diffusion constants of each component of a binary gas mixture.

Naturally, there is an enormous variety of organic components that it is possible to use for this modification and they have two distinct functions: to assist in the formation of certain networks and/or to modify certain networks.

The network modifiers are stable pendant ligands. They experience neither polymerisation nor hydrolysis. They exert their influence upon the structure in several ways. Most significantly, they can increase the rate of the hydrolysis and condensation reactions. In addition they have can control the extent of polymerisation of the sol which in turn affects the sol's suitability to be deposited as thin film.

The network formers are organic groups that do undergo polymerisation. Their polymerisation can occur at the same time as inorganic polymerisation process, or alternatively happen after the inorganic polymerisation process has run its course. The result of their action is the formation of inter-penetrating networks (IPNs). Research upon the applicability of IPNs as gas separation membranes has previously been the subject of research at this institution [2]

5.4 Template Membranes

Overview

The goal of this thesis was to synthesise porous inorganic membranes with well-defined porous morphologies and pore chemistries. As mentioned previously, the approach taken was to employ the "templating" concept within their manufacture. This technique aims to produce an inorganic network around an organic template. The removal of the template via pyrolysis creates a void within the structure of controllable size, shape and chemistry [25].

Use of the sol-gel process enables the synthesis of a hybrid organic/inorganic material. Such a material can then be converted to a *porous* ceramic by the total (or partial) removal of the template from the inorganic matrix to form an interconnected network of pores.

The resulting structure is then used as a membrane in CO_2/N_2 gas separation ...rials. (More specifically, micropores are produced by the thermally induced removal of organic ligands (i.e. templates), which normally are covalently attached to the silica network).

The bonding mechanisms of a particular template within a particular inorganic matrix can be complex. For example, there are surfactant templated silicas where the template-matrix interaction is via a non-covalent bonding mechanism and the pore structure is established in the solution stage. (Membranes can also be applied via chemical vapour deposition (CVD) [32] and templating molecules removed ...y solvent [33]). Alternatively, there are silicas that are templated by organic ligands covalently bonded to the siloxane network, where the subsequent processing strongly influences the final pore structure. The experimental work that is reported upon in this thesis (chapter 5) involves this latter type.

For the particular application of producing membranes for CO_2/N_2 separation, the basic principle involved taking a multi-component sol that was prepared via the sol-gel polymerisation route. The next stage is to physically remove varying sizes of organic molecules from the structure via pyrolysis in an attempt to obtain porosity. A brief schematic of this procedure is illustrated below in Figure 1.8

The rationale for adopting this technique as a suitable method for the production of ceramic membranes is straightforward. It was desired to synthesise a membrane to separate binary-gas mixtures. In order to accomplish this, it is necessary that such a membrane have pore sizes in the micro-porous region necessary (i.e. pore size of the order of two nanometres or less). In principle, the templating process should be an appropriate choice of manufacturing technique as it satisfies the following basic requirements:

- The size and shape of pores produced in the membrane should be determined by the size and shape of the organic templates.
- Ideally, components can be burnt out selectively in order to control porosity selectively. Having removed the desired groups, the temperature is not taken any higher.
- The porosity/total pore volume should be determined by the molar ratio of the inorganic precursor to the template precursor.

In order to discover the temperature required to remove the desired ligand(s), the thermal stability and structural evolution with temperature of these materials is characterised using conventional thermal analytical techniques such as TGA, DTA. Supplemental examination of a membrane specimen to yield more detailed structural information is accomplished by employing such techniques as FTIR, ^{13}C CP MAS NMR and ^{29}Si MAS NMR techniques (Chapter 4).

The possible candidates for use as template materials were selected from a group of multi-component silicon oxycarbide glasses that were derived from metal alkoxide precursors. These materials were chosen because it seemed likely that the loss of any organic groups due to combustion would probably tend to leave behind a structure with smaller average pore size that should be distributed uniformly over the gel network.

When a differential thermal analysis was performed upon these materials, it was observed that long before the glass transition temperature is reached, there could be several endotherms occurring at much lower temperatures. These are indicative of the burning off of chemical groups, and their absence causes voids to be left in the structure.

The consequence of this is that components can be burnt out selectively in order to control porosity selectively. Having removed the desired groups, the temperature is not taken any higher - and so there is no actual transformation into a glass.

Literature Survey

A comprehensive review of this subject is presented by Raman *et al* [28]. Loy *et al* in 1990 [34], were probably the first to describe the templating process of removing organic ligands via pyrolysis. Brinker *et al* [1] [12] [28] [30] [31], have published several papers describing what is basically the same technique as described previously within this thesis for their membrane production. In fact, the basic technique in the key paper of Raman and Brinker [1] was the initial starting point from which all of the research within this thesis evolved. They describe how an organic template approach, using sol-gel processing, is employed to synthesise microporous amorphous silica. They also report upon a finished membrane with a narrow pore size distribution comparable to that of the zeolite ZSM -5 (i.e. less than or equal to 0.5 nm).

The procedure reported upon [1] describes silica templated by organic ligands that are covalently bonded to the siloxane network. The subsequent thermal processing and pyrolysis is the essential factor influencing final pore structure in terms of size and distribution.

The chemical precursors used in one approach at membrane synthesis by Raman and Brinker [1] were methyltriethoxysilane (MTES) and tetraethoxysilane (TEOS), 3-methacryloxypropylsilane (MPS). Each molecule of MPS contains one non-hydrolysable ligand. This ligand, $H_2C{=}C(CH_3)CO_2(CH2)_3$, was considered to be the template molecule. Thus, the size and shape of the pore should be determined by the size and shape of this ligand (template). The thermal removal of these template molecules was accomplished by heating to 623 K and holding at this temperature for three hours. These MTES/TEOS derived membranes were reported as having a CO_2/CH_4 selectivity of 71.5 and the reported permeance of CO_2 was 6.8×10^{-7} mol m^{-2} s^{-1} Pa^{-1}. (Kukasabe *et al* [35] report having synthesised similar membranes with long chain alkyl ligands acting as the templates with similar results to Brinker *et al* [1] [30]).

Another combination employed by Lu and Cao *et al* [31], used methyltriethoxysilane (MTES) and TEOS. The authors' conclusion is that their observation of permselectivity results from a pore size of the order of 5Å.

In one paper [1] Brinker *et al* report upon the separating power of their synthesised membranes. (That is, the relative molar ratio of two gases with respect to each other after undergoing filtration - assuming an equal 1:1 feed mixture).

However, this was rather ambiguous as to whether or not an actual binary mixture of gases was passed through the test membrane, and the volume fraction of each separate component of the final filtrate measured *in situ* - or whether permeance measurements of individual gas of separate species were performed sequentially

and separation factors of various mixture being inferred rather than actually measured. A later paper by the same authors [30] was more precise: separation factors for various mixtures were idealised calculations based upon the flow of a series of individual gases

Single-gas permeation results cannot reliably be used to infer separation factors for gas mixtures. At most, they are merely indicative of the probable behaviour of a gaseous mixture. This is because the gas permeation behaviour of a mixture is often different from single gases due to several causes [36] [37] [38] [39] and vary according to which particular transport mechanism dominates. Common causes for variation in the permeation behaviour of single gases and mixtures are the transmembrane pressure; concentration polarisation of one species and single file permeation in micro-pores (<2 nm). For this latter, the slowest moving species partially blocks the membrane pores by larger molecules. This can impede the progress, and reduce the permeance, of the smaller molecular species.

Specific Template Membrane Systems of this Thesis

The main thrust of investigation was originally centred upon three different organic ligands: methyl, ethyl and phenyl. However, the ethyl ligand was found unsuitable for separating binary gaseous mixtures at temperatures circa 700K due to its lower pyrolysis temperature. A schematic of the key stages of the templating process appears below in Figure 1.8.

Two main classes of system were chosen: borosilicate and non-borosilicate sols. The main qualitative difference between these two systems was that the non-borosilicate sols (each with a different organic ligand) were synthesised from the co-polymerisation of two separate silanes. The borosilicate systems were the result of mixing a boron-containing precursor with a variety of single silanes.

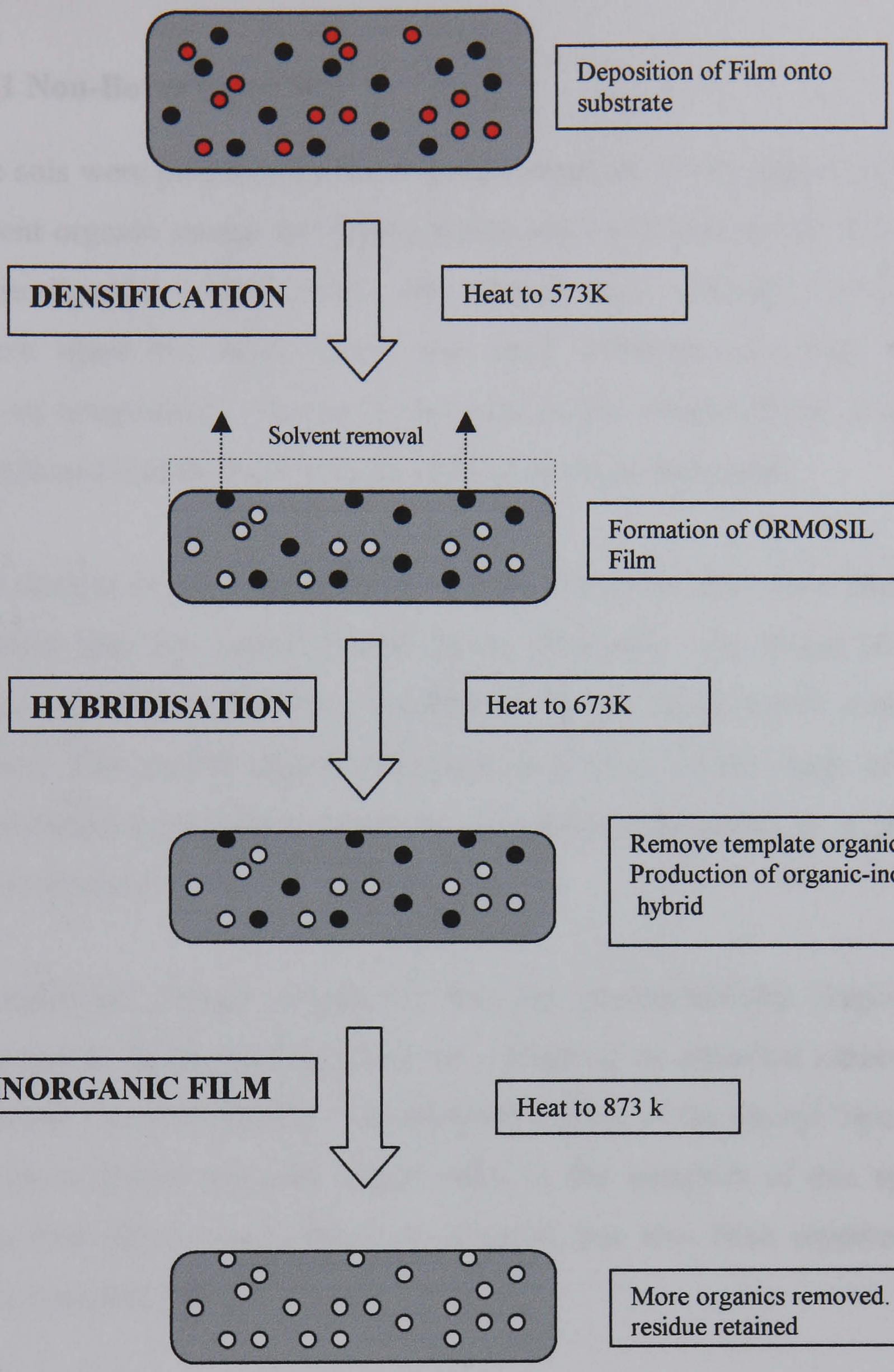

FIGURE 1.8 – Schematic of the four main stages of templating process

1.5.4.1 Non-Borosilicate Sols

These sols were prepared by the co-polymerisation of two separate silanes with different organic groups in varying molar and hydrolysis ratios. Three separate organic ligands; methyl, ethyl and phenyl were initially investigated but research upon the ethyl ligand was soon discontinued owing to its low pyrolysis temperature. Hence, it was only various combinations of methyl and phenyl based silanes that the focus of this line of investigation.

In the context of the templating philosophy, these systems were designed with the intent that the phenyl ligand (being thermally very stable [42]) should remain attached to the silica backbone and be incorporated into the final structure. The methyl ligand, being lost at a much earlier stage of pyrolysis, was intended to provide porosity by generating micropores as a result of its thermal removal.

(An additional benefit would be that the permselectivity displayed by a membrane in favour of CO_2 could be a result of its chemical attraction to the membrane's pore walls [43]. The reported affinity of the phenyl ligand towards the CO_2 molecule [43][44] might assist in the transport of this species. A similar (though weaker) chemical attraction has also been reported between CO_2 and methyl [45]).

1.5.4.2 Borosilicate Sols

These sols were synthesised in a different fashion to the non-borosilicate sols. The essential difference was that they only employed a single silane in their manufacture. This was accomplished by the mixing of a boron containing precursor -either trimethylborate (TMB) or phenylboronic acid (PBA) - in varying molar ratios with a single ethyl, methyl or phenyl based silane.

Borosilicate systems were thought to merit particular attention because of the advantages they could offer in network formation [46] [47]. Being trivalent, the

maximum functionality that boron can introduce into a system is three – which is appropriate for gels whose functionality is two to three. This also contrasts with the usual tetra-functional precursors that are normally used to dilute organo-silica systems.

One could also expect to see a greater collapse of the final gel network due to the fact that borosiloxane linkages (=B-O-Si≡) are readily severed by hydrolysis [48] [49] [50]. The appeal of this effect from the point of view of membrane manufacture is that these borosiloxane linkages can only be incorporated into the network when water is removed during heating. Delaying the incorporation of these linkages until very late on in the membrane synthesis procedure reduces the oligomeric growth of the precursor and results in a denser film.

The intrinsic disadvantage of a borosilicate system is that the borosiloxane bond itself can become unstable and form precipitates such as boric acid ($B(OH)_3$) which only has =B-OH- or =B-O-B= arrangements [51] and will therefore play no part in network formation. In addition, the sols reported upon in this thesis were catalysed under acidic conditions to a pH value 2. This behaves antagonistically against the polymerisation rate of borosilicate sols which proceed more slowly with pH values less than 4 . This is due to the OH group being too weak a nucleophile to display any significant affinity for other boric acid molecules. Another possible disadvantage with borosilicate systems is phase separation.

References

[1] Raman, N.K; Brinker, C. J. Organic "template" approach to molecular sieving silica membranes, Journal of membrane Science, 105 (1995) 273-275.

[2] Hensema, E.R. "Gas Separation Membranes", Advanced Materials, **6** (1994) p269-279.

[3] Bjorkert, U.S , "High Temperature CO_2 Permselective Planar Membranes" Ph. D. Thesis (1999), Centre for Advanced Materials, Dept. of Physics, University of Warwick.

[4] Falconer, J.L; Noble, R.D ; Sperry, D.P (1995). "Membrane Separations Technology. Principles and Applications" (Ed. R.D. Noble, S.A. Stern) - Elsevier Science B.V., Chapter 14

[5] Fain, D.E., "Technical and Economic aspects and Prospects for Gas Separation with Inorganic Membranes", Key Engineering Materials Vols. **61 & 62** (1991) 327-336.

[6] Uhlhorn, R.J.R., Huis In'T Veld, M.H.B.J., Keizer, K., Burggraaf, A.J., "High Permselectivity of Miroporous Silica-Modified γ-Alumina Membranes", Journal of Material. Science. Letters, **8** (1989) 1135-1138.

[7] Kitao, S. & Asaeda, M., "Gas Separation Performance of thin Porous Silica Membrane Prepared by Sol-Gel and CVD Methods", Key Engineering Materials, **61&62** (1991) 267-272.

[8] Kuraoka, K., Tanaka, H. & Yazawa, T., Highly Selective separation of CO_2 and He by Xerogel Coated Porous Glass Membrane, J. Mat. Sci. Let., **15** (1996) 1-3.

[9] Wu,J.C.S, Sabol, H, Smith, G.W., Flowers, D.L., Liu, P.K.T., "Characterisation of hydrogen-permselective microporous ceramic membranes", Journal of membrane Science 96 (1994) 275

[10] G. W. Scherer, "Effect of Drying on Properties of Silica Gel", Journal of Non-Crystalline Solids, **215** (1997) p155-168.

[11] Klein, L.C. & Woodman, R.H., Porous Silica by the Sol-Gel Process, Key Engineering Materials, **115** (1996) 109-124.

[12] C. J. Brinker, R. Sehgal, S. L. Hietala, R. Deshpande, D. M. Smith, D. Loy, C. S. Ashley, "Sol-Gel Strategies for Controlled Porosity Inorganic Materials", Journal of Membrane Science, **94** (1994) p85-102.

[13] Meixner, D.L; Dyer, P.N, "Characterisation of the transport properties of microporous inorganic membranes", Journal of Membrane Science, ,140 (1998) 81-95

[14] Walton, A.J., "Three Phases of Matter", Oxford University Press 2nd ed. 1992

[15] Uhlhorn, R.J.R., Keizer, K. and Burggraaf, A.J., Gas Transport and Separation with Ceramic Membranes: Part I, Multilayer Diffusion and Capillary Condensation, Journal of membrane Science, **66** (1992) 259-269.

[16] C. J. Brinker, "Sol-Gel Processing of Silica", The Colloidal Chemistry of Silica, **18** (1994) p361-402.

[17] A. B. Fuertes, T. A. Centeno, "Preparation of Supported Asymmetric Carbon Molecular Sieve Membranes", Journal of membrane Science, **144** (1998) p105-111.

[18] R. S. A. de Lange, K. Keizer, A. J. Burggraaf, "Analysis and Theory of Gas Transport in Microporous Sol-Gel Derived Ceramic Membranes", Journal of Membrane Science, **104** (1995) p81-100.

[19] W. J. Koros, G. K. Fleming, "Membrane-Based Gas Separation", Journal of Membrane Science, **83** (1993) p1-80.

[20] Kaye and Laby, "Tables of Physical Constants", Longman 15th Ed.

[21] C. J. Brinker, G. W. Scherer, "Sol-Gel Science – The Physics and Chemistry of Sol-Gel Processing", Academic Press, London, (1990).

[22] J. Zarzycki, "Past and Present of Sol-Gel Science and Technology", Journal of Sol-Gel Science and Technology, **8** (1997) p17-22.

[23] G. W. Scherer, "Thermal Expansion of a Gel Layer on a Rigid Substrate", Journal of Non-Crystalline Solids, **204** (1996) p118-124.

[24] G. W. Scherer, "Recent Progress in Drying of Gels", Journal of Non-Crystalline Solids, **147&148** (1992) p363-374.

[25] G. W. Scherer, "Cavitation During Drying of a Gel", Journal of Non-Crystalline Solids, **189** (1995) p197-211

[26] B. N. Nair, J. W. Elferink, K. Keizer, H. Verweij, "Preparation and Structure of Microporous Silica Membranes", Journal of Sol-Gel Science and Technology, **8** (1997) p471-475.

[27] Schmidt, H. & Wolter, H., "Organically Modified Ceramics and Their Applications", Journal of Non-Crystalline Solids, **121** (1990) 428-435.

[28] Brinker CJ, Raman NK, "Template Approaches to the Preparation of Amorphous Nanoporous Silicas", Chemistry of Materials, 1996, **8** 1682

[29] Brinker CJ, Yunfeng Lu, "Continuous formation of supported cubic and hexagonal mesoporous films by sol-gel dip-coating", Nature, **389** September 1997

[30] Cao, G.Z., Lu, Y.F., Delattre, L., Brinker, C.J. & Lopez, G.P., "Amorphous Silica Molecular Sieving Membranes by Sol-Gel Processing", Advanced . Materials., **8** (1996) 588

[31] Lu, Y., Cao, G.Z., Kale, R.P., Prabakar, S., Lopez, G.P. & Brinker, C.J., "Microporous Silica Prepared by Organic Templating: Relationship between the Molecular Template and Pore Structure", Chem. Mater., **11** (1999) 1223.

[32] Kodakari N, "Molecular Sieving Silica Overlayer on Tin Oxide Prepared Using an Organic Template", Journal of the Chemical Society - Chemical Communications 1995 **6** 623

[33] Malla, PB "Effect of Pore Size on The Chemical Removal Of Organic Template Molecules from Synthetic Molecular Sieves" Zeolites, vol 15, pp. 324-332 (1995)

[34] D. A. Loy, R. J. Buss, R. A. Assink, K. J. Shea, H. Oviatt, "Engineering of Porosity in Amorphous Materials. Plasma Oxidation of Hydrocarbon Templates in Polysilsesquioxanes", Materials Research Society Symposium Proceedings Vol. 346 - Better Ceramics through Chemistry VI, p825.

[35] K. Kusakabe, S. Sakamoto, T. Saie, S. Morooka, "Pore Structure of Silica Membranes formed by a Sol-Gel Technique using Tetraethoxysilane and Alkyltriethoxysilanes", Separation and Purification Technology, **16** (1999) p139-146.

[36] Asaeda, M., Tsuru, T., Manabe, T. & Hashimoto, H., "Porous Silica and Silica-Zirconia Membranes for Separation of Inorganic Gas Mixtures Including Carbon Dioxide", Proc. International Congress on Membranes and Membrane Processes, Yokohama, Japan, Aug. 1996

[37] Ohya, H., Sato, S., Ishii, A., Negishi, Y. & Matsumoto, K., "The Separation of Gaseous Mixtures With Composite Micropore Glass Membranes at High Temperature", International. Journal of Hydrogen Energy, **18** (1993) 475

[38] Arnost D., and P. Schneider, "Dynamic Transport of Multi-component Mixtures of Gases in Porous Solids," Journal of Chemical Engineering., **57** 91-99 (1995).

[39] K. Keizer,, R.J.R Uhlhorn, , Zaspalis & A.J. Burggraaf,, "Transport and Related (Gas and Vapour) Separation in Ceramic Membranes", Key Engineering Materials Vols **61** & **62**, 143-154, Trans Tech Publications

[40] Saracco G., G. F. Versteeg, and W. P. M. van Swaaij, "Current Hurdles to the Success of High-Temperature Membrane Reactors," Journal of membrane Science, **95** 105-123 (1994).

[41] Zaman J., and A. Chakma, "Inorganic Membrane Reactors," Journal of membrane Science, **92** 1-28 (1994).

[42] B. K. Sea, K. Kusakabe, S. Morooka, "Pore Size Control and Gas Permeation Kinetics of Silica Membranes by Pyrolysis of Phenyl-

Substituted Ethoxysilanes with Cross-Flow through a Porous Support Wall", Journal of Membrane Science, **130** (1997) p41-52.

[43] M. Shibata, "Porous Silica Modified by phenyltetraethoxysilane", Maku, **19** (1994) p332

[44] M. Smaïhi, T. Jermoumi, J. Marignan, R. D. Noble, "Organic-Inorganic Gas Separation Membranes: Preparation and Characterisation", Journal of membrane Science, **116** (1996) p211-220.

[45] T. Okui, Y. Saito, T. Okubo, M. Sadakata, "Gas Permeation of Porous Organic/Inorganic Hybrid Membranes", Journal of Sol-Gel Science and Technology, **5** (1995) p127-134.

[46] A. J. Ashworth, B. J. Brisdon, R. England, B. S. R. Reddy, I. Zafar, "The Permselectivity of polyorganosiloxanes", Journal of Membrane Science, **56** (1991) p217.

[47] G.D. Sorarau, F. Babonneau and C. Gervais, N. Dallabona, "Hybrid $RSiO_{1.5}$/ B_2O_3 Gels from Modified Silicon Alkoxides and Boric Acid." Journal of Sol-Gel science and Technology 18 (2000) p11

[48] L. C. Klein, N. Giszpenc, "Sol-Gel Processing for Gas Separation Membranes", Ceramic Bulletin, **69** (1990) p1821-1830

[49] A. D. Irwin, J. S. Holmgren, J. Jonas, "Solid State ^{29}Si and ^{11}B NMR Studies of Sol-Gel Derived Borosilicates", Journal of Non-Crystalline Solids, **101** (1988) p249.

[50] A. D. Irwin, J. S. Holmgren, T. W. Zerda, J. Jonas, "Spectroscopic Investigations of Borosiloxane Bond Formation in the Sol-Gel Process", Journal of Non-Crystalline Solids, **89** (1987) p191.

[51] K.H. Yang & A.J. Woo, "Solid State ^{1}H and ^{29}Si NMR Studies of Silicate and Borosilicate Gel to Glass Conversion", Bulletin of the Korean Chemical Society, **17** (1996) p696

[52] A. M. Wootton, Silicon Oxycarbide Glasses and Glass-Ceramics, PhD Thesis, University of Warwick, (1998).

Chapter 2

Experimental Techniques.

1. Material synthesis

As mentioned in chapter one, two general classes of material were investigated during the course of this research: non-borosilicate systems and borosilicate systems. As both these systems are sol-derived, their synthesis route was similar enough for a generic description to be presented below which could apply to either. This is represented by a schematic that appears in Figure 2.1 (Adapted from Brinker [1] [2]) All the precursors used in this thesis were of commercial grade AR and were supplied by either Aldrich Chemicals Ltd or Lancaster Chemicals Ltd.) .

Unless precursors have very similar hydrolysis rates, the usual approach is to partially hydrolyse the least reactive precursor before the addition of the second. Hence, as is shown in Figure 2.1, the less reactive precursor was always prepared first (mixed at various temperatures for varying amounts of time) prior to the combination with the second component.

The hydrolysis ratios of silane/precursor: H_2O for the non-borosilicate systems was initially varied between 2 and 4 but a standard ratio of 3 was later adopted. The hydrolysis ratio of the borosilicate systems was always maintained at 2.

The stirring stage for all the binary sols was always performed at approx. 313 K and after 5 to 20 minutes, whilst the sol was still liquid, the required volume

was decanted and bottled. It was then refrigerated for future use as membrane material. The remainder was stirred further at temperature until a sharp increase in viscosity was observed. This indicated the threshold of the gel stage. After a few more minutes this (by now very viscous) solution was poured into a petri dish and allowed to cool.

Gelation was normally observed after one hour and complete gelation within 24 hours. The gels were then covered and left to age at room temperature for one to three weeks to allow complete gelation and polymerisation to occur. These aged gels were then dried at 373 K for 3-4 days. These xerogels were then ground into powders for use in structural analysis examinations (chapter 4).

The preparation of the "second component" in Figure 2.1 was slightly different for each precursor.

The PBA precursor was prepared in a slightly more elaborate way than the other systems [3]. It was first dissolved in a minimum amount of methanol and then heated and stirred for approx. 20 minutes at 308 K. The water was not added at this stage but was previously initially included as a total water requirement for both precursors when the silane was prepared.

2.2 Membrane Production

In order to have a high throughput (i.e. high volume flow per unit surface area) *any* membrane must be made as thin as possible. This basic design criterion requires that, in order for a membrane to retain a reasonable degree of mechanical strength, it must be supported by a porous substrate.

All of the membranes investigated in this thesis are thin films deposited as a sol onto a flat porous support substrate. Therefore, this section will section will describe the coating procedure and the pre-treatment of substrates.

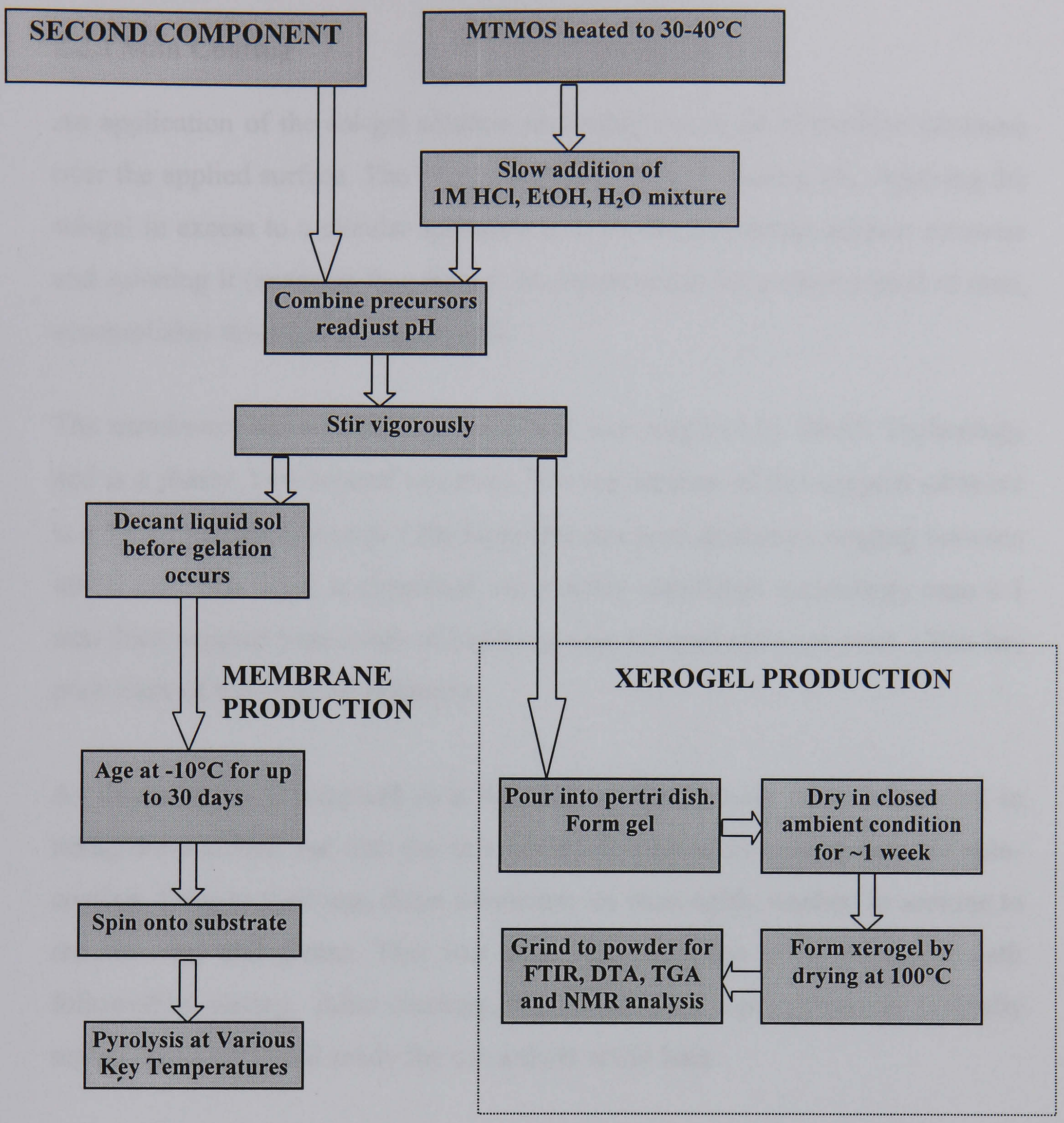

Second component:
PBA (Phenyl Boronic Acid); TMB (Trimethylborate); DPDMOS (Diphenyldimethoxysilane); PTMOS Phenyltrimethoxysilane.

FIGURE 2.1 - Generic Process of Membrane Production.

2.2.1 Spin Coating

An application of the sol-gel solution preferably has to be of uniform thickness over the applied surface. The chosen technique is spin-coating [4]. Applying the sol-gel in excess to a circular specimen of a porous membrane support substrate and spinning it (ensuring that there is no eccentricity) for a short period of time, accomplishes this objective quite well.

The membrane support substrate used here was supplied by IMAS Technology and is a planar, two-layered structure. The top stratum of this support substrate is a 15-20 μm thick porous TiO_2 layer that has pore diameters ranging between 40-50 nm. This layer is deposited via powder metallurgy technology onto a 1 mm thick support base made of highly porous sintered stainless steel. (This has pore sizes of the order of microns).

As this material is supplied as a flat sheet, it lends itself particularly well to being die-punched out into the thin one-inch wide discs appropriate for spin-coating. Prior to their use, these substrates are thoroughly washed in acetone to remove dust and grease. This was done via immersion in an ultrasonic bath followed by rinsing. After cleaning, these discs were kept in clean hermetically sealed containers until ready for use a short while later.

With a membrane applied onto such a substrate via spin-coating there is a continuous gradation of pore size before the feed gas enters the active separation layer.

The spin coater was purpose-built for this research. A schematic of its main features appears in Figure 2.2. The coated substrate is placed on top of a spindle. This spindle is a small-bore pipe that rotates. The substrate is held in place whilst spinning by the suction action a rotary pump evacuating the bore.

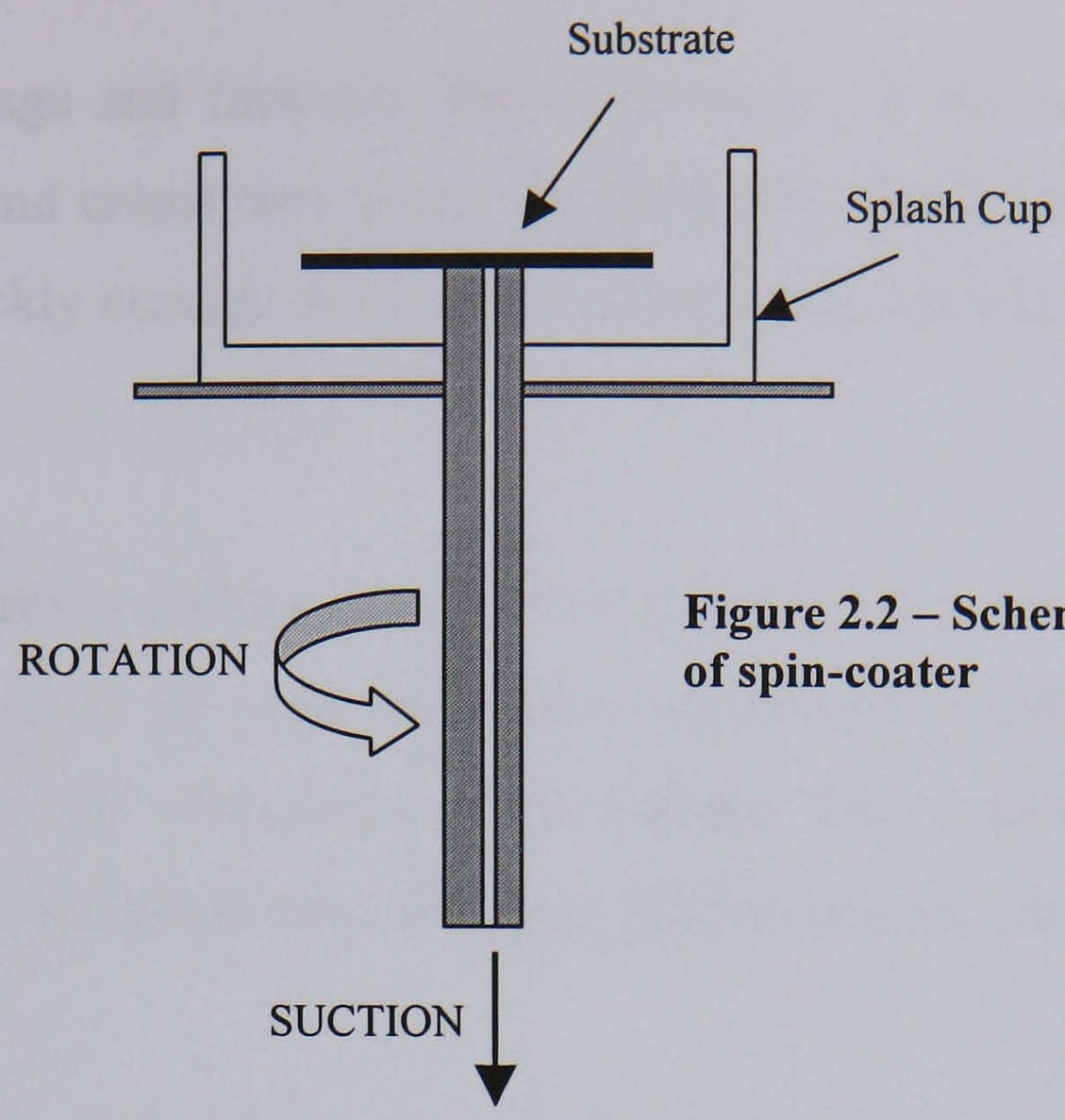

Figure 2.2 – Schematic of spin-coater

To minimise the chance of dust particulates etc. ruining the deposited film the spin-coating apparatus was located within a laminar flow cabinet. Typical spinning speeds were 2,500 to 3000 rpm and sustained for 20 to 30 seconds. Whilst spinning, a dark circular band concentric to the axis of rotation could be seen. It increased in diameter until eventually it got to such a size that it "dropped off" the edge of the substrate. This then meant that the sol had completely covered the substrate disk.

2.2.2 Densification

Once applied, the sol has to be dried and heat-treated. The right drying rate is crucial and has to be extremely slow, as rapid evaporation causes large capillary stresses (proportional to the drying rate) to develop and can cause cracking [1] [5]. However, there is a dilemma, as it is the faster drying rates that produce the desired smaller pore sizes - so a trade off has to be achieved. (This was found empirically by an exhaustive process of trial-and-error).

Heating causes shrinkage and increases the surface area of the membrane as components burn off and create new pores. Evolved gases build up in pressure and cannot escape quickly enough through the small pores, leading to eruptions and further cracking.

In addition to an increase in surface area due to the formation of new pores, the drying of the coating layer of such composite membranes actually causes a *volume reduction* due to the evaporation of the solvent. This volume reduction causes mechanical stresses, which can ultimately lead to defects, particularly for glassy polymers.

To get closest to the desired structure from both drying and heat treatment, the general approach is to heat the sample up very slowly from ambient temperature to the final heat-treatment temperature on a very slow ramp [1]. This was typically less than one degree per minute. A typical example of a spin-coated film that has been thermally converted to a membrane is shown in Figure 2.3. The result is a uniform layer of controllable thickness of the order of a micron or two.

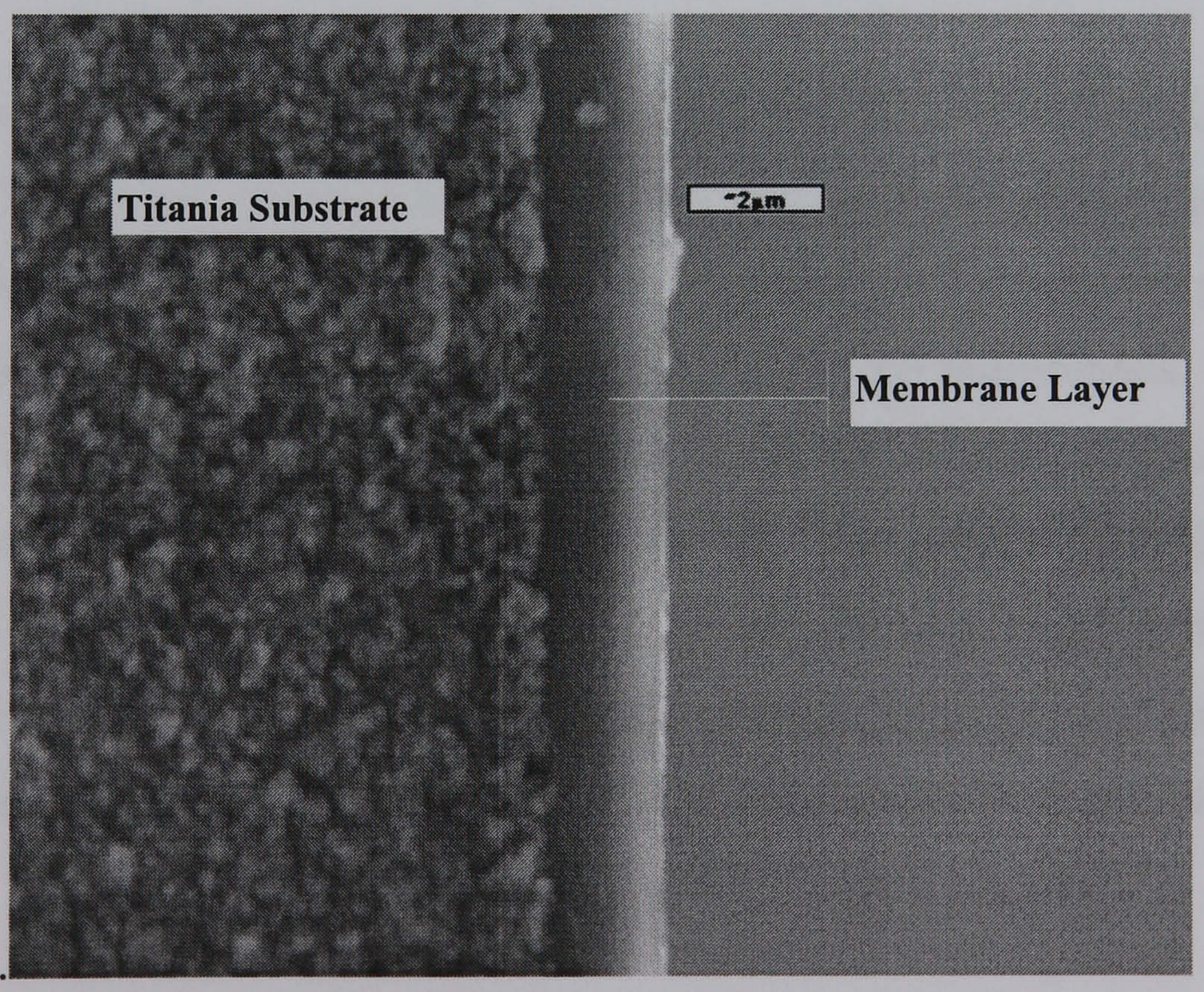

Figure 2.3 – Example of a spin-coated membrane deposited upon the stainless steel/titania substrate

2.2.2.1 Heating Regimes

Heating regimes were devised in accordance with the results of thermal analyses (section 4.4 of chapter 4). The common aim for all the systems was that densification should occur before the removal of template molecules. The main thermal processing domains are illustrated in Figure 2.4.

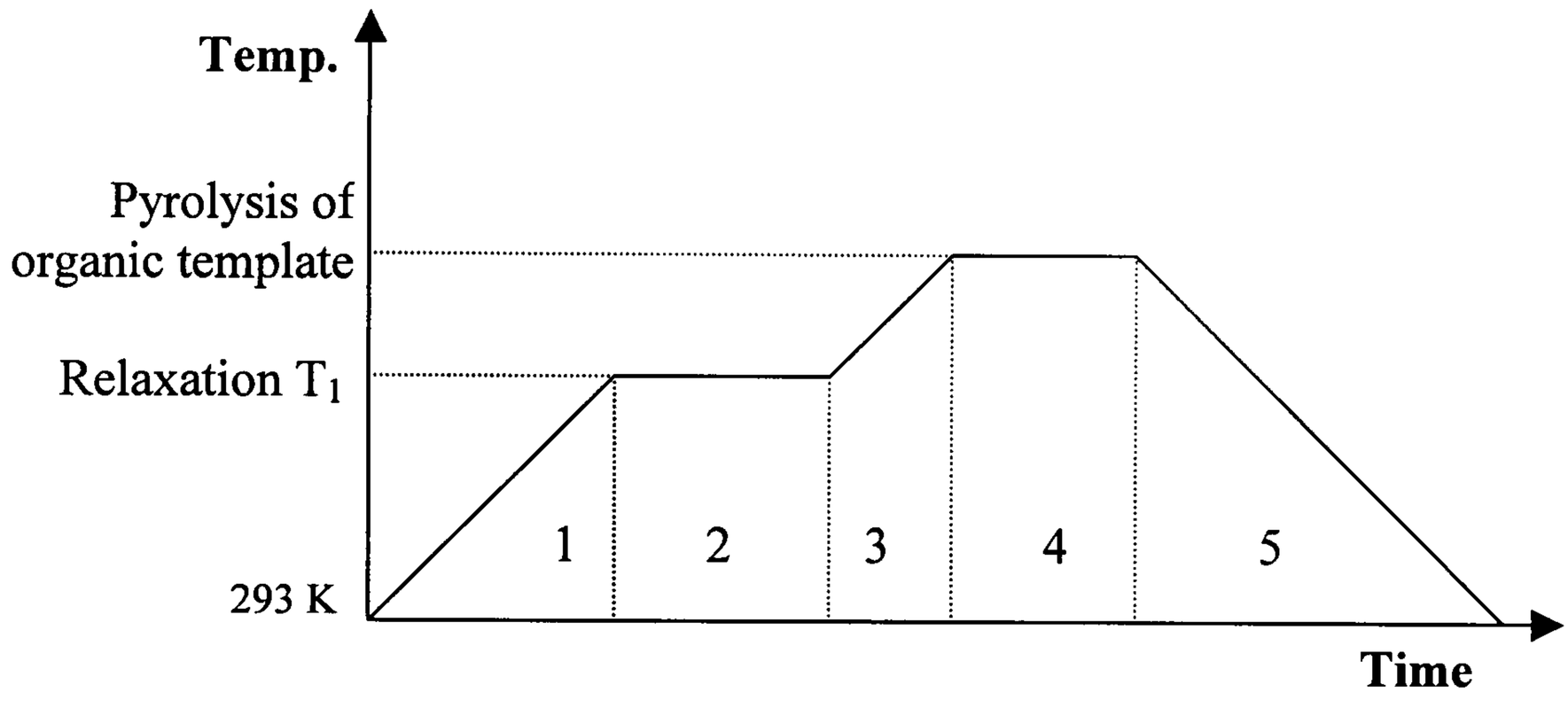

FIGURE 2.4 – Schematic of thermal processing procedure.

One caveat must be made. The results of DTA and TG analyses (section 4.4 of chapter 4) upon xerogel powders guided the design of the thermal processing route of the membranes. However, thermal analyses of the powders proceeded at a different rate than was actually the case for the membranes. It is also uncertain as to whether or not thin films of a sol deposited as a liquid, react in the same way to thermal environments as the xerogel powders derived from the same sol. If this is not the case, then the DTA and TG analyses of powders will not truly reflect the situation of a thin film undergoing pyrolysis. Instead, they may just be an approximation of the real circumstances and timing of chemical events.

The five main temperature-time domains that are shown in Figure 2.4 are a mixture of heating, isothermal and cooling regimes. The heating and cooling ramp rates for thermal regions (1), (3) and (5) were very slow (1 degree/min) to minimise mechanical stresses and network collapse within the film as discussed in section 2.2.2. The isothermal states (2) and (3) were typically maintained for four hours.

(An additional reason for using such a low ramp rate for heating and cooling was that fact that the substrate possessed thin sheet geometry. Being a part-metal laminated structure with strata of differing thermal expansion coefficients meant that sudden increases in temperature would cause the substrate to bend slightly. Any distortion of the substrate's surface (if even only on a small scale) could result in cracking of the deposited membrane).

Also tried, were heat treatments regimes that reached a temperature plateau at a level below the threshold-temperature necessary for organic template removal. However, results from these membranes were very inconsistent and not at all repeatable and the approach was soon discontinued.

The membrane deposition procedure was usually repeated at least once in order to obtain a structure with at least two active (stratified) layers. This was considered prudent, as it would repair any defects present in the first layer. Although great care was taken in the preparation of substrates and application of sols, it was considered possible that some contamination defects might still have occurred when depositing the first layer. The likeliest causes would be small-particulate contamination (dust etc.), microscopic air bubbles in the sol itself and surface irregularities of the support substrate.

From a practical point of view, the production schedule of membranes was handicapped by the long processing time required to obtain xerogels of the sols

that were to be used for membrane production. This meant that the waiting time for the thermal analyses data relevant to a particular sol to become available was measured in weeks. The most efficient use of time was to proceed with membrane production from the new sol anyway. The thermal regimes for a new sol had to be initially guided by previous results upon other similar systems. Then, when the proper data became available, the new sol's thermal processing route was then adjusted (if found necessary to do so).

2.3 Permeation Measurements

The permeation measurements taken from trials upon all of the membranes reported upon in this thesis were performed upon apparatus that was designed and built by this author. Details of its performance and construction (including a novel *in-situ* ultrasonic binary-gas analyser) are presented in chapter 3.

The flow of feed gas, retentate and permeate were all measured directly and the transducer outputs logged on a computer via an 11-bit A/D converter. The same was true for simultaneous pressure measurements on either side of the membrane. It was also part of the design that external gas analysis devices could be connected to feed gas, retentate or permeate. An external heating module around the membrane housing also permitted permeation trials at temperatures up to 400K to be performed.

2.3.1 Permeability Calculations

The molar throughput of gas through a test membrane was measured directly by the mass-flow meters (chapter 3).

The basic relationship between molar throughput (n) and permeability (F) is given by Equation (2.1)

$$n = AF\frac{\Delta p}{l} \qquad \textbf{(2.1)}$$

(Where A is the membrane's area, p is the transmembrane pressure difference and l is the thickness of the membrane).

However, it is very difficult, without destroying the membrane for SEM inspection of its cross-section, to say with any degree of certainty exactly what the membrane's thickness l actually is.

A more practical way of expressing a membrane's performance is to use the concept of *permeance (Q)*. This is the normalising of a membrane's permeability for unit thickness. Hence, Equation (2.1) becomes Equation (2.2) that only depends upon quantities that can be measured directly (i.e. n and A)

$$Q = \frac{F}{l} = \frac{n}{A} \qquad \textbf{(2.2)}$$

2.4 Thermal Analyses

Thermal analyses were performed upon the powders of ground xerogels that were derived from the same sols used for membrane synthesis.

Differential Thermal Analysis (DTA)

The specific apparatus used was a "Stanton Redcroft" SRDTA 673.4. Experiments were over the range from 283 K to 1100 K in oxygen and nitrogen atmospheres. Sample weights were typically of the order of 70 mg. Platinum crucibles were always used and a heating rate of 5K/min was standard. The reference material was quartz which always produced a small endotherm at 847 K (α -β quartz transition temperature).

The technique was employed to determine the temperatures where key structural events occurred within the membrane materials. The conventional report from a

DTA is represented as continuous trace of endothermic or exothermic chemical processes as a function of temperature.

Thermogravimetric Analysis (TG)

This is a complementary technique to DTA and its purpose is to report weight loss of a sample when exposed to a continuous variation in temperature. From a basic knowledge of the starting compounds it then possible to obtain empirical chemical formulae of the species that are lost at key temperatures.

The specific apparatus used was a "Stanton Redcroft" TG 750/770. Once again experiments were conducted over the temperature range of 283 K to 1100 K in oxygen and nitrogen atmospheres. Sample weights were typically of the order of 25mg and again platinum crucibles and again a heating rate of 5K/min were standard. Analysis was carried out on the powdered xerogel of each membrane material under both oxidising (air) and inert (N_2) atmospheres.

2.5 MAS NMR

MAS NMR of powdered xerogels were used to measure the development of the membrane materials with temperature. The NMR specimens were powders from various systems that were pyrolysed to what thermal analyses had indicated as being the key temperatures for those systems. The MAS NMR spectra obtained were specific to three separate nuclei: ^{13}C; ^{11}B and ^{29}Si.

The ^{13}C MAS NMR was used to track the behaviour of organic components of the precursors with temperature. The ^{29}Si MAS NMR was employed to reveal detail of the formation of the silica backbone within the polymerised networks as the temperature was increased. Finally, the ^{11}B MAS NMR was specific to the borosilicate systems and mainly provided an insight into the evolution of boron to oxygen bonds of the BO_3 and BO_4 species.

MAS NMR is the standard technique for the determining of nearest neighbour and next nearest neighbour species for a particular atomic nucleus [6]. This technique is an especially sensitive analytical tool for short-range amorphous materials. The basic report from NMR spectroscopy gives a spectral peak that corresponds with a specific generating site.

The basic principle of NMR is that those nuclei that have a magnetic moment associated with them will tend to become aligned in the presence of an external magnetic field. (i.e. those nuclei with a molecular spin number **I** >0) However, because nuclei possess angular momentum they precess about the direction of the applied field.

The energy of interaction between the applied field and the nuclear magnetic fields is quantised. Hence, only certain orientations (2**I** + 1) of the nucleus relative to the applied field are permitted in accordance with quantum-mechanical principles. A transition from one orientation to another involves the absorption or emission of a quantum of electromagnetic radiation, the frequency of which is equal to the precessional frequency. The energy of such a transition is given by Equation (2.3).

$$\Delta E = h\gamma B_0/2\pi \qquad \textbf{(2.3)}$$

(Where γ is the magnetogyric ratio (different for each nucleus), h is Planck's constant and B_0 is the strength of the applied field).

From (2.3) it follows that resonance occurs when transitions between orientations are induced by the application of a radio signal, whose frequency (ν) matches that of precession:

$$\nu = \gamma B_0/2\pi \qquad \textbf{(2.4)}$$

As the orbital electrons shield the nucleus to a certain extent from the external magnetic field then, at a given frequency, nuclei in different electronic (i.e. chemical) environments will resonate at slightly different values of the applied field. This is the phenomenon known as the "chemical shift" and provides the insight into the configurations of molecular complexes.

(The main factors affecting chemical shifts are atomic coordination number; the type of nearest neighbour atoms; bond angles; connectivity of the structural unit (Q_n) and next nearest neighbour atoms.)

2.5.1 Experimental Details of MAS NMR

Three separate types of MAS NMR investigations were performed: carbon; boron and silicon. For each elemental examination, the frequency, external field, pulse parameter and chemical reference standard all differed. These are summarised in table 2.1 overleaf.

For the cross-polarisation technique employed in the ^{11}C CP MAS NMR, a pulse sequence that differed significantly from normal MAS NMR was employed and is represented pictorially in figure 2.5 below.

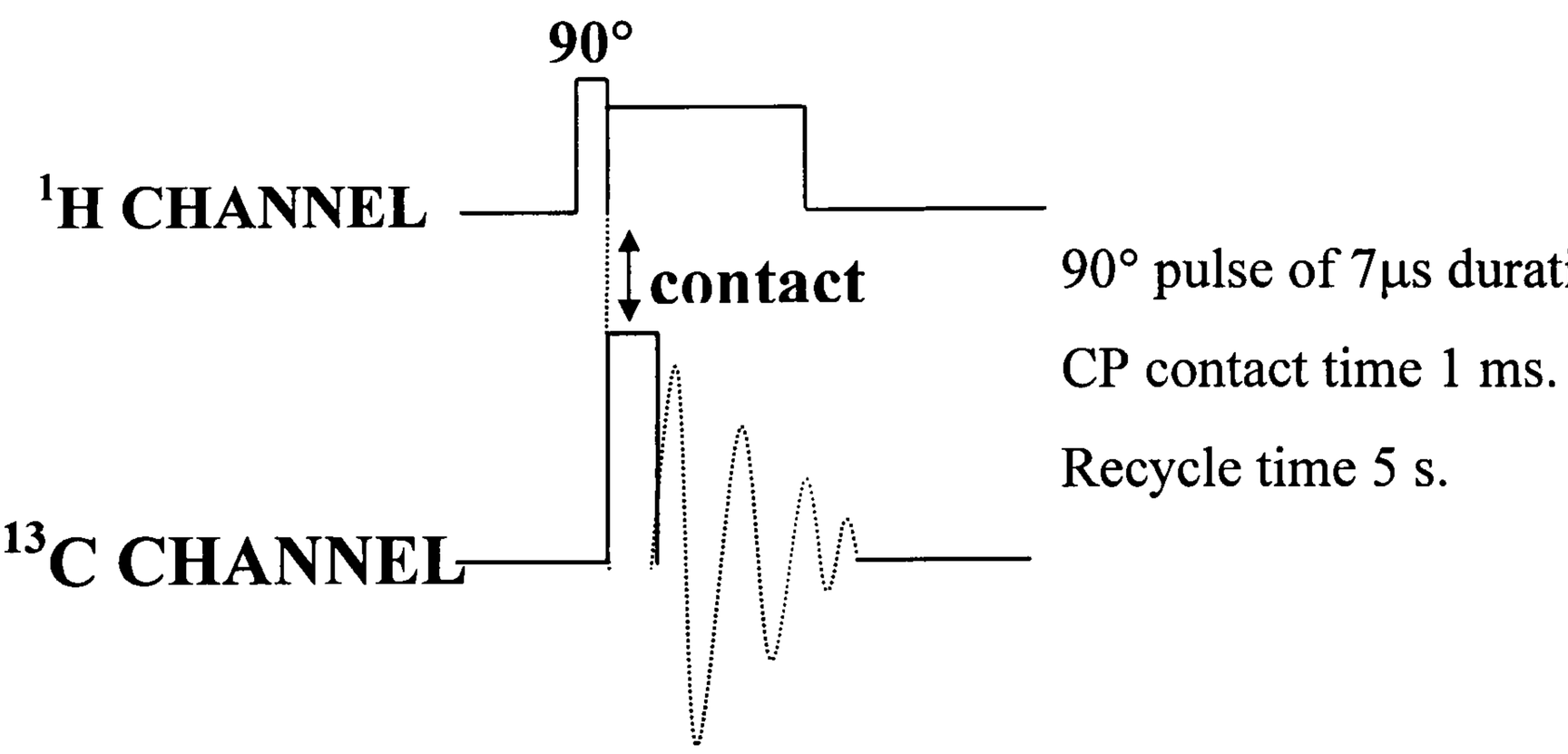

FIGURE 2.5 - Schematic of pulse sequence employed for ^{11}C CP MAS NMR

Nucleus	Frequency/ MHz	Pulse width/ μs	Repetition Time/ s	Spinning Speed./kHz	Reference
^{11}C	78.790	See Fig. 2.5	5	3.8 – 4.2	Adamantine
^{29}Si	59.627	(2π/6)	20	3.5	TMS
^{11}B	192.546	0.9	2	20.4	Boric Acid

Table 2.1 – Experimental Details for MAS NMR Spectroscopy.

Note:

The ^{11}C and ^{29}Si results were obtained using a Bruker MSL 300 spectrometer operating with a field strength of 7.05 Tesla. The ^{11}B investigations were performed upon a Bruker MSL 600 spectrometer operating with field strength of 14.1 Tesla.

2.6 FTIR Spectroscopy

Fourier transform infrared spectroscopy (FTIR) of the membrane materials was performed upon a Bruker Vector 22 FTIR. The use of this apparatus was courtesy of the Department of Chemistry of the University of Warwick.

No special preparation of the samples was necessary. (One caveat is that when cleaning the instrument prior to testing new samples, no solvents were used as they might introduce artefacts into the resulting spectra. Instead all surfaces were dry-wiped). The spectra produced by this instrument were obtained from a range of dry xerogel powder that had been previously exposed to various temperatures within the pyrolysis regime described above in section 2.2.2.1. This particular apparatus used a Bruker Single Reflection Diamond attenuated total reflection system (ATR) and all spectra were obtained from the sample powders located on the test bed and open to the external laboratory atmosphere. The spectral range was from 2000 cm^{-1} to 400 cm^{-1}.

This technique was especially useful in that not only did it perform examination of bulk specimens but was also permitted the *in situ* examination of actual membranes. It was therefore possible to investigate synthesised active separation layers both before and after they had been exposed to gas permeation trials. Hence, it was possible to determine whether any CO_2 absorption had actually occurred during the membranes' exposure to this feed gas. (Section 4.3.2). In addition, from a structural point of view, it was possible to detect if there was any gross chemical differences between the bulk and the film.

FTIR spectroscopy supplemented (and in some instances complemented) the MAS NMR observations very well. As with the MAS NMR investigations, the important structural information obtained related to observing the structural and chemical evolution of the membrane materials at various key temperatures within their thermal treatment regimes.

2.7 SEM Microscopy

All scanning electron microscopy (SEM) was performed upon a JEOL 6100. Examinations for the most part were restricted to observing the morphology and quality of the deposited membranes upon their substrates [7]. Two views were desired: topographic (membranes' surfaces) and cross sectional.

In order to obtain cross-sectional images, samples were prepared by fracturing the circular membrane-coated substrates as nearly as possible into two semicircular fragments. This would then give a cross sectional view that ran radially from the centre to circumference of the substrates. One then had sufficiently wide specimens to be able to determine whether the membrane layer varied in thickness across the top of substrate. It also provided large enough pieces for topographic inspection over sufficiently well separated

locations on the membrane's surface to discount any possibility of unrepresentative local sampling.

Specimens were mounted with conductive carbon epoxy onto standard aluminium stubs and gold-coated. Images were normally acquired with an accelerating voltage of 10 kV and the instrument in secondary electron mode.

Energy dispersive x-ray analysis (EDX) was performed upon some cross-sectional samples where it was suspected that sol had actually seeped into the bulk of the membrane substrate itself

2.8 Atomic Force Microscopy

Atomic Force Microscopy (AFM) was used to obtain topographic data relating to the surface flatness of the stainless steel/titania substrate. This was performed upon a Burleigh model ARIS-3300 and no special sample preparation techniques were required.

References

[1] C. J. Brinker, G. W. Scherer, "Sol-Gel Science – The Physics and Chemistry of Sol-Gel Processing", Academic Press, London, (1990).

[2] Raman, N.K; Brinker, C. J. Organic "template" approach to molecular sieving silica membranes, Journal of membrane Science, 105 (1995) 273-275.

[3] A. M. Wootton, Silicon Oxycarbide Glasses and Glass-Ceramics, PhD Thesis, University of Warwick, (1998).

[4] R.G.Larson abd T.J. Rehg, "Spin Coating", S.F. and Schweizwer (eds.) "Liquid Film Coating", Chapman and Hall (1997)

[5] G. W. Scherer, "Thermal Expansion of a Gel Layer on a Rigid Substrate", Journal of Non-Crystalline Solids, **204** (1996) p118-124.

[6] R. Dupree and D. Holland "MAS NMR: a New Spectroscopic Technique for Structure Determination in Glasses and Ceramics" Appearing in "Glasses and Glass Ceramics", M. H. Lewis Ed., Chapman and Hall, London (1989) p1

7] P.J Goodhew & F.J. Humphreys, "Electron Microscopy and Analysis", Taylor and Francis (1992)

Chapter 3

Permeation Measurement Apparatus

3.1 General Design

Permeation trials were performed upon apparatus designed and built solely by the author. The basic functions of the system are the measuring of permeance for single gases; binary gas permeance measurements and the separation factor analysis of binary gases. In addition, if required, these measurements could also be taken at temperatures up to 400 K. Construction was stainless steel where possible and pipes were high quality 3/16"walled stainless steel tubing and all connections were made with Swagelock™ vacuum unions

The device was also designed so that separate analysis of the feed, retentate and filtrate gases could be performed. In the absence of a gas chromatograph, these analyses were performed by a novel ultrasonic gas analyser. (section 3.3). Though lacking the resolution of a chromatograph, this device could adequately resolve the molar fractions of a binary mixture of CO_2 and N_2 to a confidence limit of 1% by volume.

A schematic representation of the apparatus is shown in Figure 3.1 and accompanying photographs in plate 3.1. Data acquisitions were fully automated. For this purpose the pressure gauges, mass flow meters (MKS 1170A) and humidity sensor were connected to a computer through an 11-bit AD converter

The basic design philosophy was to incorporate as much flexibility as possible in the measurement of the flow of gases through a membrane under the influence of a transmembrane pressure gradient. An uncommon feature is that by setting the retentate exhaust to a rotary pump (Figure 3.1), sub-atmospheric pressures became available on the high-pressure side of the membrane.

The device operates in an absolute pressure-difference mode. That is, high and low-pressure sides of the membrane are completely separate and the only path between them lies through the test membrane. The low-pressure side is controlled and maintained by a rotary pump. This means that (unlike the majority of test equipment used by researchers in this field) no sweep gas was used.

The purpose of a (usually inert) sweep gas is to sweep away the permeating products and to decrease their concentration on the far side of the membrane. The result is a concentration gradient of the permeating species across the membrane and a transmembrane pressure difference. However, there are two basic drawbacks to this technique.

- The presence of a (non-inert) species of sweep gas on the far side of a membrane can impede the permeation of other chemical species.

- Counter diffusion of the inert sweep gas can affect the gas permeation behaviour of the feed components. This has to be mathematically compensated for later in the analysis of resullts.

It was decided at the initial design stage that this approach with its attendant requirement of conditioning was too uncertain and unquantifiable to be relied used in the testing of new membranes. Hence, the technically more difficult route of maintaining an absolute pressure drop via evacuation was chosen.

(Another advantage of the chosen approach is that more realistically simulates the conditions of a membrane in a practical working environment).

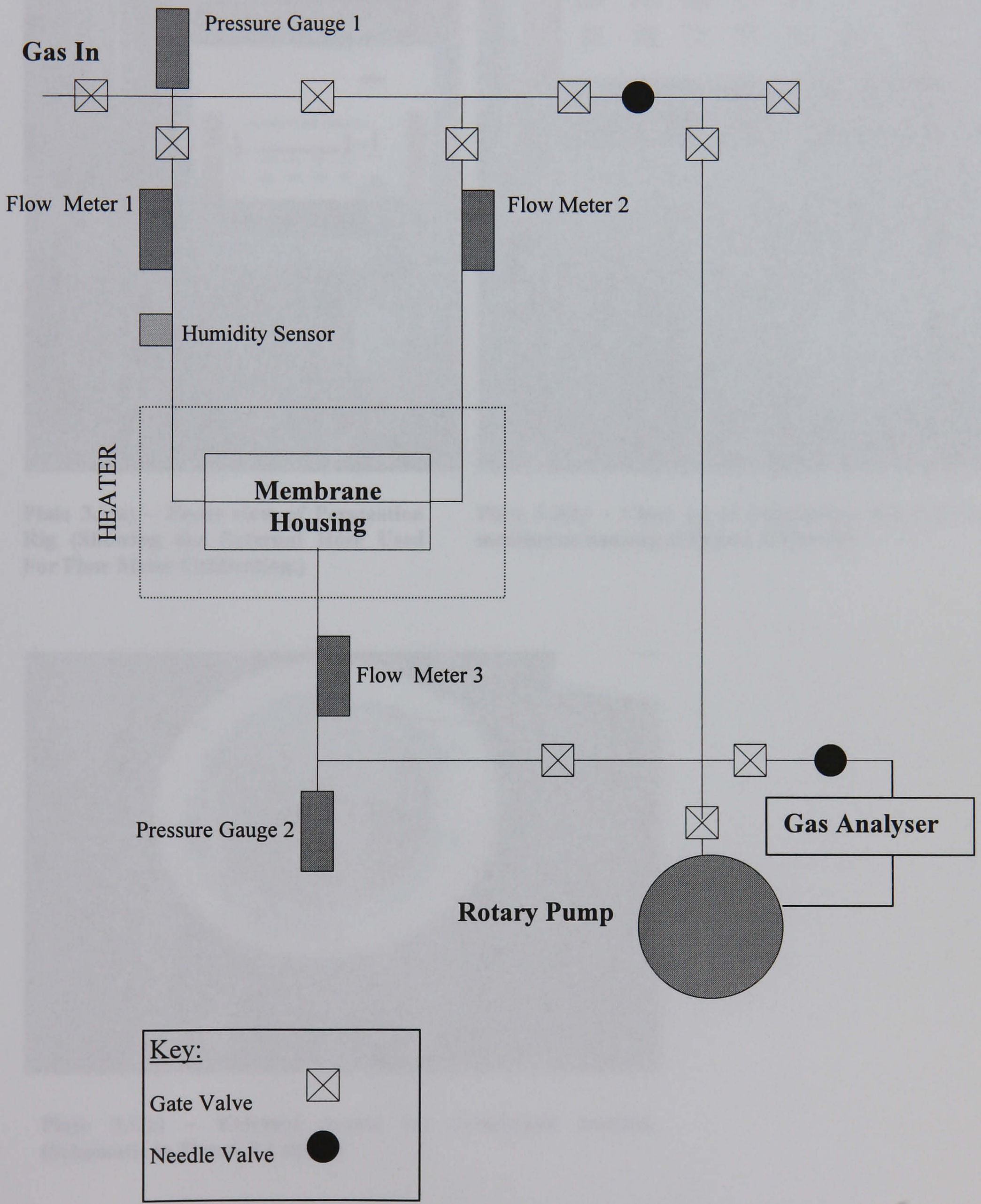

Figure 3.1 – Schematic of Gas Permeation measurement Apparatus.

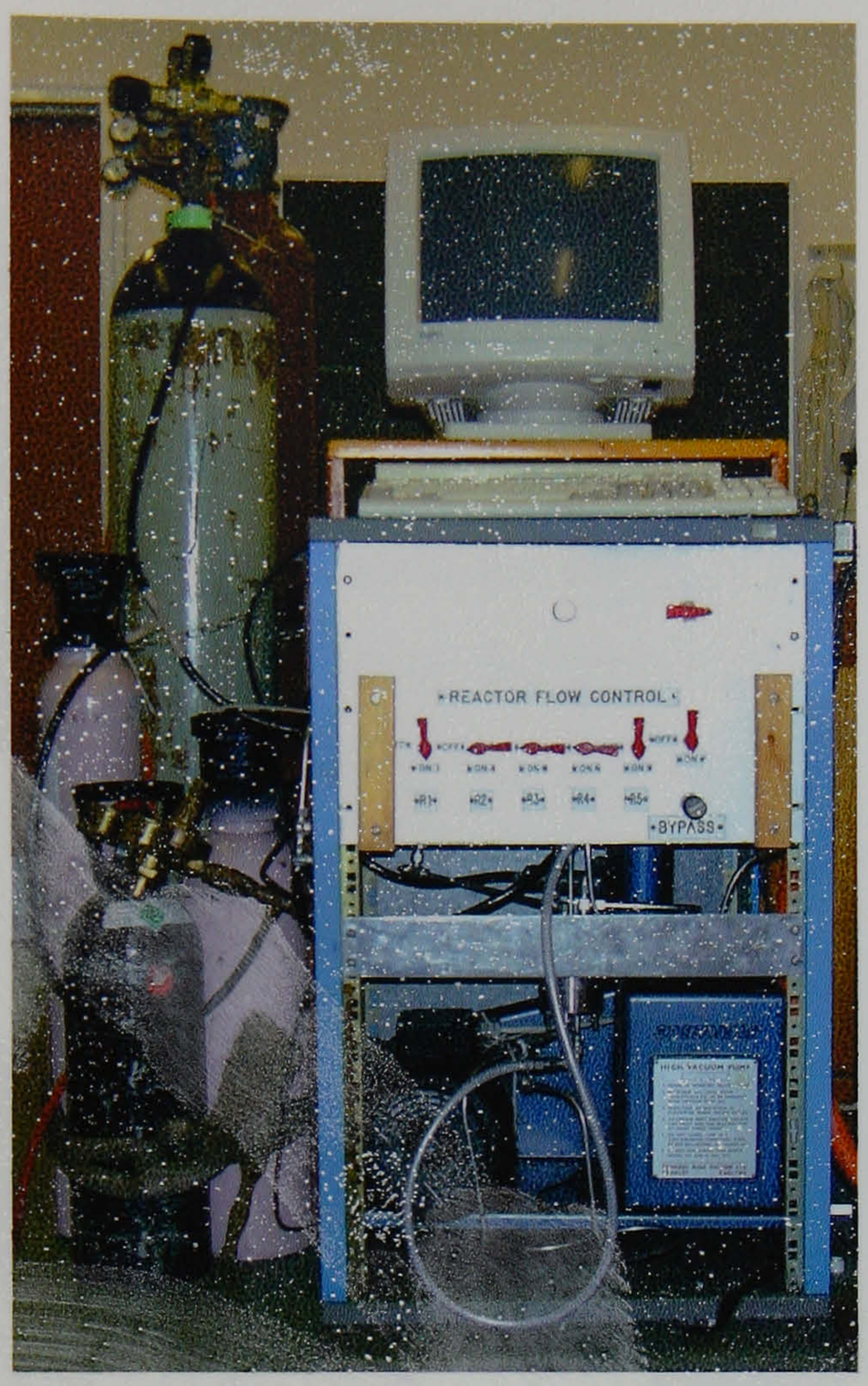

Plate 3.1(a) – Front view of Permeation Rig (Showing the External Hose Used For Flow Meter Calibration.)

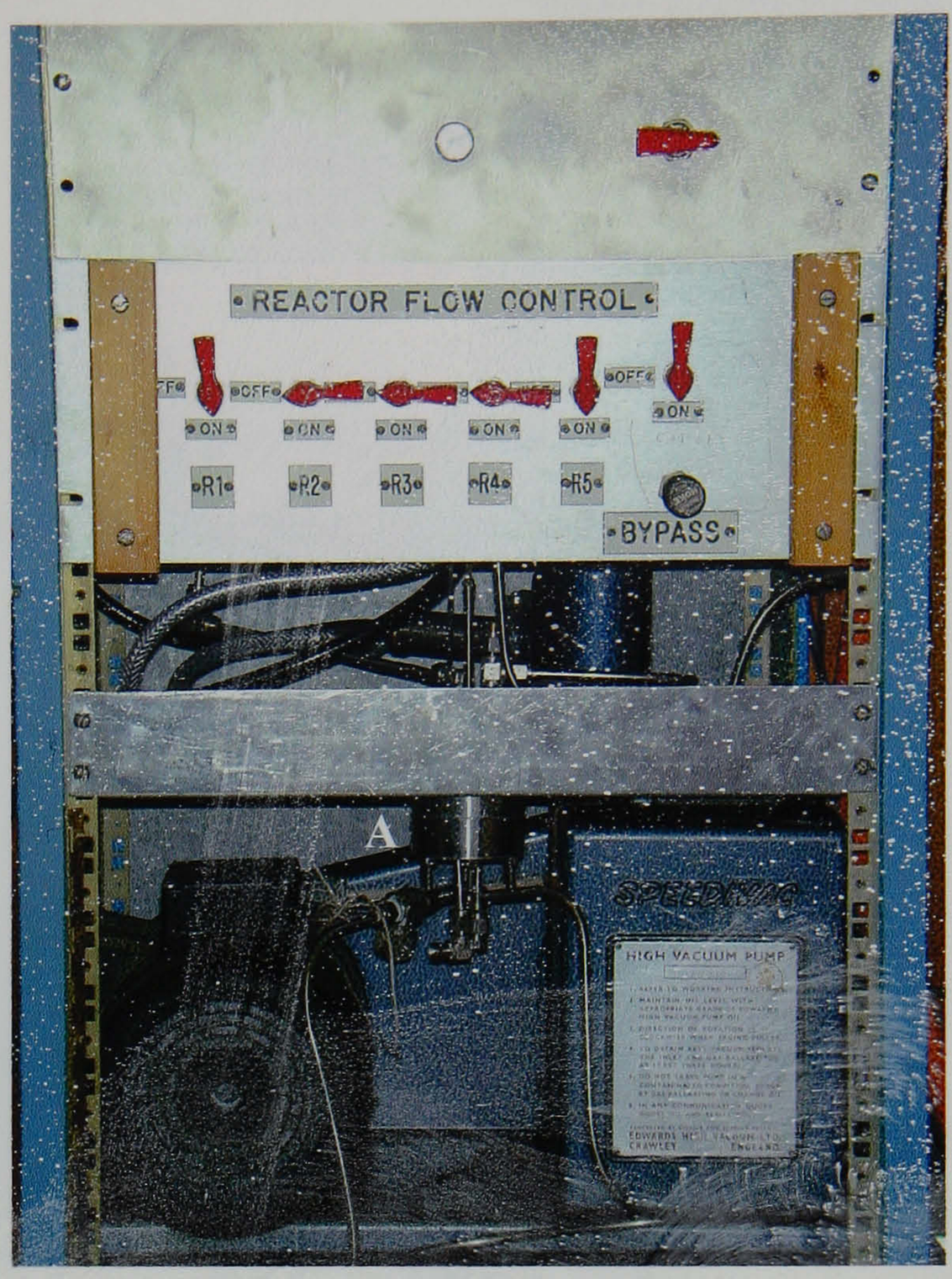

Plate 3.1(b) – Close up of Permeation Rig ("A" is membrane housing of Figure 3.3 below)

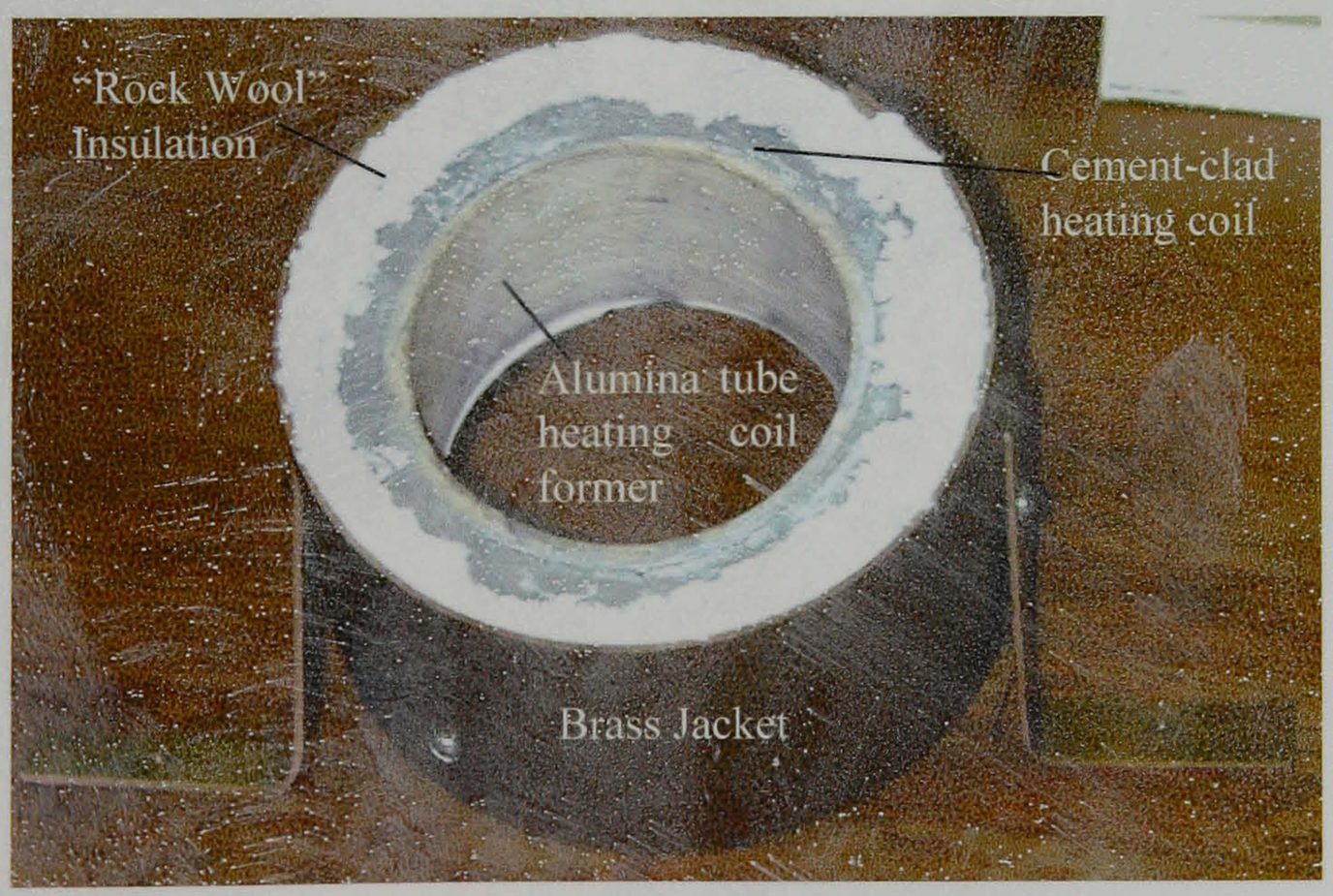

Plate 3.1(c) – External heater for membrane housing. (Schematic in Figure 3.1 above)

Plate 3.1 – Gas Permeation Rig for evaluation of membrane behaviour.

3.2 Sample Preparation.

The membrane-coated substrates were prepared for the permeation rig by first being mounted upon the ledge of an aluminium annulus. A secure gas seal was formed by securing the membranes in place within the annulus with epoxy. This is illustrated in Figure 3.2 below.

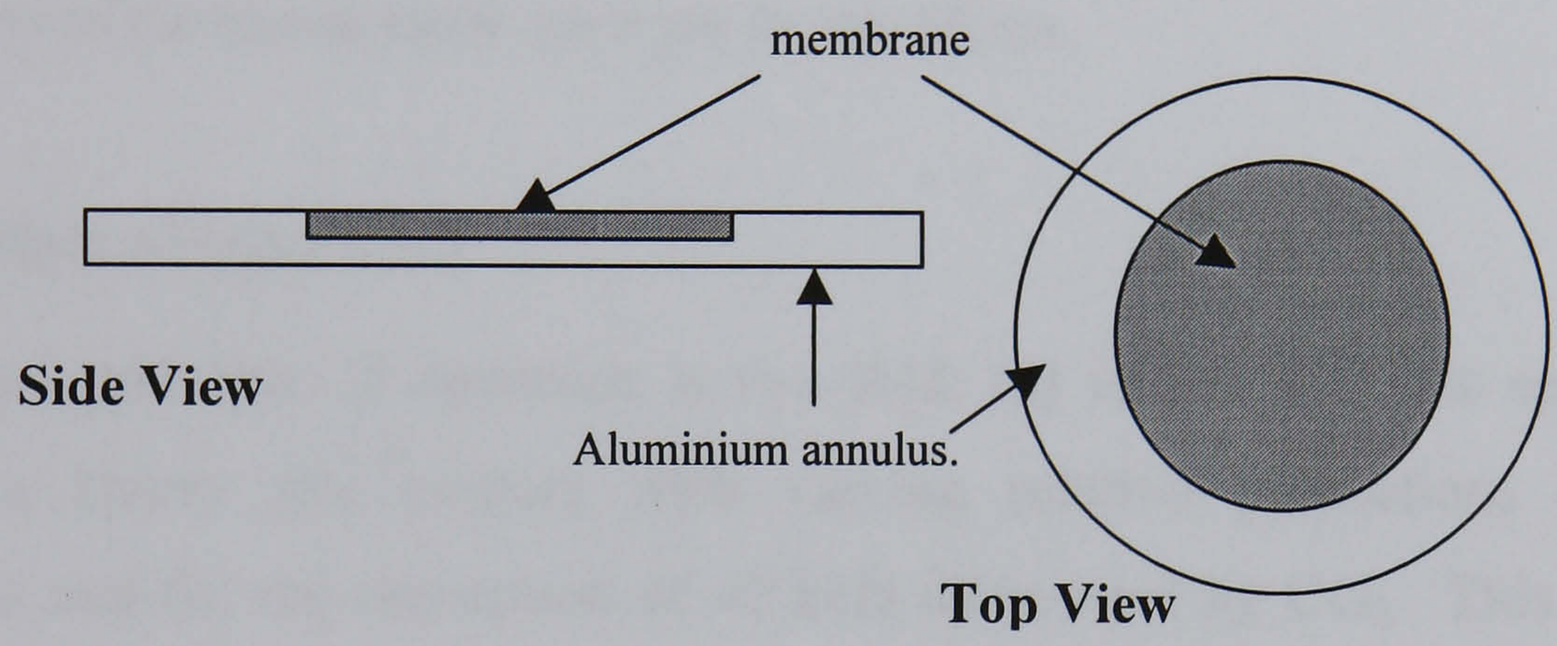

Figure 3.2 Sample Preparation

After being mounted, the sample membrane was then placed in the test cell, which was the kernel of the permeation test apparatus. This is shown in figure 3.3.

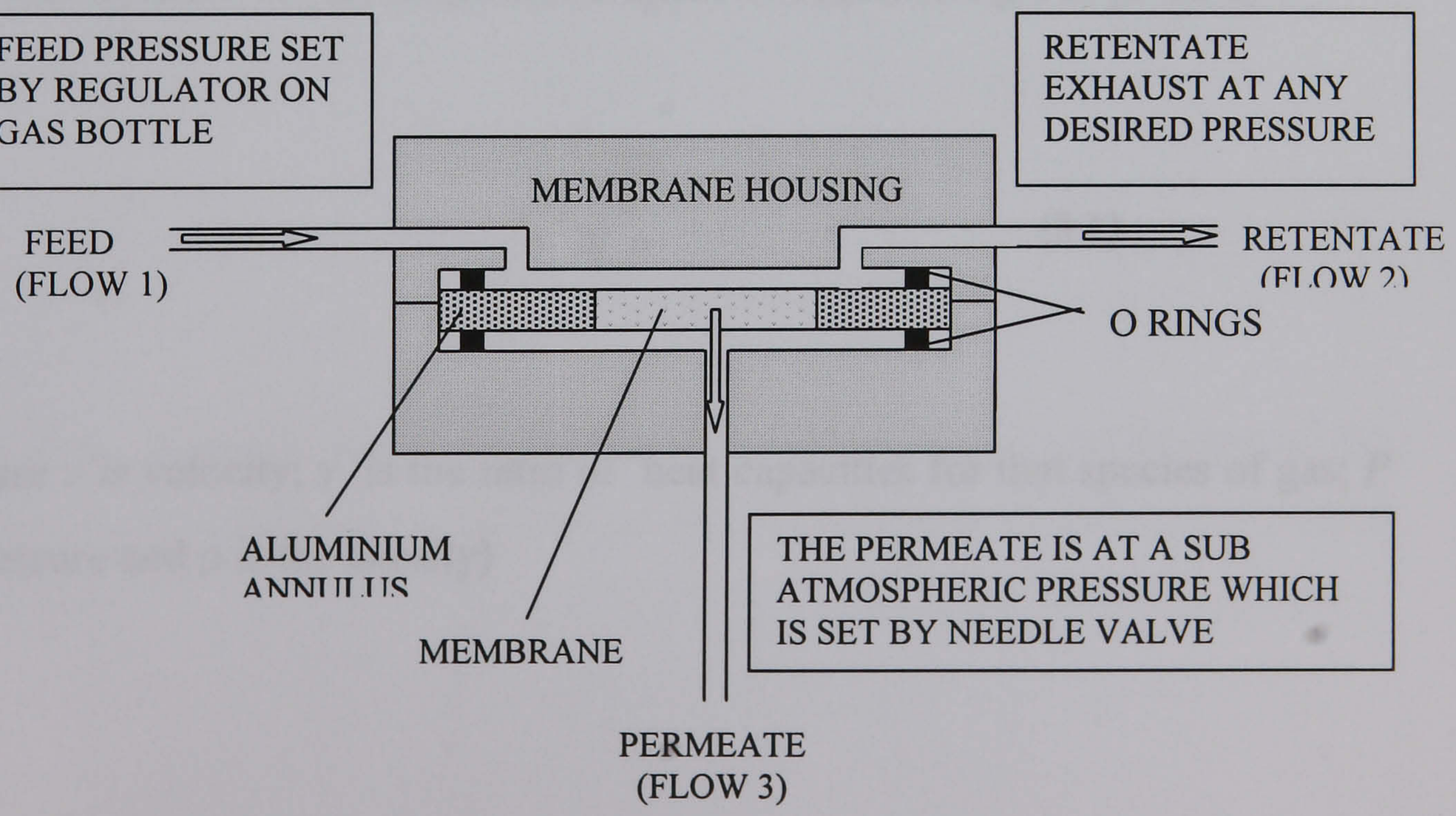

FIGURE 3.3 – Schematic diagram of the membrane module.

3,3 Novel Ultrasonic Gas Analyser.

The gas analyser that is shown in Figure 3.1 (a schematic of which is presented in Figure 3.5) was a novel device built by this author. Its purpose was to measure the respective molar fractions of a volume of a binary gas mixture of CO_2 and N_2 (though other gases can be used). The confidence limit is 1% by volume but this is adequate for the purposes of measuring separation performance of the membranes reported in this thesis.

3.3.1 Principle of Operation

The physical principle of operation is two-fold: (a) variation of the speed of sound in a binary gas mixture with varying relative proportions of the constituents and (b) the absorption of 40 kHz ultrasound by CO_2. This meant that the device could employ two separate principles - each acting as a control measurement upon the other,

Variation in the Speed of Sound

The basic relation for the longitudinal speed of sound in a gas is given by :

$$v = \sqrt{\frac{\gamma P}{\rho}} \qquad \textbf{(3.1)}$$

(Where v is velocity; γ is the ratio of heat capacities for that species of gas; P is pressure and ρ is the density)

Manipulation of the ideal gas equation allows us to express Equation (3.1) as:

$$v = \sqrt{\frac{\gamma RT}{m}} \qquad \textbf{(3.2)}$$

(Where R is the universal gas constant; T is the thermodynamic temperature and m is the molar mass of that species expressed in grams).

The speed of sound in a miscible binary mixture of gases is then found by simply substituting the average values of γ_{Ave} and m_{Ave} into Equation (3.2). Hence if the volume molar fraction of species A is designated by x and that of species B by (1-x) then:

$$\gamma_{Ave} = x\gamma_A + (1-x)\gamma_B \qquad \textbf{(3.3)}$$

Similarly,

$$m_{Ave} = xm_A + (1-x)m_B \qquad \textbf{(3.4)}$$

Combination of Equations (3.2), (3.3) and (3.4) now leads to the expression for the speed of sound in a binary mixture v_{mix} as given in Equation (3.5) below:

$$v_{mix} = \sqrt{\frac{\gamma_{Ave} RT}{m_{Ave}}} \qquad \textbf{(3.5)}$$

The effect upon the speed of varying the relative molar proportions of the components in a binary gaseous mixture of CO_2 and N_2 is illustrated overleaf in figure 3. 4

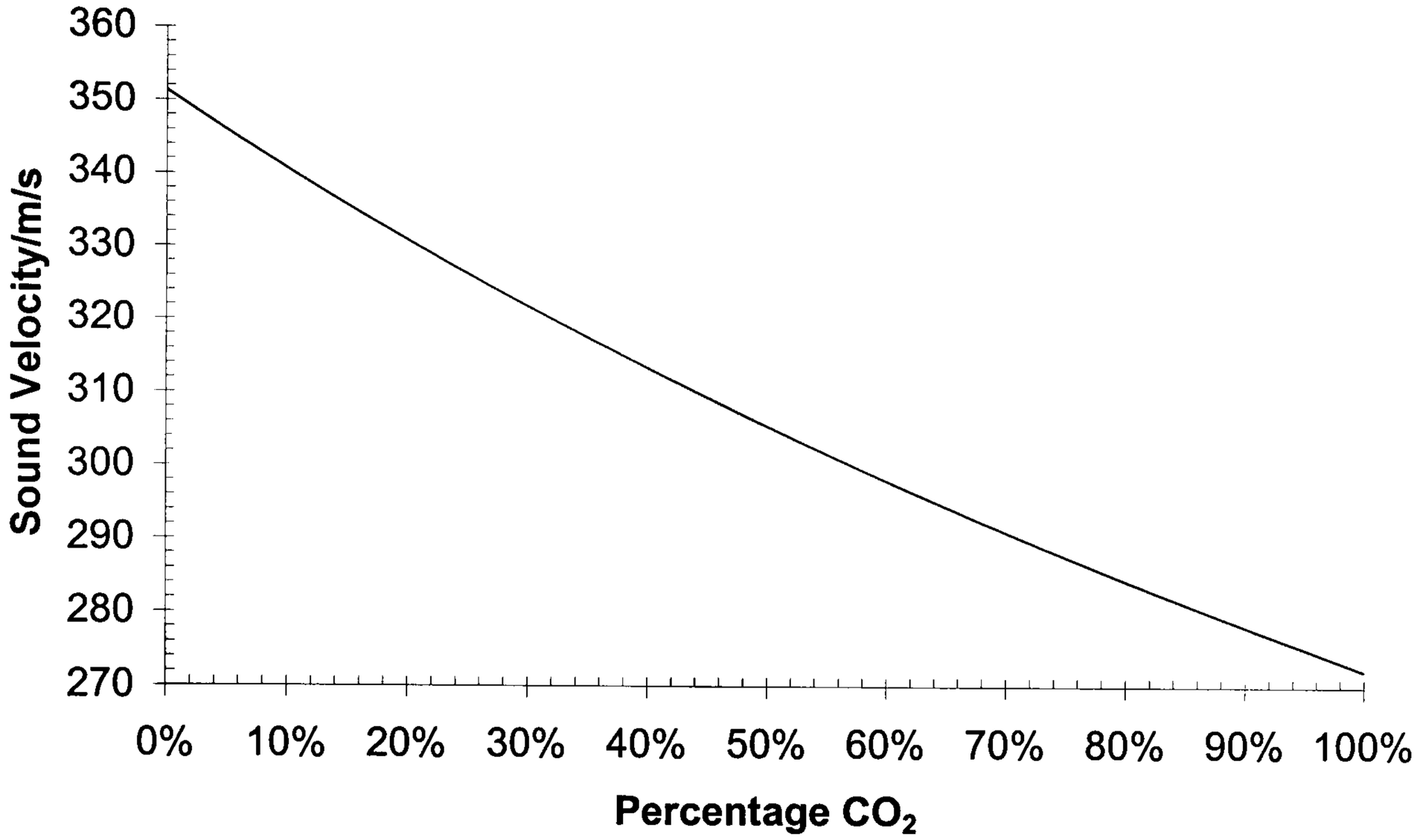

Figure 3.4 – Graphical representation of the variation of the speed of sound within a binary mixture of N_2 and CO_2 as the molar volume of each of the components changes.

The speed of sound in the gaseous mixture is found in two ways:

- Measurements of the phase shift due to the transmission lag of a continuous beam between the two transducers.
- The time of flight of a pulse of sound (leading edge of square wave) between the two transducers.

Owing to the small wavelengths of the sound beam, a time-delay phase shift could be many multiples of a single wavelength of the source beam – making conventional phase shift measurements meaningless. Therefore a "phase shift multiplier" was devised by the author. Essentially it is hardwired counter which converted the phase shift due to a change in velocity in sound across a fixed gap in terms of the number of whole wavelengths (plus the remainder) of the original oscillator signal. The result is then converted to an analogue voltage output that represents the degree of phase shift on a linear scale.

With a temperature measurement acquired by a thermocouple (in accordance with Equation (3.2) the relative proportions of the binary mixture could then be calculated.

The (inherently more accurate) continuous beam method was used for transducer frequencies of 150 kHz; the time of flight method was used for transducers which had centre frequencies of 40 kHz.

Absorption of 40kHz Ultrasound by CO_2

CO_2 absorbs ultrasound between frequencies 10-100kHz, peaking at 40kHz. This was discovered as it was the centre frequency of the originally used transducers. Accompanying this absorption is a corresponding velocity dispersion. The reason for this velocity dispersion is based upon molecular relaxation phenomena:

The ratio of specific heats of a gas $C_p/C_v = \gamma$ and as a general rule obeys the relation [1]:

$$\gamma = (f + 2) / f \qquad \textbf{(3.6)}$$

(Where: f is the number of degrees of freedom of the gas molecule.)

In any polyatomic gas, the heat from the adiabatic compressional phase is distributed in both the external translatory degrees of freedom and also in the internal ones. However, in the case of CO_2 undergoing excitation at frequencies between 10 kHz -100 kHz (and peaking at around 40 kHz), the compressional half cycles become too short in duration for this interchange of energy to occur. This results in the active degrees of freedom of the molecule being reduced - and in accordance with Equation (3.6) above, the specific heat ratio γ is increased.

As the speed of sound in any gas is proportional to $\gamma^{1/2}$, the result is a velocity dispersion.

From consideration of the rationale presented above, it is possible to explain the observed velocity dispersion. It seems that the speed of adiabatic compressional half cycles which reduces the degrees of freedom of the CO_2 molecule and thereby changing its ratio of specific heats γ - results from excitation by a *continuous wave in an equilibrium condition*.

Therefore, a logical inference is that the propagation of the *leading edge* of a *single* isolated pulse, of *width equivalent to a single half cycle*, should not cause any reduction in the degrees of freedom of the CO_2 molecule. Hence the speed of its propagation should not be affected by any velocity dispersion. The actual velocity of propagation in an otherwise dispersive medium could then be established by a simple time of flight method of a single pulse.

Speed of sound measurements were then taken from time of flight method. (A brief pulse rather than a continuous beam did not experience velocity dispersion by the presence of CO_2. Later, the continuous beam method was used again with specially constructed PZT transducers operating at 150 kHz.)

However, the degree of absorption was a very useful control experiment owing to the extreme sensitivity that the amplitude of a 40kHz beam showed to CO_2. (Surprisingly, investigations in this area date back as far as the 1920's [2] [3]) Calibrations were performed against known mixtures of 100%; 50% and 10% CO_2: N_2 and the rectified signal amplitude was found directly proportional to the percentage composition of CO_2 – provided pressure was the same value for each measurement.

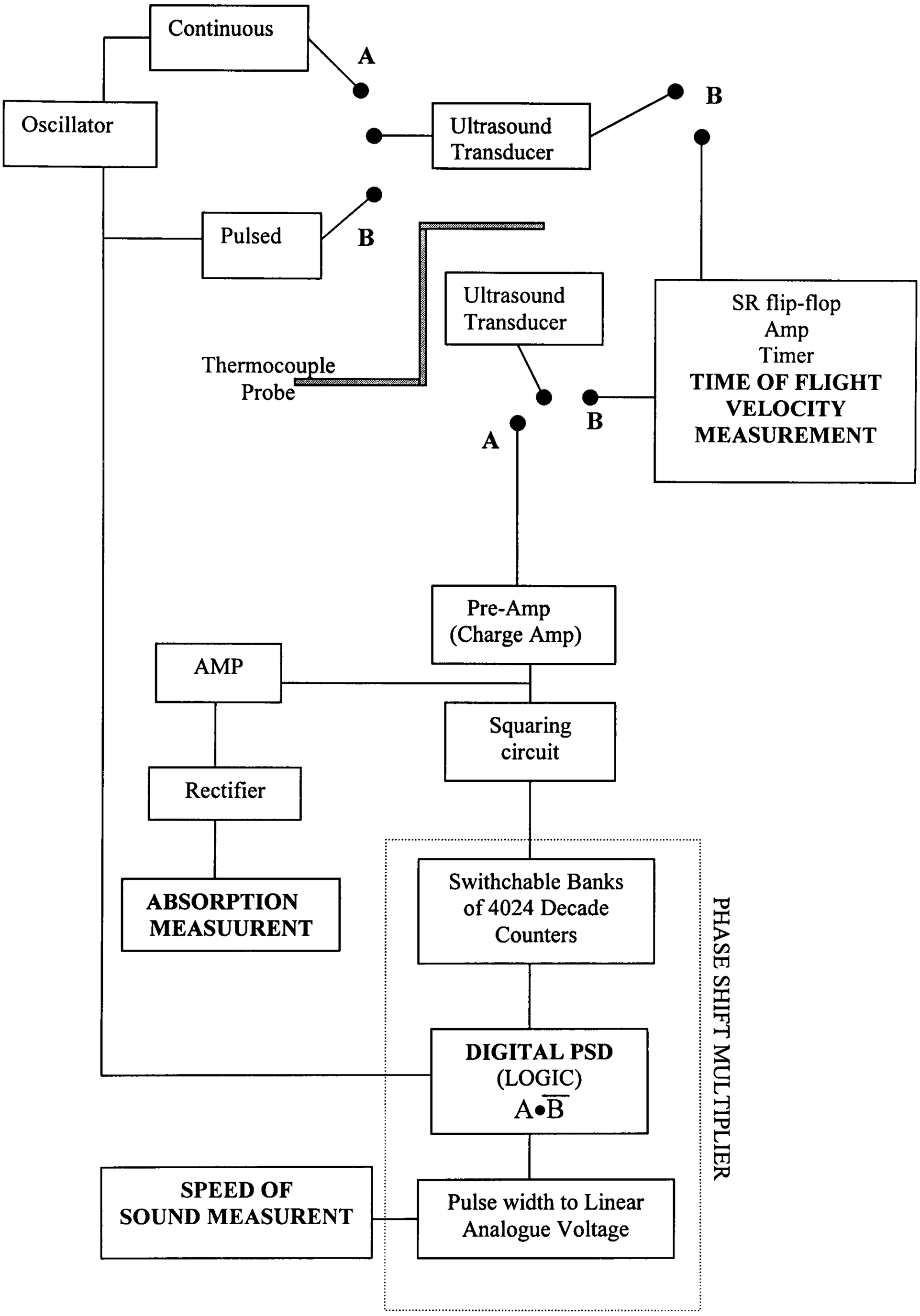

Figure 3.5 Schematic of Binary Gas Analyser. (Note all low pressure measurements were 0.5 bar or higher)

References

[1] T.F Hueter and R.H. Bolt, "Sonics", Wiley and Sons 3rd ed.(1955)

[2] S.J. Haldane, "Methods of Air Analysis", Griffin and Co. London 1920

[3] W.D. Keidel, "Nuovo Cimento," **5,** Supp, 2, 610 1927

Chapter 4

The Structural Evolution of Membrane Materials

4.1 Overview

Of all the non-borosilicate systems investigated, those which performed best in terms of CO_2 transport were those which were deposited from sols which contained both phenyl and methyl ligands. This finding was echoed for borosilicate systems in as much that it was the methyltrimethoxysilane (MTMOS) with varying molar fractions of the phenyl boronic acid precursor (PBA) which produced membranes with the best performance in terms of separation and durability.

As previously described in chapter one, there was a major difference taken in the synthesis route of the non-borosilicate and borosilicate systems. For non-borosilicate systems, the desired organic ligand was introduced via co-polymerisation of two silanes. For the borosilicate systems, organic ligands were added via organo-substitution with a suitable precursor.

Hence, in the case of the non-borosilicate systems the organic ligand - prior to any loss via pyrolysis – was covalently attached directly to the backbone of the silica network. The situation with the borosilicate systems was that the desired ligand is

more labile. That is, because the organic ligand is attached directly to a boron atom it can only form an indirect link to the silica network via borosiloxane bonds.

From a theoretical point of view, the main advantages offered by borosilicate systems are based upon the fact that boron is trivalent [1] Therefore the maximum functionality that boron can introduce into a system is three – which is appropriate for gels whose functionality is two to three. It also contrasts with the usual tetrafunctional precursors, which are frequently used to dilute organo-silica systems [2] [3].

Also, one could expect that borosilicate systems would experience a greater collapse of the gel network due to the fact that borosiloxane linkages (=B-O-Si=) are easily cleaved by hydrolysis. The consequence of this being that such linkages are incorporated into the network only when water is removed during heating. This sequence of events reduces the oligomeric growth of the precursor and results in a denser deposited film being synthesised.

The theoretical disadvantages of borosilicate systems however, are that the borosiloxane bond itself is unstable and could lead to precipitates, such as boric acid and trimethyl borate, being formed [2][4]. Phase separation is also a possibility and another consideration is that boron alkoxides experience comparatively rapid hydrolysis. Design limitations are also introduced by the fact that polymerisation is considerably constrained under values of pH 4 due to the OH ligands of the boric acid being insufficiently strong nucleophiles to express reasonable affinity for other boric acid molecules.

For both borosilicate and non-borosilicate systems, Differential Thermal and Thermogravimetric analyses (DTA and TGA) of the relevant xerogels indicate that generally speaking the methyl ligand is lost at around 550K. However, the phenyl

ligand remains until a temperature of 770K has been attained. NMR and FTIR techniques were then employed to supplement the analysis of the structure of these xerogels at these structurally significant temperatures.

4.2 Characterisation via NMR

The experimental conditions for all the NMR investigations reported upon within this chapter have been previously summarised in section 2.5.1 and Table 2.1

4.2.1 Carbon (^{13}C) CP MAS NMR of Non-Borosilicate Systems

This structural evolution with temperature of the phenyl and methyl xerogels is illustrated below in Figure 4.1 by the relevant ^{13}C (CP MAS) NMR spectra. The samples investigated were 30:70 molar ratios of PTMOS: MTMOS xerogels (r = 4), which were co-polymerised from the silanes PTMOS and MTMOS. These were then heated to the key pyrolysis temperatures of 523K, 673K and 873K.

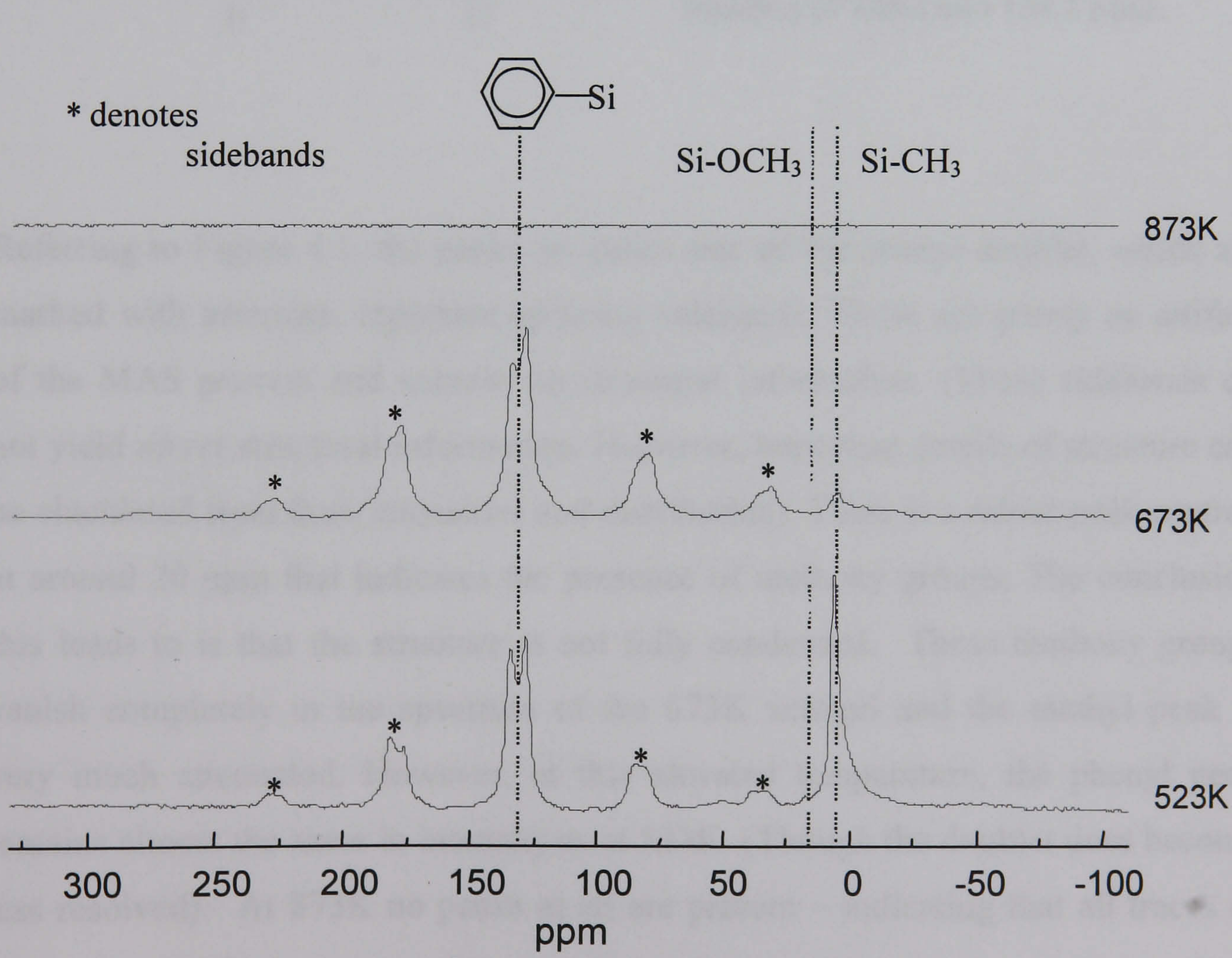

FIGURE 4.1 – ^{13}C CP MAS NMR spectra for key temperatures of 30:70 PTMOS:MTMOS xerogel (r=4).

From inspection of Figure 4.1 above, one can see that for the specimen heated to 523K there is a conspicuous peak centred around 6.4 ppm. This is due to the presence of the methyl ligand. The accompanying doublet with maxima at 128.4 and 134.3 ppm is indicative of a phenyl ring. The representation of this structure as a doublet within this particular spectrum is due to the diversity of the local chemical environments of each of the carbon atoms within the phenyl ring. This is illustrated further in Figure 4.2 below.

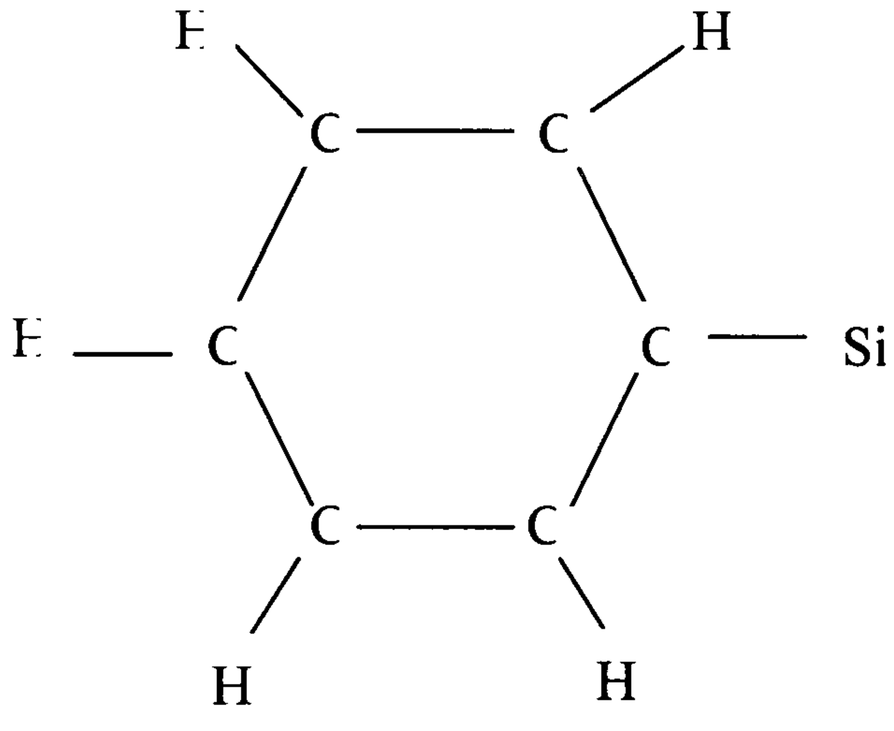

FIGURE 4.2 – The distinct chemical environment around each carbon atom within the phenyl ligand – responsible for the appearance of the doublet with maxima at 128.4 and 134.3 ppm.

Referring to Figure 4.1, the peaks on either side of the phenyl doublet, which are marked with asterisks, represent spinning sidebands. These are purely an artifact of the MAS process and contain no structural information. (These sidebands do not yield *direct* structural information. However, important details of structure can be elucidated from their intensities and distribution). There is a minor peak centred at around 20 ppm that indicates the presence of methoxy groups. The conclusion this leads to is that the structure is not fully condensed. These methoxy groups vanish completely in the spectrum of the 673K xerogel and the methyl peak is very much attenuated. However, at this elevated temperature, the phenyl peak remains almost the same in intensity as at 523K. (Though the doublet does become less resolved). At 873K no peaks at all are present – indicating that all traces of

carbon (and hence all organic groups) have been completely removed from the specimen.

The same specimens were then exposed to a different NMR technique: non-quaternary suppression. This technique enables a closer examination of non hydrogen-bonded carbon atoms to be conducted. (The rationale for this approach being that a single carbon atom within the phenyl group is attached to silicon, as illustrated Figure 4.2 above). These spectra appear below in Figure 4.3.

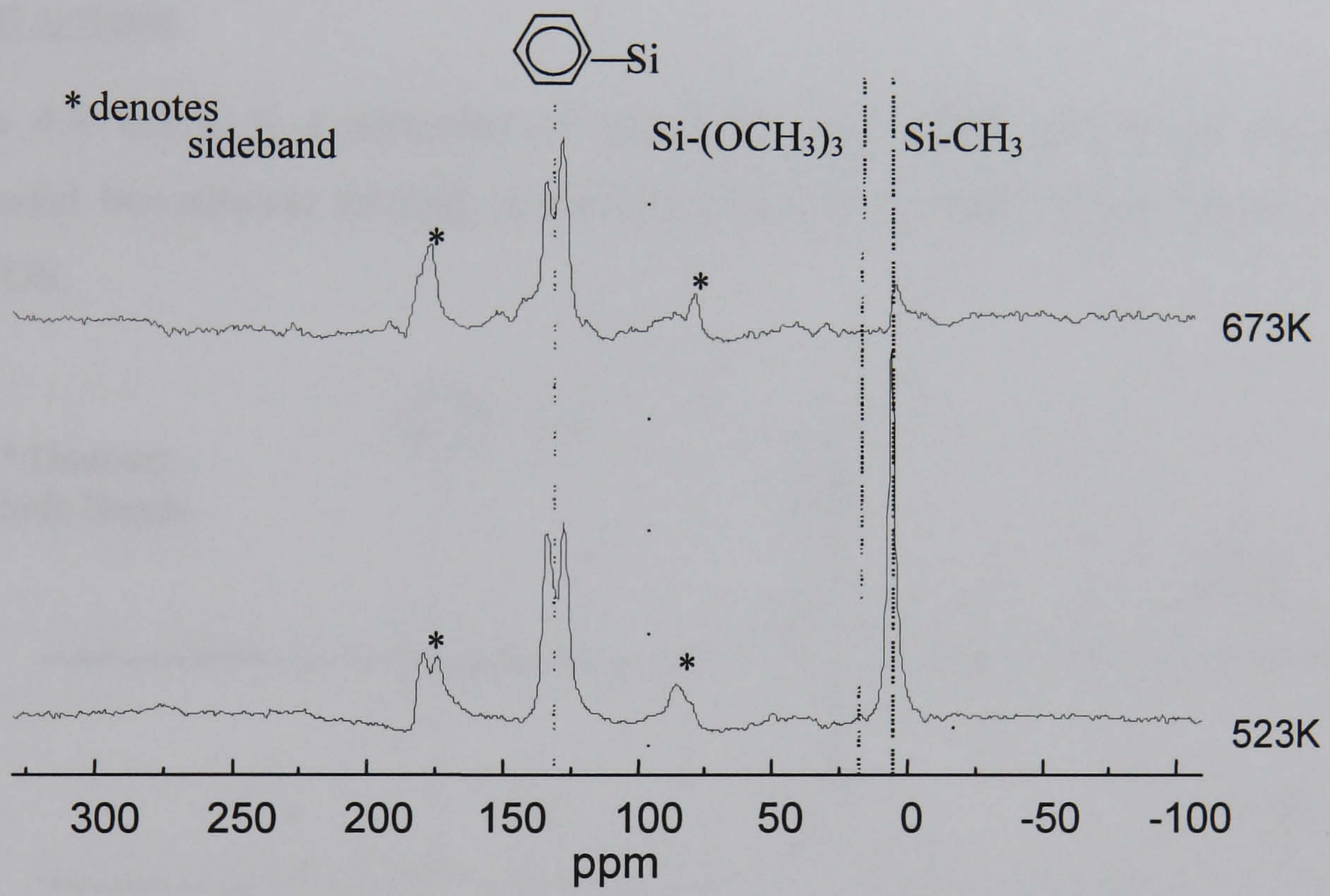

FIGURE 4.3 – ^{13}C CP MAS NMR spectra of 30:70 PTMOS:MTMOS xerogel (r=4) with non-quaternary suppression.

Unfortunately, the non-quaternary suppression technique was not very useful for elucidating further structural information from these specimens. Indeed, qualitatively the spectra presented in Figure 4.3 do not differ significantly from those presented in Figure 4.1, which relied upon ^{13}C CP MAS NMR alone. (This

was most probably due to the fact that methyl and phenyl groups themselves produce residual signals).

4.2.2 Carbon (^{13}C) CP MAS NMR of Borosilicate Systems

The most successful borosilicate membranes (see chapter 5) were synthesised from the co-polymerisation of the phenyl boronic acid (PBA) precursor with MTMOS; ETMOS and PTMOS respectively.

Methyl systems

Figure 4.4 below is a summary of the ^{13}CP MAS NMR spectra of the most successful borosilicate derived membrane: PBA in a 20:80 molar mixture with MTMOS.

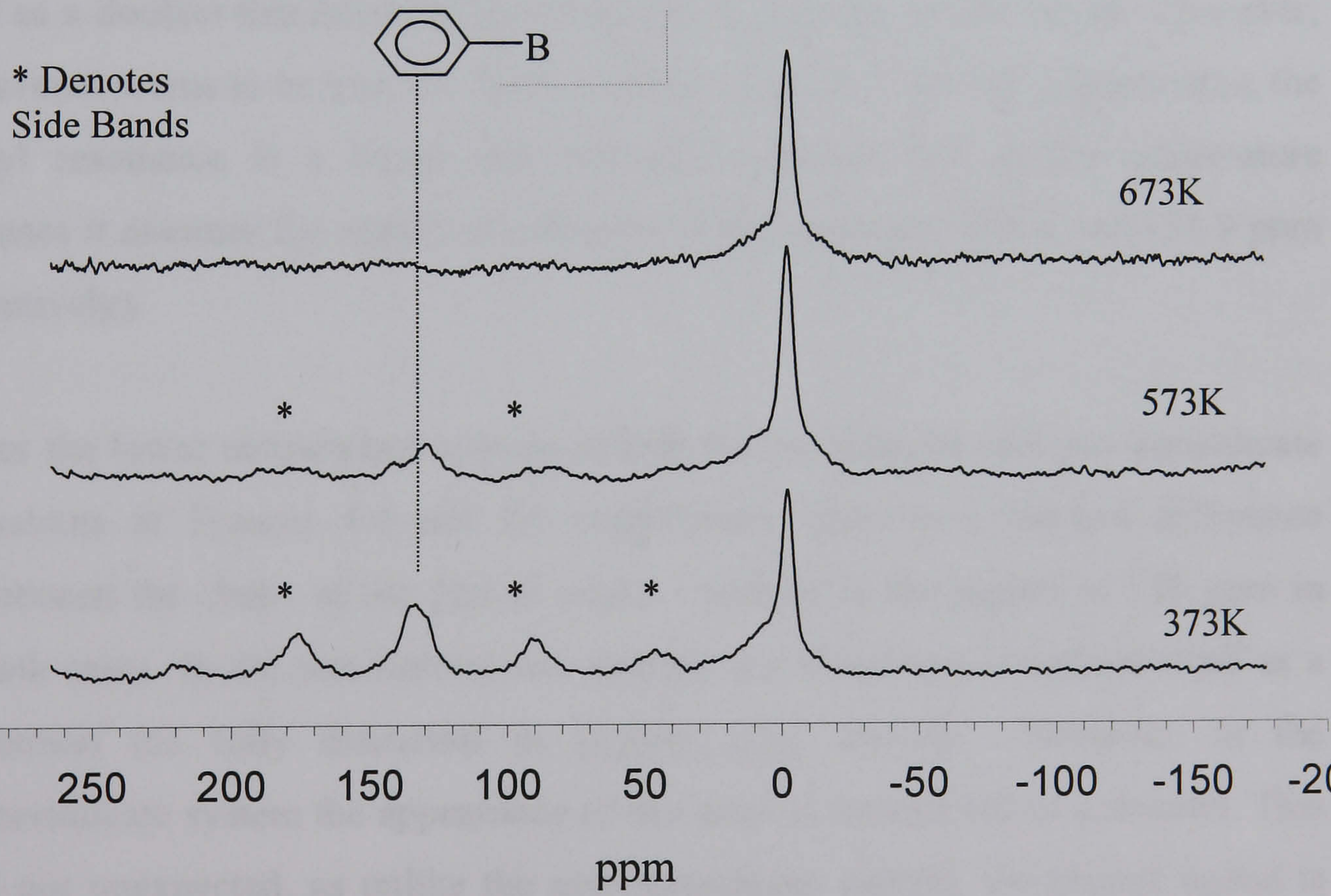

FIGURE 4.4 – ^{13}C CP MAS NMR of 20:80 PBA: MTMOS at key pyrolysis temperatures.

From inspection of Figure 4.4 above, it can see that the specimen pyrolysed at 573K exhibits a major peak that is centred on –3.2 ppm. This is due to the presence of the methyl ligand. There is a "shoulder" upon the left-hand side of this peak. After deconvolution, this can be attributed to an additional resonance that is centred on 9.7 ppm. As with the non-borosilicate example, this left hand "shoulder" is almost certainly due to the presence of methoxy groups. Similarly, it would appear the borosilicate specimen is also not fully condensed at this (higher) temperature.

The second major feature in the spectra of both the borosilicate and non-borosilicate systems examined here, is a spectral feature – identified as a phenyl resonance - that is located in the region of 130 ppm for both classes of system. In the representative non-borosilicate system discussed above, this feature manifests itself as a doublet that becomes less resolved at elevated temperatures. However, the reverse seems to be true for the borosilicate system. At lower temperatures, the phenyl resonance is a broad and unresolved feature but as the temperature increases it assumes the aspect of a doublet (with maxima at 128.4 and 134.9 ppm respectively).

1) For the lower temperature spectra of both the borosilicate and non-borosilicate systems of Figures 4.4 and 4.1 respectively, there is a marked difference between the shape of the phenyl peaks - centred in the region of 130 ppm in both cases. In the non-borosilicate system, this resonance manifests itself as a doublet (as fully discussed in section 4.2.1 above). However, in the borosilicate system the appearance of this peak is unresolved as a doublet. This is not unexpected, as unlike the non-borosilicate system, the phenyl ligand is not directly bonded to the silica backbone and now has boron atom in place of the silicon – c.f. Figure 4.2 above. This leads to the characteristic line

broadening of spectral features caused by the quadrupole interaction with ^{11}B nuclei.

2) This phenyl component of the 20:80 PBA: MTMOS xerogel is far less resilient to the effects of heating, as the ratio of the intensities between the methyl: phenyl peaks at 673K illustrates. For the non-borosilicate system illustrated in Figure 4.1 the intensity of the methyl peak at 673K (whilst initially being the dominant spectral feature at lower temperatures), has been reduced to a very small fraction of that of the phenyl resonance. However, for the borosilicate system illustrated in Figure 4.4 the reverse is true: at 673K the phenyl resonance has sunk below the level of background noise, whilst the methyl peak is still a very prominent feature. The rationale for this behaviour is that the phenyl group for the borosilicate system is not as tightly bound to the network as it lacks the direct covalent bond between the organic ligand and the silicon atom.

This demonstrated volatility of the organic component with elevated temperature as compared to the non-borosilicate system is good supporting evidence that the templating process (i.e. the selective removal of organic groups to provide selective porosity) is active.

Phenyl System

Figure 4.5 below presents the results of the ^{13}CP MAS NMR spectra of another successful borosilicate derived membrane: PBA in a 20:80 molar mixture with phenyltrimethoxysilane (PTMOS). As with the PBA: MTMOS system described above, the spectra presented in Figure 4.5 show the presence of the main resonance from the silane itself. Another feature, centred around 130 ppm, has previously been identified as the phenyl peak. There is a striking difference

between this system and the previous one: the extreme volatility of the phenyl component. In fact, the phenyl appears to have vanished completely at only 473K whereas with the previous system it was present in significant quantities at a temperature 100 K higher. As with the previous system, this behaviour is reasonable empirical confirmation of the fact that specific organic molecules can be controllably removed from the structure. The fact that this removal of the phenyl ligand happened at the lowest temperature of any other system should be an advantage in membrane synthesis. This is because, in terms of temperature, it significantly precedes the thermal densification stage that should then allow for a more controllable porous film formation process (see chapter 2).

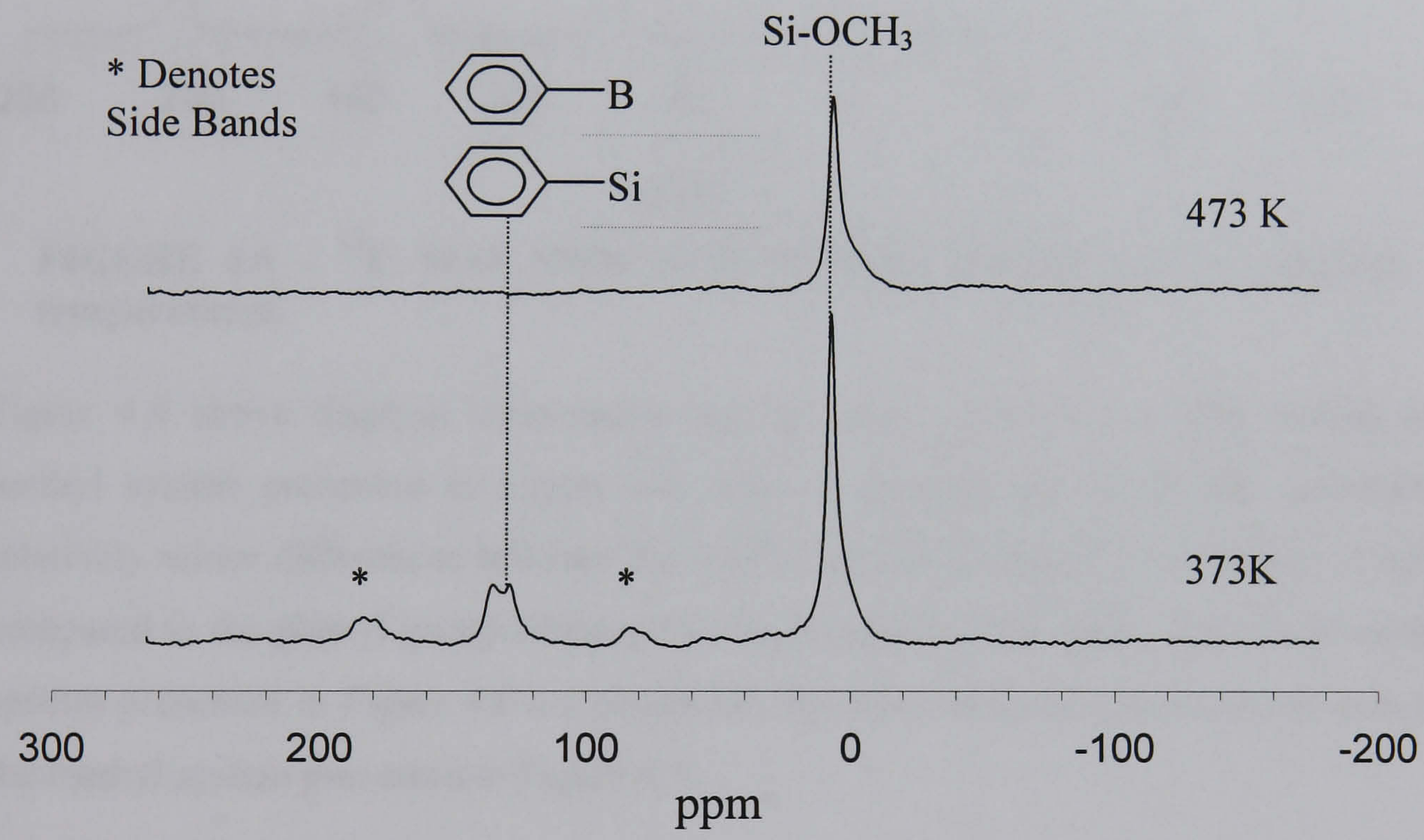

FIGURE 4.5 – ^{13}C CP MAS NMR spectra of 20:80 PBA:PTMOS at key pyrolysis temperatures.

Ethyl Systems

Figure 4.6 below shows the results of the ^{13}CP MAS NMR spectra of the final borosilicate system in this series: PBA in a 20:80 molar mixture with ethyltrimethoxysilane (ETMOS).

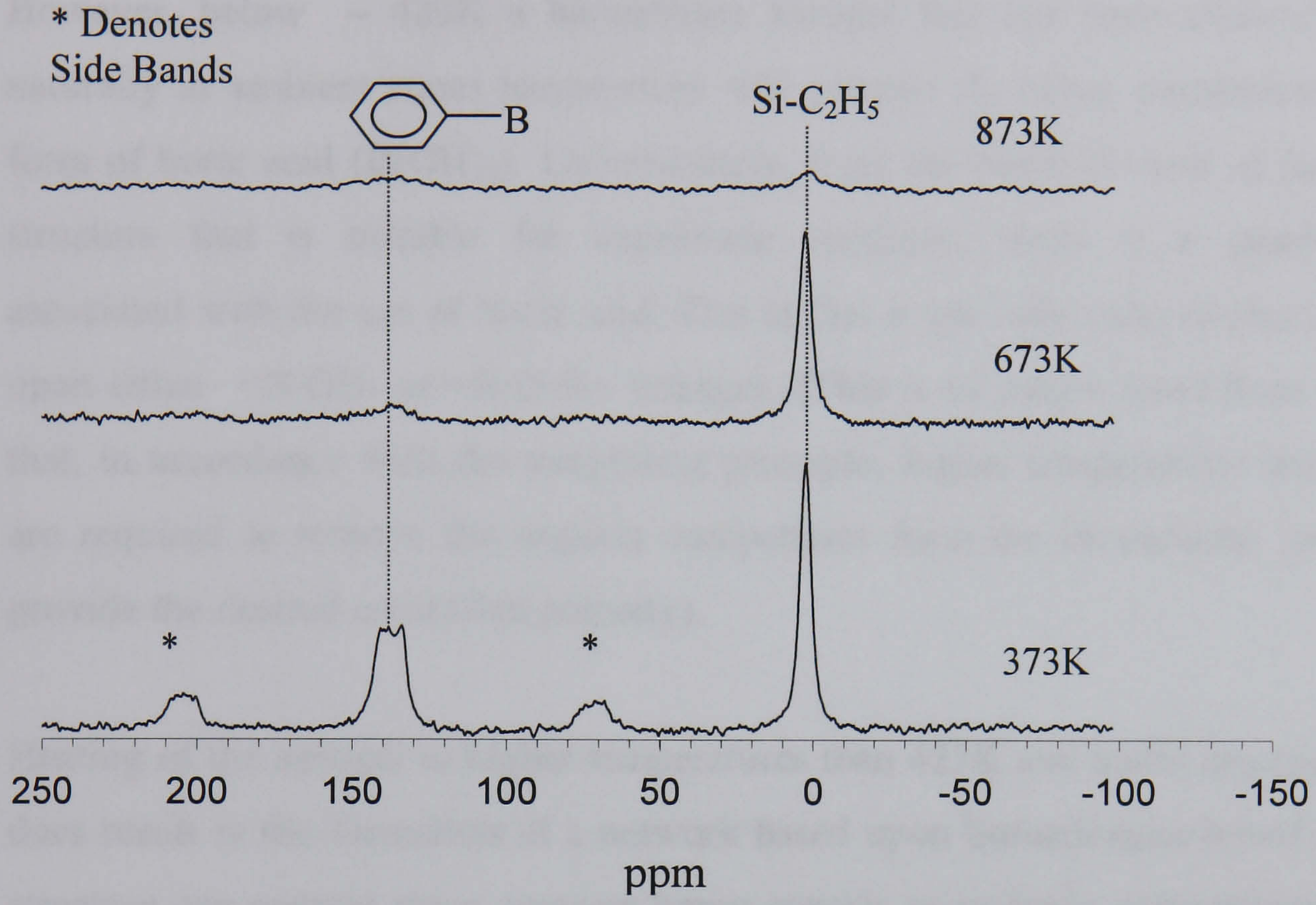

FIGURE 4.6 – ^{13}C MAS NMR of 20:80 PBA: ETMOS at key pyrolysis temperatures.

Figure 4.6 above displays temperature spectra whose profiles are very similar to the methyl system presented in Figure 4.4. This is unsurprising when one considers the relatively minor differences between the methyl and ethyl groups when either of these is compared to the phenyl group. Hence, the salient points of the ethyl system's temperature spectra presented in Figure 4.6 are essentially the same as those previously discussed for the methyl system presented in Figure 4.4.

4.2.3 ^{11}B MAS NMR of Borosilicate Systems

Before drying, a borosilicate gel system does not possess the borosiloxane bond (=B-O-Si=) to any significant degree and so naturally no extensive silica-backboned structure can exist. However, following the chemical condensation reaction and the subsequent removal of water and solvent by heating, this situation changes.

However, below ~ 423K a borosilicate xerogel that has been allowed to dry naturally at ambient room temperature will possess its boron constituent in the form of boric acid ($B(OH)_3$). Unfortunately, from the point of view of forming a structure that is suitable for membrane synthesis, there is a disadvantage associated with the use of boric acid. This is that it can only form networks based upon either =B-OH- or =B-O-B= linkages. (This is of course apart from the fact that, in accordance with the templating principle, higher temperatures than 423K are required to remove the organic components form the borosilicate system to provide the desired controlled porosity).

Heating of the xerogel to higher temperatures than 423K and under dry conditions does result in the formation of a network based upon borosiloxane bonds. Such a structure can possess three separate boron species as its basic components. These are BO_3 (in two forms: symmetric trigonal BO_3 and asymmetric BO_3) and a tetrahedral BO_4 group [2] [3].

Figure 4.7 displays the ^{11}B MAS NMR spectra obtained from a single specimen of 20:80 PBA : ETMOS xerogel at various key temperatures. The resolution is quite low due to the comparatively large quadrupole-coupling constant of ^{11}B. Hence, the identification of chemical species has to indirectly arrived at via the results of deconvolution analyses which reveal the specific spectral resonances of each temperature spectrum of Figure 4.7.

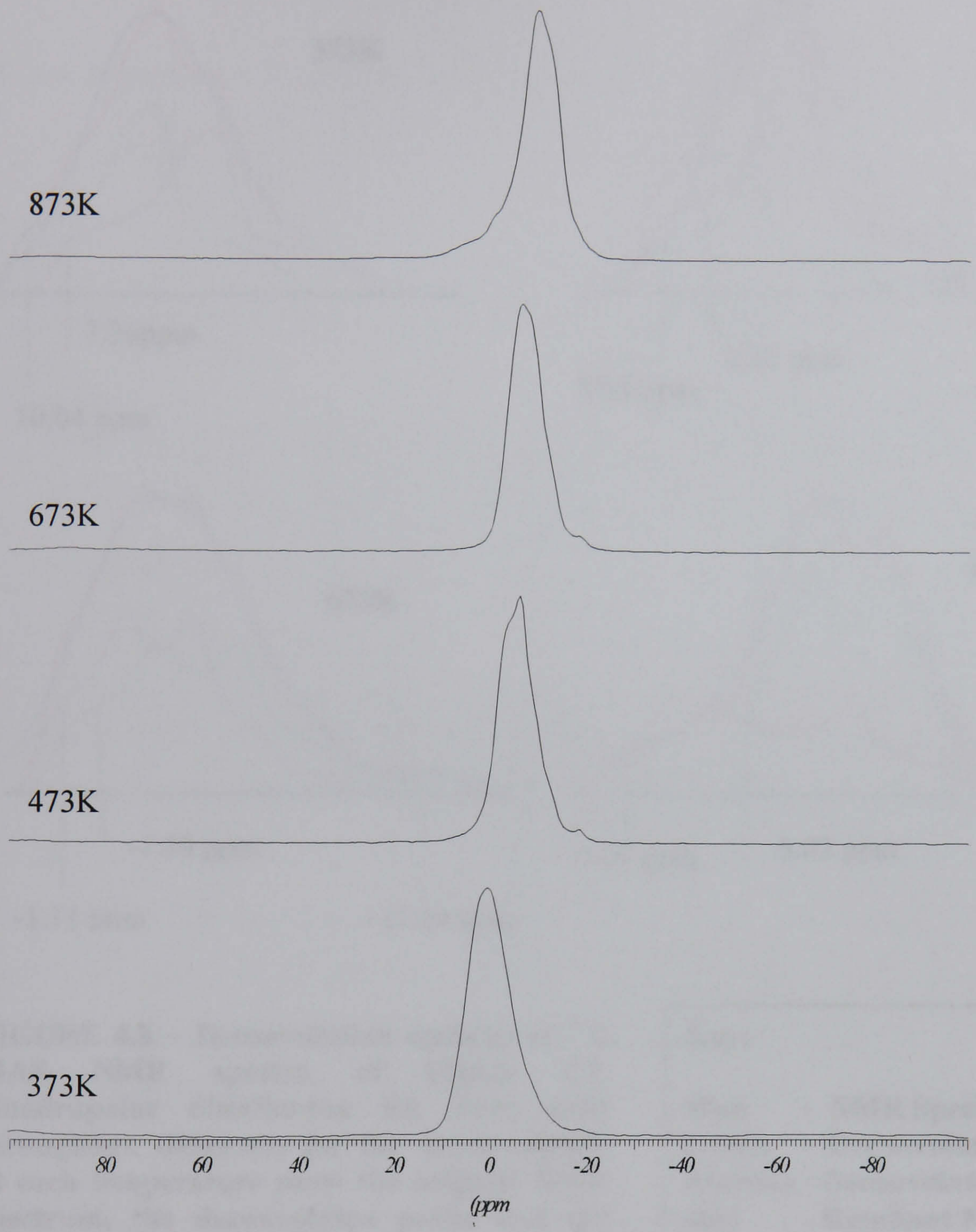

FIGURE 4.7 – ^{11}B MAS NMR of 20:80 PBA: ETMOS at key Pyrolysis Temperatures

For all spectra, deconvolution analysis with Gaussian curve fitting, revealed at least two major peaks for each ^{11}B MAS NMR spectral feature. Their positions relative intensities are presented below in Figure 4.8.

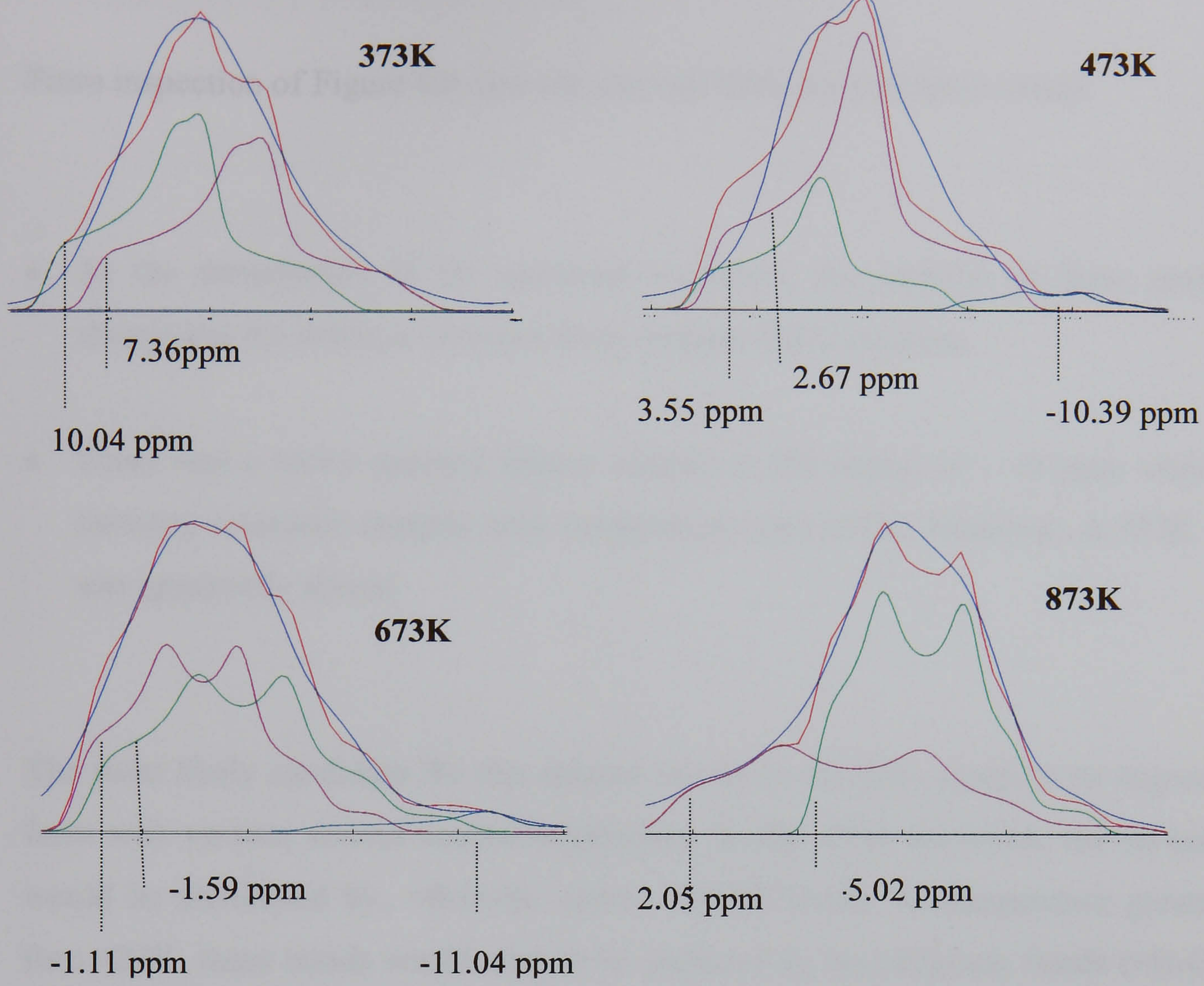

FIGURE 4.8 – Deconvolution analysis of ^{11}B MAS NMR spectra of Figure 4.7. Quadrupolar distribution fits were used throughout. Diagrams for the deconvolution at each temperature show the original NMR spectrum, the deconvoluted peaks and the resultant fit (see key opposite).

Key:

Blue - NMR Spectrum
Green - Deconvoluted Peak
Maroon - Deconvoluted Peak
Red - Resultant Fit

From inspection of Figure 4.8, one can see that there are two basic trends:

- As the temperature of the specimen increases, the position of these peaks change but the distance between them remains fairly constant.

- There was a minor spectral feature centred in the region of – 18 ppm whose intensity increased steadily with temperature until 673K. However, at 873K it was apparently absent.

The most likely candidate for this species would be the BO_3 group in its trigonal form with various second nearest neighbours. In the 373K specimen, the xerogel would be dominated by =B-O-B= and/or =B-OH bonds. At temperature greater than 423K, these bonds would start to be replaced by borosiloxane bonds (=B-O-Si=). However, it is unlikely that full condensation occurs at 873K and is certainly not the case for the membrane synthesis temperature of approx. 673K – as is apparent from the ^{13}C CP MAS NMR spectra of section 4.2.2 and Figure 4.5.

The minor spectral feature centred in the region of – 11 ppm, whose intensity increased steadily with temperature until 673K is sufficiently far removed from the main spectral feature to represent a different species. The chemical shift between this small feature and the main one, is of the order of 12 ppm. It is postulated that this represents a very small amount of the tetrahedral BO_4 species

4.2.4 Silicon (^{29}Si) MAS NMR

4.2.4.1 Non-borosilicate system

In addition to ^{13}C CP MAS NMR to trace the organic components of the 30:70 PTMOS: MTMOS sols, silicon NMR investigations at various key pyrolysis temperatures were conducted. Figure 4.9 is a presentation of ^{29}Si (MAS) NMR spectra of the same specimens presented above in the ^{13}C NMR investigations (Figure 4.1). Corresponding deconvolution analyses appear in Figure 4.10.

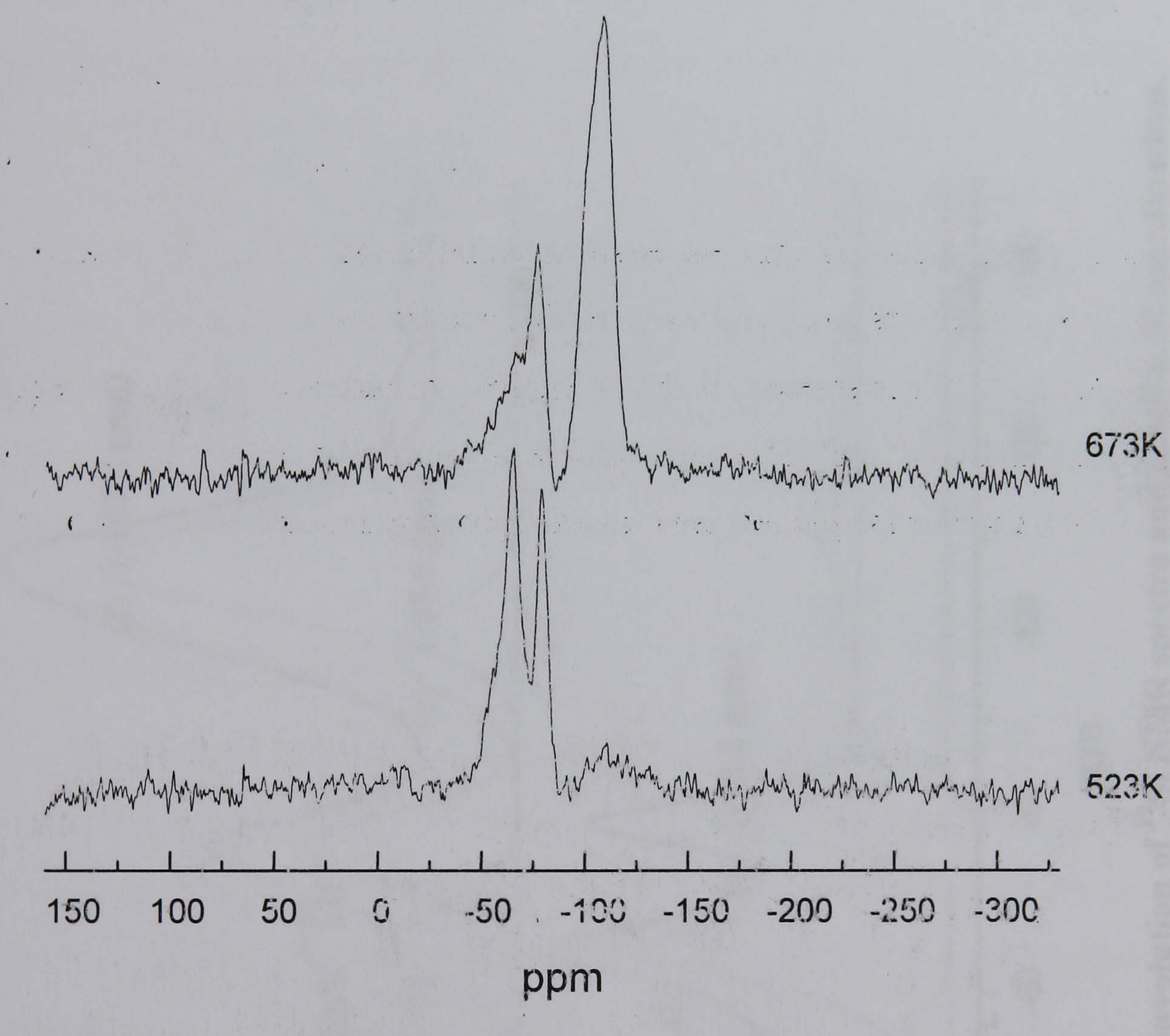

FIGURE 4.9 -- ^{29}Si MAS NMR spectra of 30:70 PTMOS:MTMOS xerogel (r = 4). (These spectra were analysed via deconvolution software that fitted profiles according to a Gaussian distribution).

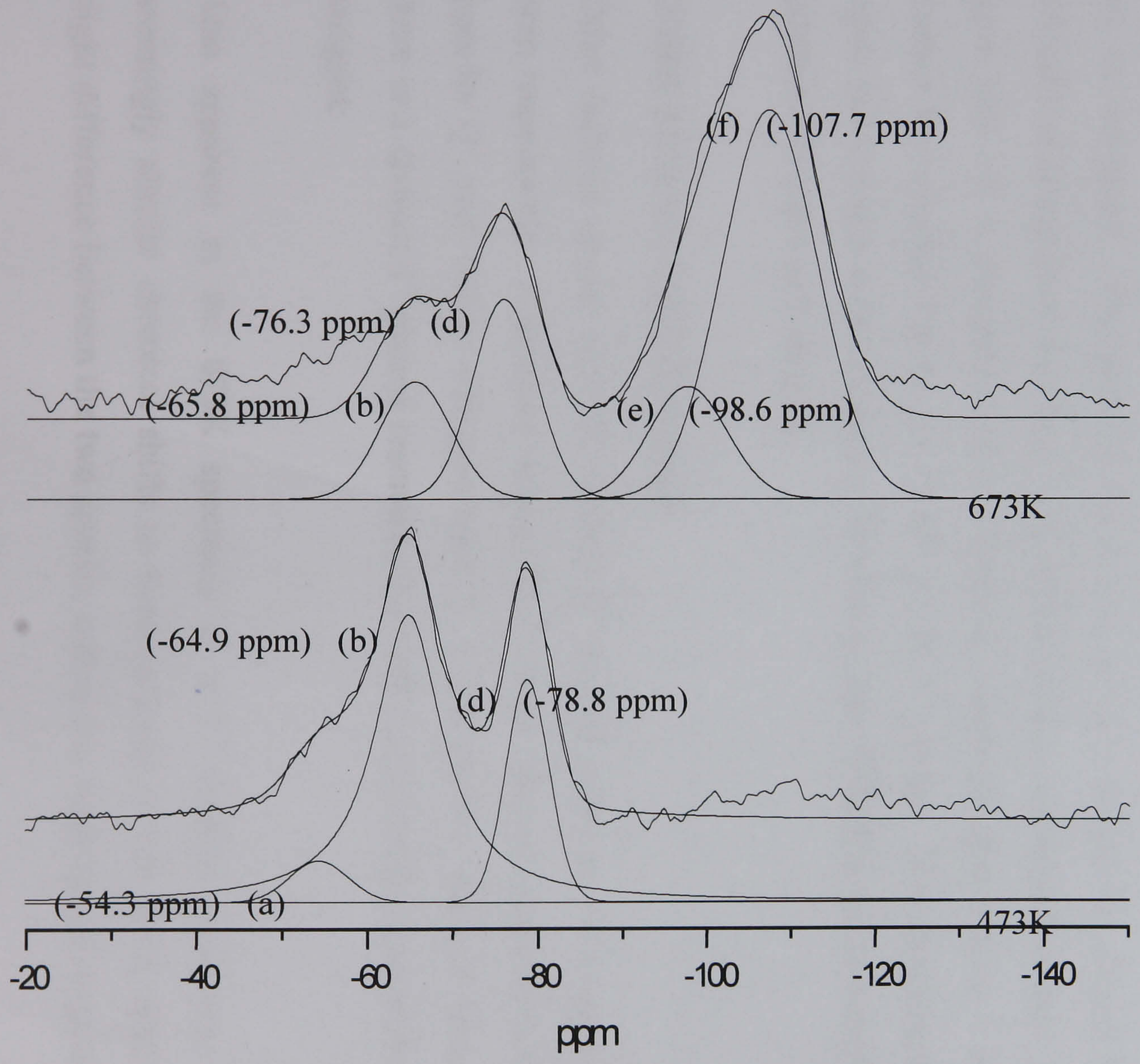

FIGURE 4.8 – Deconvolution of ^{29}Si NMR spectra and possible Si coordinations.

(a) T^2 (methyl)	**(b) T^3 (methyl)**
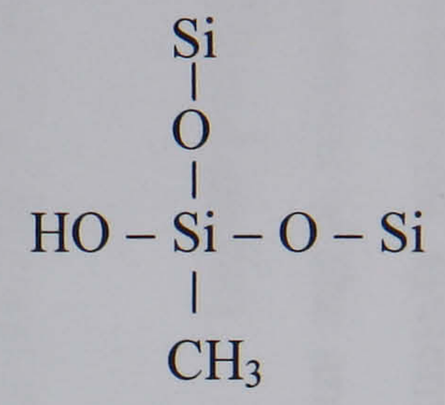	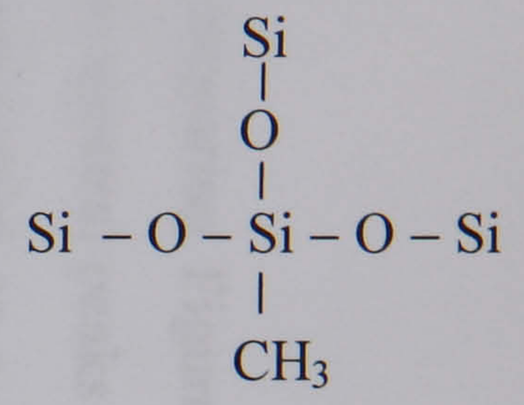
	(d) T^3 (phenyl)
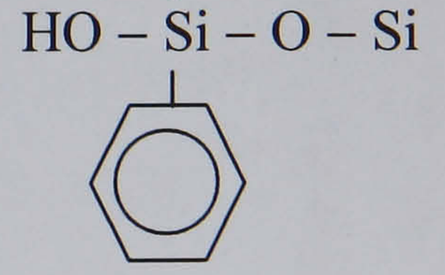	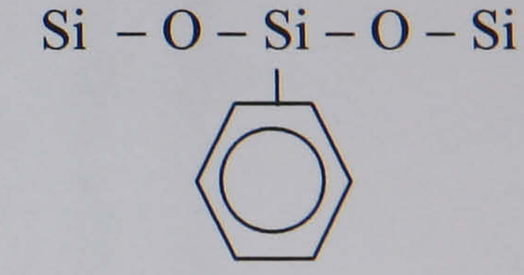
(e) Q^3	**(f) Q^4**
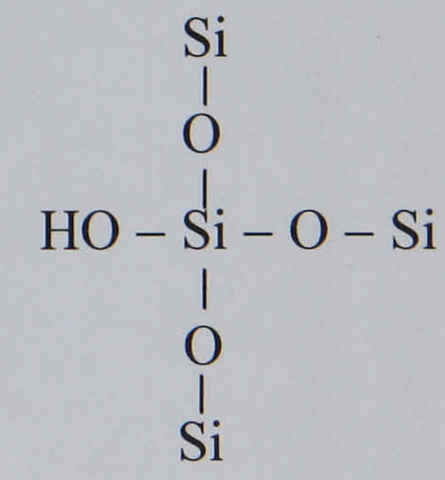	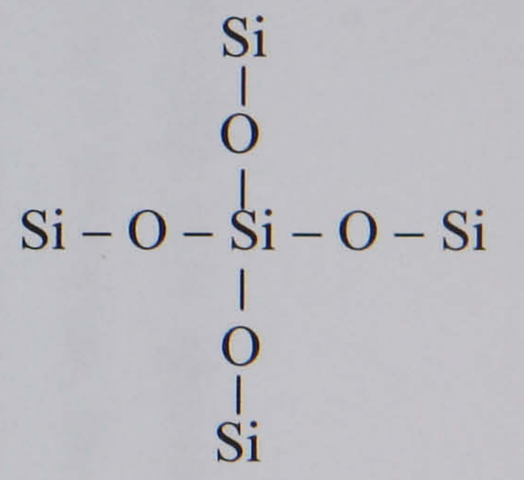

Comparing Figure 4.10 with the spectra presented previously, it is apparent that the spectral peaks were much broader than with the ^{13}C NMR. However, this is not unexpected as a FWHM of the order of 10-20 ppm is characteristic of highly disordered systems. In this instance, the high degree of disorder is an intrinsic property of the amorphous silica itself. (Arising from the extremely variable Si-O-Si bond angle).

Salient Features of 523K Specimen

From inspection of Figure 4.10, at 523K peaks appear at -54.3 ppm and -64.9 ppm respectively. These are thought to be the methyl T^2 and methyl T^3 species respectively. (Literature values for these species range from -54 to -56 ppm and -61 to -66 ppm). The peak at -78.8 ppm is taken to be the phenyl T^3 species. (Smaihi *et al* reported that the T^3 (phenyl) resonance occurred between -77 and -80 ppm [6]). It is probable that a T^2 phenyl resonance also occurs – however, it cannot be resolved due to the width of the T^3 peaks. This conclusion is based upon the fact that in the absence of methyl groups, Smaihi *et al* observed T^2 and T^1 peaks at -70 ppm and -62 ppm.

Salient Features of 673K Specimen

Other features appear at 673K, namely Q^4 and Q^3 peaks at -107.7 ppm and -98.6 ppm respectively. (Literature values [5] for these features range from -98 to -100 ppm for Q^3, and -105 to -110 ppm for Q^4). In the spectral range of -50 to -92 ppm, there is a distinct T^3 phenyl resonance for both temperatures represented by these samples.

Also apparent in the 673K specimen is a T^3 methyl resonance exhibiting seemingly similar chemical shifts to those present in the 523K specimen. The slight difference between the two spectra within this range can be explained by the

differences in the absolute amount of T^2 phenyl that is actually present at both of the pyrolysis temperatures represented. Also, the ratio of the peaks' intensities between T^3 methyl and T^3 phenyl is greatly reduced in the 673K specimen as compared to the 523K sample. This is a corollary to the previous conclusion that the methyl ligand is mostly removed from the siloxane at this temperature. (In this temperature domain, the presence of T^2 phenyl and T^2 methyl species might still be significant in terms of membrane performance. However, it is not possible to reliably determine their presence- or absence – from the spectrum of this temperature illustrated in Figure 4.4. This is due to the limitations of spectral broadening and poor signal to noise ratio for these species).

4.2.4.2 ^{29}Si MAS NMR of Borosilicate Systems

The ^{29}Si MAS NMR spectra at various pyrolysis temperatures of the xerogel of the most successful sol for membrane synthesis (see chapter 5) are presented in Figure 4.11.

As previously, Gaussian-Lorentzian functions were used to calculate the positions and intensities of the peaks revealed in the deconvolution analyses of these results, and are presented in Figure 4.12.

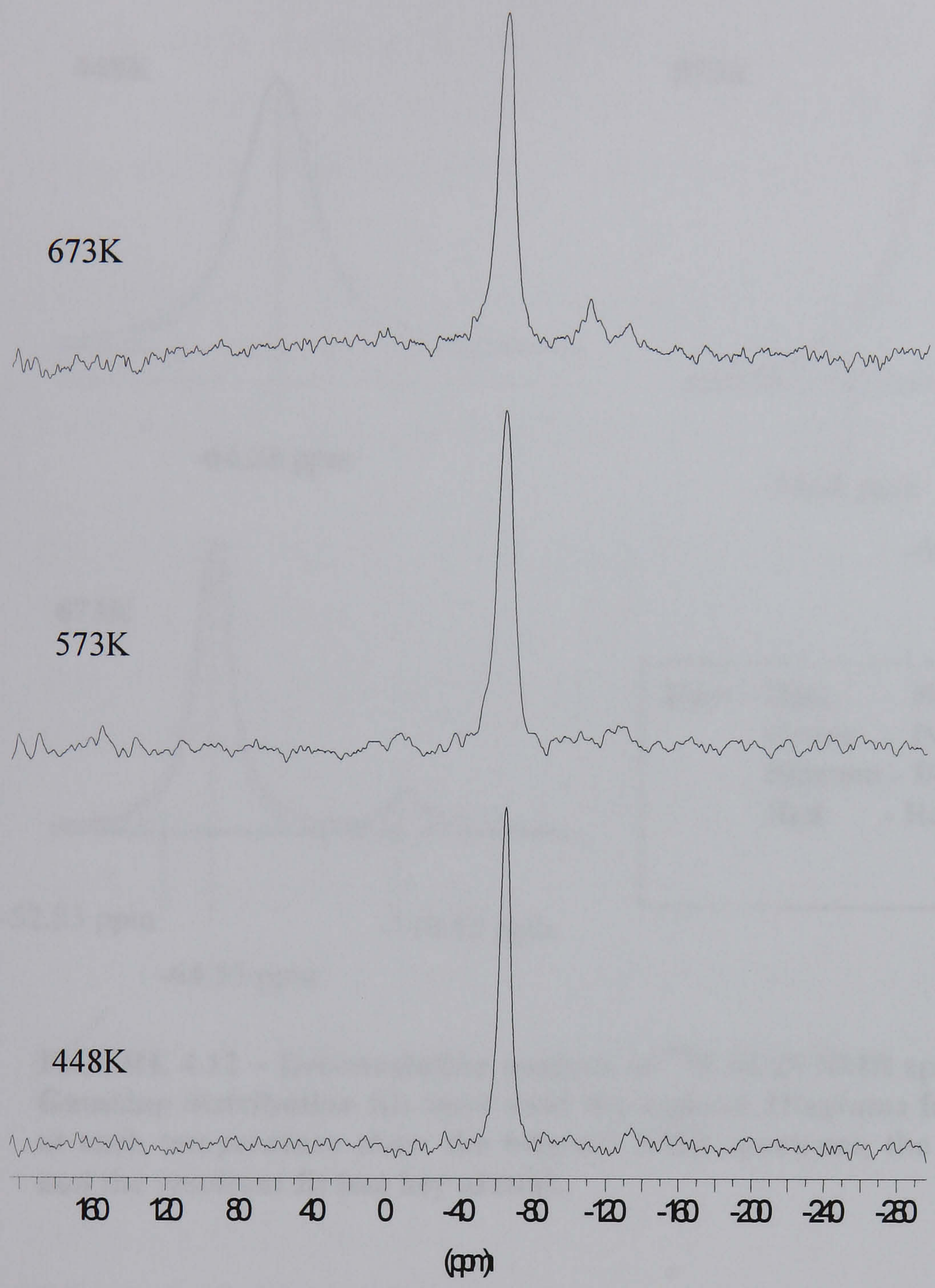

FIGURE 4.11 – ^{29}Si MAS NMR Spectra of 20:80 PBA: MTMOS at various pyrolysis temperatures

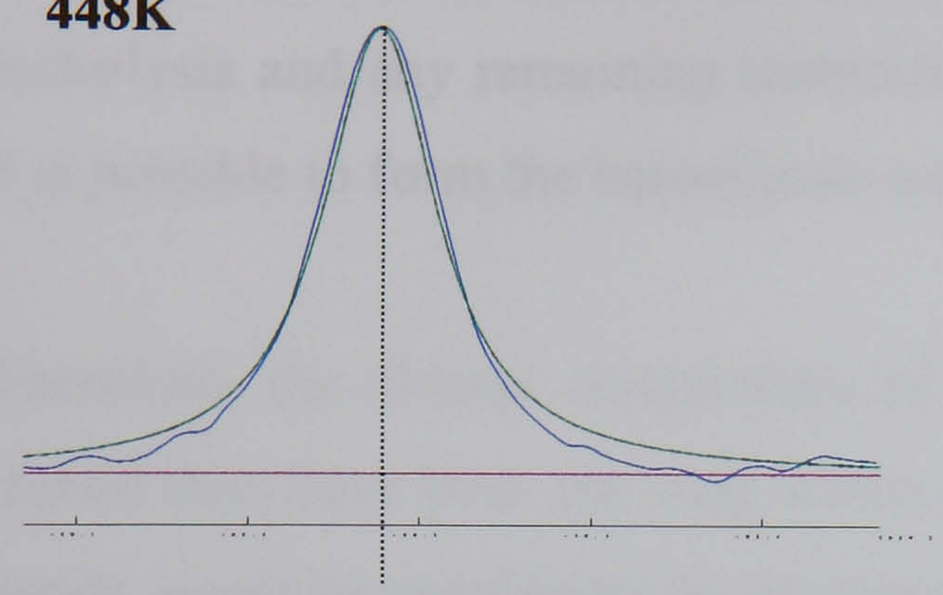

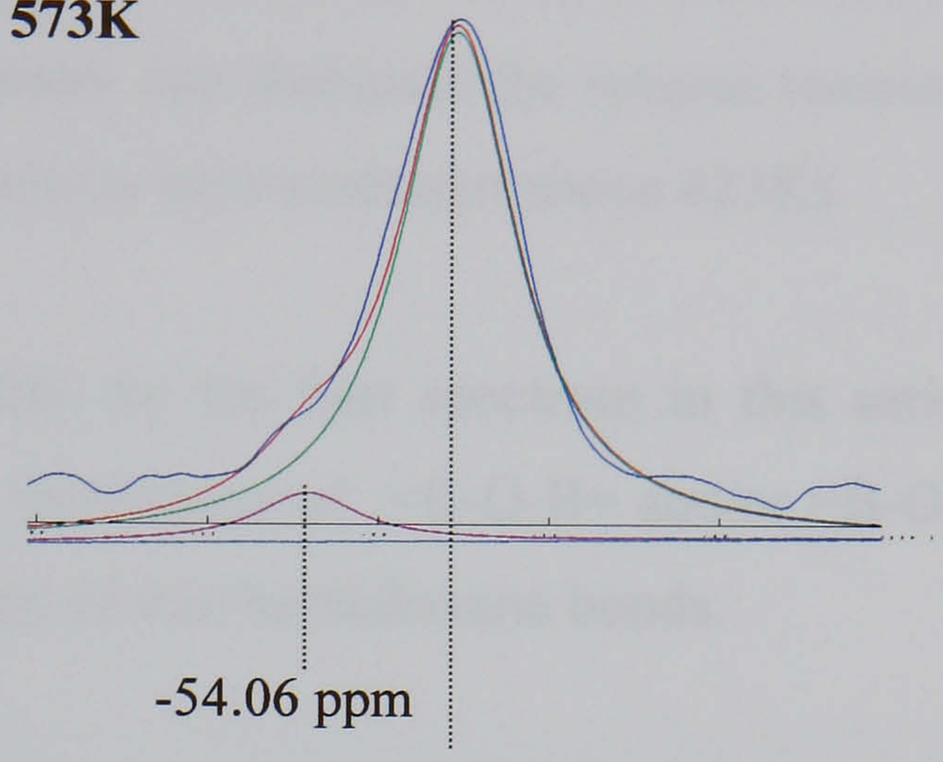

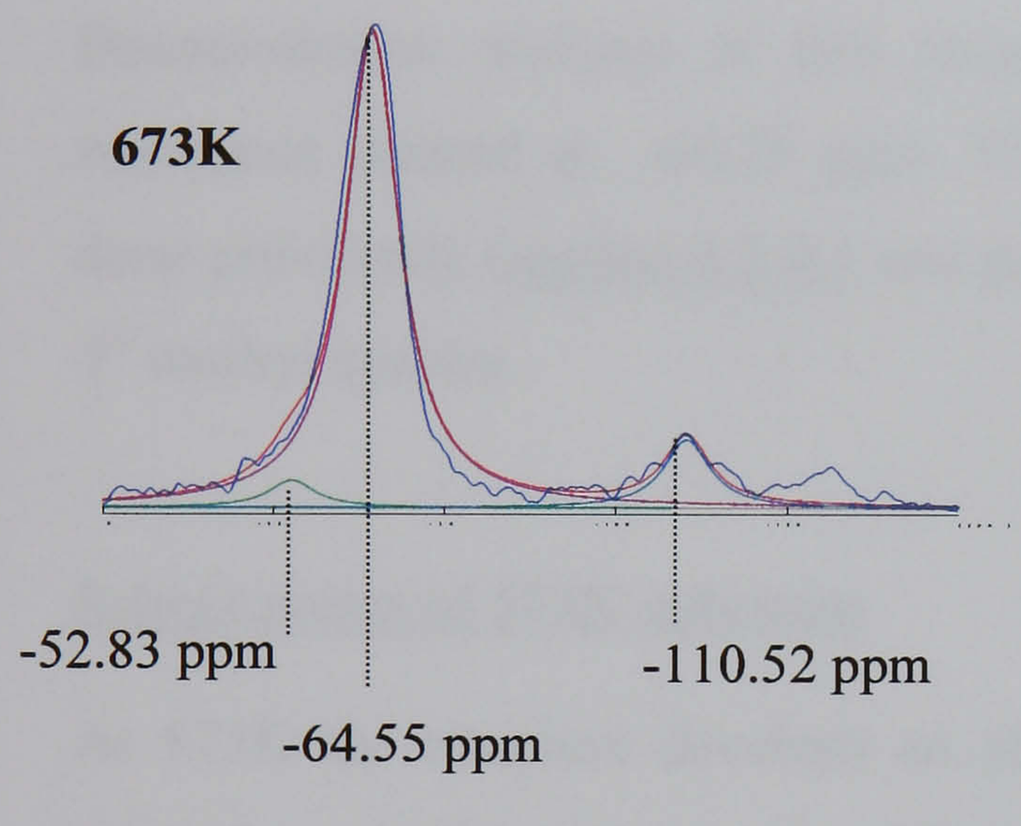

Key: **Blue - NMR Spectrum**
Green - Deconvoluted Peak
Maroon - Deconvoluted Peak
Red - Resultant Fit

FIGURE 4.12 – Deconvolution analysis of ^{29}Si MAS NMR spectra of Figure 4.11. Gaussian distribution fits were used throughout. Diagrams for the deconvolution at each temperature show the original NMR spectrum, the deconvoluted peaks and the resultant fit (see key above).

Salient points of 448K spectrum

From inspection of Figure 4.12 one can see that there is a continuous evolution of the structure with temperature. The initial pyrolysis temperature was chosen, as it is above the threshold where excess solvent and water should have been removed from the xerogel.

(The condensation reaction in borosilicates occurs via the cross-links between Si and B atoms resulting in the formation of =B-O-Si≡ bonds. However, as hydrolysis and any remaining molecular water can dominate the reverse reaction, it is possible to form the borosilicate network by heat treatment above 423K).

Therefore, the chosen temperature of 448K for the first spectrum in this series should then have been the cusp where the dominance of =B-O-B= and/or =B-OH bonds would be supplanted by the formation of true borosiloxane bonds.

Deconvolution analysis at this temperature reveals the presence of a single resonance centred at -64.28 ppm. With reference to the deconvolution analyses done previously (section 4.2.4.1 and fig. 4.10) this peak was identified as being the T^3 methyl species.

Salient points of 573K spectrum

At 573K the structure develops an additional feature: relatively small resonance centred at –54.06 ppm. Again, with reference to section 4.2.1 and fig.4.8 this was identified as being the T^2 methyl species.

Salient points of 673K spectrum

This temperature was chosen as it represented the usual peak pyrolysis temperature when synthesising membranes from the sol. From inspection of Fig. 4.9(a), it can be seen that in addition to the two structures represented by the peaks in the 573K spectrum, there now appears a small resonance that has emerged at -110.52 ppm. Cross-referencing to the summary of species in fig 4.8 has identified this peak as indicating the presence of the SiO_4 Q^4 species.

4.2.5 Comparison between borosilicate and non-borosilicate ^{29}Si NMR

The non-borosilicate and borosilicate systems examined above differ chemically. The former is a co-polymer between methyl and phenyl based silanes (PTMOS and MTMOS), whilst the latter results from the mixture of a boron-containing phenyl based organic precursor and a methyl based silane (PBA and MTMOS respectively). Therefore, one would not expect to observe any phenyl species in the ^{29}Si MAS NMR spectra of the borosilicate system.

(It is appropriate to emphasise at this point, that Q species cannot be formed by the hydrolysis of T precursors. As the pyrolysis process described in chapter 2 occurs in air, then the CH_3 groups combine with oxygen at around 520K. An OH then replaces the CH_3 group and the combustion by-products are CO_2 and H_20).

However, there is a crucial empirical difference in the borosilicate system and the non-borosilicate system examined in section 4.2.1. From examination of the series of ^{29}Si spectra illustrated in figs. 4.9 and 4.9(a) there was the apparent absence in the evolution with temperature of the borosilicate system of any SiO_3OH Q^3 sites. This is unexpected, as one might assume that the SiO_3OH Q^3 species would precede the formation of the SiO_4 Q^4 species within a regime of constantly increasing temperature.

There are two possible rationales, which singly (or in combination) may account for this difference between the two systems:

- If any quantity of the SiO_3OH Q^3 species was present in the spectra presented in fig. 4.9 and 4.9(a) then they were below the level of background noise. If this is the case, then many than usual more data-acquisitions by the spectrometer would be necessary to obtain a reasonable signal intensity.

- Another possibility that presents itself is that, as mentioned previously in section 4.1, the borosiloxane bond itself is unstable and can lead to precipitates. One such is boric acid and its presence would make the borosilicate solution more acidic. Consequently, a more acidic condition would make the condensation reaction proceed more quickly and thereby increase the number of Q^4 sites.

4.3 Characterisation via FTIR spectroscopy

4.3.1 FTIR Analysis of Non Borosilicate System

The same specimens of methyl/phenyl xerogels (representing key pyrolysis temperatures) that were exposed to NMR spectroscopy were also studied using FTIR spectroscopy. These spectra are presented below in Figures 4.13 and 4.14. Also presented below in Table 4.1, is a key for the main IR absorption frequencies which are relevant for these xerogels.

Wavenumber (cm^{-1}) at: 523K	673K	873K	Vibration Assignment
694	694	-	Benzene ring with 5 adjacent H atoms
737	737	-	Benzene ring with 5 adjacent H atoms
786	787	797	Si – O
993	1015	1043	Si – O
1250	-	-	Si – CH_3
1380	-	-	CH_3
1413	-	-	O – H (bending)
1429	1429	-	Benzene ring
1462	-	-	CH_3
1593	1593	-	Benzene ring
2829-3124	-	-	OCH_3

TABLE 4.1 – A summary of the FTIR adsorption assignments at key pyrolysis temperatures, based on a 30/70 PTMOS:MTMOS xerogel (r = 4).

The designation of each frequency to represent a specific chemical feature and molecular vibration was accomplished by contrasting the spectrum of a phenyltrimethoxysilane xerogel with that of a methyltrimethoxysilane xerogel. Finally, reference was made to IR literature values [4] [7].

As a complementary technique to NMR, FTIR spectroscopy supplements the NMR findings very well. Common results to both techniques were the retention of the phenyl ligand at 673K and removal of the methyl ligand at the same temperature.

It was also confirmed that at 673K that other organic remnants (such as methoxy groups) had also been removed. In addition, it was shown more clearly than was possible with NMR, that the amounts of hydroxyls present were greatly reduced.

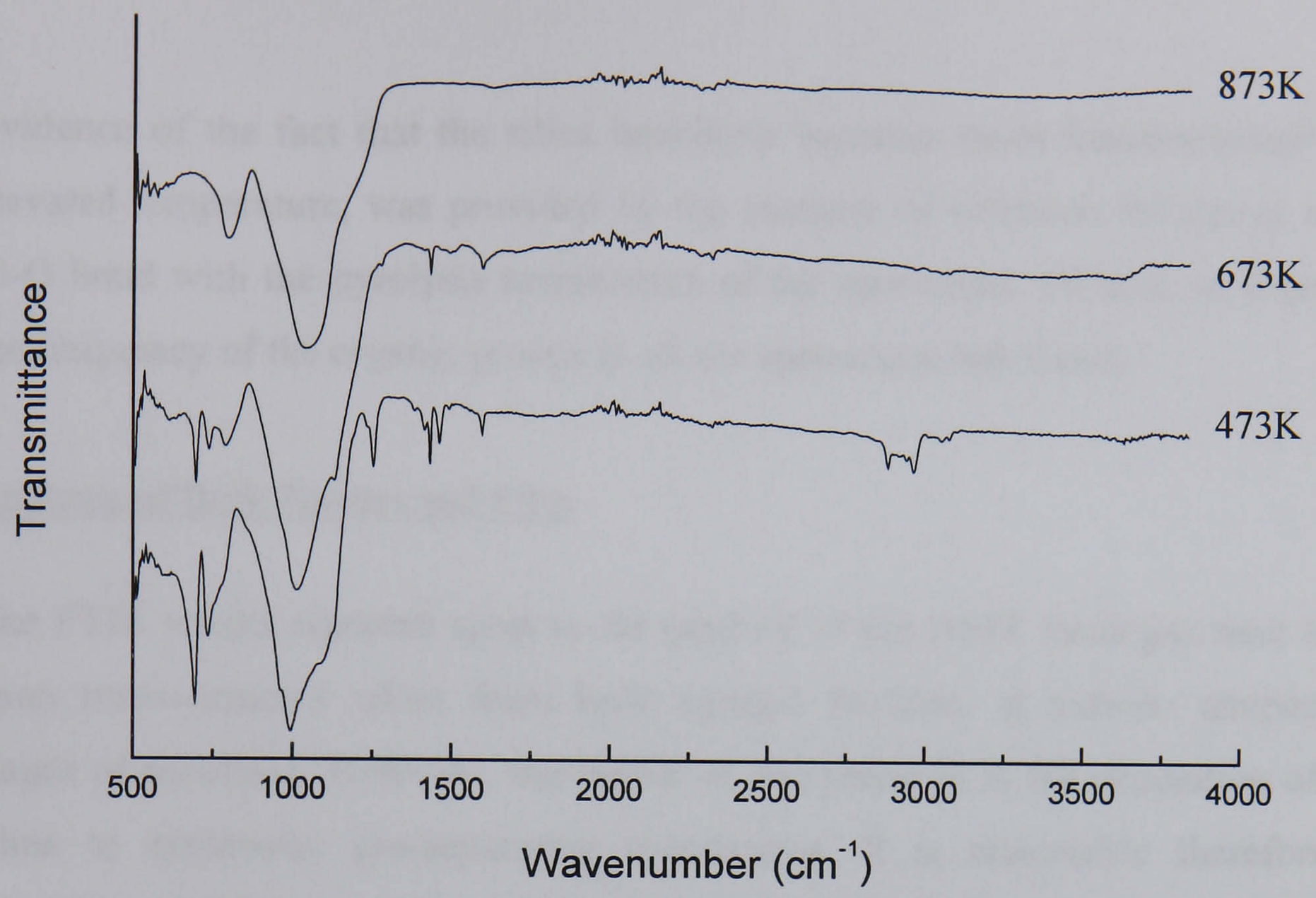

FIGURE 4.13 – FTIR spectra of a 30/70 PTMOS/MTMOS xerogel (r = 4) at key pyrolysis temperatures.

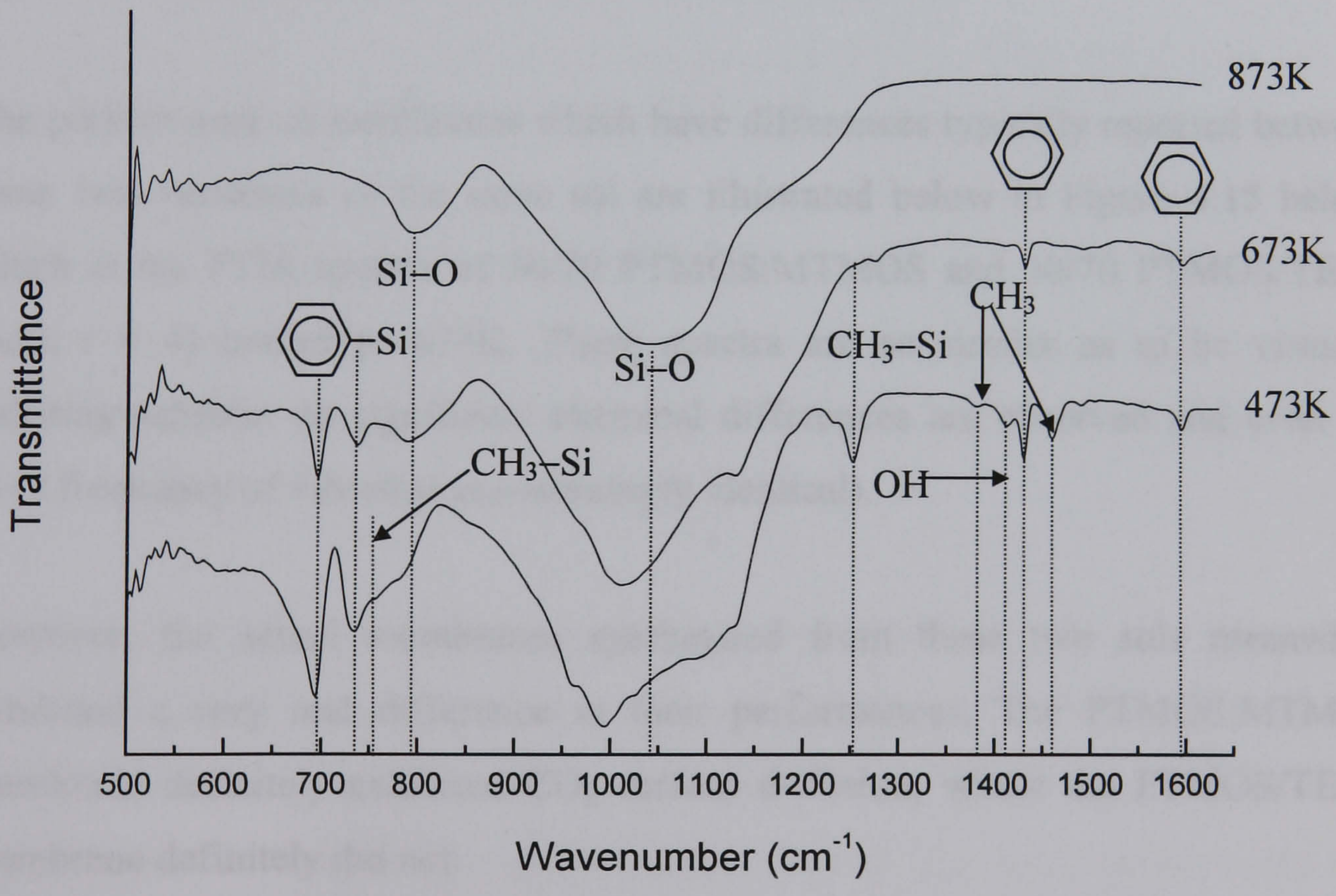

FIGURE 4.14 – FTIR spectra of a 30/70 PTMOS/MTMOS xerogel (r = 4) at key pyrolysis temperatures in the fingerprint region.

Evidence of the fact that the silica backbone becomes more interconnected with elevated temperature, was provided by the increase of vibration frequency of the Si-O bond with the pyrolysis temperature of the specimens. (Whilst, as expected, the frequency of the organic groups in all the specimens was fixed).

Analysis of Bulk Powder and Film

The FTIR results reported upon so far (and all of the NMR findings) were based upon measurements taken from bulk xerogel powders at various temperature stages of pyrolysis. However, the theme of this research is the deposition of thin films to synthesise gas-separating membranes. It is reasonable therefore, to consider whether or not this approach of analysing the bulk xerogel powders truly reflects the nature of a deposited thin film of the same sol.

The performance of membranes which have differences typically reported between these two variations of the same sol are illustrated below in Figure 4.15 below, which is the FTIR spectra of 30/70 PTMOS:MTMOS and 30/70 PTMOS/TEOS (both r = 4) heated to 673K. These spectra are so similar as to be virtually indistinguishable: no significant chemical differences are observed and even the Si-O frequency of vibration are seemingly identical).

However, the actual membranes synthesised from these two sols meanwhile exhibited a very real difference in their performances. The PTMOS:MTMOS membrane definitely exhibited CO_2 surface diffusion, whilst the PTMOS/TEOS membrane definitely did not.

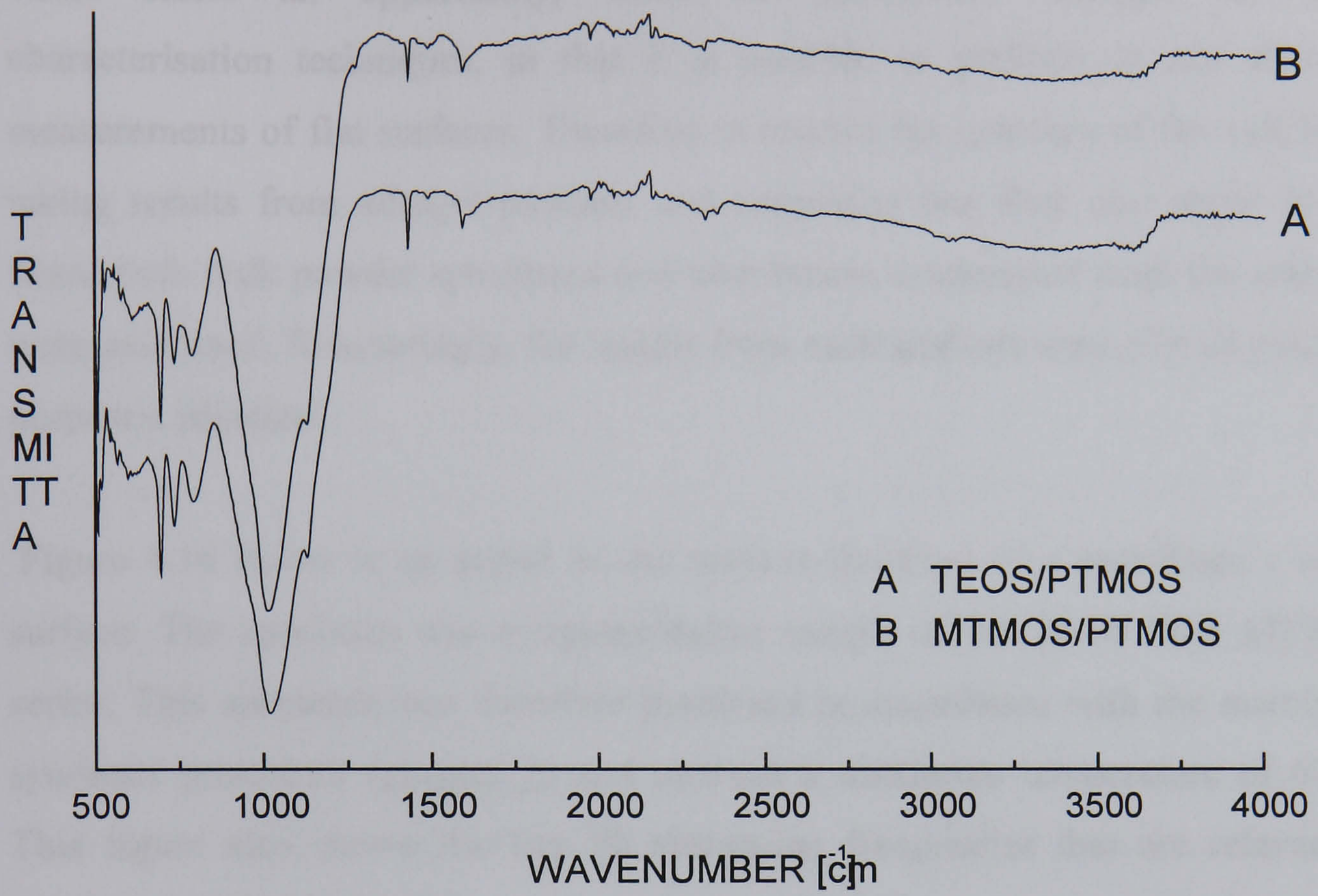

FIGURE 4.15 – A comparison of FTIR spectra obtained from TEOS/phenyl and methyl/phenyl xerogel heated to 673K (both r = 3).

4.3.2 FTIR Analysis of Borosilicate Systems

The FTIR analysis of the borosilicate system concentrates upon the xerogels of the sol which gave the best results in terms of membrane performance and durability: the 20:80 PBA: MTMOS composition.

As discussed in the end of the previous section, all of the FTIR and NMR results reported upon so far were based upon measurements taken from bulk xerogel powders. Concern was expressed as to whether or not it was valid to analyse bulk xerogel powders and assume that the results would also apply to deposited thin films of the same sol.

FTIR offers an opportunity, which is uncommon amongst the usual characterisation techniques, in that it is possible to perform *in situ* chemical measurements of flat surfaces. Therefore to resolve the question of the validity of taking results from xerogel powders and supposing that they also apply to thin films, both bulk powder specimens and membranes synthesised from the same sol were examined. Reassuringly, the results from each analysis were, for all practical purposes, identical.

Figure 4.16 below is an actual *in situ* surface-spectrum of a membrane's active surface. The specimen was a representative sample of the 20:80 PBA MTMOS series. This specimen was therefore pyrolysed in accordance with the membrane synthesis procedure (chapter 2) and attained a maximum temperature of 673K. This figure also shows the key IR absorption frequencies that are relevant to hybrid borosilicate gels [4].

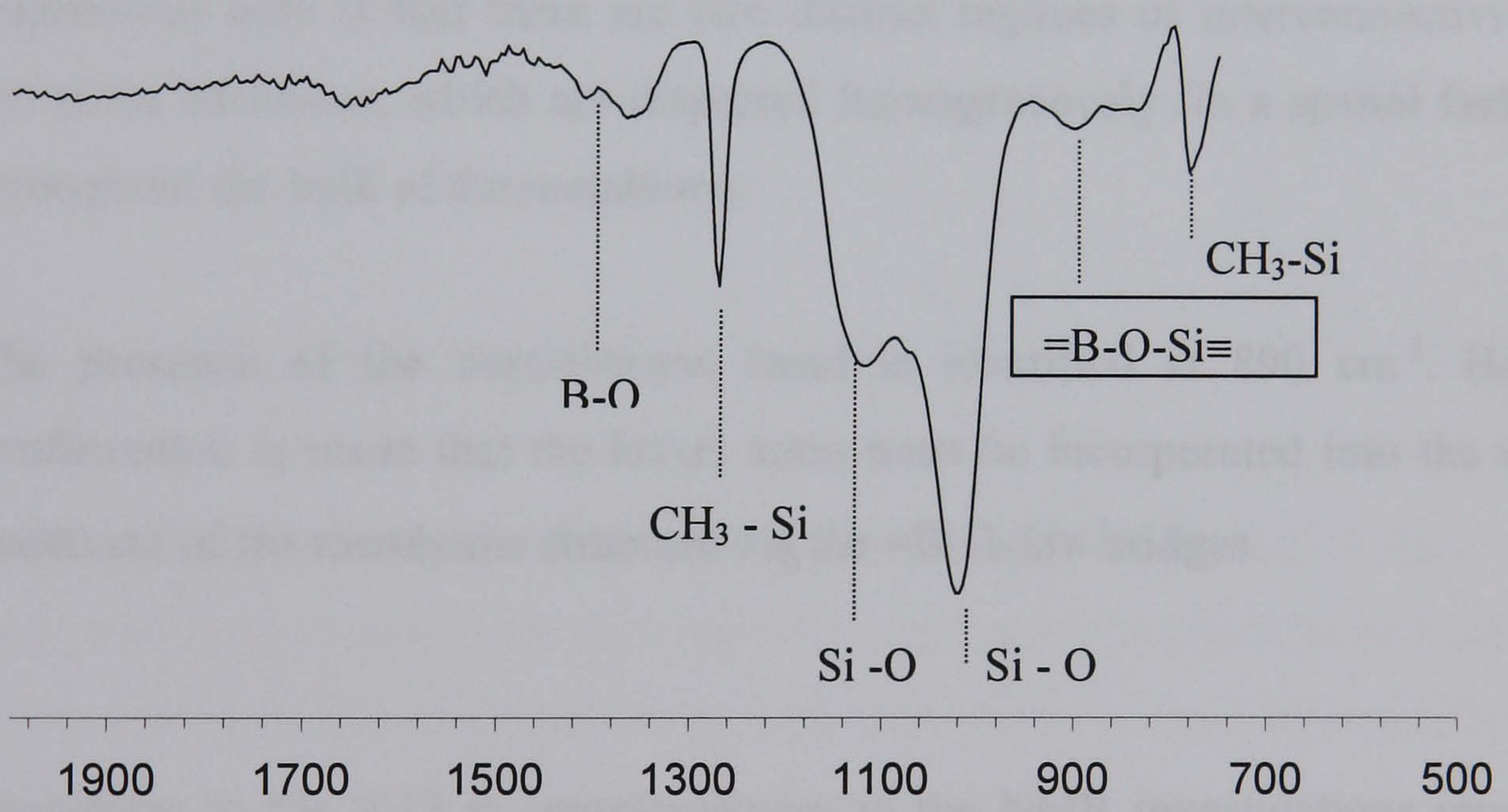

FIGURE 4.16 – *in situ* FTIR of the actual flat surface of a membrane synthesised from 20: 80 PBA: MTMOS sol pyrolysed at 673K. (This spectrum does not significantly differ from FTIR spectrum of bulk xerogel powder that had been exposed to the same thermal processing).
NB: The scale appears reversed compared to other FTIR spectra. However, this was the format of the spectrometer's report.

There are several points of interest concerning the spectrum presented in Figure 4.16:

1) Firstly, the presence of the B-O bond is confirmed by the absorbance band between 1500 to 1300 cm^{-1}. This is the initial test of whether or not there is actually any boron is present in the sample – especially as a decrease in the boron content of this class of sol during drying and gelation is common.

2) The presence of the Si-O bond is indicated by two well-defined troughs at 1120 and 1015 cm^{-1} respectively. The curious aspect of this result in comparison with the non-borosilicate spectra illustrated in the previous section is that there is no broadness or spectral spreading. In fact, the opposite appears to be the case, there are two sharply defined Si-O absorbance frequencies. The implication here is that there are two distinct regimes of interconnectivity of the silica backbone, which are dispersed homogeneously (in a spatial fashion) throughout the bulk of the membrane.

3) The presence of the borosiloxane bond is identified at 890 cm^{-1}. Hence, confirmation is made that the boron atom must be incorporated into the silica backbone of the membrane structure via the =B-O-Si≡ bridges.

The spectrum in fig. 4.13 is complementary to the NMR investigations reported previously. In some ways it offers a more refined approach to analysing the structure of a membrane as it can directly analyse the chemical structure of a membrane *in situ*. In addition, the direct observation of such structures as the borosiloxane bond is probably easier to accomplish via this type of spectroscopy.

The most intriguing aspect of Figure 4.16 is the identification of two distinct classes of Si-O bond. It is suggested that this is due to the presence of boron increasing the interconnectivity of the silica network via B-O-Si bridges. The reason for the two distinct classes of interconnectivity could then be due to the simple fact some domains within the network contained boron whilst others did not.

The molar ratios of this sol of boron to silicon were 20:80 and it is usual for some of the boron content of this class of sol to be lost during drying and gelation. If one postulates that boron was responsible for the formation of the higher order of interconnectivity of the silica backbone, then it would be expected that only the minority of the Si atoms would benefit from this enhanced cross-linking. From inspection of Figure 4.16 this would indeed appear to be the case. The depth of the absorbance trough of the Si-O frequency representing a higher order of interconnectivity of the silica backbone (1120 cm^{-1}) is much less than that of the Si-O absorbance frequency representing a lower order of interconnectivity.

4.4 Thermal Analysis

Thermal analysis is the standard tool for characterising the chemical changes that a xerogel might experience when exposed to a continuous increase in temperature. In the context of this investigation, it is used to provide baseline measurements of gross chemical changes to support (or otherwise) the conclusions presented previously within this chapter.

4.4.1 Silanes.

Figure 4.17 below pertains to the two silanes that were used for synthesising the most successful membranes. (Both non-borosilicate and borosilicate systems). Illustrated below, are the main temperature regions where major mass loss in both PTMOS and MTMOS actually occurred.

In this instance, precise quantification of mass-losses can be somewhat problematic. This is because mass is actually lost from two sources: by the pyrolysis of the organic template and from the removal of additional organic compounds such as the methoxy and hydroxyl groups. Hence, care must be taken when attempting to quantify the amount of template removed within a given temperature region. With this caveat in mind, the figures for the weight losses portrayed in Figure 4.17 are summarised in Table 4.2 below.

	Total weight loss observed (%) (20 - 800°C)	Theoretical weight loss of the fully condensed xerogel (%)
MTMOS	16.0	10.5
PTMOS	38.2	53.5

TABLE 4.2 – A comparison between the weight loss observed with that expected for a fully condensed material, for MTMOS and PTMOS precursors.

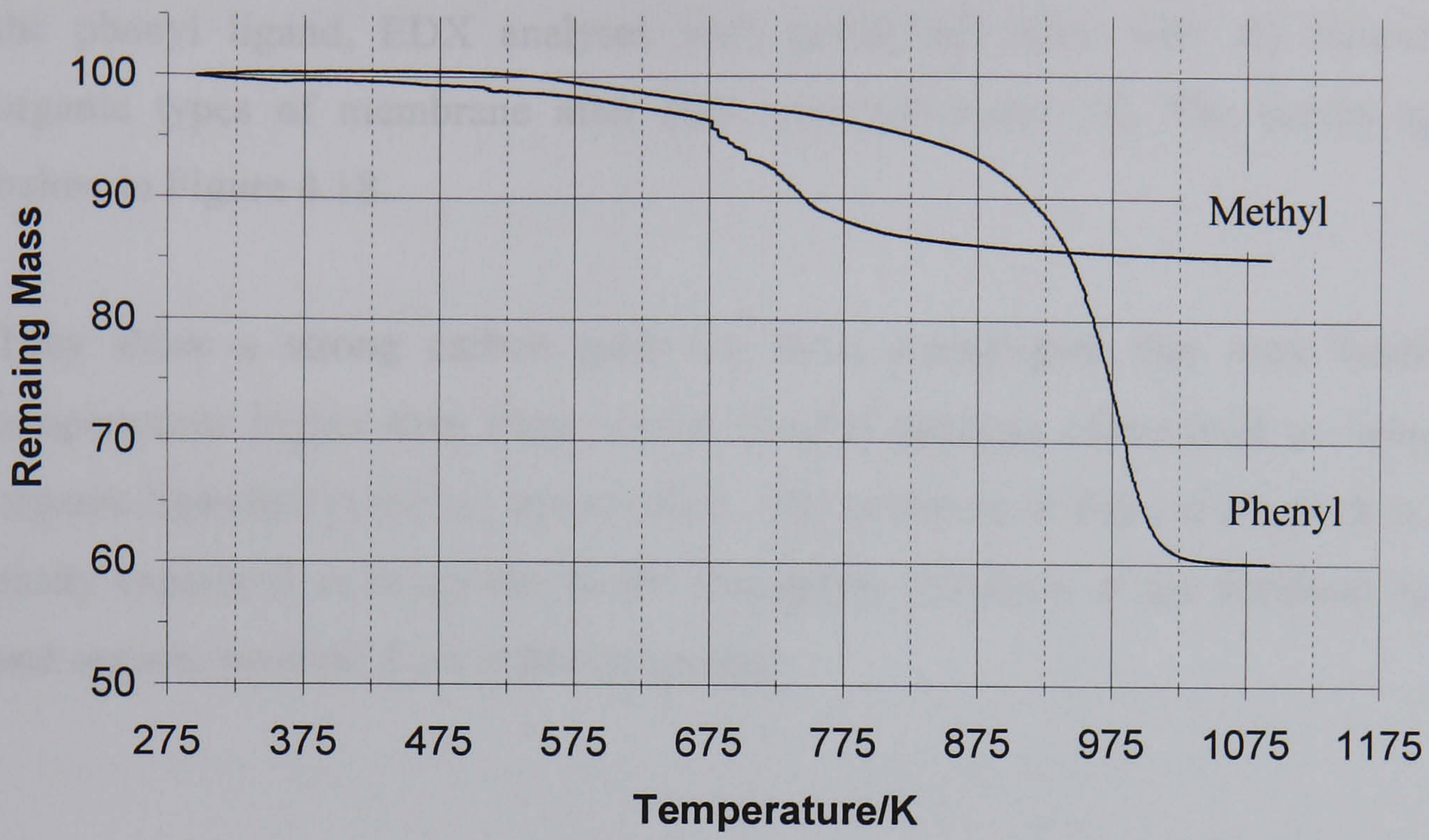

FIGURE 4.17 – TGA thermograms of MTMOS and PTMOS in air.

The calculation of the theoretical mass loss (as mentioned in Table 4.2) is based upon the assumption that xerogel contains no methoxy or hydroxyl groups. The results of these calculations are then cross-referenced with the empirical observations of mass loss.

One conclusion from the data presented in Table 4.2 is that the PTMOS xerogel does not experience a high enough loss of mass to be consistent with all of the carbon actually being removed from within the phenyl ligand. One possible explanation for this inconsistency is that insufficient oxygen is available for complete pyrolysis to occur. (Xerogels derived from PTMOS precursors have been reported to retain a high carbon content when heated in an inert atmosphere [8]).

To test this hypothesis of whether or not carbon was actually being retained within the phenyl ligand, EDX analyses were performed upon both the hybrid and organic types of membrane after they were pyrolysed [9]. The results appear below in Figure 4.18.

They show a strong carbon peak for those membranes that were heated to temperatures higher than those which thermal analysis determined as being the organic ligand(s) pyrolysis temperature. The presence of this carbon peak is most easily explained as being due to the incomplete pyrolysis of the template ligands and organic residual from methoxy groups.

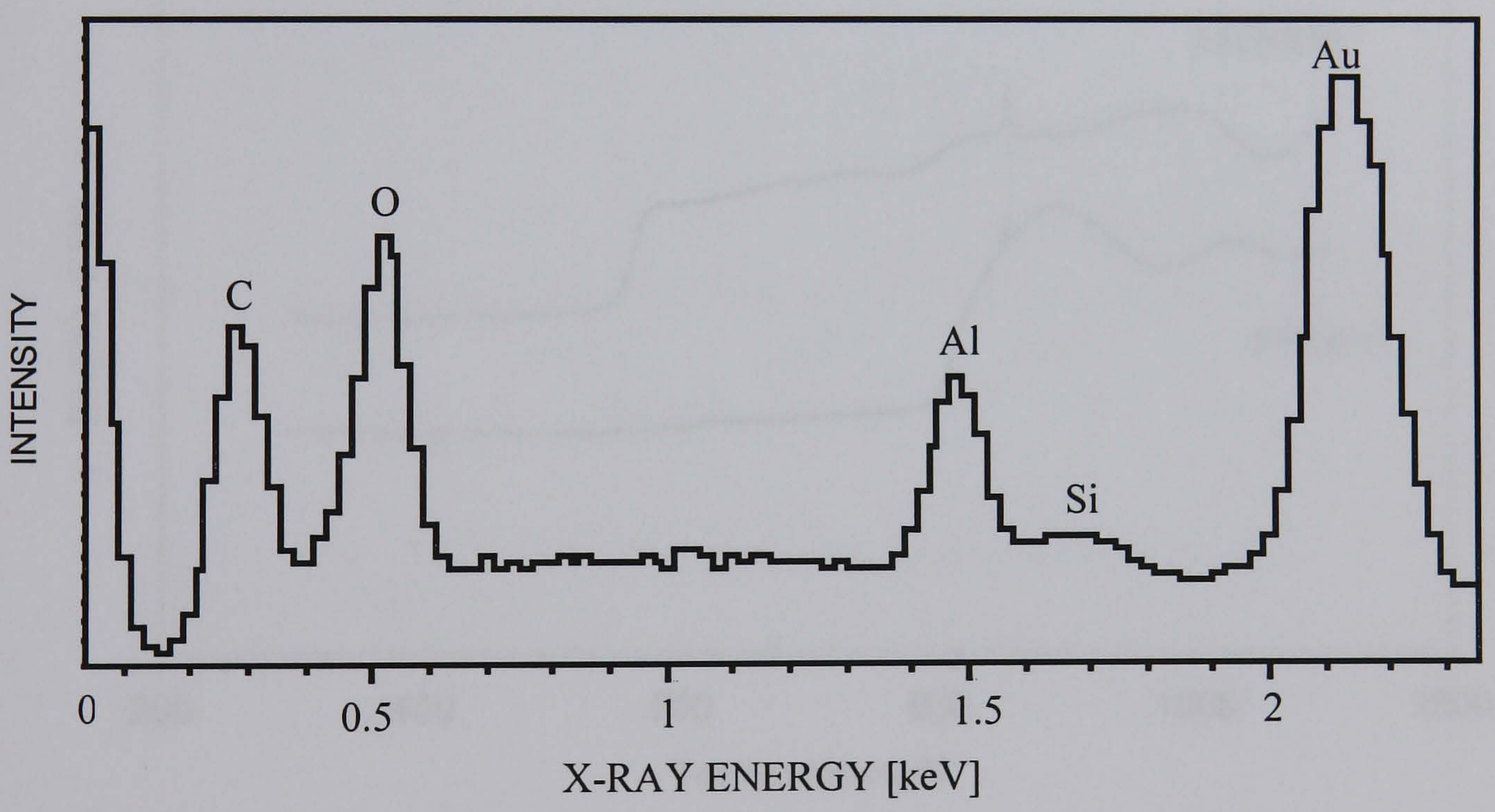

Figure 4.18 – EDX analysis of a membrane derived from MTMOS.

4.4.2 Thermal analysis of a representative non-borosilicate system.

As mentioned in preceding sections, the most successful non-borosilicate membranes were based upon the co-polymerisation of PTMOS and MTMOS silanes in a 30:70 phenyl/methyl ratio.

With this in mind, Figure 4.19 compares and contrasts the DTA thermograms of MTMOS and PTMOS derived xerogels. The principal features are the oxidation of the methyl and phenyl ligands that manifest themselves as large exotherms that appear at 553Kand 793K. (There is another feature that appears at 846K but this is purely an artefact caused by the apparatus's quartz reference).

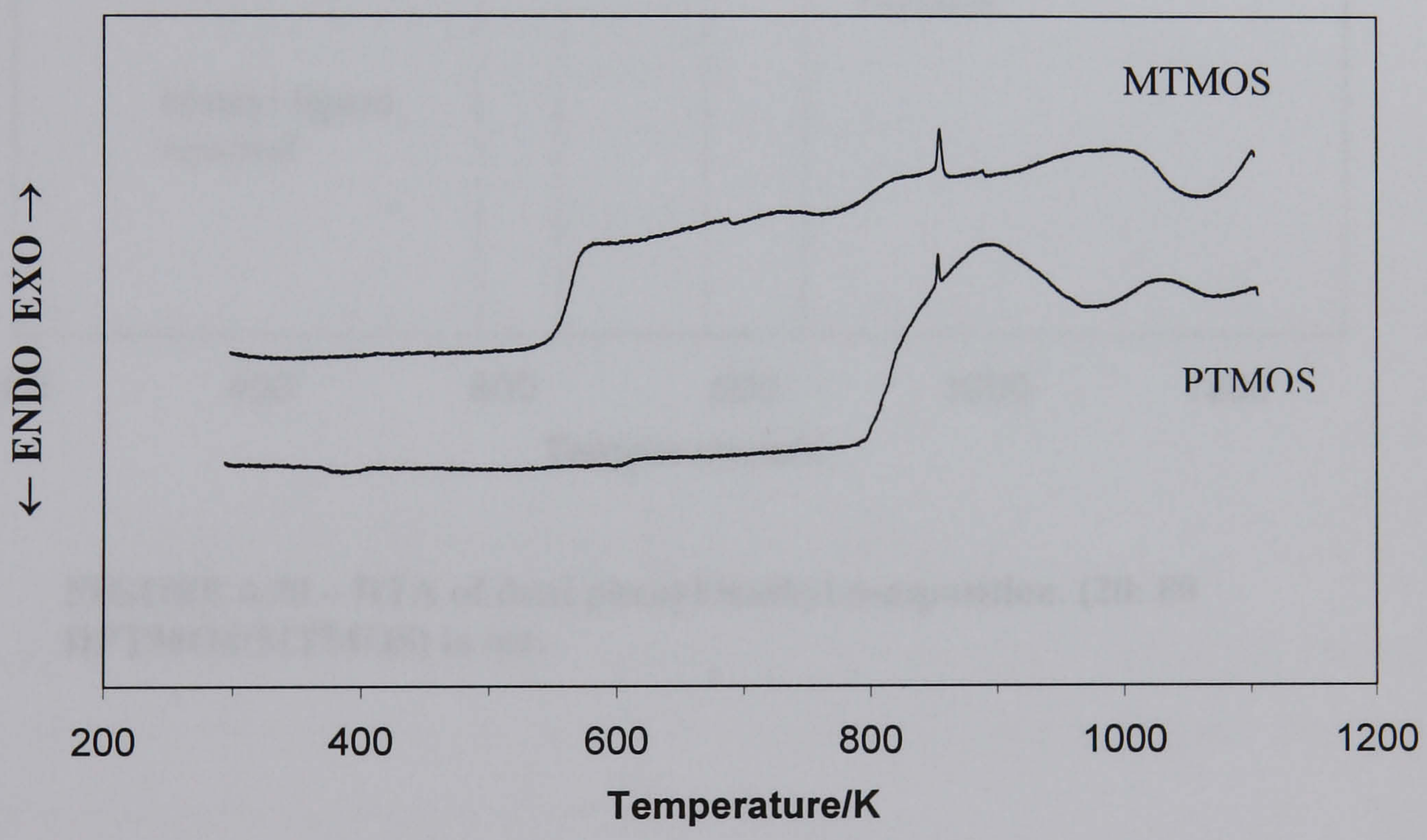

FIGURE 4.19 – DTA of PTMOS and MTMOS xerogel powders in air.

Figure 4.20 below, illustrates the similar thermal behaviour that is observed for those materials that contain both phenyl and methyl groups together.

(However, there is one subtle difference. The observed temperature where mass is lost on a DTA trace is offset by approximately 70K on the corresponding TGA trace. This is because less time is required to measure the breaking of chemical bonds (via DTA) than the much slower process of actual physical removal of the by-products of combustion via diffusion (TGA). This is easily remedied by applying a much slower heating rate but is rather impractical as it would make experiments inconveniently long in duration).

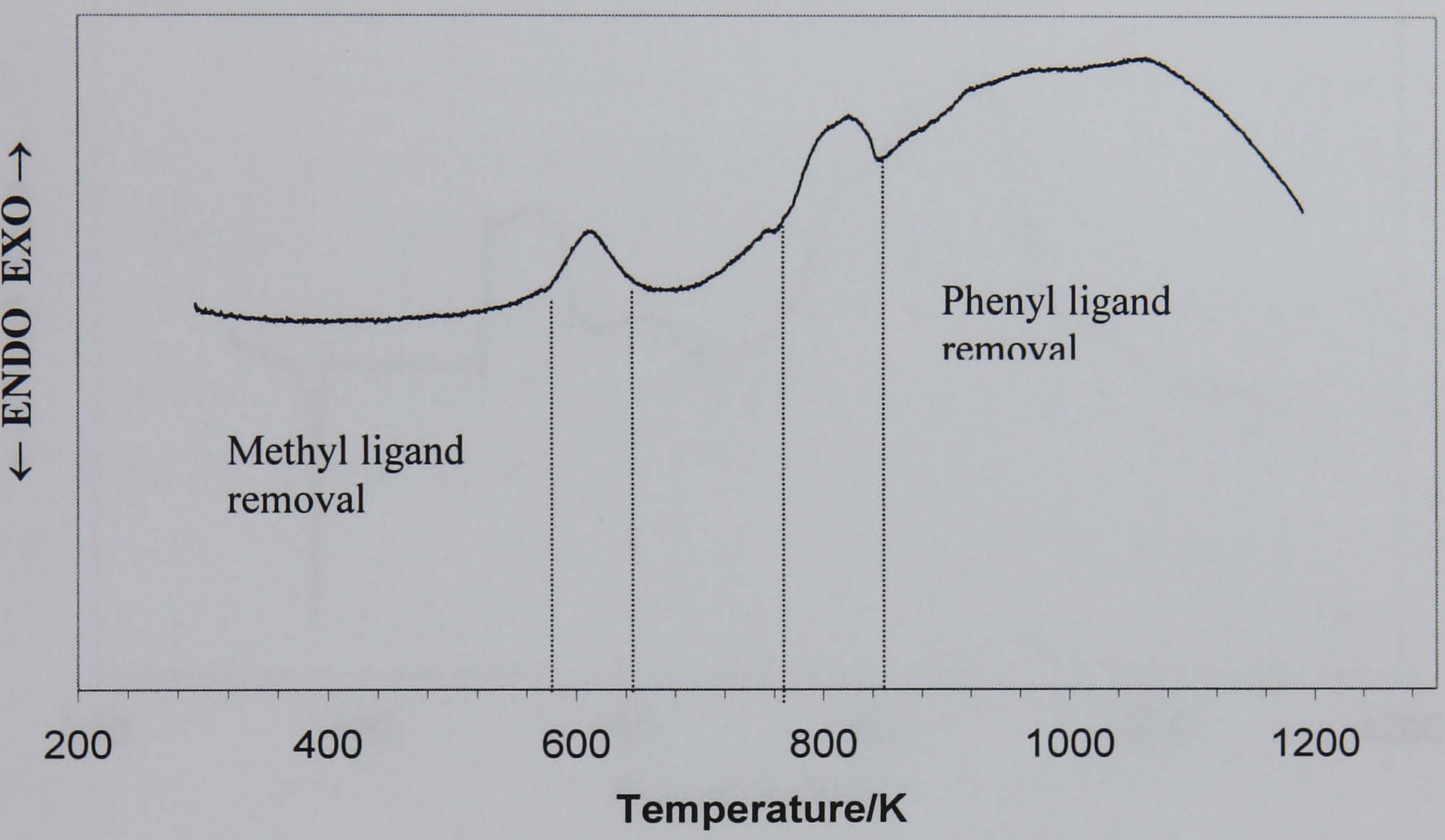

FIGURE 4.20 – DTA of dual phenyl/methyl composition. (20: 80 DPTMOS/MTMOS) in air.

4.4.3 Thermal analysis of a representative borosilicate system.

The most successful borosilicate membranes were synthesised from sols of 20:80 PBA: MTMOS. The analysis of the MTMOS has been detailed above in sections 4.2.1 and 4.2.2._The DTA of a xerogel of this sol is presented below in Figure 4.21.

Knowledge of the thermal conversion process is necessary in order to control the pyrolysis during the membrane synthesis process. From inspection of the DTA trace of Figure 4.21, one can see that long before the glass transition temperature is reached that there were several exotherms occurring at much lower temperatures. These seem indicative of the burning off of chemical groups, whose absence

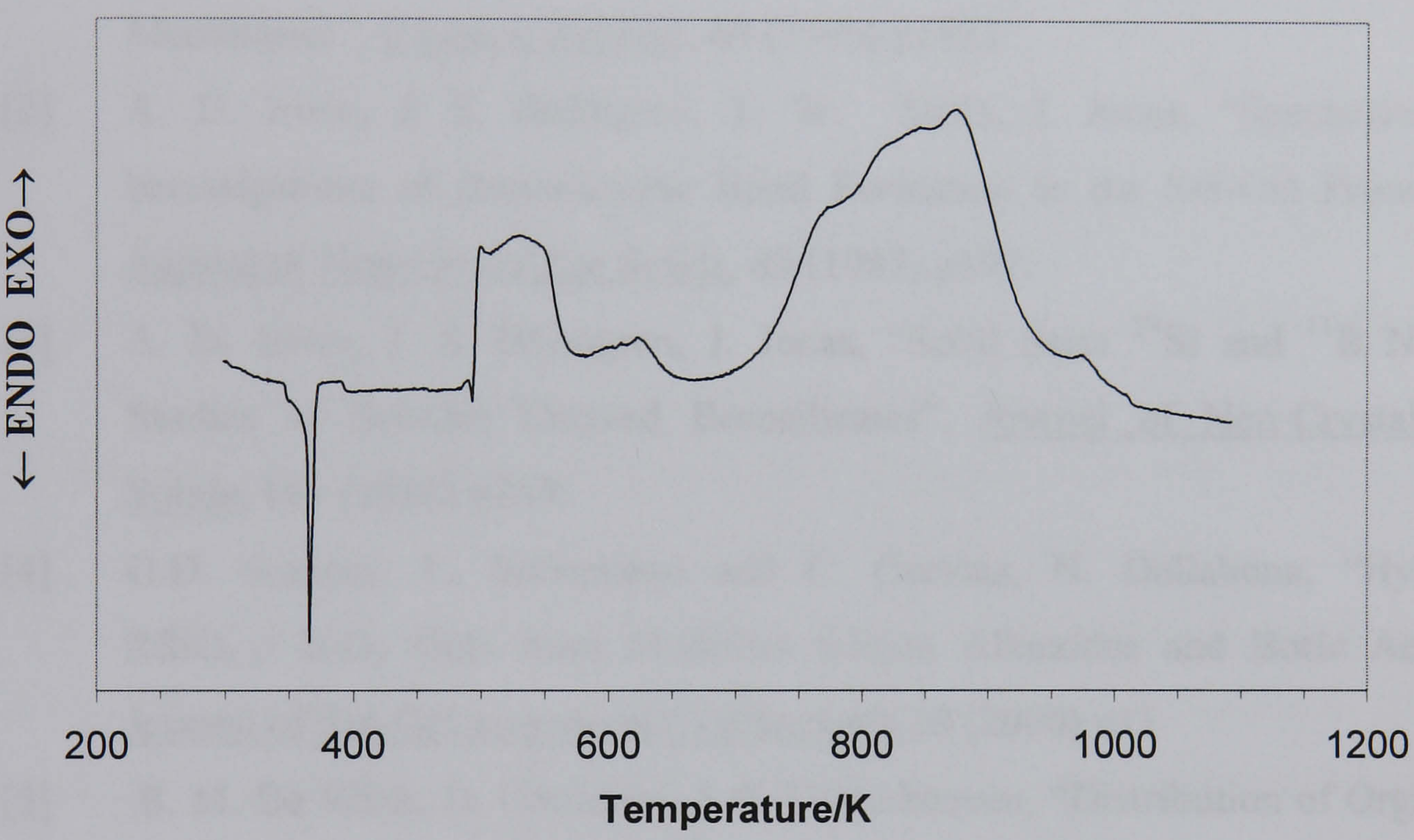

FIGURE 4.21 – DTA of 20:80 PBA: MTMOS in air.

should have caused voids to be left in the structure. Figure 4.21 shows the various key stages of the pyrolysis process in air, where (presumably) organic template molecules were removed from the matrix.

The main features of this thermogram are:

- The loss of water and condensation products in the region of 373K to 473K.
- The combustion of the phenyl ligand from phenyl boronic acid precursor results in the evolution of benzene within the region of 490K to 620K.

- The second major exotherm between 670K and 890K is thought to be due to extensive incorporation of boron into the siloxane network in the form of borosiloxane bonds.

References

[1] L. C. Klein, N. Giszpenc, "Sol-Gel Processing for Gas Separation Membranes", Ceramic Bulletin, **69** (1990) p1821

[2] A. D. Irwin, J. S. Holmgren, T. W. Zerda, J. Jonas, "Spectroscopic Investigations of Borosiloxane Bond Formation in the Sol-Gel Process", Journal of Non-Crystalline Solids, **89** (1987) p191.

[3] A. D. Irwin, J. S. Holmgren, J. Jonas, "Solid State ^{29}Si and ^{11}B NMR Studies of Sol-Gel Derived Borosilicates", Journal of Non-Crystalline Solids, **101** (1988) p249.

[4] G.D. Sorarau, F. Babonneau and C. Gervais, N. Dallabona, "Hybrid $RSiO_{1.5}$/ B_2O_3 Gels from Modified Silicon Alkoxides and Boric Acid." Journal of Sol-Gel science and Technology 18 (2000) p11

[5] B. M. De Witte, D. Commers, J. B. Uytterhoeven, "Distribution of Organic Groups in Silica Gels Prepared from Organic-Alkoxysilanes", Journal of Non-Crystalline Solids, **202** (1996) p35

[6] M. Smaihi, T. Jermoumi, J. Marigan. "Structural Study of Poly(phenylsilsesquioxane) Sol-Gel materials, Chemistry of Materials, **7** (1995) p2293-2299.

[7] D. H. Williams, I. Fleming, "Spectroscopic M ethods in Organic Chemistry", McGraw-Hill, London (1995).

[8] H. Zhang, C. G. Pantano, "Synthesis and Characterisation of Silicon Oxycarbide Glasses", Journal of the American Ceramic Society, **73** (1990) p958-963.

Chapter 5

Membrane Characterisation and Performance

5.1 Membrane Synthesis and Characterisation

Overview

This chapter is spilt into two main parts:

1) Sections 5.1 To 5.2.3 relate to the necessary considerations of experimental procedure and treatment of the substrate that had to be addressed before the synthesis of a successful membrane could be accomplished.
2) Sections 5.2.4 onwards, catalogue and discuss the experimental findings.

It was found that the successful synthesis of membranes depends greatly upon being able to accurately characterise each specimen produced, in terms of the feed gas flowing through it, past it (feed side) and the mean pressure across it. This was especially true when characterising the performance of membrane specimens in response to a mixed feed gas.

A careful measurement procedure can indicate which mechanisms dominate the transport of gas through a membrane and provide useful information as to the pore structure of the deposited membrane film. Such measurements were used extensively to guide the development of membrane preparation and application procedures.

Permeance performance information also provides useful feedback regarding the effectiveness of a particular deposition and drying/pyrolysis regime. Two membrane films, prepared from the same sol, can differ quite dramatically in

their relative performances if exposed to seemingly minor variations in their respective preparation processes.

5.1.1 Choice of Membrane Support Substrate

General Considerations

The membrane films investigated here have a thickness of the order of microns, and as mentioned previously, are supported upon a high-flux porous substrate.

The usual requirements for any substrate are that they possess the following basic qualities: -

- High permeability;
- High mechanical strength (to prevent flexion and rupture) under pressure;
- Be as thin as possible, to offer the least resistance to flow as possible;
- To be chemically and thermally very stable;
- Of paramount importance is that any substrate should also be capable of having an active membrane deposited upon it that is as uniform and thin as possible. This requires a very even surface and excellent wetting property when used with the chosen membrane-deposition technique.

The Stainless Steel : Titania Substrate.

The choice of substrate was a planar one, as this allowed for the easy deposition of thin films from a sol. However, rather than the usual choice of α-alumina – which is supplied usually as being at least 2mm thick – an alternative stainless steel/TiO_2 composite manufactured by IMAS Technology was chosen. This substrate's manufacture uses powder technology to apply a 20 - 40 μm thick macroporous layer on top of another highly porous (macroporous) layer of sintered stainless steel.

The total thickness of this chosen substrate is approximately 240 μm – which in principle should allow for a gas flow of at least an order of magnitude than the

much thicker α-alumina. A schematic of this substrate construction and an SEM micrograph of the same appear below in figs 5.1 and 5.2a.

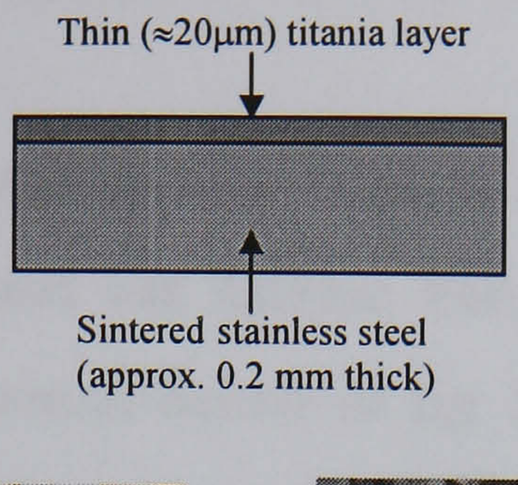

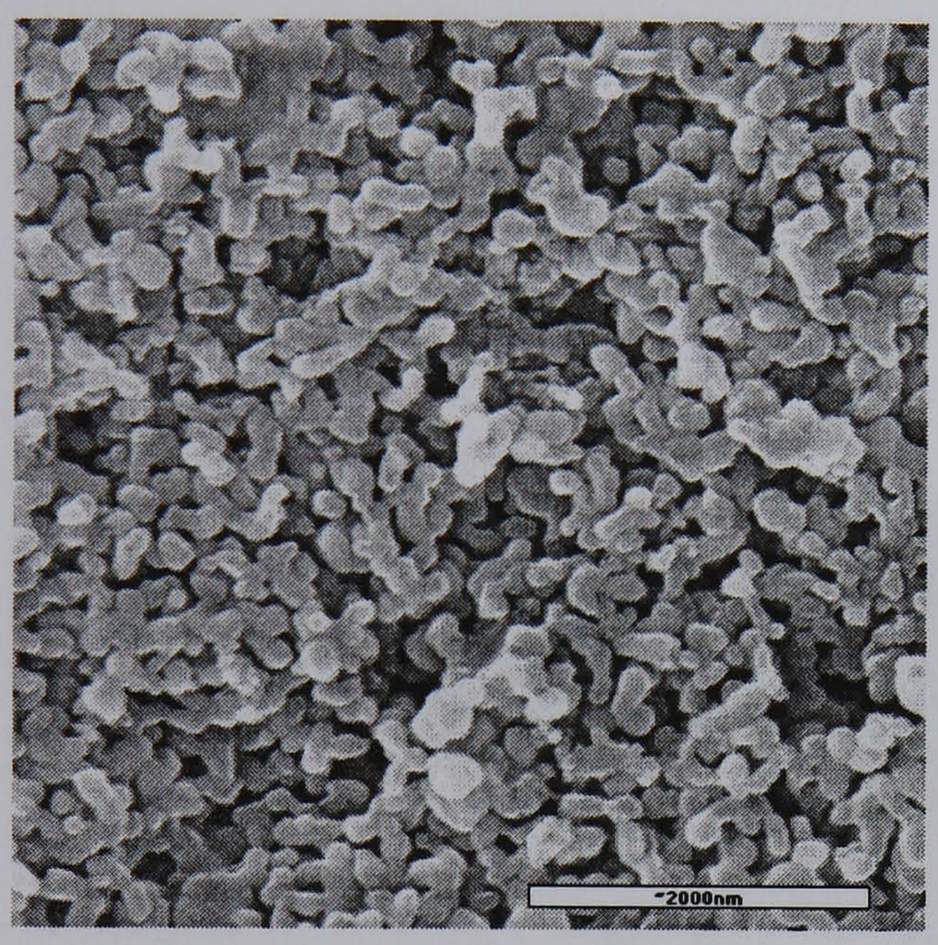

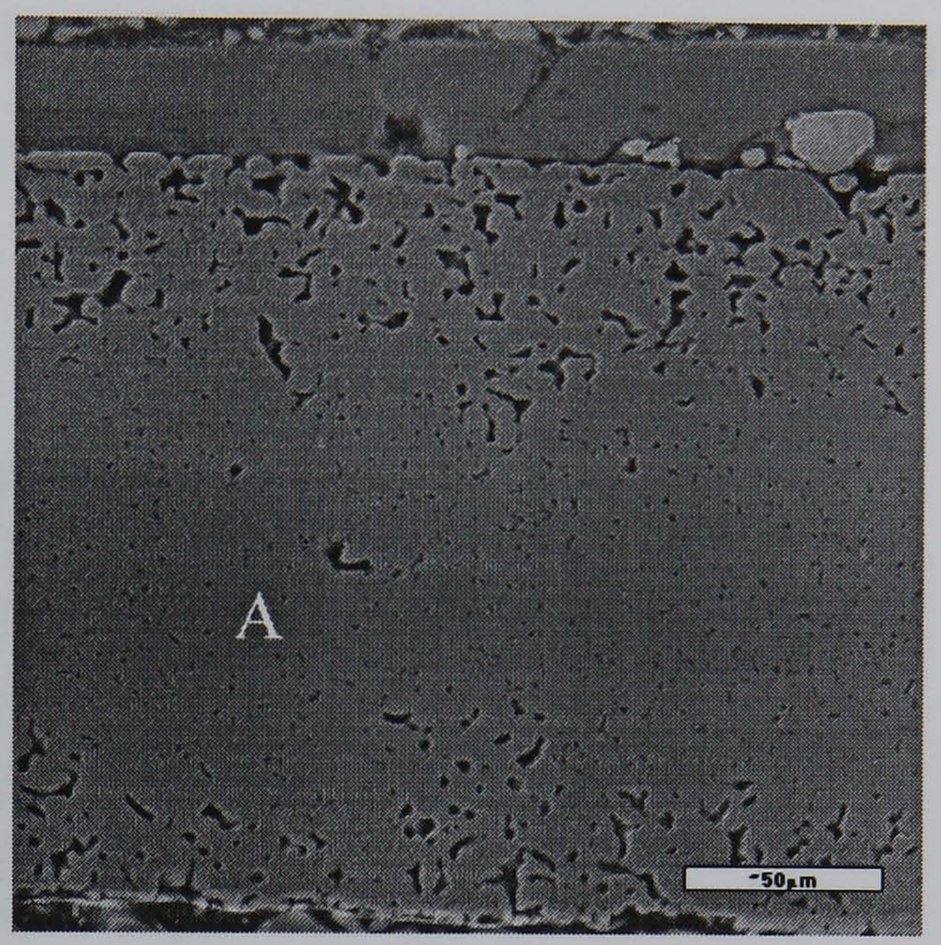

Figures 5.1 Schematic and 5.2 SEM Micrographs of TiO_2 Membrane Support Substrate. Micrograph on LHS is the stainless steel layer labelled "A" on RHS micrograph.

The TiO_2 overlayer in Figure 5.2 averaged a thickness of around 20μm.. However, Figures 5.2 and 5.3 show that significant variations in thickness occur. There were even (rare) occasions where the stainless steel actually protruded beyond the surface of the TiO_2 top layer. The results of the mechanical and thermal tests that were performed upon this substrate are presented below in table 5.1.

Mechanical Property	**Value**	**Error**	**Unit**
Young Modulus, E	380	± 5%	MPa
Yield Point, σ_u	32	± 5%	MPa
Ultimate Tensile Strength σ_B	76	± 5%	MPa

Table 5.1 : Measured mechanical properties for stainless steel: titania substrate

As the aim of this project is to separate gases at high temperature, the thermal cycling results are very promising: after 500 cycles there was no indication of any decline in the mechanical properties of this support substrate.

The structural features, overall surface flatness and effective pore size of the TiO_2 top layer were evaluated via Atomic Force Microscopy (AFM). These topographic results are presented below in fig 5.3 and showed: variations of vertical undulations (Z dimension) to be well within 100 nm.; and a pore between the sintered particles of titania of size of approximately 100 nm.

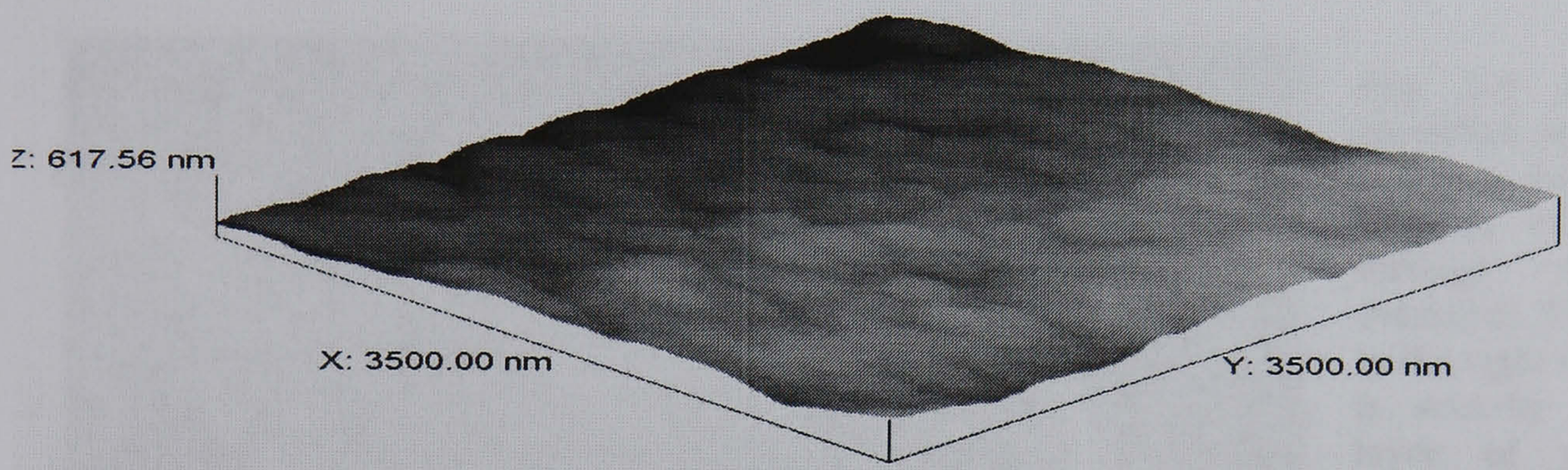

Fig 5.3 AFM Inspection of TiO2 Overlayer of Support Substrate

The permeance of the support substrate to N_2 (for transmembrane pressure differences ~ one bar) was of the order of 5×10^{-5} mol s^{-1} m^{-2} pa^{-1}. This is orders of magnitude higher than the permeance of the membrane layers and is due to its comparatively larger pore size. The stainless steel: titania substrate operates in the transitional regime between Knudsen diffusion and viscous flow. This is not unexpected, as the ratio of the pore radius of the titania to the free mean paths (r/σ) of CO_2 and N_2 are 2.24 and 1.50 respectively. The larger ratio of CO_2 implies that viscous flow has a larger contribution for this species when it flows through the substrate.

Imperfections in the Support Substrate

Occasionally, some samples that failed to demonstrate any permselectivity also had higher than expected permeation rates. Minor defects can have a totally debilitating effect upon permselectivity and yet not be so serious as to present an obvious case of viscous flow. In these instances, the technique of evaluating the flow vs. mean pressure gradient is a powerful tool for ascertaining the existence of small defect(s). The effect of an imperfect substrate upon the performance of the final membrane structure is significant. An example of this (fortunately rare) fault is presented in Figure 5.4.

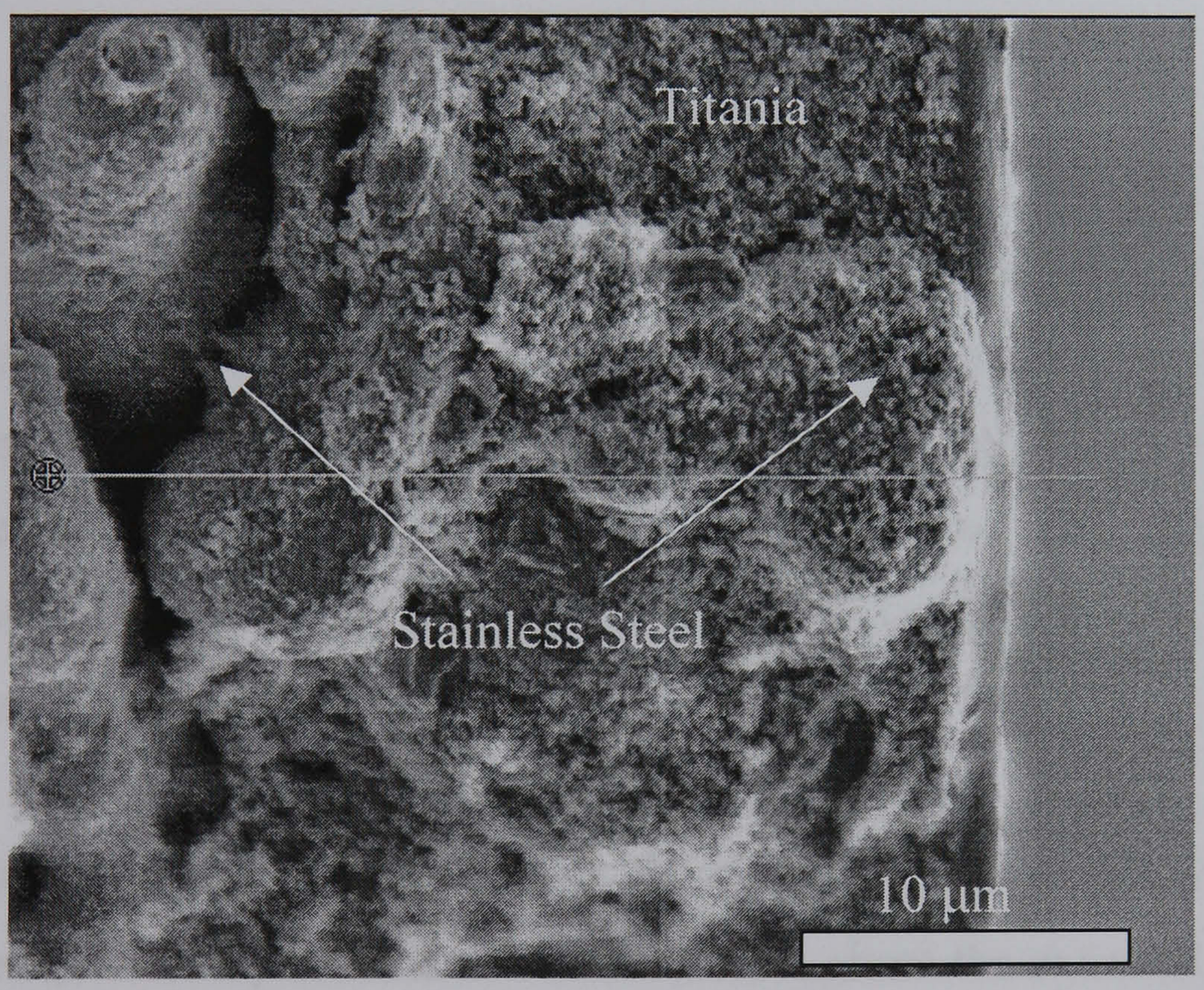

Fig 5.4 Example of imperfect substrate. The stainless can clearly be seen to be protruding through the titania overlayer. The thin layer to the right of the picture is actually an inactive layer of an alumina based sol which has been applied as an "undercoat" in order to prevent a catastrophic failure of the system once a membrane proper has been deposited

5.1.1.2 Effect of Substrate upon Permeation Rates

When a membrane is supported by a porous substrate, the result is a multi-layered structure with various strata of differing thicknesses and porosities. The usual analogy to describe such a multi-layered structure is that of several electrical resistances that are connected in series. The permeance is now likened to the conductance of the circuit (i.e. 1/R). Hence, the total permeance (Q) of the entire layered structure is:

$$Q = \frac{1}{\left(\frac{1}{Q_1} + \frac{1}{Q_2} + \frac{1}{Q_3} + \ldots . \frac{1}{Q_n}\right)} \qquad \textbf{(5.1)}$$

(Where n is the total number of layers in the structure).

Equation (5.1) shows that unless there are two or more layers of similarly low permeability, then the lowest value of conductance (i.e. highest resistance) will dominate the behaviour of the whole structure. This fact is reiterated here because the necessity arose in some instances (section 5.1.2.1 below) of treating the stainless steel: titania substrate with an additional layer – that was not actually active in the gas separation process.

5.1.1.3 Seepage of Sol into Substrate

It was observed that some (dilute) non-borosilicate sols of low viscosity had actually seeped into the substrate. Following the application of these dilute sols onto the stainless steel: titania substrates, SEM examination revealed that the desired discrete layers had not formed upon the substrates' surfaces. Subsequent EDX analyses showed high Si K_α intensities throughout the bulk of the substrate.

Having been drawn down into the titania over-layer the sol could be easily spread laterally as well as vertically throughout the extremely porous stainless steel under-layer as a result of centrifugal spreading during spin-coating. The rate of sol penetration varies with the viscosity of the sol. For viscous sols, the speed of penetration into the substrate is low and the membrane will densify during pyrolysis before a significant volume of the sol enters the substrate.

5.1.1.4 Prevention of Sol Seepage into Substrate

A remedy was devised that consisted of a pre-treatment of the substrates, which consisted of a coating (approximately 1 μm thick) of alumina-sec-butoxide sol

that originated as part of a related research project at Warwick [1]. The purpose of this "undercoat" (though decreasing the overall permeance) was to act as sealant that prevented seepage of the sol into the bulk of the support substrate.

Therefore, some of the results presented below are for membrane systems where the substrate was pre-treated with this "undercoat" before deposition of the membrane layer(s). The introduction of this additional layer reduces the overall permeance of the membrane/substrate combination. This reduction in permeance will be significant if the pore size of the additional preventative layer is of a similar order to that of the membrane itself. This "undercoat" of alumina sol is shown in Figure 5.5. Figure 5.6 illustrates the successful application of a membrane layer to a pre-treated substrate. EDX inspection also showed that the alumina-sec-butoxide sol did not penetrate the titania layer. (The effective pore size of this "undercoat" layer has been evaluated as being within the 3-4nm size range [1]).

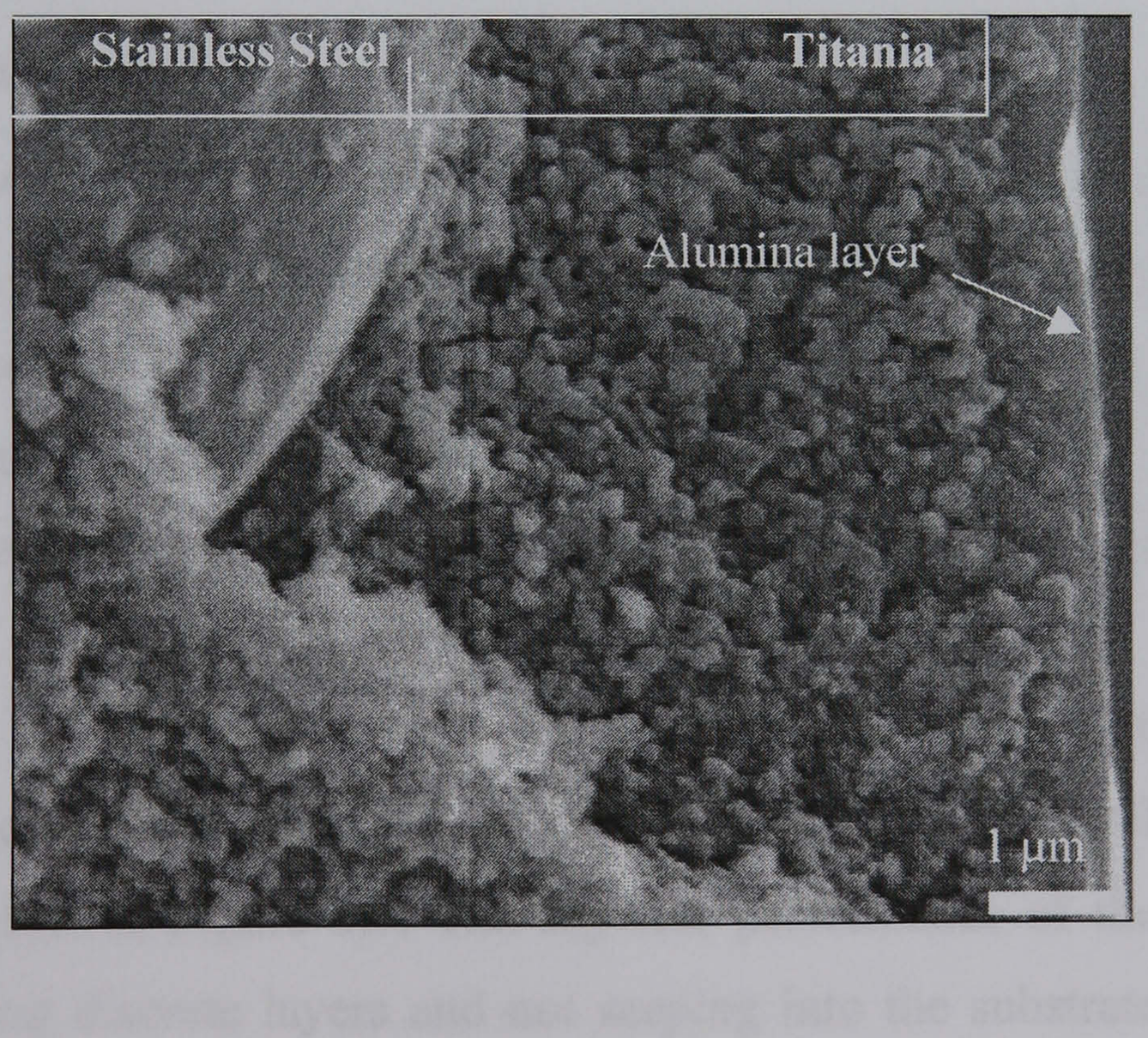

FIGURE 5.5 - An SEM micrograph illustrating the cross-section of a stainless steel: titania substrate with the additional alumina "undercoat".

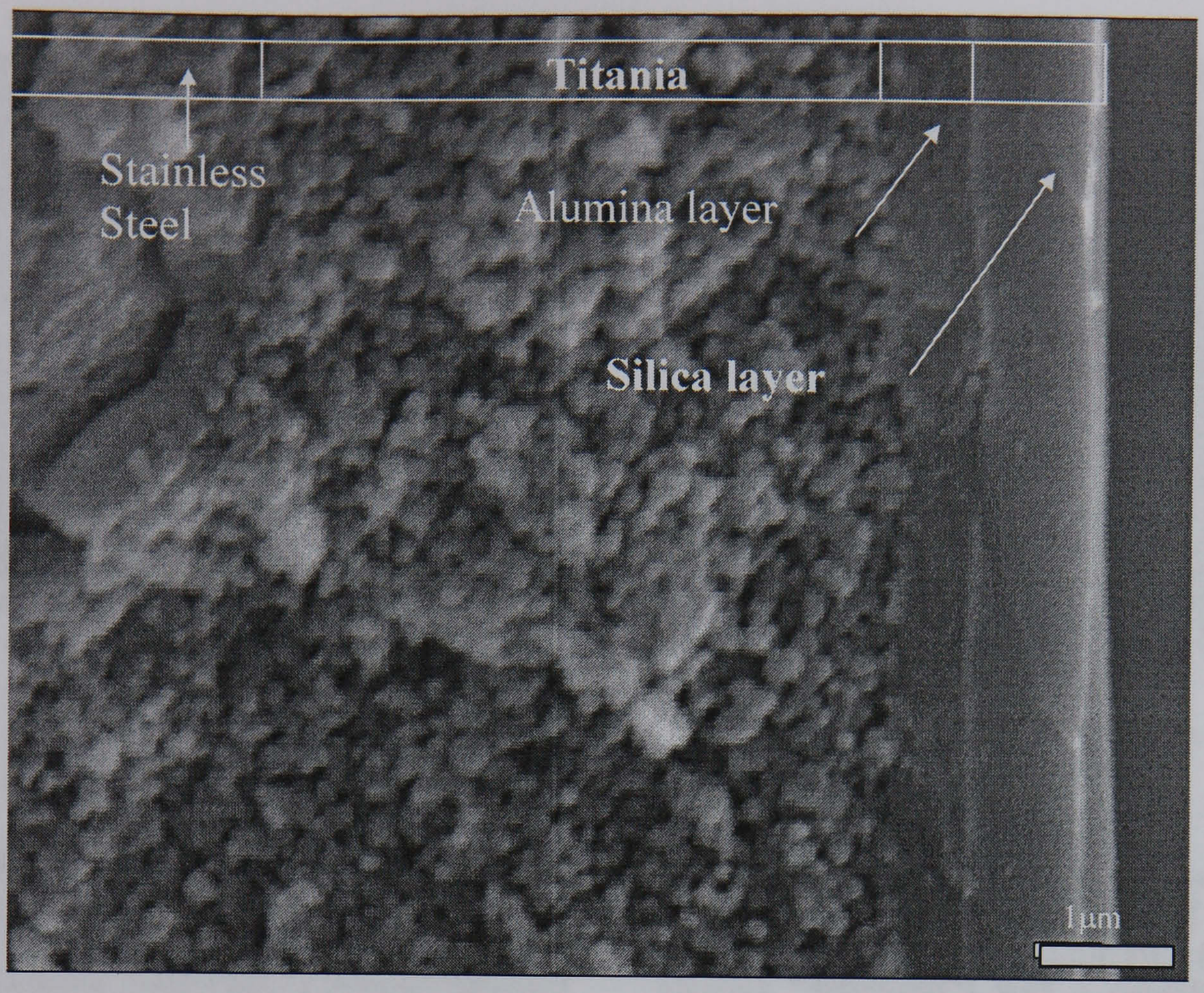

FIGURE 5.6 – Micrograph illustrating the successful application of a membrane layer atop of the pre-treated support substrate. This cross-section is of double-layered membrane with an the alumina "undercoat".

5.1.15 Borosilicate sols

Seepage of sol into the bulk of the stainless steel: titania substrate was never found to be a problem when depositing membrane layers from borosilicate sols. Crack-free coatings of sub-micron thickness were also the norm when depositing membranes from borosilicate sols. Hence, the use of the preventative alumina sol "undercoat" upon the substrate was dispensed with.

The absence of any detectable penetration into the bulk of the untreated substrates (i.e. those without an "undercoat") by these borosilicate sols is illustrated below in Figure 5.7. The superior performance of the borosilicate sols in forming discrete layers and not seeping into the substrate was mainly because they were inherently more viscous than the non-borosilicate sols. Therefore, it takes longer for the suction of the spin-coater's specimen-location system to draw sol down through the pores of the titania support

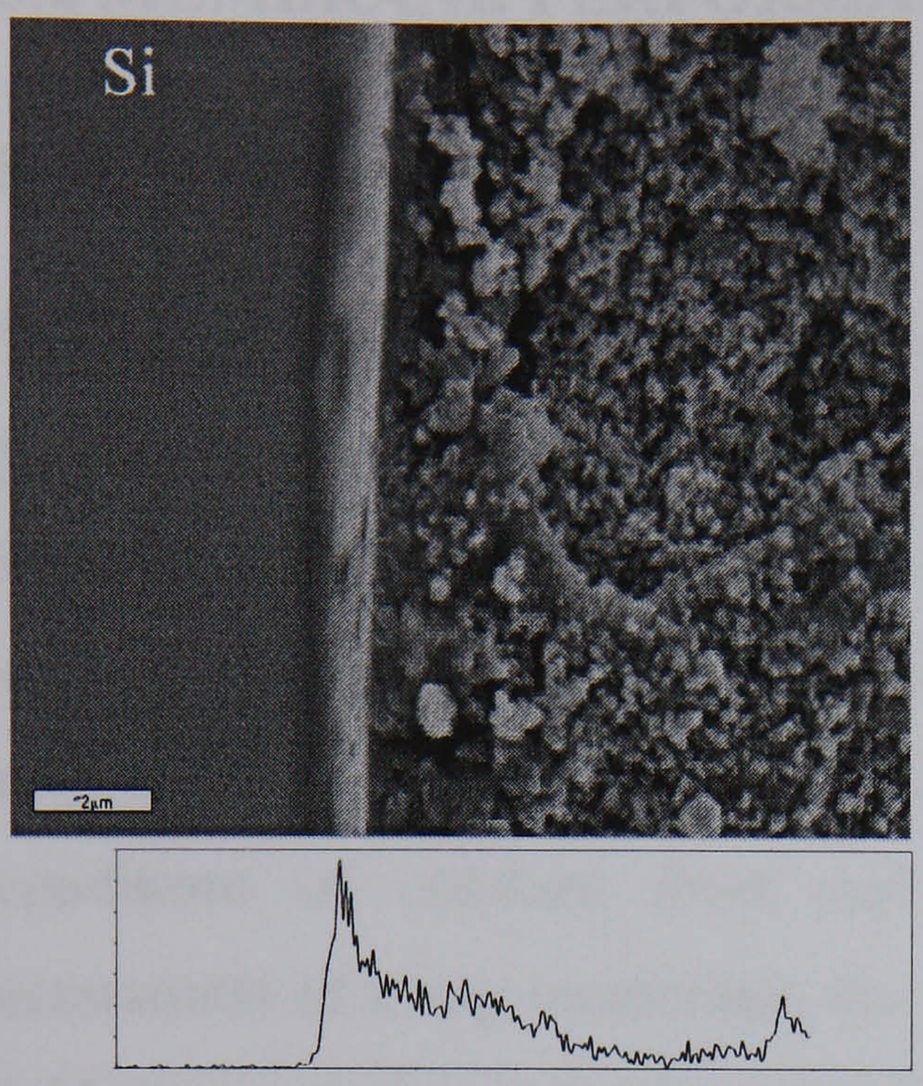

FIGURE 5.7 – Typical EDX maps and cross-sectional topographic lines-cans of a stainless steel: titania substrate (no alumina "undercoat") with a deposited active gas separation membrane based upon a boron containing precursor. No appreciable seepage of silicon into the bulk of the substrate is apparent.

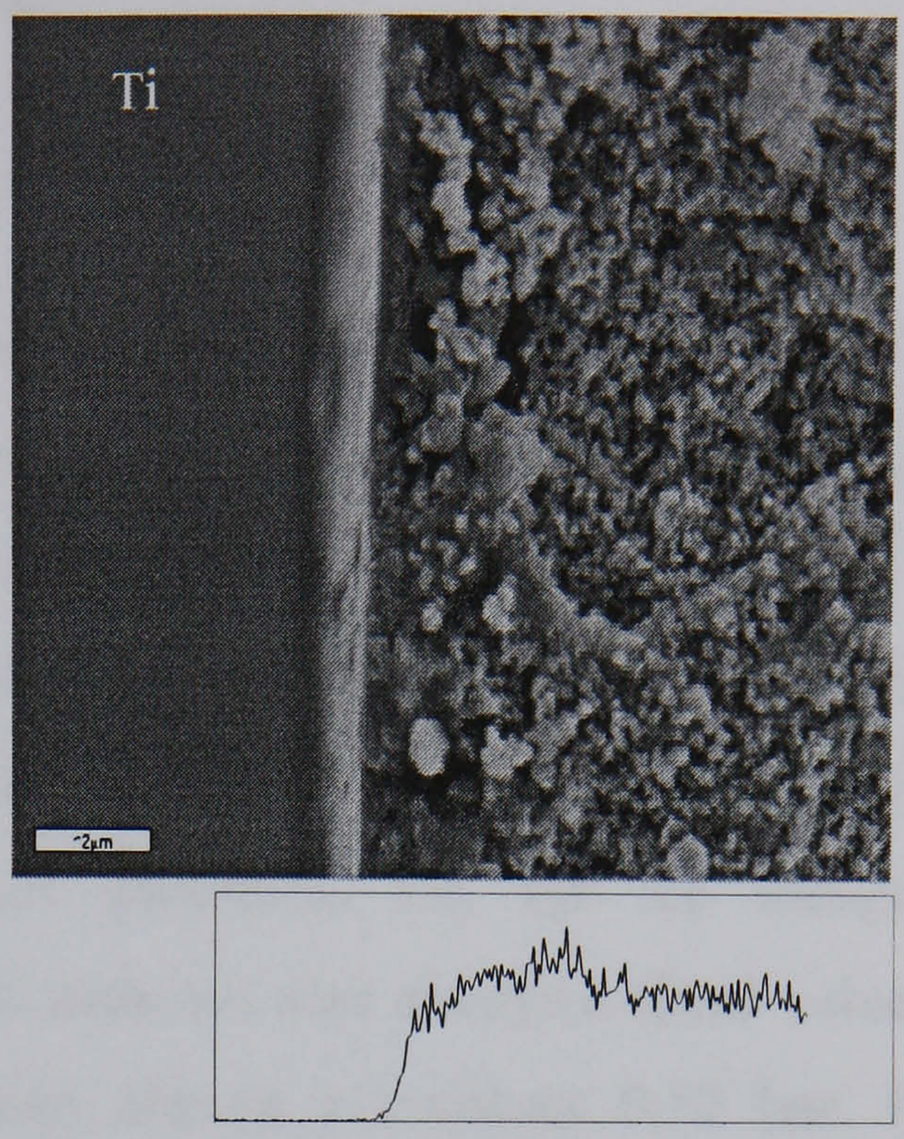

Figure 5.7a Typical EDX maps and cross-sectional topographic lines-cans of a stainless steel: titania substrate (no alumina "undercoat") with a deposited active gas separation membrane based upon a boron containing precursor.

In addition, whilst being more viscous the borosilicate sols did not suffer the usual fate of making sols more viscous. That is, producing membranes which were prone to cracking. This was largely because the borosilicate sols spread more easily across the surface of the support substrate whilst being spun. This quality of easily being spread could be because boric acid - which is readily formed from the hydrolysis of boron alkoxides - does not undergo permanent polymerisation under aqueous conditions. Instead, it merely forms weak hydrogen bonds. The resultant sol has a lower contact angle upon the surface of the titania support and is more susceptible to centrifugal spreading.

5.2 MEMBRANE PERFORMANCE

5.2.1 Evaluation Methodology.

The usual method of evaluating membrane performance is to measure gas permeation as a function of mean pressure across the membrane. As many hundreds of specimens were tested during the course of this research, for the sake of expediency, the results presented below were obtained using a two-fold method of data collection. All specimens were initially tested under identical conditions of constant front and back pressures. I.e. for the inaugural assessment of every membrane, the feed pressure was always a fixed value of 1.55 bar and the permeate pressure was always a constant 0.52 bar. If a specimen demonstrated selectivity then it would warrant further investigation under a full range of mean pressure testing and binary gas analysis. If a specimen was obviously flawed then it could be immediately discarded without taking up any further valuable machine time. (Further testing under a full range of mean pressures was also conducted upon some selected specimens - which initially demonstrated no selectivity – in order to obtain an estimate of effective pore size).

Great care was taken to ensure that all data points measurements were collected under conditions of steady state before changing the front and back pressure for the next measurement. Data reproducibility for all specimens was accomplished by repeated trials with differing pressure steps and dwell times between measurements with both increasing and decreasing pressure sweeps.

5.2.2 Membrane Systems

The results presented below were obtained from membrane specimens of varying compositions and pyrolysis states. They fall into two distinct categories: boron and non-boron containing sols. The reason for this demarcation is that it was found that the presence of a boron precursor with a

specific silane had more potential to improve selectivity, overall robustness and durability than those without. Also, there is a distinction between those membranes that were deposited upon substrates that had been pre-treated with an alumina sol "undercoat".

5.2.3 Reproducibility in Membrane Synthesis

As mentioned previously in section 5.1 it was found that two membrane films, prepared from the same sol, can differ quite dramatically in their relative performances if exposed to seemingly minor variations in their respective preparation processes.

Permeation performance could not just be dependent upon very minor variation(s) in synthesis, which were introduced deliberately. It was also found that significant variation in permeation could also occur amongst a batch of specimens that apparently experienced an identical synthesis and preparation regime. A number of factors could be responsible for this, most of which involve the formation of defects, which are a ubiquitous problem in ceramic membrane synthesis. The size and surface chemistry of such defects usually depend on such things as drying speed, the number and size of air-borne particulates in the preparation atmosphere, the thermal processing schedule and the flatness of the substrate. Time dependency is a consideration and is discussed further in section 5.2.5

5.2.4 Permeation Measurements

The majority of the results presented below represent single-gas measurements. However, for a selected group of membranes some binary gas analysis was also performed. There is a often a difference between single and multiple gas trials as the separation factor obtained is dependent upon which specific mass transport mechanism is dominant. In addition, two (or more) separate mechanisms can be operating within a membrane at the same time. These can

either work to reinforce each other's effectiveness – or could also be working antagonistically against each other. Basically, the differences between single and multiple gas species measurements might be attributed to four main influences:

- In pores with diameters larger than 50 nm where molecules of differing gas species and molecular weights (at the same temperature) will exchange momentum with each other.
- Concentration of permeate exhibiting a back-pressure which causes a resistance to further flow
- Non-separable back diffusion
- In pores less than 2 nm the progress of the slower moving species impedes the flow of the faster moving gas molecules resulting in "single file" molecular progress.

5.2.4.1 Non-Boron Containing Sols

As mentioned previously in section 5.1.1.3 the non-boron containing sols had a tendency to seep into the bulk of the substrate and not form discrete layers atop of the support substrate. Therefore, for the same sols were applied to some substrates which had been pre-treated with the alumina sol "undercoat" and some representative results appear in Figure 5.9 below.

From inspection of Figure 5.9, one can see that the performances of the differing molar ratios of diphenyl/methyl membranes were considerably improved in terms of both CO_2 permeability and CO_2/N_2 (and CO_2/He) single-gas permselectivity. This was a typical finding for these systems and demonstrates the advantage offered by the alumina sol "undercoat" to the non-borosilicate systems.

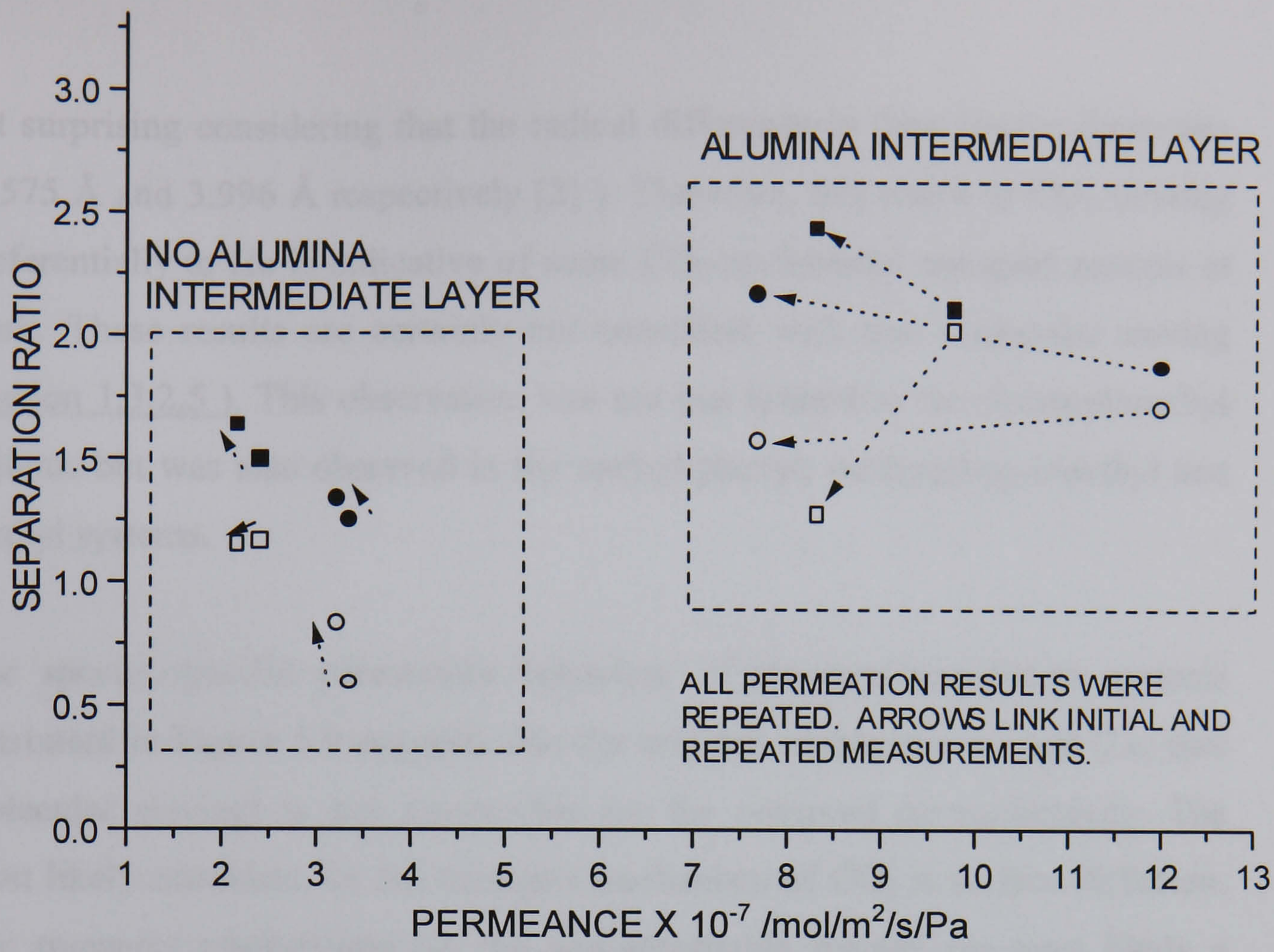

FIGURE 5.9 – Permeation performance some no-boron containing sols with the alumina "undercoat" and normal substrates. Solid markers refer to CO_2/N_2 single-gas permselectivities and open points to CO_2/He. Square markers refer to 20/80 diphenyl/methyl (hydrolysis ratio of 2) membranes and circular points to 40/60 diphenyl/methyl (hydrolysis ratio of 2).

The comparatively low permeance of the membranes without the alumina sol "undercoat" can be explained as being due to the seepage of the sols into the bulk of the substrate. To have inhibited their overall performance to such a degree, this seepage must have almost totally sealed the pores of the substrate.

The results represented in Figure 5.9 also show that CO_2 flowed preferentially to helium (separation factors up to 2). The possibility of systematic error was eliminated by exhaustive checks and calibration trials of all experimental measurement apparatus.

It is widely reported in the literature that helium usually displays a higher permeance than carbon dioxide through porous inorganic membranes. This is

not surprising considering that the radical difference in their kinetic diameters (2.575 Å and 3.996 Å respectively [2]). Therefore, this result of CO_2 flowing preferentially to He is indicative of some CO_2-preferential transport process at work. These results are certainly not consistent with true molecular sieving (section 1.3.2.5). This observation was not just limited to the diphenyl/methyl systems but was also observed in the methyl/phenyl; methylphenyl/methyl and methyl systems.

The species-specific permeation behaviour of the non-borosilicate systems illustrated in Figure 5.9 suggests that the original templating concept (i.e. true molecular sieving) is not responsible for the observed permselectivity. The most likely candidate for the transport mechanism of CO_2 is surface diffusion. The transport mechanisms for the non-adsorbable species are most likely a combination of Knudsen diffusion and activated diffusion. (This conclusion is further supported by the variation of permeation with temperature profiles of single gas permeation in section 5.2.7 and section 5.3.2 which deals with separation behaviour of binary feed gases).

5.2.4.1.1 Rationale for Permeation Behaviour in Terms of Structure

In chapter 4 of this thesis (section 4.2.4), the generic ^{29}Si MAS NMR results for non-borosilicate xerogel powders indicate that as the pyrolysis process proceeds, the template molecules are replaced by Q^3 sites. These have been assigned as bearing hydroxyl groups. Condensation of these groups leads to the formation of siloxane linkages.

However, the pyrolysis behaviour of thin films might differ from the pyrolysis behaviour of xerogel powders. Should this be true then it is feasible that the formation of siloxane linkages observed in xerogel powders may not necessarily occur to the same degree within thin films. A rationale for this would be that the siloxane backbone of a deposited membrane might be too inflexible to permit the formation of siloxane linkages. If this were the case

and the formation of siloxane linkages were indeed suppressed, then upon oxidation, the organic template molecule would be substituted by the hydroxyl groups that are the by-products of combustion. These would then line the internal surface of a membrane's pore wall and act as surface diffusion sites.

Support for this hypothesis is supplied by Li *et al* who synthesised silica membranes - using a similar synthesis route to that reported here – and reported a preferential CO_2/He selectivity [3]. Li *et al* also reported that permeance was inversely proportional to temperature for all gases studied. This observation also suggests that a surface diffusion mechanism was present (as discussed in section 1.3.2.3 of chapter 1).

5.2.4.2 Borosilicate Sols

The boron containing sols studied in this research contained the phenyl boronic acid and trimethyl borate precursors. These were added in differing molar ratios to methyl, ethyl and phenyl silanes. Representative results of the hundreds of trials upon those membranes that were derived from sols based upon methyltrimethoxysilane are presented in Figure 5.10.

These sols were deposited upon membranes that had not been pre-treated with the alumina sol "undercoat. It was noticed very early on in this project that they did not enjoy any significant improvement in separation performance (section 5.1.1.5). In fact, the only noticeable difference when depositing borosilicate membranes upon a substrate that had been pre-treated with the alumina sol "undercoat" was a sharp decrease in permeance. This can be attributed to the fact (confirmed by EDX analysis) that unlike the non-boron containing sols where the unprimed substrate became saturated, very little seepage into the bulk of the substrate occurred. Depositing discrete layers of uniform thickness upon an uncoated substrate was relatively simple to accomplish.

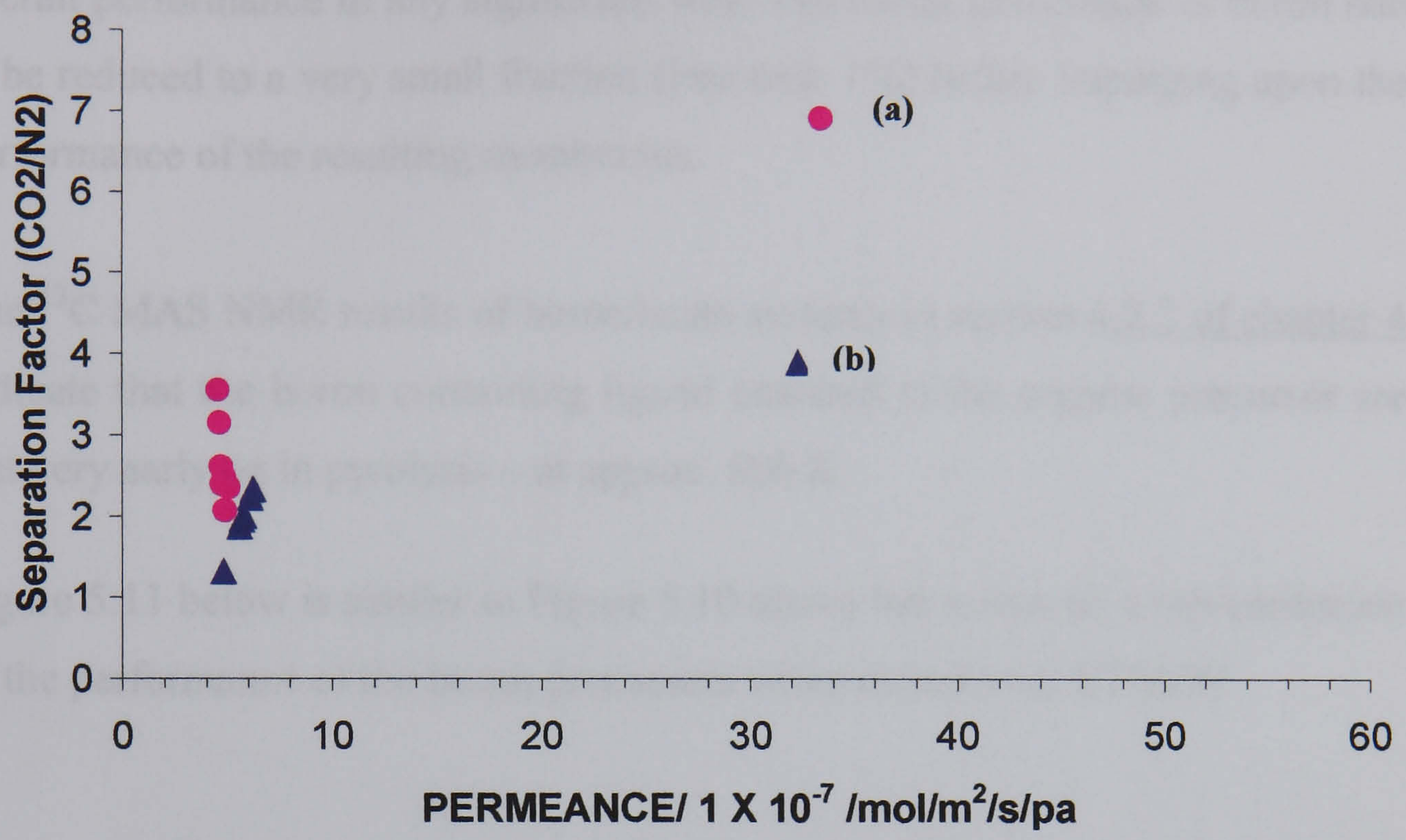

Fig 5.10 Grouped results of single gas separation factor vs. permeance for boron containing sols. Single data point representing an average of at least 3 similar trials – with the exception of those labelled (a) and (b) which were "one-off" results. Boron present as the precursors trimethyl borate and phenyl boronic acid mixed in various molar ratios with methyltrimethoxysilane. (Circles represent PBA and triangles TMB. Hydrolysis ratio was 2). Note the general trend that the PBA precursor has generally superior separation performance but poorer permeance.

Figure 5.10 represents the results of hundreds of trials represented as grouped data. The data points labelled as (a) and (b) however, are "one-offs" which were only accomplished once in over a hundred trials. Membranes synthesised from the very same sols from under seemingly identical conditions did not repeat the atypical results (a) and (b) – which not only displayed superior permselectivity compared to the norm but greater permeance as well. This is an example of the inherent problem of reproducibility for these types of inorganic membrane described above in section 5.2.3.

The hydrolysis ratio of all the samples in Figure 5.10 was 2. This was found to be the optimum for best performance and so was adhered to for all borosilicate specimens.

One curious fact is that the molar ratios of boron containing precursor to silane for all the results above varied enormously from 50% to 5% and did not alter overall performance in any significant way. The molar percentage of boron had to be reduced to a very small fraction (less than 1%) before impinging upon the performance of the resulting membranes.

The ^{13}C MAS NMR results of borosilicate systems in section 4.2.2 of chapter 4 indicate that the boron containing ligand attached to the organic precursor are lost very early on in pyrolysis – at approx. 600 K.

Figure 5.11 below is similar to Figure 5.10 above but is instead a representation of the performance of the boron precursors when mixed with ETMOS.

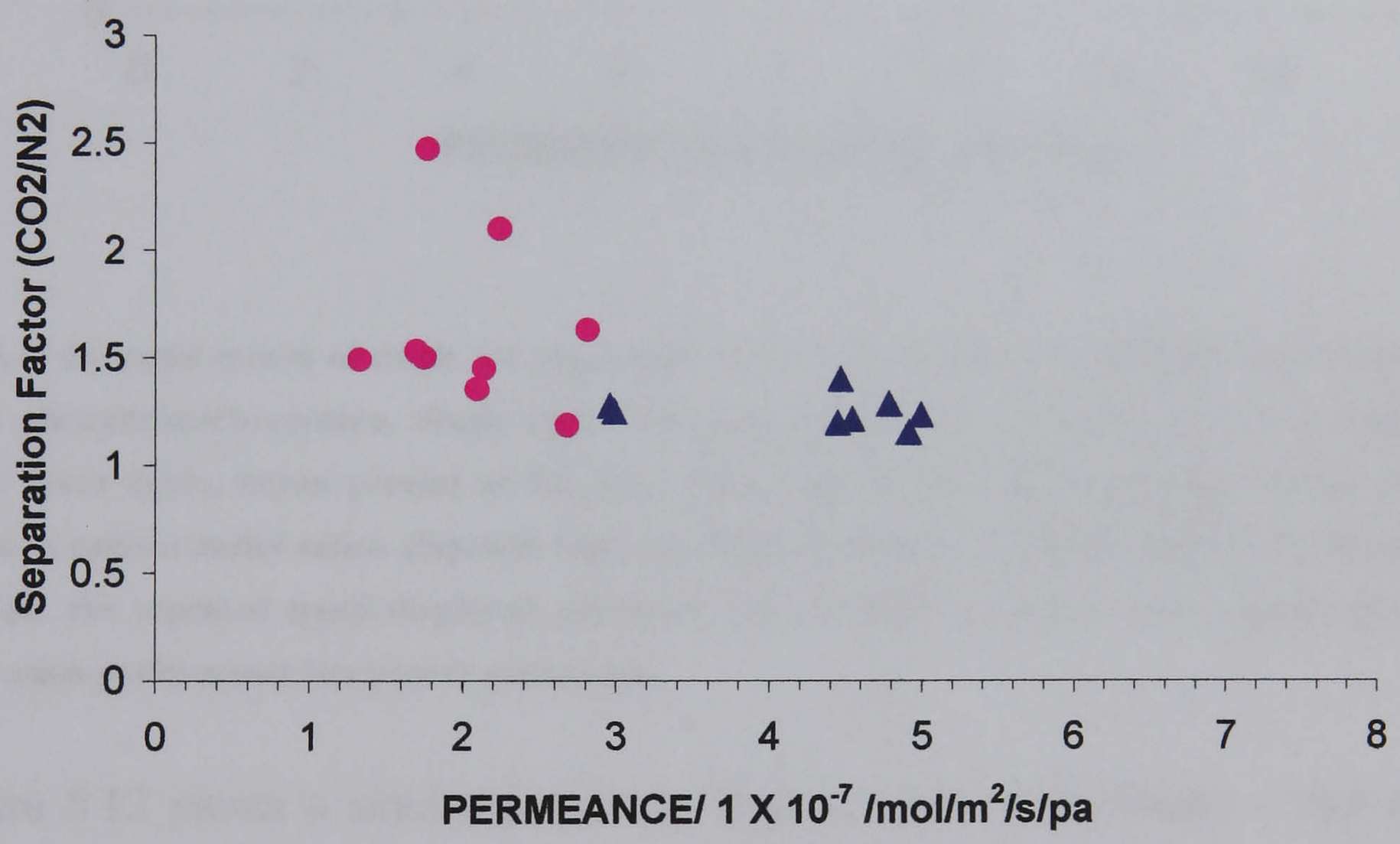

Fig 5.11 Grouped results of single gas separation factor vs. permeance for borosilicate sols based upon ethyltrimethoxysilane. Single data point representing an average of at least 3 similar trials. Once again, boron present as the precursors trimethyl borate and phenyl boronic acid mixed in various molar ratios. (Circles represent PBA and triangles TMB. Hydrolysis ratio was 2). Note the repeated trend displayed previously that the PBA precursor has generally better separation performance but poorer permeance.

The final borosilicate sols investigated were based upon phenyltrimethoxysilane and the two precursors trimethyl borate and phenyl boronic acid. These results are presented below in Figure 5.12.

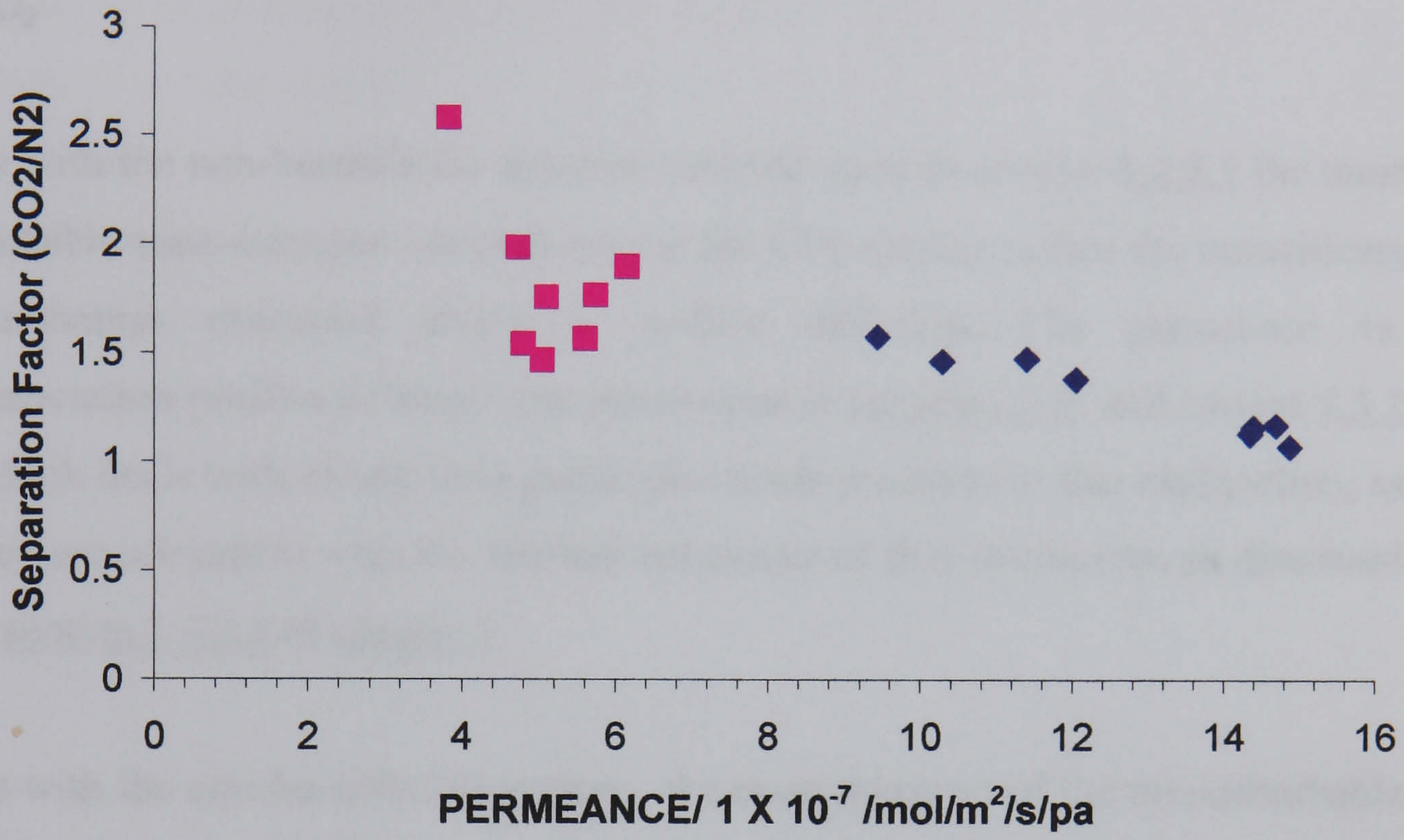

Fig 5.12 Grouped results of single gas separation factor vs. permeance for borosilicate sols based upon phenyltrimethoxysilane. Single data point representing an average of at least 3 similar trials. Once again, boron present as the precursors trimethyl borate and phenyl boronic acid mixed in various molar ratios. (Squares represent PBA and diamonds TMB. Hydrolysis ratio was 2). Note the repeated trend displayed previously that the PBA precursor has generally better separation performance but poorer permeance

Figure 5.12 paints a similar picture to those presented previously – that the PBA precursor seems to enable greater permselectivity (though at the expense of permeance) than the TMB precursor.

5.2.4.2.1 Rationale for Permeation Behaviour in Terms of Structure

As with the non-borosilicate systems, it would appear from the results presented in Figures 5.10 –5.12 for the borosilicate systems that true molecular sieving, (i.e. discrimination by a membrane's pore towards a gas molecule solely due to that molecule's kinetic diameter) does not play any significant

part in the permselectivity process. This is because although the CO_2 molecule is larger than the N_2 molecule (3.996 Å compared to 3.681 Å [2], some permselectivity ratios of CO_2 : N_2 were at over 7: 1 .If true molecular sieving had been active then the smaller species N_2 would have flowed quicker than CO_2

As with the non-borosilicate systems reported upon in section 5.2.4.1 the most probable mass-transport mechanism for the CO_2 species within the borosilicate membranes examined above is surface diffusion. The permeance vs. temperature profiles of single gas permeation in section 5.2.7 and section 5.3.2 (which deals with binary feed gases) also lends credence to this explanation, as they are consistent with the thermal behaviour of this mechanism as discussed in section 1.3.2.3 of chapter 1.

As with the non-borosilicate systems, the mass transport of the non-adsorbable species is most likely a combination of Knudsen diffusion and activated diffusion (section 1.3.2.5 of chapter 1).

However, unlike the non-borosilicate systems, the ^{29}Si MAS NMR spectra of the borosilicate systems do not show the presence of any significant number of Q^3 species (Figure 4.12 of chapter 4). In the non-borosilicate systems, the Q^3 species were assumed to link with hydroxyl groups to form surface diffusion sites and were abundant in the fully pyrolysed non-borosilicate specimens (as shown in Figure 4.10 of chapter 4.)

The apparent absence of Q^3 species in the borosilicate systems could be an indirect consequence of borosiloxane bonds – the presence of which was confirmed by FTIR spectroscopy (Figure 4.16 of chapter 4) . The borosiloxane bond is unstable and can lead to precipitates such as boric acid. This would lower the pH of the borosilicate sol. As discussed in section 1.5.2.2 of chapter 1, a more acidic condition would make the condensation reaction proceed more

quickly and thereby increase the number of Q^4 species. (To such an extent, that the Q^3 species were undetectable by the ^{29}Si MAS NMR detailed in Figure 4.12 of chapter 4).

In the non-borosilicate systems, the surface diffusion sites are taken to be hydroxyl groups attached to Q^3 silicon coordinations. In the apparent absence of Q^3 sites in the borosilicate systems, the only analogous environment is the T^2 (methyl) group SiO_2 CH_3OH shown in Figure 4.12 of chapter 4. However, this T^2 species is present in only very small quantities. Therefore, unlike the non-borosilicate systems where the opportunity for hydroxyl - Q^3 linking is abundant, the proportion of hydroxyl-based surface diffusion sites for the borosilicate systems would be very small and their contribution in this fashion limited.

Other surface diffusion sites within the borosilicate systems could be due to silane coupling. MTMOS was the most successful silane system for the borosilicate membranes and it is known that methyl does possess a chemical affinity towards CO_2.

However, phenyl is known to possess a far stronger chemical affinity towards CO_2 molecule and inspection of Figures 5.12 (phenyl) and 5.10 (methyl) shows that the phenyl based silane (PTMOS) borosilicate systems displayed lower permselectivity ratios than the methyl (MTMOS) based borosilicate systems.

The fact that surface diffusion for CO_2 in the MTMOS based systems was superior to the PTMOS system – despite the latter's greater chemical affinity towards CO_2 – could be due to two factors (acting either singly or in combination).

Firstly, Takaba *et al* [4.] present evidence that there is an optimum level of chemical affinity to maximise surface diffusion. Simply maximising the chemical affinity (as with the phenyl based borosilicate systems) could actually inhibit this mechanism, as the CO_2 molecule will tend to become attached to the pore wall rather than diffuse along it.

The second factor which could act to promote the surface diffusion of CO_2 in methyl based borosilicate systems is that the network formation based upon borosiloxane bonds is superior in methyl based borosilicate systems. Babeneau *et al* have reported that the formation of homogenous borosilicate gels and the degree of the incorporation of boron into the network via B-O-S bridges is highly dependent upon the alkyl group used in the silane precursor [5].

5.2.5 Time- Dependent Performance

Non-Borosilicate Sols

Figure 5.9 (section 5.2.4.1) showed that permeance measurements had been repeated (arrows linking successive measurements) and significant differences are apparent between sequential measurements. Normally one might assume that this was due to poor instrumentation. However, this varying permeance was a very common occurrence. In fact, for most of the non-borosilicate specimens, the same permeance result (under the same experimental conditions) could not be achieved twice in succession.

At first, it was thought possible that this effect might be an artefact of the instrumentation. (Especially as permeance sometimes increased and at other times decreased between sequential measurements). Figure 5.13 illustrates the change of permeance between successive measurements.

A degradation in permeance with time is apparent for all gas species. At first, this was blamed upon moisture adsorption - which is a ubiquitous problem with silica membranes and discussed in section 5.1.2.3. However, it seemed that in this case, *only CO_2 was being effected*. Closer inspection of the results showed a very slight – but very real - progressive change in CO_2 permeance over the normal 200s collection period. The flow rates of N_2 He and Ar remained constant.

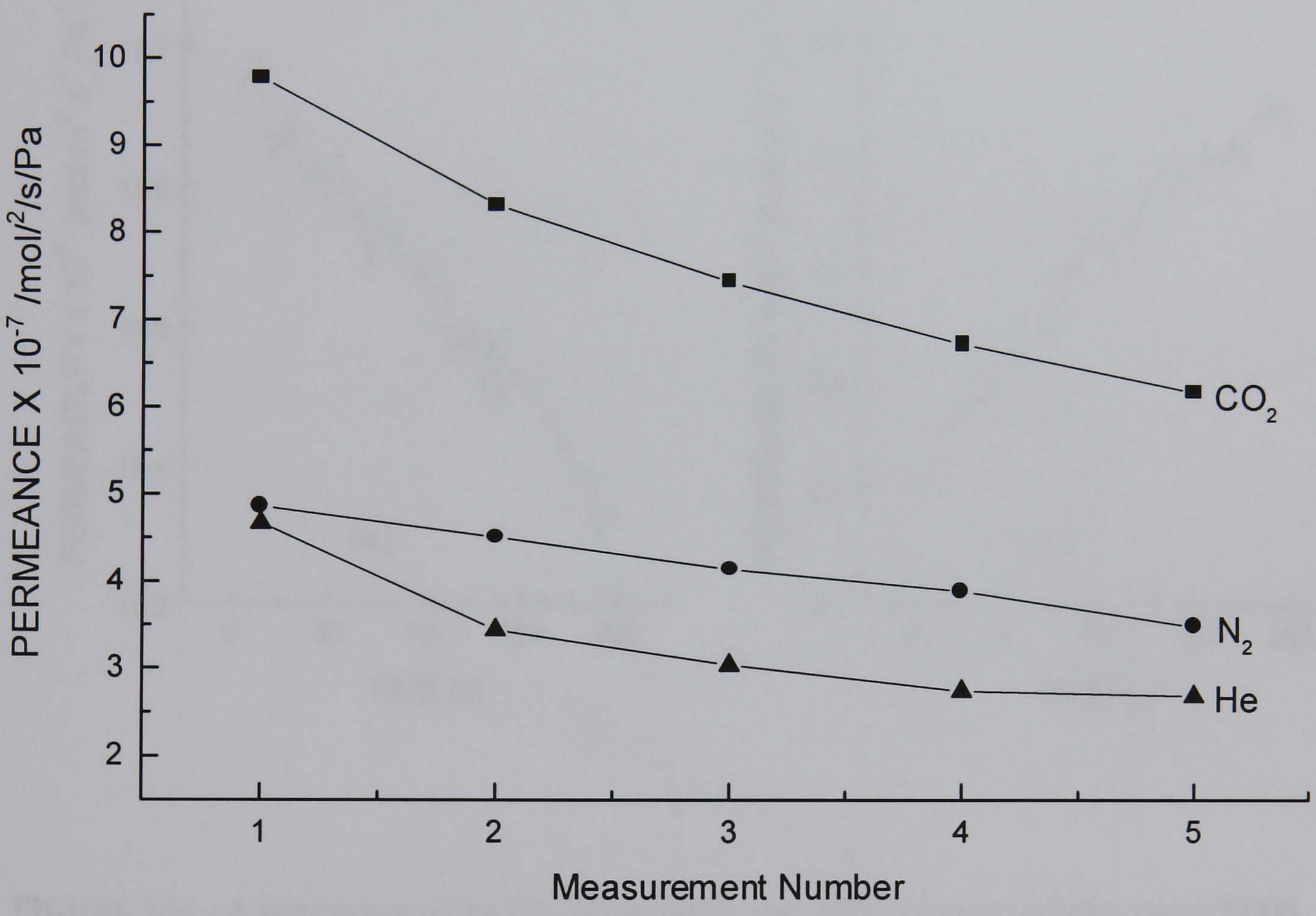

Figure 5.13 – Change in permeance with successive measurements (same experimental conditions)

At first, the CO_2 permeance increases, reaches a maximum, and then gradually decreases non-linearly. This is illustrated in Figure 5.14 below and explains why consecutive measurements upon the same specimen often yielded differing results.

This effect was investigated in greater depth by extending the sampling-time period to far beyond the 200 seconds normally used for data acquisition. Figure 5.15 shows that whilst the permeance of N_2 and He remain constant over time, the CO_2 permeance drops markedly. Additional permeance measurements identified a characteristic CO_2 permeation curve, illustrated in Figure 5.16.

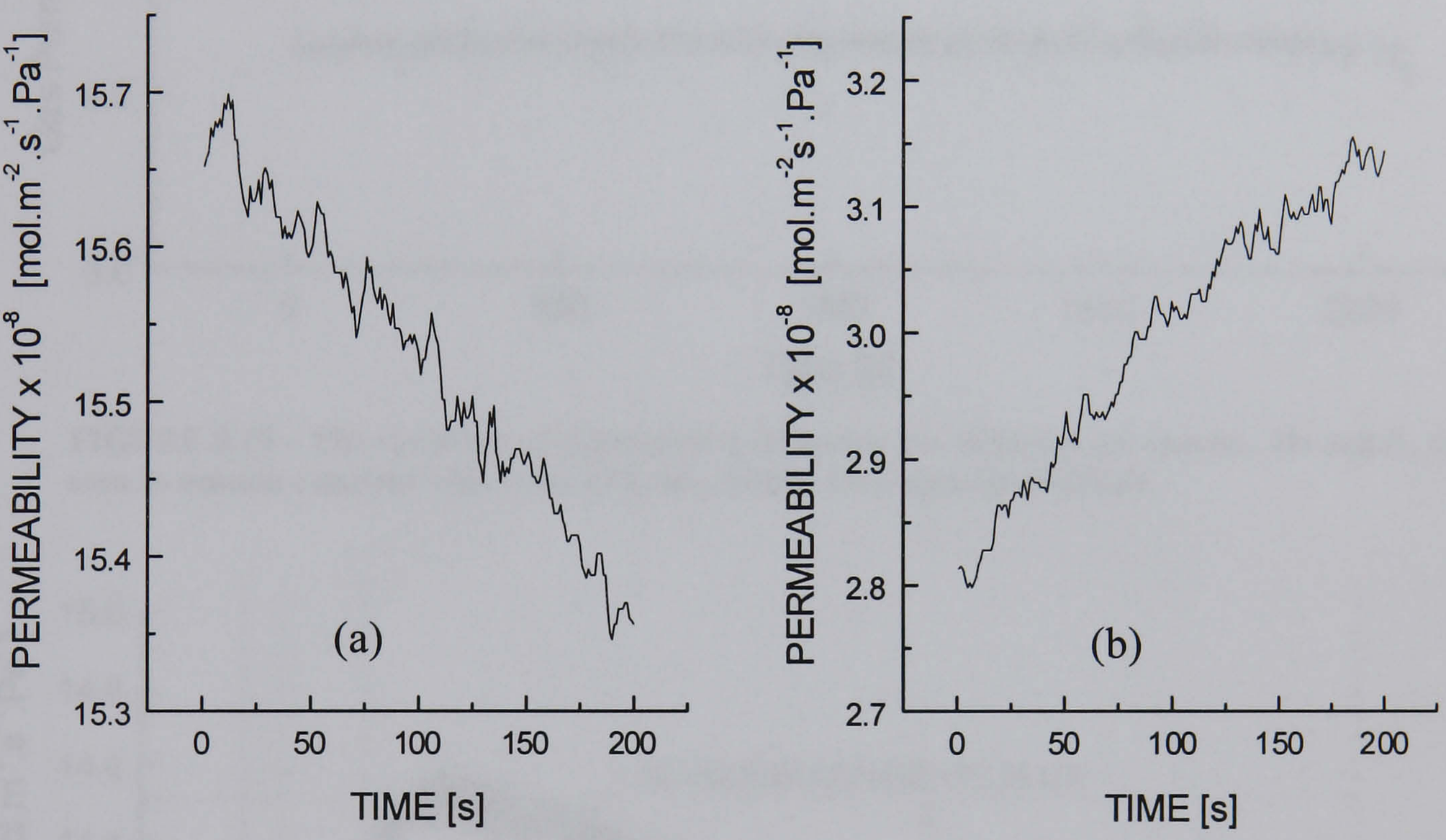

FIGURE 5.14 – A comparison of the CO_2 permeability-time profiles of two samples; (a) ph/TEOS 30/70 r = 10 and (b) methyl r = 2. No previous measurements had been performed on either sample.

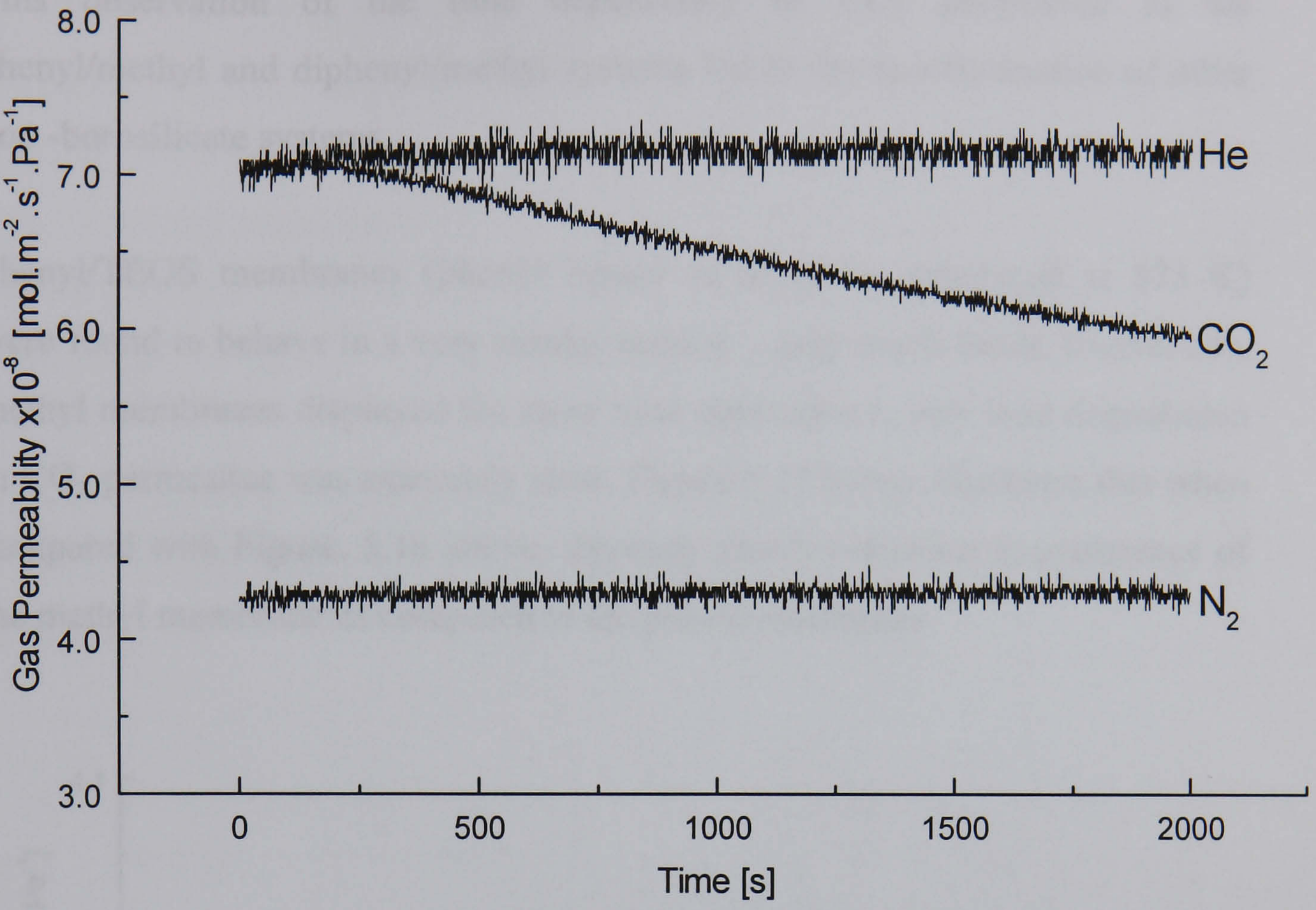

FIGURE 5.15 – The variation of permeability with time for different gas species. He and N_2 can be seen to remain constant with time, CO_2 meanwhile decreases significantly.

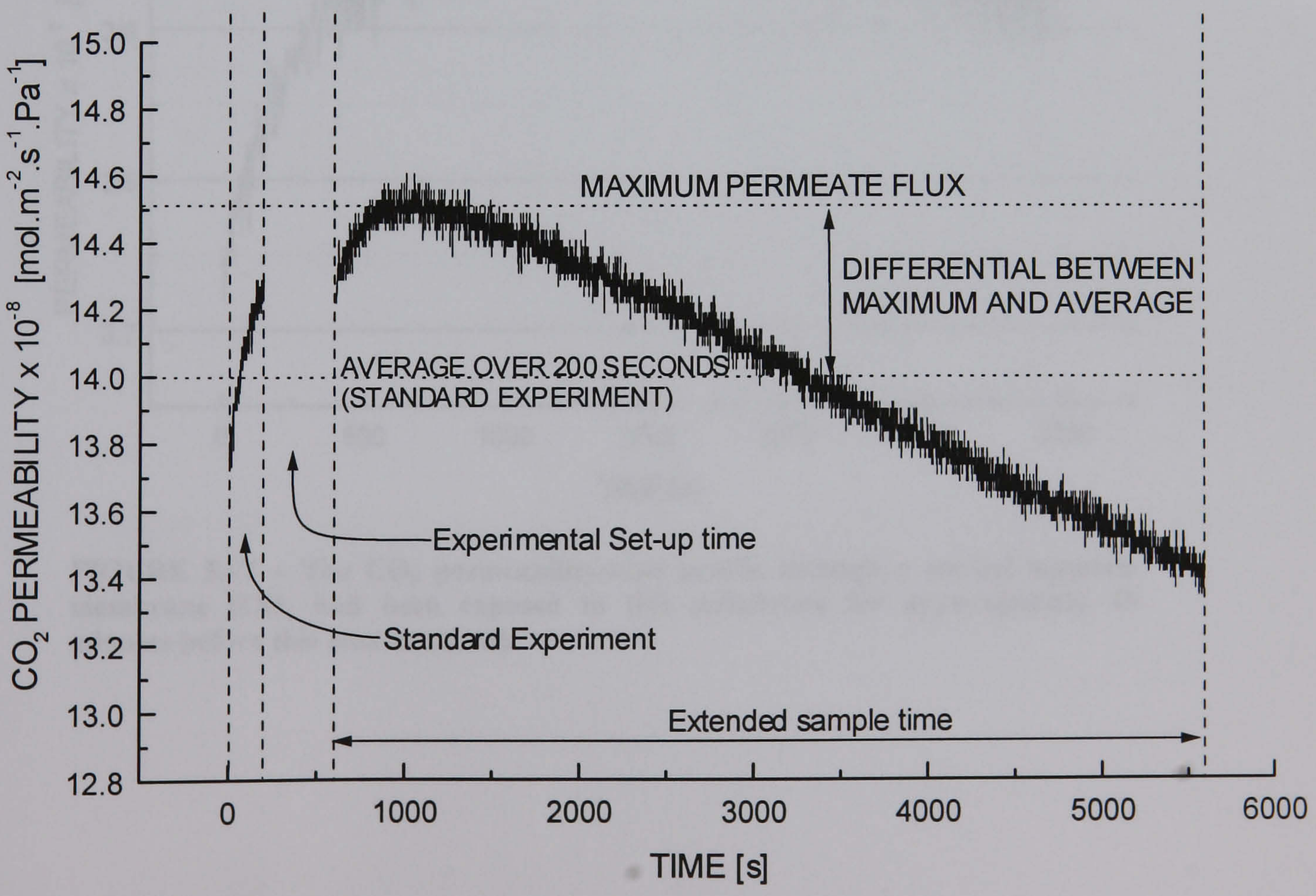

FIGURE 5.16 – The characteristic CO_2 permeability – time curve.

This observation of the time dependency of CO_2 permeance in the phenyl/methyl and diphenyl/methyl systems led to the re-examination of other non -borosilicate systems.

Phenyl/TEOS membranes (phenyl ligand as template- pyrolysed at 873 K) were found to behave in a very similar fashion – only much faster. Conversely, methyl membranes displayed the same time dependency, only here degradation in CO_2 permeance was extremely slow. Figure 5.17 below illustrates this when compared with Figure. 5.16 above, showing clearly reduction in permeance of the methyl membrane as compared to the phenyl membrane.

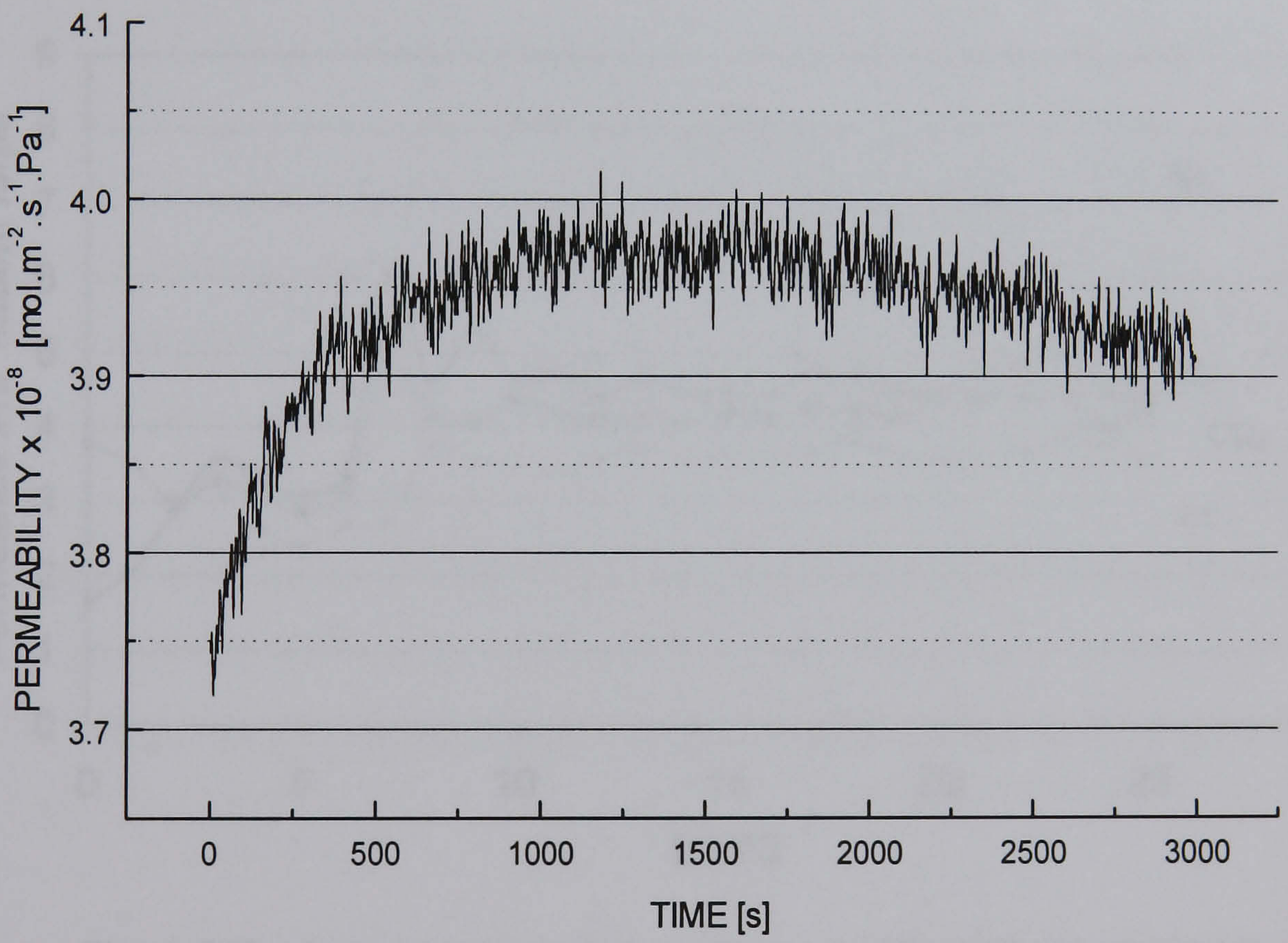

FIGURE 5.17 – The CO_2 permeability-time profile through a methyl template membrane (CO_2 had been exposed to this membrane for approximately 45 minutes before this measurement).

Borosilicate Sols

As mentioned previously, the overall performance of the borosilicate sols was superior to the non-borosilicate systems – and also far more robust and durable. This durability extended to the degradation of CO_2 permeance with time and the degradation in performance of the non-borosilicate systems described above, was not observed over the same time periods.

However, permeance measurements with four gas species were conducted on consecutive days over the period of a month and the results are presented below in Figure 5.18

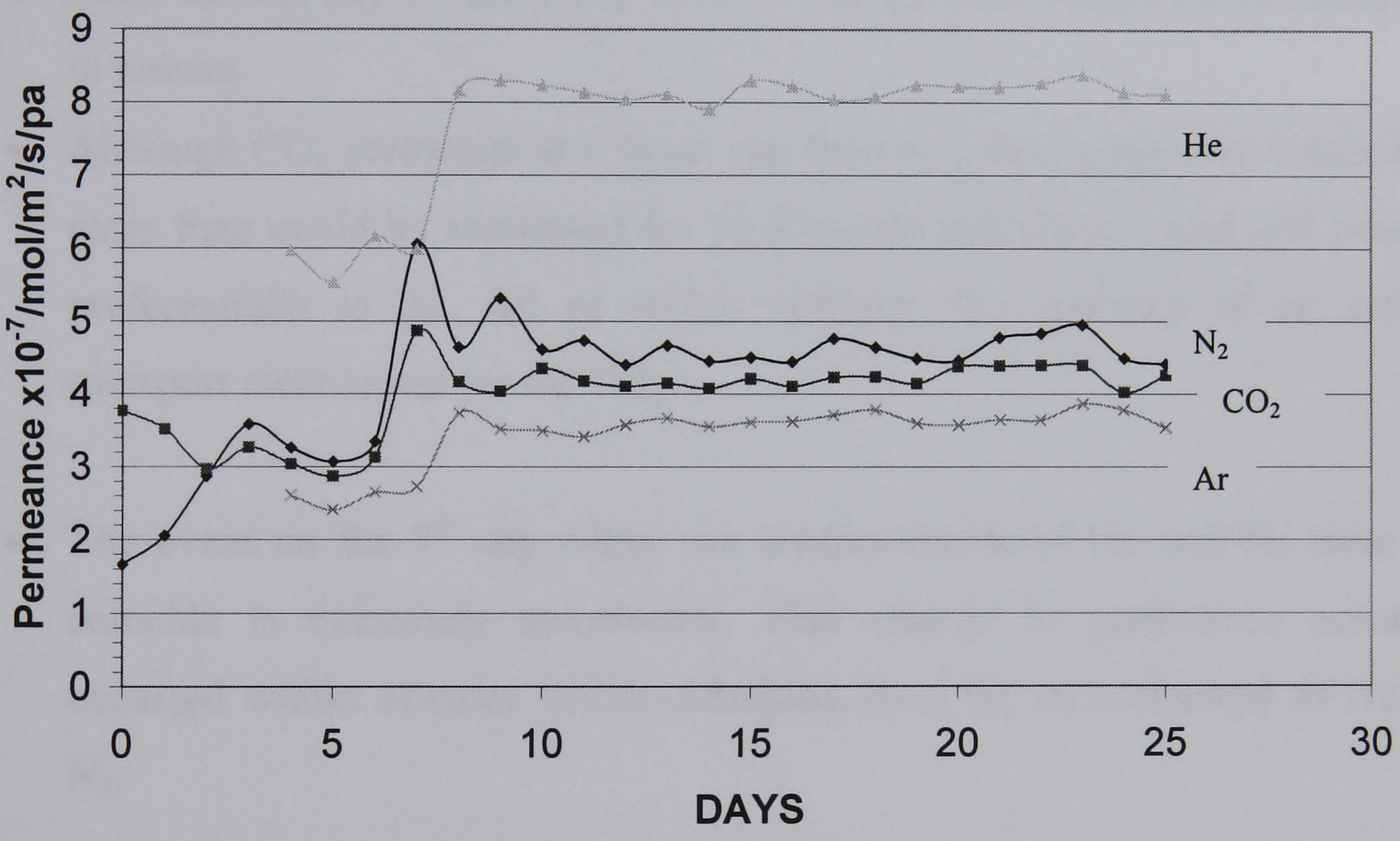

Figure 5.18 – Long term permeance performance of borosilicate sol membrane (PBA precursor with MTEOS in 20% molar ratio).

The original CO_2 permeance was approximately twice that of nitrogen but fell after a few days to be less than that of nitrogen. Inert gas measurements were included after day four. This decision was based upon the reasoning that being chemically inert, that these gases would act as useful indicators of any physical process occurring within the membrane.

This membrane was purposely chosen because it was an uncharacteristically poor representative of the group of membranes based upon PBA precursor and MTEOS – the reasoning being that any degradation in performance, or gross changes in physical behaviour, would be more noticeable in such a sample.

From inspection of Figure 5.18, the salient points of interest are:

- After the 4th day all the gases seem to change their respective permeances in unison.
- Although CO_2 permeates at a lower rate than N_2 , their respective values are more than could be accounted for by Knudsen diffusion. – and still passed preferentially to Ar. All of which indicates the presence of an active transport mechanism for the CO_2.

- The event on the 7^{th} day where the measurements of He and N_2 seem to coincide is extremely noteworthy. This change in permeance actually occurred within minutes whilst switching from the measurement of He to N_2.

Taken in context with the profiles of all the gases in this plot, it would appear that the increase in permeance before reaching a steady state condition after about the 9^{th} day is due to the gradual purging of clogged pores within the membrane and/or the substrate. The drastic leap in permeance that was witnessed within a space of minutes on the 7th day between the He and N_2 measurements must have been such an event.

The oscillations in the permeances of all the gases after about the 10^{th} day when a seeming steady state had been achieved could be due to random purging and clogging of the membrane and/or the substrate. (Attempts were made to analyse whether or not this non-linear behaviour was chaotic behaviour but the number of data points was insufficient).

5.2.6 CO_2 Absorption of Non-Borosilicate and Borosilicate Systems.

Figure 5.18 shows that the borosilicate sols do suffer from CO_2 permeance degradation. *However, this process is very much slower than in the non-borosilicate systems – and more importantly seems to settle into a steady state condition indefinitely.*

From the evidence summarised by figs. 5.15 to 5.17 that absorption of CO_2 of the non-borosilicate systems is also occurring. However, unlike the borosilicate systems it would appear that for the non-borosilicate systems, the degradation in CO_2 permeance is a continual process. This is empirical evidence that suggests that in the non-borosilicate systems that chemi-sorption dominates over physisorption. As discussed in section 5.2.4.1.1 and 5.2.4.2.1, the chemisorption observed in the non-borosilicate systems could be due to the action of the abundant Q^3 species becoming linked with hydroxyl groups and acting not only as surface diffusion sites for CO_2 but also chemisorption sites as well. In addition, with phenyl based (PTMOS) non-borosilicate systems, the strong chemical affinity of phenyl towards CO_2 could act as a chemisorption site.

In the borosilicate system, the reverse seems to be true. Some chemisorption does occur: CO_2 starts as being passed selectively to N_2 but from inspection of Figure 5.18, their relative positions have swapped after about three days. If chemisorption were active in this period then the sites have become saturated

after this time. The only chemisorption site which is analogous to the Q^3 – OH species in the non-borosilicate systems would be the T^2–OH. However, from inspection of the deconvoluted ^{29}Si MAS NMR spectra of the borosilicate system in Figure 4.12 of chapter 4, one can see that only a very small quantity of this species is present in the fully pyrolysed borosilicate systems.

After the third day the ratio of permeances of N_2 to CO_2 averaged approx. 1.08 :1 . This was less than could be accounted for by Knudsen Diffusion (i.e proportional to the square root of their masses and theoretically 1.25: 1 for N2 : CO_2) . This suggests that some mechanism was acting preferentially towards CO_2 and the likeliest mechanism is surface diffusion and for the non adsorbable species a combination of activated diffusion and Knudsen diffusion. (As discussed in sections 5.2.4.1.1. and 5.2.4.2.1)

The periodic modulation of the permeance of CO_2 from the third day onwards is shadowed by similar synchronised behaviour of all the test gases (including the inert ones He and Ar). This then is indication of the physical state of the interior of the membrane in terms of continuous clogging and catastrophically unclogging its pores on a micro-scale. (As commented on in the notes in section 5.2.5. for the 7th day observation)

5.2.7 Permeation and Temperature.

Non borosilicate systems

Figure 5.19 shows the temperature dependency of permeance for some non-borosilicate systems (Sequential measurements for each temperature). The CO_2 permeance falls rapidly to less than that of both N_2 and He. After cooling these trials were then repeated. It was then discovered that the permeation performance of each specimen remained at the level attained after the inaugural temperature trial. This result was typical for all (phenyl containing) systems investigated.

The permeability of N_2 and He were also decreased with temperature – which is consistent with the functional relationship between temperature and flow for both Knudsen diffusion and also surface diffusion mechanisms. The He/N_2 separation ratios were in the 1.6-2.0 range (Knudsen 2.65).

It is therefore reasonable to assume gas transport might be a result of a combination of both surface diffusion and Knudsen diffusion. Unlike CO_2, this decrease in N_2 (and He) permeability with temperature was found to be reversible.

For methyl membranes, the trend was similar to above but the decrease in permeability is less than with the methyl/diphenyl membranes. Also, unlike the phenyl membranes, the degradation in permeability of the methyl membranes was found to be partially reversable upon cooling.

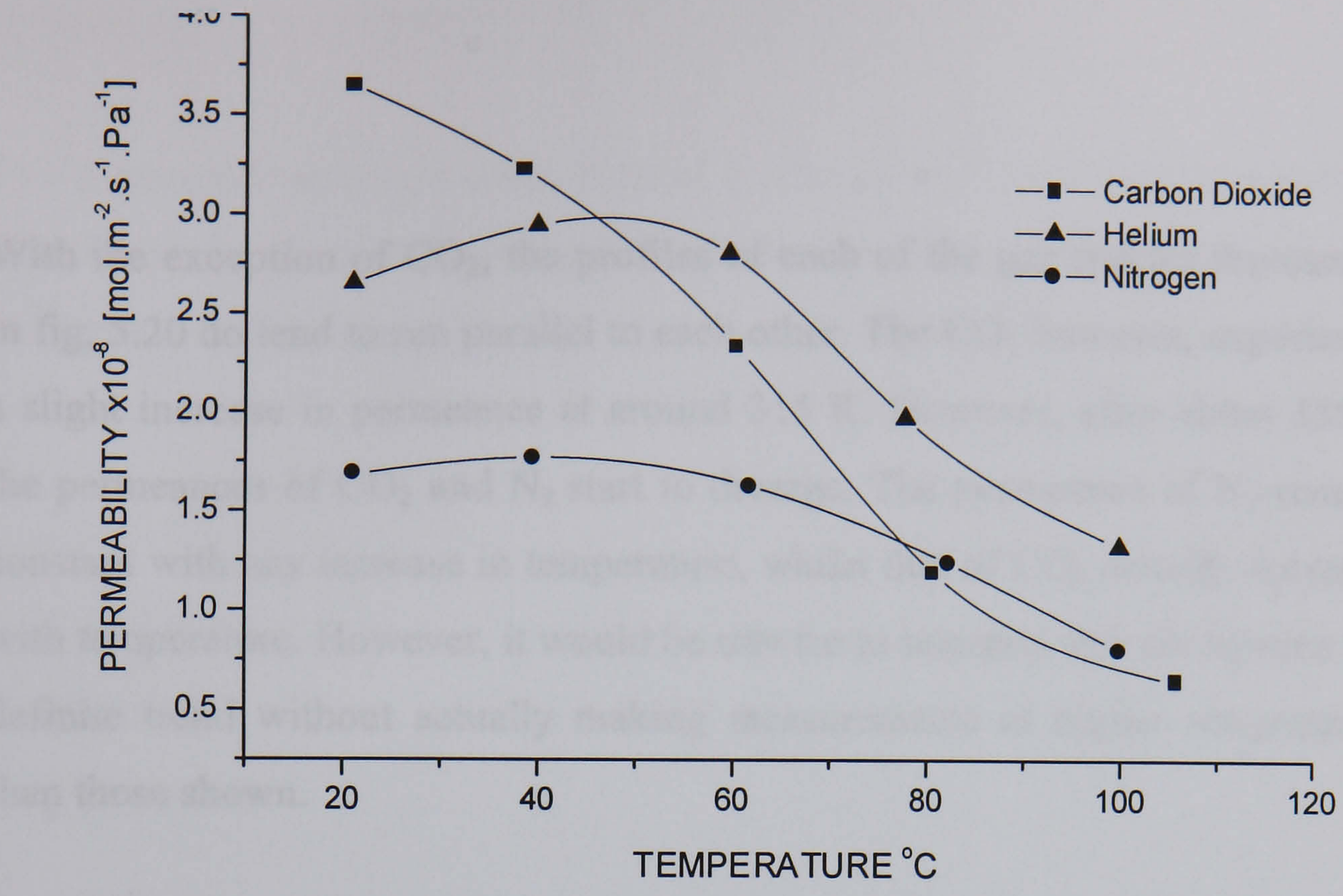

FIGURE 5.19 – The temperature dependency of permeability. (Gases were tested in the order N_2, CO_2, He.) The results shown were obtained from a diphenyl/methyl (40/60) membrane heated to 400°C.

Borosilicate Membranes

Figure 5.20 shows the temperature dependency of permeance for a borosilicate system.

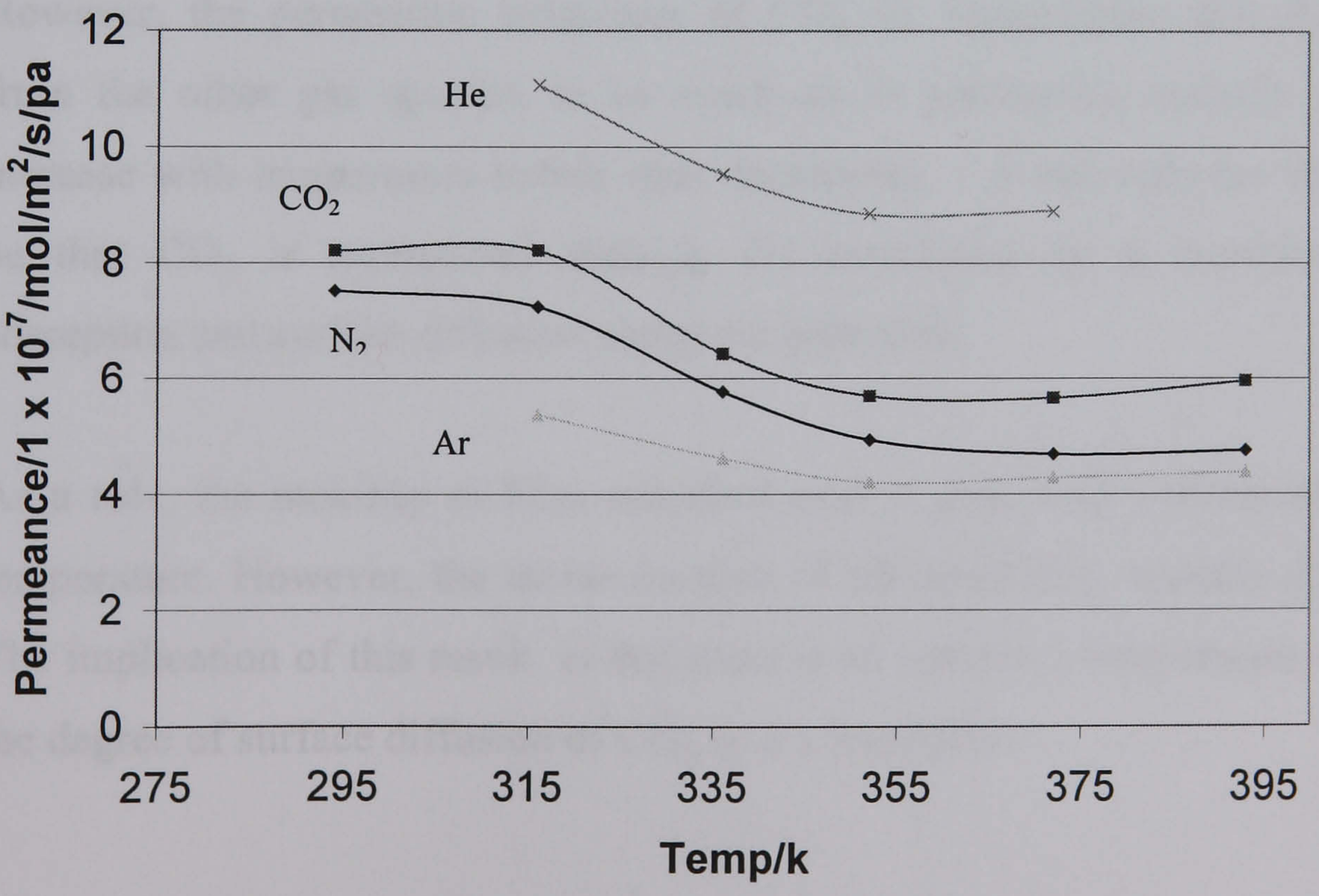

Figure 5.20 – Permeance of Borosilicate membrane (TMB precursor MTEOS 20% molar ratio).

With the exception of CO_2, the profiles of each of the gas species represented in fig, 5.20 do tend to run parallel to each other. The CO_2 however, experiences a slight increase in permeance at around 315 K. However, after about 355 K, the permeances of CO_2 and N_2 start to diverge. The permeance of N_2 remains constant with any increase in temperature, whilst that of CO_2 actually increases with temperature. However, it would be unwise to interpret this divergence as a definite trend without actually making measurements at higher temperatures than those shown.

Generally speaking, the permeance of all the gas species represented in Figure 5.20 appear to decrease in proportion to $T^{1/2}$ up to about 360K. Above this temperature, this general decrease in permeance seems to level off - and might even be starting to increase. This effect is most apparent for Ar permeance and can be explained by a combination of an increase of the mean free path of Ar with temperature and also the exhibition of the greater influence of activated diffusion rather than Knudsen diffusion at elevated temperatures.

However, the permeation behaviour of CO_2 vs. temperature initially differs from the other gas species, in as much as its permeance actually starts to increase with temperature before then decreasing. A rationale for this might be that CO_2 is transported through the membrane by a combination of adsorption and surface diffusion along the pore wall.

As a rule, the mobility of CO_2 adsorbed onto a pore wall will increase with temperature. However, the molar fraction of adsorbed CO_2 actually decreases. The implication of this result is that there is an optimum temperature at which the degree of surface diffusion of CO_2 is at a maximum.

The permeance vs. temperature profiles for the phenyl boronic acid containing sols differ slightly to those containing phenyl boronic and are presented below in Figure 5.21 for CO_2 and N_2.

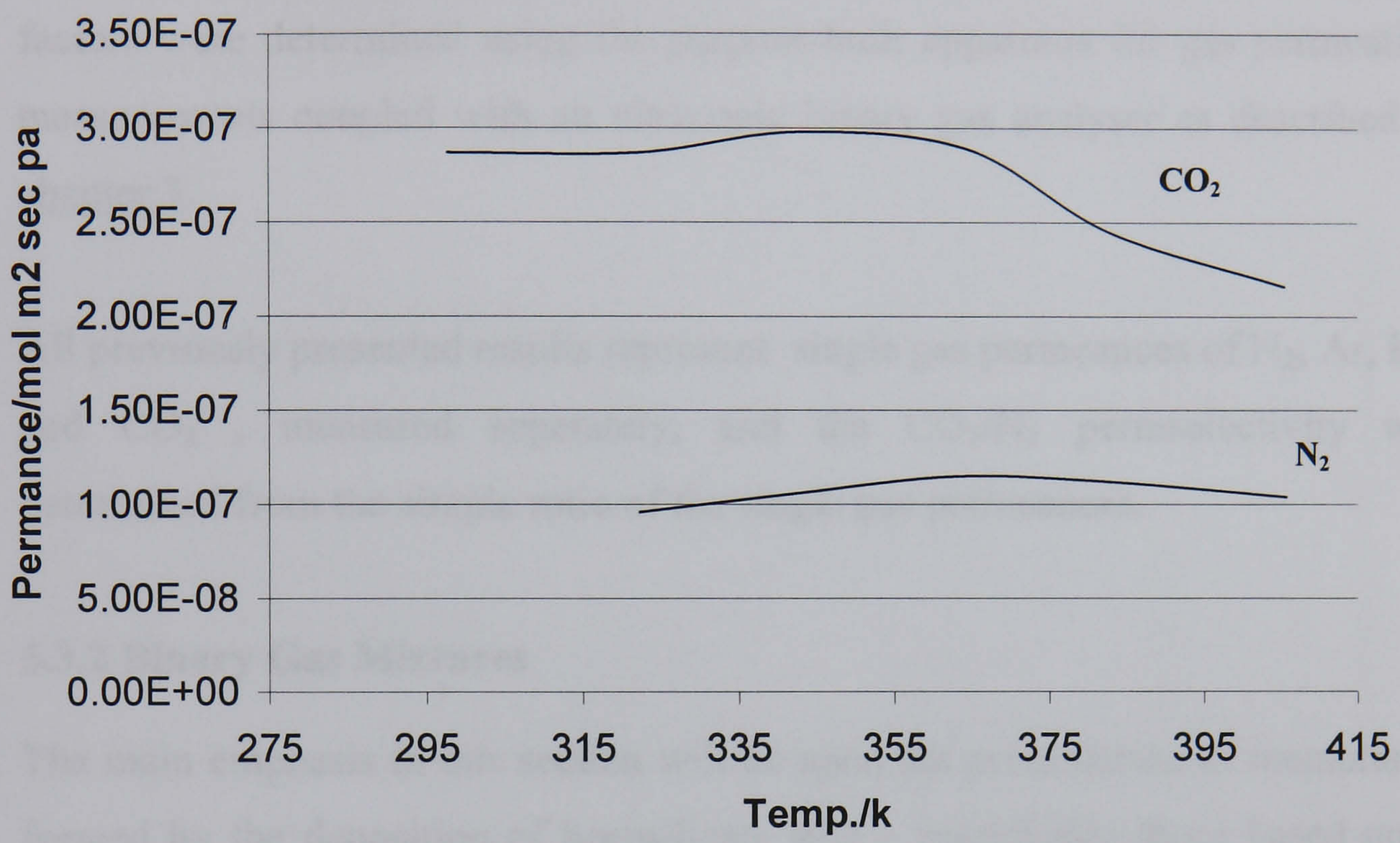

Fig. 5.21 - Permeance vs, temperature behaviour of MTEOS sols containing PBA precursor.

5.3 Permselectivity and Separation Factors

5.3.1 Single gas permselectivity

The gas permeance results presented previously and their attendant separation factors were determined using the purpose-built apparatus for gas permeation measurements coupled with an ultrasonic binary gas analyser as described in chapter 3.

All previously presented results represent single gas permeances of N_2, Ar, He, and CO_2 , measured separately, and the CO_2/N_2 permselectivity was determined from the simple ratio of the single gas permeances.

5.3.2 Binary Gas Mixtures

The main emphasis in this section will be upon the presentation of membranes formed by the deposition of borosilicate sols – specifically those based upon MTMOS with the phenyl boronic acid precursor. This is because of all the membrane systems investigated during this thesis, they were the ones which performed best in terms of selectivity and durability.

The separation factor of CO_2 to N_2, was calculated according to the relation:

$$\frac{Y_{CO_2}\left(1-X_{CO_2}\right)}{X_{CO_2}\left(1-Y_{CO_2}\right)}$$

(Were X_{CO2} was the CO_2 composition of the feed gas and Y_{CO2} that of the permeate measured after steady state had been attained).

Variations of the separation factor of a particular membrane were measured as a function of several variables: feed composition; pressure difference; temperature; and the ratio between the volumes of permeate and retentate.

This last was found to be one of the dominant variables to affect a membrane's performance in terms of both and separation factor. Figure 5.22 below represents the performance of one of the better membranes in this study: a deposited sol of methyltrimethoxysilane (MTMOS) with a phenyl boronic acid (PBA) precursor mixed in a molar ratio of 4:1

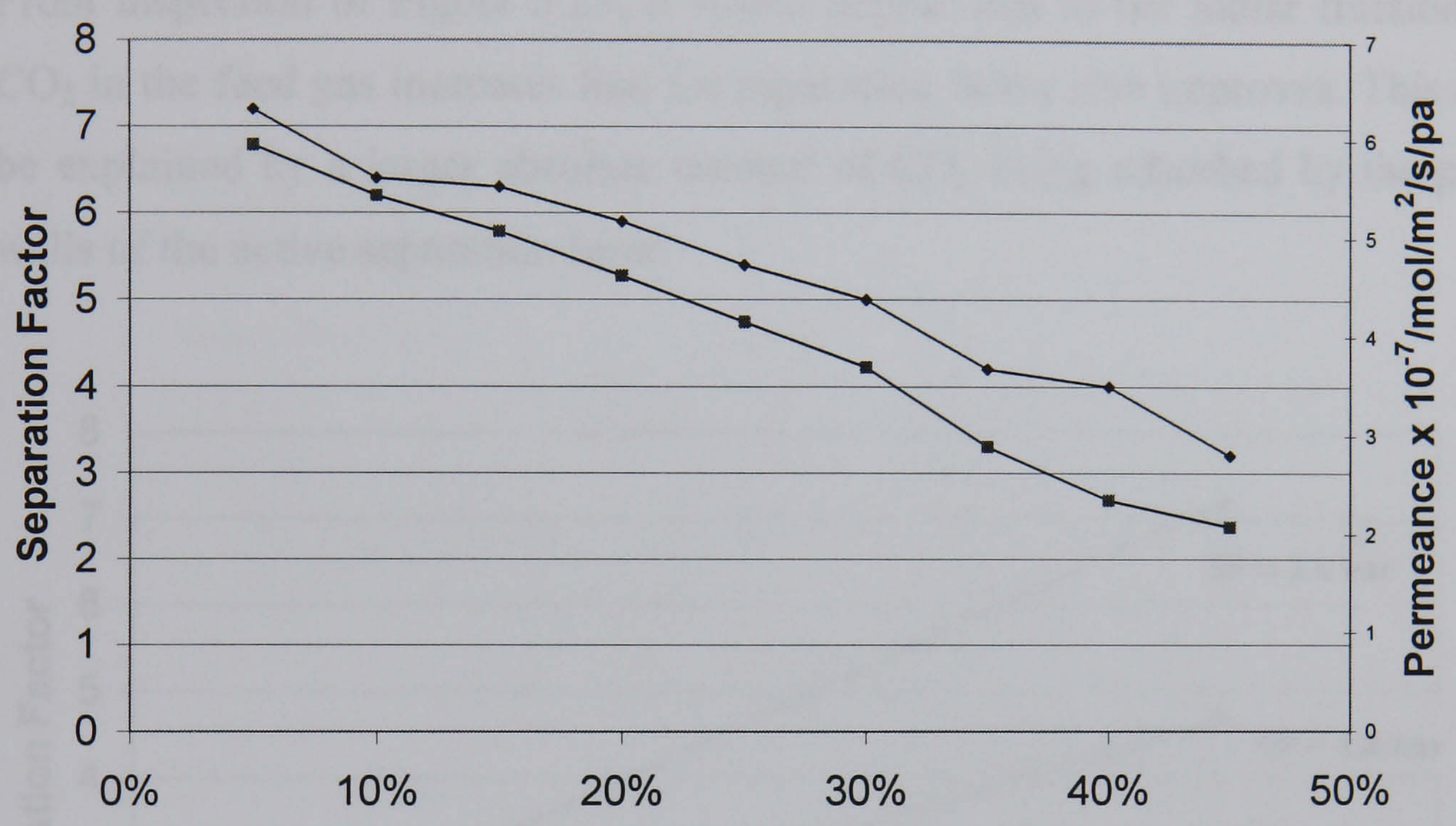

Figure 5.22 – Room temperature CO_2:N_2 binary gas permeances (lower trace) and binary gas separation factors (upper trace) vs. ratio of the volume of permeate to retentate. Feed gas was a binary mixture was a 50:50 C02:N2 and membrane was a deposited sol of MTMOS and a PBA precursor in a 20% molar ratio.

As the volume ratio of permeate to retentate falls, both the CO_2: N_2 separation factor and binary gas permeance increases. A rationale for this observation is that there is an accumulation of the retained N_2 at the site of the pore entrance that impedes CO_2 adsorption along the pore wall. Any reduction in the volume ratio of permeate to retentate basically means that more of the feed gas will flow past parallel to the membrane's surface (feed side) and be vented to the external atmosphere. Whilst reducing the absolute volume of gas passing through the membrane, this will in effect reduce the concentration of the CO_2-inhibiting N_2 build-up at the entrance to the pore wall. Hence, the overall separation efficiency would be improved.

Figure 5.23 below illustrates the variation in the separation factor of a binary CO_2: N_2 gaseous mixture as both the molar fraction of CO_2 in the mixture and the transmembrane pressure difference change. (This particular inquiry was limited by the availability of only two pre-bottled molar mixtures of CO_2: 10% and 50%).

From inspection of Figure 5.23, it would appear that as the molar fraction of CO_2 in the feed gas increases that the separation factor also improves. This can be explained by a larger absolute amount of CO_2 being adsorbed by the pore walls of the active separation layer.

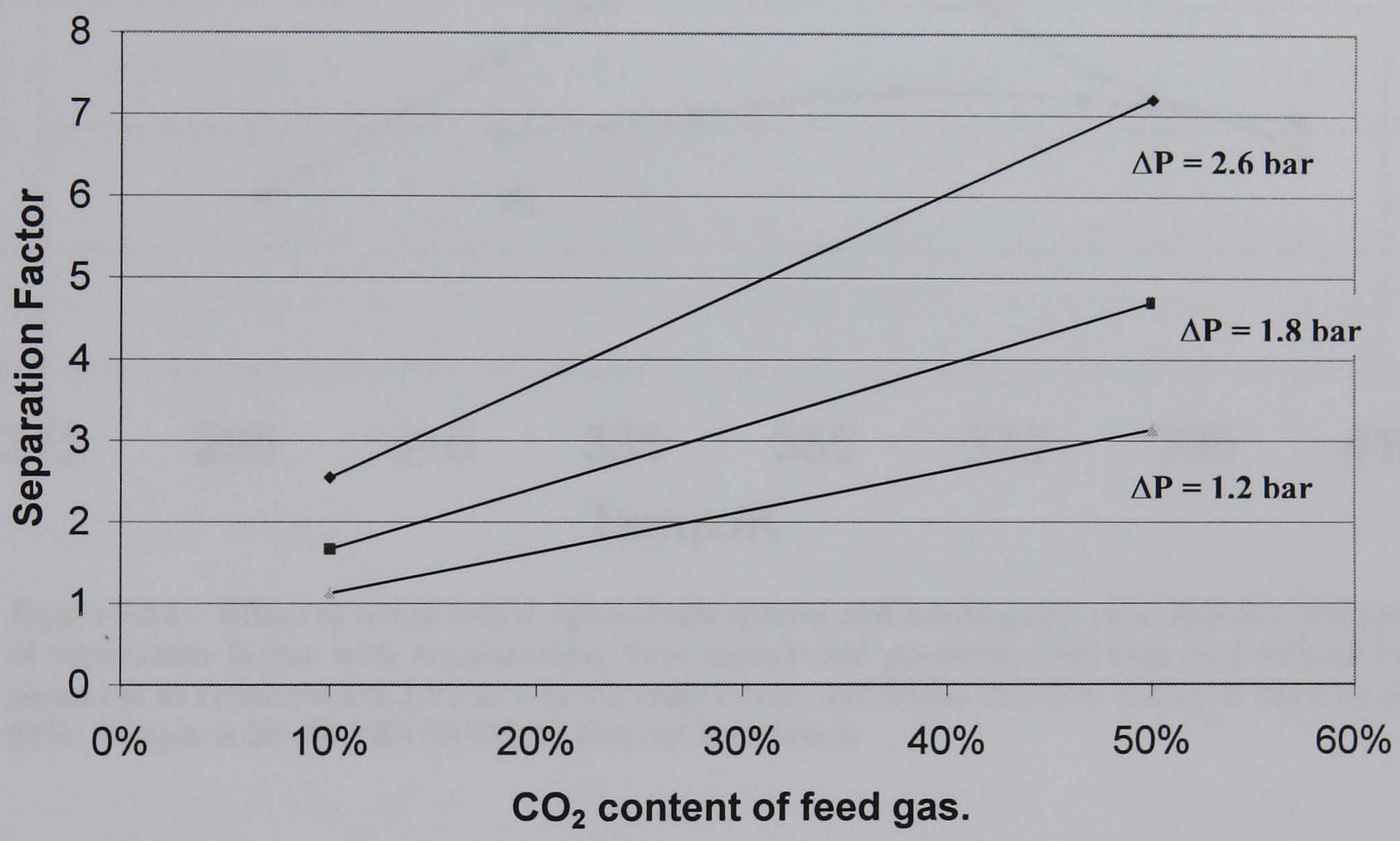

Figure 5.23 – Room-temperature separation factor of a binary CO_2: N_2 gas mixture Vs. molar CO_2 content at various transmembrane pressure differences. The volume ratio of permeate to retentate was kept fixed at 20% and membrane tested was a deposited sol of MTMOS and a PBA precursor in a 20% molar ratio.

Figure 5.20 above, illustrated the effect of temperature upon single gas permeability. In contrast, Figure 5.24 below shows the effect on temperature upon the separation of a binary gas mixture of CO_2 and N_2. The transmembrane pressure difference and volume ratio of permeate to retentate were kept

constant at 1.9 bar and 0.2 respectively and the molar fraction of CO_2 in the feed gas was 50%.

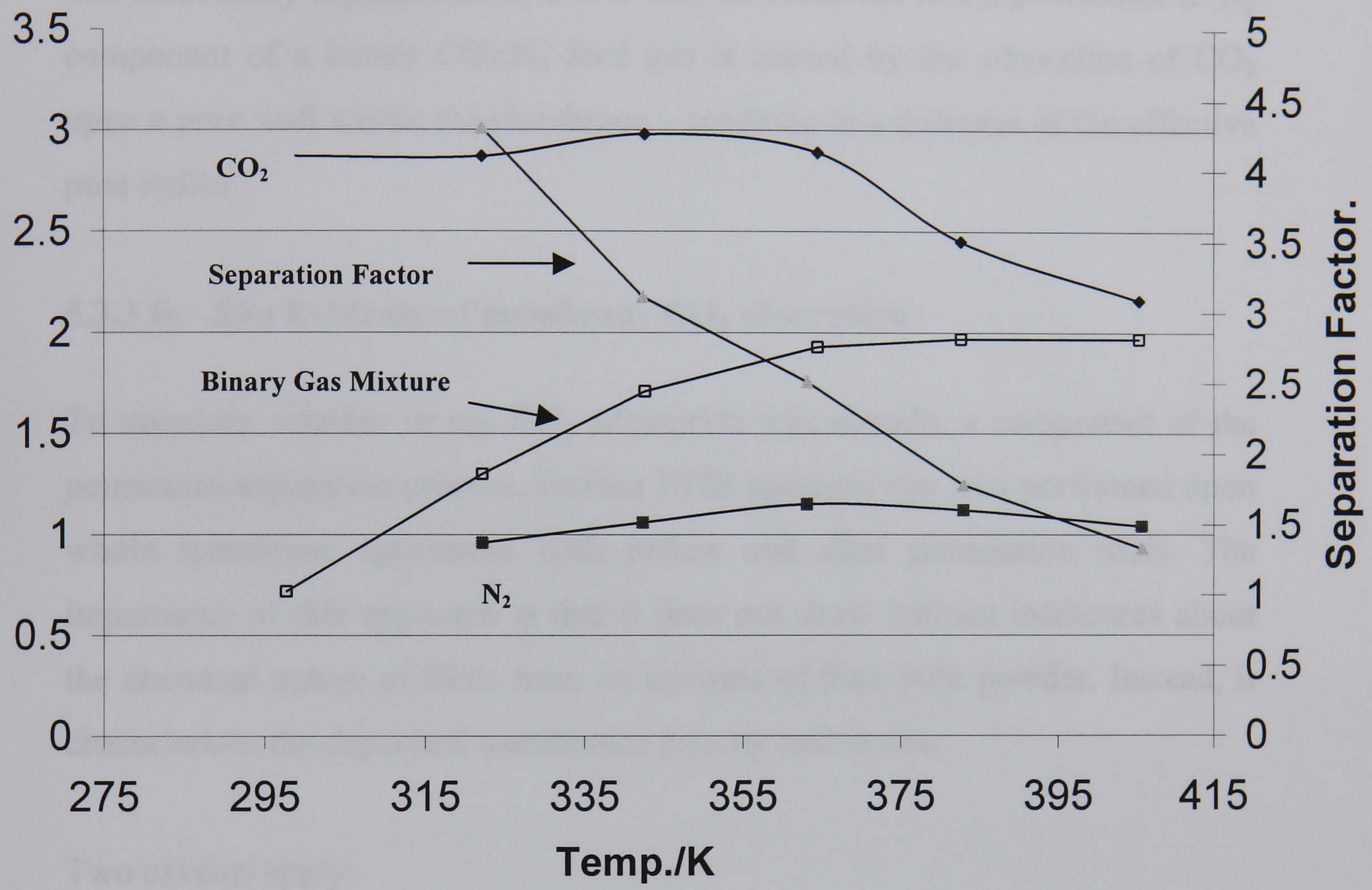

Figure 5.24 – Effect of temperature upon single species and mixed gases. Also shown is the variation of separation factor with temperature. Transmembrane pressure difference and volume ratio of permeate to retentate are 1.9 bar and 0.2 respectively and molar fraction of CO_2 in the feed gas was 50%. Sample is 20: 80 PBA:MTMOS derived membrane.

From inspection of Figure 5.24, it can be seen that the single gas species permeance (and hence permselectivity) differs from that of the 50% binary CO_2: N_2 mixture. With increasing temperature, the permeance of the binary mixture actually increases whilst the separation factor of the binary feed gas actually decreases.

For all the membranes reported here, the separation factor values of a binary mixture feed gas-containing CO_2 and N_2 in varying molar fractions were higher than those of the single-gas permselectivities alone.

The most likely explanation for this is that the reduction in the permeance of N_2 component of a binary CO_2:N_2 feed gas is caused by the adsorption of CO_2 upon a pore wall within the membrane – resulting in a decrease of the effective pore radius.

5.3.3 *In –Situ* Evidence of membrane CO_2 absorption

To ascertain whether or not CO_2 adsorption was actually a component of the permeance/separation process, surface FTIR spectroscopy was performed upon whole membrane specimens both before and after permeation trials. The importance of this approach is that it does not draw indirect inferences about the chemical nature of films from an analysis of their bulk powder. Instead, it characterises the deposited membranes directly and *in situ*.

Two caveats apply:

- Firstly, the process of testing each specimen involved a diamond-tipped indentor. This destroyed the membranes' integrity, making it impossible to obtain a surface spectrum followed by testing in the permeation rig and to take a final measurement after the run was complete. The "before and after" spectra had to be obtained from two separate specimens. However, all specimens were part of the same production batch and exhaustive statistical sampling techniques were employed.

- Secondly, it was not possible to replace the ambient atmosphere within the FTIR spectrometer and hermetically replace it with an inert species such as nitrogen – so atmospheric CO_2 could have been present. However, a background calibration was performed before each spectrum was obtained

and tests run after such a background was taken - but in the absence of any specimen - always returned the expected flat line spectrum.

Figures 5.25(a) to 5.25 (d) below represent a typical "before and after" spectrum of a MTMOS with a 20% molar fraction PBA precursor. The specimens were sampled at at least 15 different locations over their surface in order to discount the possibility of any spurious and atypical local phenomena.

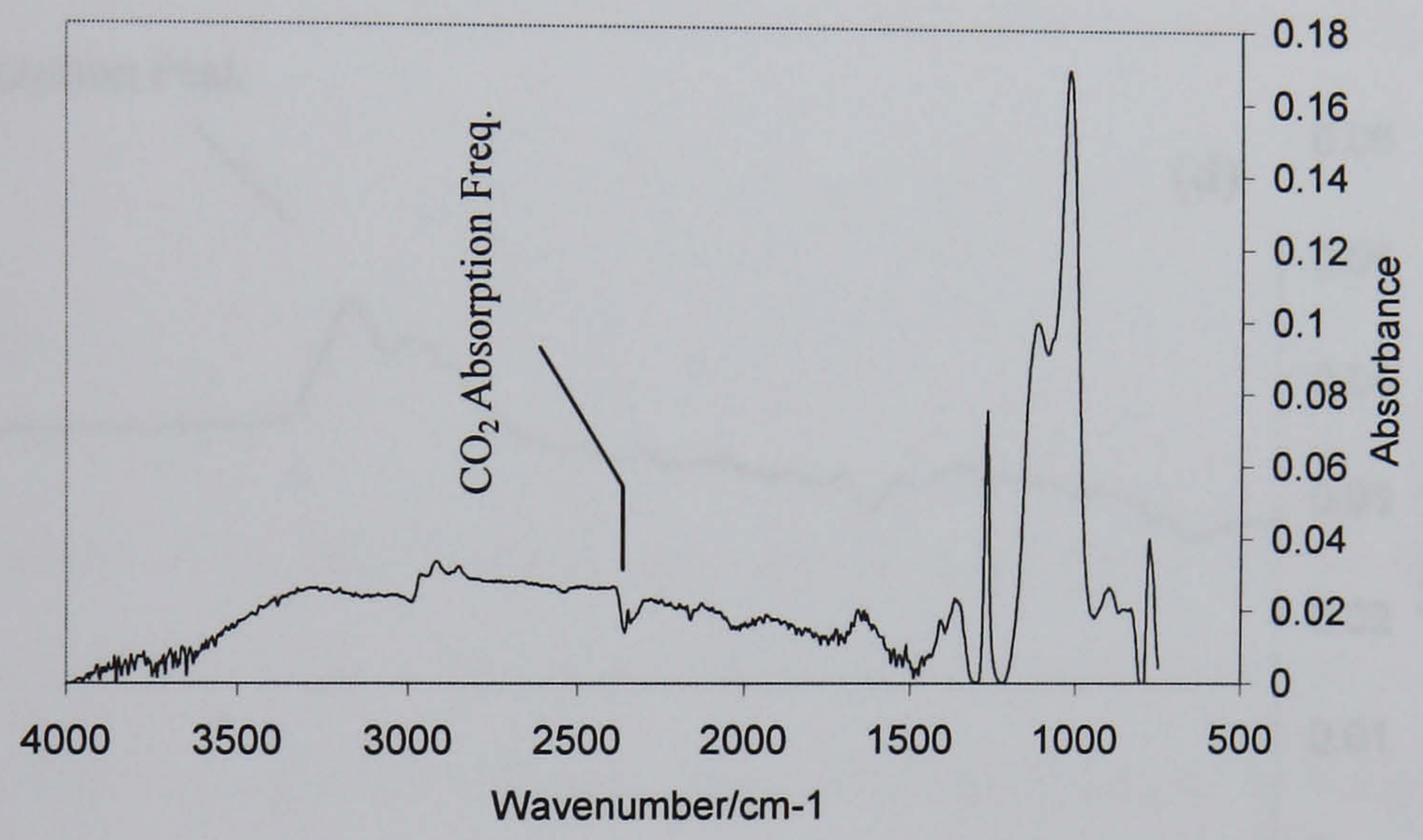

Figure 5.25(a) – Representative spectrum of MTMOS:PBA membrane before exposure to permeation trial. CO_2 doublet at approx. 2350 cm^{-1} is suppressed. Though broad convex baseline on LHS side indicative of water absorption by membrane and/or support substrate.

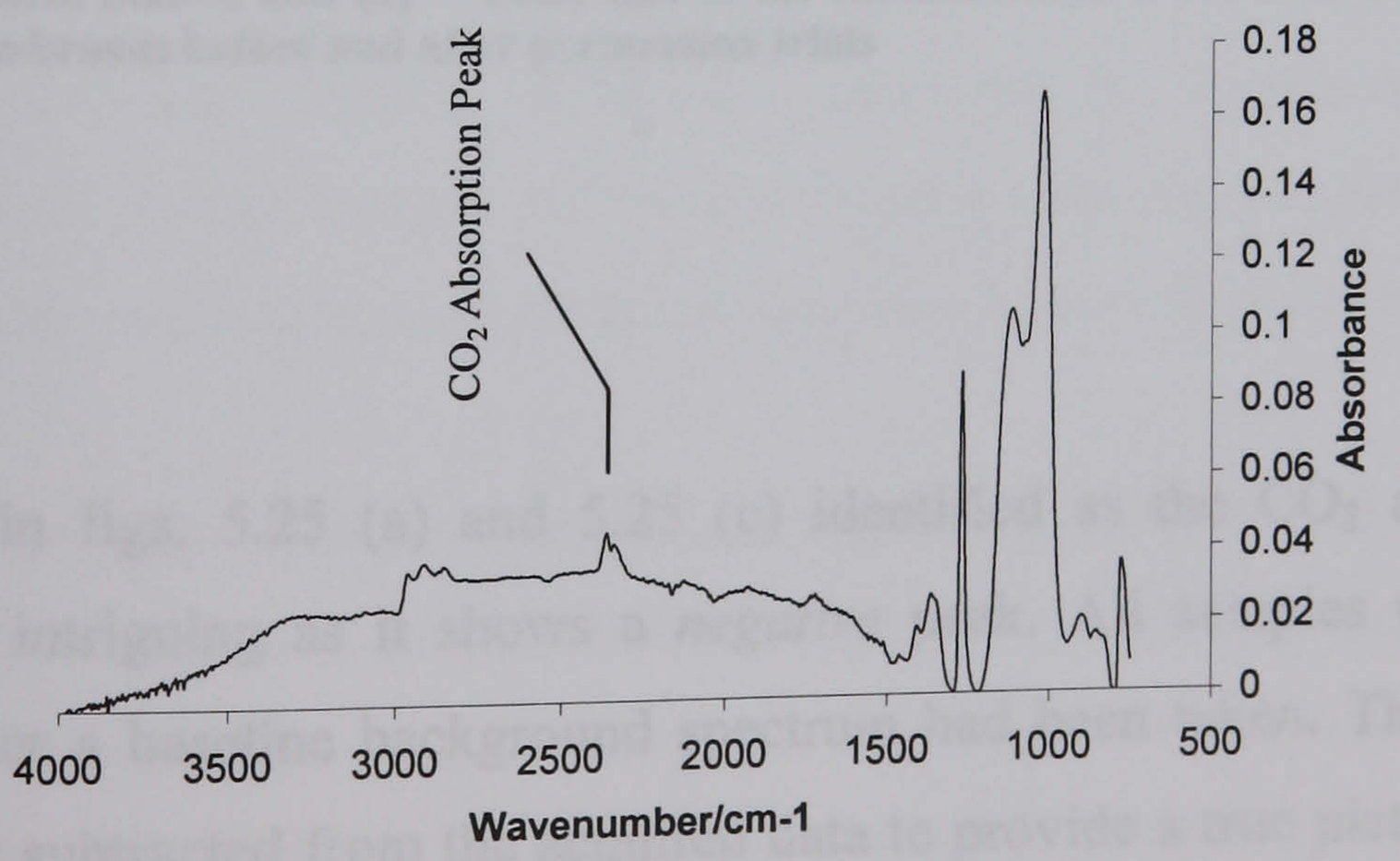

Figure 5.25(b) – Representative spectrum of MTMOS:PBA membrane after exposure to permeation trial. CO_2 doublet at approx. 2350 cm^{-1} is pronounced. Though still indication of water absorption by membrane and/or support substrate.

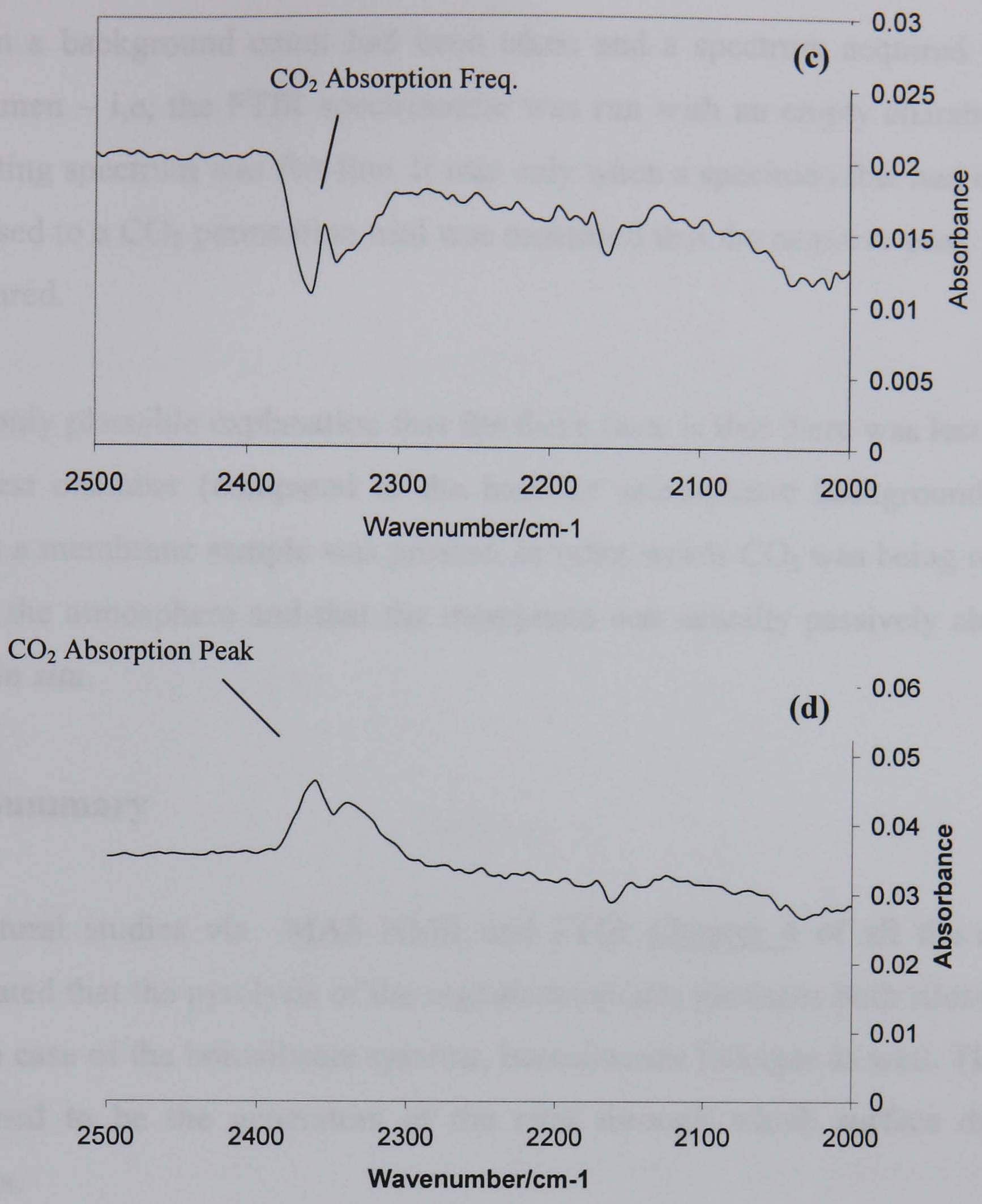

Figures 5.25 © and (d) - Close ups of the surface FTIR of MTOS:PBA membranes before and after permeation trials

Comment

The feature in figs. 5.25 (a) and 5.25 (c) identified as the CO_2 absorption frequency is intriguing as it shows a *negative* peak. All samples were only examined after a baseline background spectrum had been taken. This is then automatically subtracted from the acquired data to provide a true picture of the chemical nature of the specimen.

When a background count had been taken and a spectrum acquired with no specimen – i,e, the FTIR spectrometer was run with an empty chamber – the resulting spectrum was flat-line. It was only when a specimen that had not been exposed to a CO_2 permeation trial was measured that the negative peak for CO_2 appeared.

The only plausible explanation that fits these facts is that there was less CO_2 in the test chamber (compared to the baseline atmospheric background count) when a membrane sample was present. In other words CO_2 was being removed from the atmosphere and that the membrane was actually passively absorbing CO_2 *in situ*.

5.4 Summary

Structural studies via MAS NMR and FTIR Chapter 4 of all the systems indicated that the pyrolysis of the organic templates produces both siloxane and in the case of the borosilicate systems, borosiloxane linkages as well. These are assumed to be the generators of the sites through which surface diffusion occurs.

From the results presented within this chapter, it would appear that for the non-borosilicate systems, surface diffusion seems to be improved by the incorporation of phenyl ligands within the siloxane network. However, this is associated with accelerated adsorption and decrease in overall performance.

For the borosilicate systems, the most successful system had a methyl backbone and decreased in its performance only very gradually. Afterwards its performance remained constant - except for long-term modulations of Figure 5.18 which were mirrored by the inert species as well. Thermally rejuvenating the degraded non-borosilicate membranes did not meet with success. However, the borosilicate systems did partially respond to this treatment and regained a

significant fraction of their original performance. The conclusion is that in both the non-borosilicate and borosilicate systems, the mass-transport mechanism for CO_2 is surface diffusion, whilst that of the other non-adsorbable gases is a mixture of Knudsen diffusion and activated diffusion.

The degradation of the non-borosilicate systems is due to the large amount of Q^3-OH species acting as chemisorption sites. (in addition to the phenyl ligand of the silane). The analogous species within the borosilicate systems is the T^2-OH group which is only present in very small quantities within the borosilicate systems and this is reflected in the gross difference in chemisorption behaviour of the two classes of system.

References

[1] Bjorkert, U.S , "High Temperature CO_2 Permselective Planar Membranes" Ph. D. Thesis (1999), Centre for Advanced Materials, Dept. of Physics, University of Warwick.

[2] Kaye and Laby, "Tables of Physical Constants", Longman 15th Ed.

[3] Z. Li, K. Kusakabe, S. Morooka, "Preparation of Thermostable Amorphous Si-C-O Membrane and its Application to Gas Separation at Elevated Temperature", Journal of Membrane Science, **118** (1996) p159

[4] H. Takaba, K. Mizukami, M. Kubo, A. Stirling, A Miyamoto, "The Effect of Gas Molecule Affinities on CO_2 Separation, from the CO_2/N_2 Gas Mixture using Inorganic Membranes as Investigated by Molecular Dynamics Simulation", Journal of Membrane Science, **121** (1996) p251

[5] G.D. Sorarau, F. Babonneau and C. Gervais, N. Dallabona, "Hybrid $RSiO_{1.5}$/ B_2O_3 Gels from Modified Silicon Alkoxides and Boric Acid." Journal of Sol-Gel science and Technology 18 (2000) p11

[6] F. Scheinmann, "An Introduction to Spectroscopic Methods For the Identification of Organic Compounds Volume 1: NMR and IR Spectroscopy", Pergamon Press (1970)

Chapter 6.

Conclusion

6.1 Templating Process

For both the non-borosilicate and borosilicate systems reported within this thesis, the attempt to produce porous gas-selective membranes by the selective thermal removal of the organic components of the deposited sol did result in selective behaviour of the active layer.

However, the mechanism of gas selectivity does not appear to be consistent with true molecular sieving (i.e. discrimination solely in terms of molecular diameter). Instead, for both classes of system, the transport mechanism for CO_2 appears to be surface diffusion.

Pyrolysis of the organic templates produces both siloxane and in the case of the borosilicate systems, borosiloxane linkages as well. These are assumed to be the generators of the sites through which surface diffusion occurs The mass-transport

process for the non-adsorbable gases (in both classes of system) appears to be a mixture of Knudsen diffusion and activated diffusion.

6.2 Differences Between Borosilicate and Non–Borosilicate Systems

In general, it was found that the borosilicate systems are more robust and durable, do not degrade so quickly and possess superior gas separation properties to the non-borosilicate systems. The borosilicate derived membranes were also less likely to possess surface cracks and gross physical defects.

For the non-borosilicate systems, surface diffusion of CO_2 seems to be enhanced by incorporating phenyl ligands (with a strong CO_2 affinity) within the siloxane network. However, this is associated with accelerated CO_2 adsorption and decrease in overall performance.

For the borosilicate systems, the most successful membranes had a methyl backbone and performance degraded very slowly. Afterwards its performance remained constant. Thermally rejuvenating the degraded non-borosilicate membranes was not possible. However, the borosilicate systems did partially respond to this treatment and regained most of their original performance.

The degradation of the non-borosilicate systems is due to the large amount of Q^3-OH species acting as chemisorption sites. (in addition to the phenyl ligand of the silane). The analogous species within the borosilicate systems is the T^2-OH group which is only present in very small quantities within the borosilicate systems and this is reflected in the gross difference in chemisorption behaviour of the two classes of system.

The fact that surface diffusion for CO_2 in the MTMOS based borosilicate systems was superior to the phenyl based non-borosilicate systems– despite the latter's greater chemical affinity towards CO_2 – could be due to two factors (acting either singly or in combination).

1) Firstly, there is an optimum level of chemical affinity to maximise surface diffusion. Simply maximising the chemical affinity could actually inhibit this mechanism, as the CO_2 molecule will tend to become attached to the pore wall rather than diffuse along it.

2) The second factor is simply that the network formation within borosilicate systems could be superior to non-borosilicate systems.

   Hence the number, size and homogeneity of the pores within a borosilicate system would be improved in comparison with the non-borosilicate systems. Also, the associated benefits of better network formation are that there are fewer (seemingly minor) cracks and defects that can seriously affect membrane performance.